Characterization of Electrode Materials for Aqueous-Based Electrochemical Capacitors Using Spectroscopy, the Boehm Titration and Spectroelectrochemistry

by

Sarah L. Goertzen

Submitted in partial fulfillment of the requirements for the degree of Master of Science

at

Dalhousie University
Halifax, Nova Scotia
July 2010

DALHOUSIE UNIVERSITY

DEPARTMENT OF CHEMISTRY

The undersigned hereby certify that they have read and recommend to the Faculty of Graduate Studies for acceptance a thesis entitled "Characterization of Electrode Materials for Aqueous-Based Electrochemical Capacitors Using Spectroscopy, the Boehm Titration and Spectroelectrochemistry" by Sarah L. Goertzen in partial fulfillment of the requirements for the degree of Master of Science.

Dated: July 26, 2010

Supervisor (Research Supervisor): _____

Readers (Examining Committee): _____

_____

_____

Departmental Representative: _____

DALHOUSIE UNIVERSITY

DATE: July 26, 2010

AUTHOR: Sarah L. Goertzen

TITLE: Characterization of Electrode Materials for Aqueous-Based Electrochemical Capacitors Using Spectroscopy, the Boehm Titration and Spectroelectrochemistry

DEPARTMENT OR SCHOOL: Department of Chemistry

DEGREE: MSc CONVOCATION: October YEAR: 2010

Table of Contents

List of Tables

List of Figures

Abstract

In this research various techniques were used to study surface groups on carbon electrodes, including the spectroscopic techniques UV-Vis-NIR, FTIR, PAS, XPS and XAS, as well as the Boehm titration. The methods determined to give the best insight to the surface functionalities on the carbon were XPS, XAS and the Boehm titration. The Boehm titration methodology was standardized before use. An *in situ* method of examining surface groups using spectroscopy during electrochemistry was attempted. Spectroelectrochemistry is a useful way to gain information on how electrochemistry affects electrodes during experimentation; however, it was unsuccessful for the carbon used and remains to be developed. Polymerization of the copolymer of PANI and PPy as a potential electrode material for ECs was achieved by electrochemical cycling and was studied through spectroelectrochemical measurements. Overall, the research completed included the initial stages to studying electrodes for electrochemical capacitors using analytical, non-electrochemistry techniques in conjunction with electrochemistry.

List of Abbreviations and Symbols Used

AFM: Atomic Force Microscopy
Ag/AgCl: silver/silver chloride reference electrode
ATR: Attenuated Total Reflectance
CSF: carbon surface functionality
CLS: Canadian Light Source
CV: cyclic voltammogram
DRIFTS: Diffuse Reflectance Infrared Fourier Transform Spectroscopy
EC: electrochemical capacitor
FTIR: Fourier Transform Infrared
Hupd: underpotential deposition of adsorbed hydrogen
ITO: indium tin oxide
NEXAFS: Near Edge X-ray Absorption Fine Structure
OTE: optically transparent electrode
PAS: Photoacoustic Spectroscopy
PANI: polyaniline
PPy: polypyrrole
RSD: relative standard deviation
SCE: saturated calomel electrode
SD: standard deviation
SHE: Standard Hydrogen Electrode
SGM Beamline: Spherical Grating Monochromator Beamline
TPD: Temperature-Programmed Desorption
UV-Vis-NIR: Ultraviolet-Visible-Near Infrared
XAS: X-ray Absorption Spectroscopy
XPS: X-ray Photoelectron Spectroscopy

Acknowledgements

Firstly, I would like to thank Dr. Heather Andreas for giving me the opportunity to study at Dalhousie and for teaching me so much over these two years. Thank you also for having confidence in my abilities to carry out this project.

Many people contributed to the research included in this thesis. Thank you to Jennifer Black for the powder electrodes used in FTIR and UV-Vis-NIR spectroscopy, and to Bryanna Wood for the cloth samples studied in UV-Vis-NIR spectroscopy. For the standardization of the Boehm titration, thanks to Kim Thériault for carrying out many of the titrations for CO_2-removal through degassing, and to Anthony Tarasuk for the titrations from CO_2-removal through heating experiments. I would like to particularly acknowledge those who performed spectroscopic measurements on my samples: Christopher Felix in the Faculty of Dentistry for ATR-FTIR measurements, Dr. Zeynel Bayindir for the XPS measurements and analysis carried out in the Department of Physics at Dalhousie, Dr. Brant Billinghurst at the Canadian Light Source for PAS measurements, and Tom Regier for some of the XPS and XAS measurements, and for training at the Canadian Light Source. A huge thank you goes to Stephanie Thomas for instruction on the UV-Vis-NIR spectrometer. Thanks also to Zachary Cormier for doing some of the XAS measurements at the CLS while I slept, and to Dr. Peter Wentzell for help with uncertainty calculations in the Boehm titration.

Thanks to my fellow labmates, who were always helping me out and generally making the working environment enjoyable: Jenn Black, Alicia Oickle, Michelle Everist and Zac Cormier, as well as the undergrad students.

Lastly, thank you to my friends and family! Thank you to my friends and family in Ontario, who kept in touch with me and kept me entertained with stories. Thanks to my friends in Halifax, who welcomed me to the department and who kept me from feeling alone in a new province. Finally, thank you to Tyler, who continually gave me love, fun times, and the confidence to carry on when I needed it most.

Chapter 1 Introduction

The electrochemical capacitor (EC), also called a supercapacitor and an ultracapacitor, is a charge-storage device. ECs are used for applications such as memory backup for electronic devices,[1, 2] and are of interest as systems for energy storage in emission-free vehicles.[1-5] Other charge-storage devices include batteries and fuel cells. Batteries and fuel cells are high energy devices, whereas capacitors are high power devices. ECs principally utilize an alignment of charge, called the double-layer, to store charge. This will be described in further detail in Section 2.1. Because charging and discharging in the double-layer involves a charge rearrangement, and not a chemical reaction, ECs charge and discharge quickly and this is what gives them high power.[1, 2] The redox reactions of batteries and fuel cells, on the other hand, provide high energy.[2]

The goal of this project is to observe surface changes on electrodes during electrochemical experiments; specifically, to characterize the electrode materials used for ECs in the Andreas lab at Dalhousie University. The method chosen to do this will ultimately be through spectroelectrochemistry: performing spectroscopy on electrodes during electrochemical experiments.

The first electrode material studied was carbon. Carbon is often used as an electrode material for ECs because it is inexpensive, has a high surface area available to store charge, and comes in many forms (e.g. fibres, powders, and nanotubes).[6] Carbon electrodes can exhibit pseudocapacitance, a capacitor-like redox reaction (explained in Section 2.1). The principle type of carbon used in this research is known to have pseudocapacitance caused by the formation of quinone reactions.[7-9] It is possible,

however, that there are other surface groups that can contribute to pseudocapacitance as well, but are not yet known on this carbon. The project to utilize spectroelectrochemistry was undertaken to observe whether surface groups can be formed by electrochemistry alone, and if so, at what conditions. Spectroelectrochemistry could also answer questions regarding whether surface groups are present but do not contribute to pseudocapacitance and so are undetectable by electrochemistry. Ideally, a way to form more surface groups contributing to pseudocapacitance at potentials different from the quinone will eventually be discovered. Electrochemistry itself can cause the quinone groups to develop, and so it is conceivable that this may cause other groups to form as well. Although the entire project encompasses spectroelectrochemistry, the focus of the carbon-related portion of this thesis was to initiate the spectroscopy area of the research.

Polymers are also used as electrodes for ECs, and spectroelectrochemistry has been used in polymer literature studies. Polyaniline and polypyrrole were chosen to be studied in this research because they are two of the most well-known polymers, and there is a significant amount of literature to compare to the observations made in this thesis. A copolymer of these has also been made before and has recently been suggested for use as electrodes in ECs specifically.[10] A spectroelectrochemical study had not yet been done during the formation of the copolymer, nor had the copolymer been made by electrochemical cycling. These two studies were consequently undertaken in this thesis, to determine whether the copolymer could be formed using electrochemical cycling, and to observe the electropolymerization of the copolymer using UV-Vis-NIR spectroscopy.

Background information on all topics relevant to this thesis is covered in Chapter 2. Chapter 3 describes the experimental procedures used for all research performed throughout this work. The initial steps of this project, including testing of different spectroscopic techniques to find a suitable one for the carbon electrodes studied, were covered in Chapter 4. A chemical technique, the Boehm titration, was also chosen to characterize the surface groups of the carbon under study. The methodology of the Boehm titration was standardized in Chapter 5, and the standardized procedure was applied to the examination of carbon samples Chapter 6. The results from the polymer electrode studies are chronicled in Chapter 7. Chapter 8 includes conclusions and future studies.

Chapter 2 Background

2.1 Electrochemistry

Electrochemistry is the study of reactions involving the transfer of electric charge between an electrode and a chemical species, as well as how the properties of the chemical species involved change with the charge transfer.[11] The build up of charge on an electrode/electrolyte interface is illustrated using the electrochemical double-layer model (Figure 1a). In the electrochemical double-layer, the electrode is charged, and this charge is balanced by ions in electrolyte, lining up along the surface of the electrode to balance the charge,[2, 11] and this can be modelled more simply using the parallel plate model (Figure 1b). The double-layer model is based on an electrostatic alignment of charge, with no electron transfer at the interface (no species oxidized or reduced).

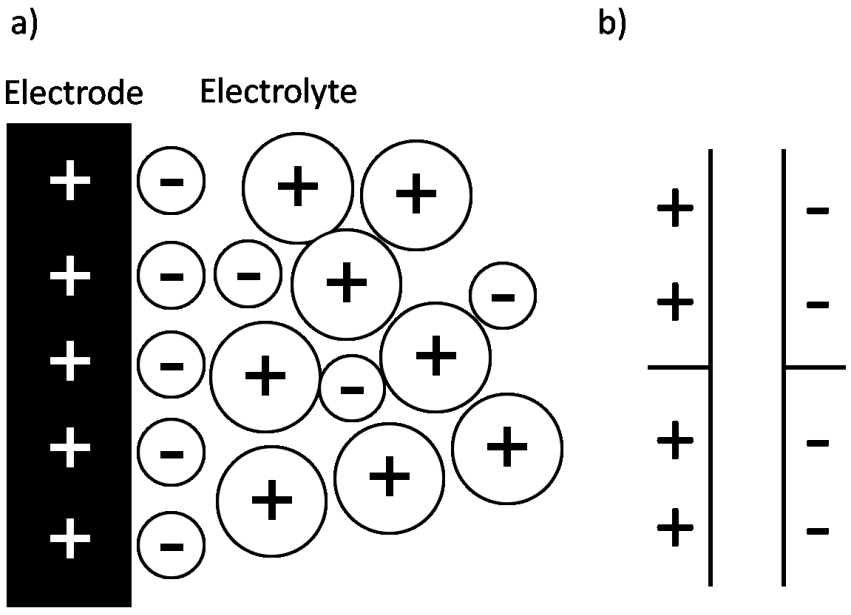

Figure 1. Charge build up modelled by a) the electrochemical double-layer model and b) the parallel plates model.

The ability to store charge for a certain voltage is called capacitance. It is defined by:[12]

$$C = \frac{dQ}{dV} = \frac{\varepsilon \varepsilon^{o} A}{d} \qquad (1)$$

where C is the capacitance, Q is charge, V is voltage, ε is the dielectric constant of the solvent in the double-layer, ε^{o} is the dielectric constant for a vacuum, and A is area of the electrode. d is the distance between the surface of the two layers of charge; between the plates in the parallel plate model, and in the double-layer model between the surface of the electrode and the ions aligned in the electrolyte.

The double-layer is not the only way in which to store charge; pseudocapacitance contributes to charge storage as well. Charge storage due to the double-layer is about 0.18 electrons per surface atom, as compared to 1-2 electrons per surface atom when pseudocapacitance is involved.[3] Pseudocapacitance is a phenomenon where a redox (oxidation or reduction) reaction with capacitive behaviour occurs on the electrode, in which the electron transfer is not the rate-limiting step.[5, 13] The advantage to pseudocapacitive ECs compared to traditional batteries is that pseudocapacitive processes are reversible,[5, 6] whereas many battery redox reactions are irreversible due to phase changes that occur with their charging and discharging processes,[4, 5] A capacitor with double-layer charge storage has a nearly constant capacitance (ability to store charge per potential) over its entire potential range, but systems with pseudocapacitive reactions have higher capacitance at potentials where the reactions occur. All systems have both the double-layer and pseudocapacitance, but their contribution to overall capacitance varies. Some systems, such as certain polymers[6] or RuO_x[13], exhibit mostly pseudocapacitance whereas other systems, such as

the carbon used in this research, store charge mostly through both the double-layer with some contribution from pseudocapacitance. The source of the pseudocapacitance in carbon will be discussed in Section 2.2.

There are three electrodes used in the electrochemical setup employed in this research: the working electrode, the reference electrode and the counter electrode. The working electrode is the electrode under study and the reference electrode is the electrode against which the potential is measured. In this research a Standard Hydrogen Electrode (SHE) was primarily used as the reference electrode, where the potential of its half-reaction is 0.000 V. The SHE consists of platinum black, 1 M H^+ and 1 atm H_2. The silver/silver chloride (Ag/AgCl) reference electrode was also used, which contains a silver wire coated with AgCl in a KCl solution and is capped at the bottom with a porous frit. It has a potential of +0.222 V vs. SHE when 1 M KCl is used. Current flows between the third electrode in the electrochemical setup, the counter electrode, and the working electrode.

Cyclic voltammetry is often used to study how current flows through an electrode upon application of a potential. In a cyclic voltammetry experiment, a potential (E) is applied to the electrode and varied at a constant sweep rate (v), and current (I) is measured. The resulting current vs. potential profile is called a cyclic voltammogram (CV). Sweeping from low to high potential can cause oxidation of the electrode, and the reverse can cause reduction. Features in the CV, such as peaks, are indicative of redox reactions occurring on the electrode surface.[11] To calculate capacitance from a CV at a given potential, the following equation is used:

$$C = \frac{I}{v} \tag{2}$$

A characteristic of capacitive and pseudocapacitive systems is reversibility, which can be observed in a CV based on its shape; a reversible CV is one that is a mirror image about the x-axis, and has vertical lines when the potential direction is switched.[3] Figure 2 is an example of a reversible CV.

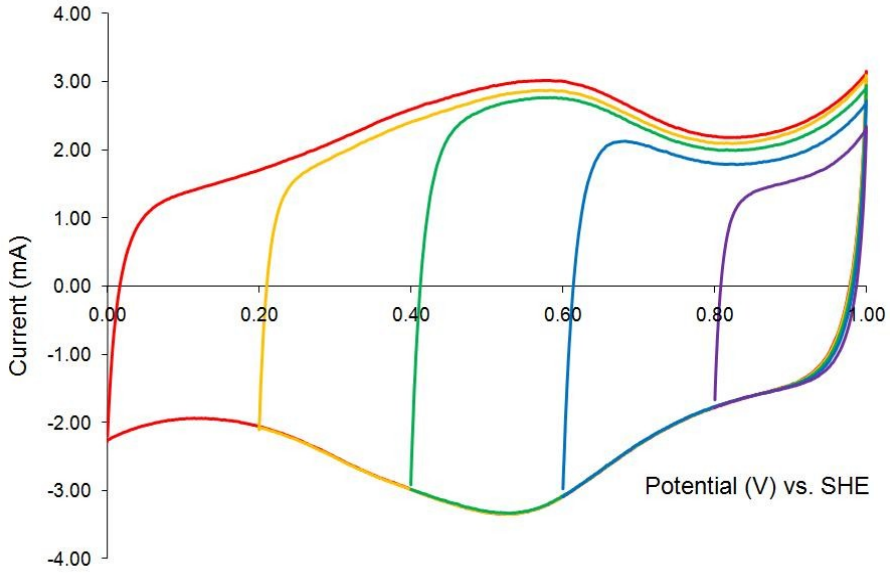

Figure 2. Reversible CV of a Spectracarb 2225 carbon cloth electrode, electrochemically cycled at 1.0 mV/s in 1.0 M H_2SO_4.

2.2 Carbon Surface Functionalities

Various factors affect performance of electrochemical capacitors employing carbon electrodes, particularly specific characteristics of the carbon itself. The distribution of heteroatoms, i.e. carbon surface functionalities (CSFs), is one factor that affects electrochemical capacitors; certain CSFs are responsible for the redox reactions leading to pseudocapacitance in carbon electrodes.[3, 14, 15] For example, carbons may have surface quinone groups which can be electrochemically reduced to hydroquinones

(Reaction 1),[7] resulting in a peak in the CV ca. 0.5 V vs. SHE[7-9] (Figure 2). Oxide functional groups present on carbon can cause the sample surface to exhibit Brønsted acidity or basicity, observed by neutralisation with base and acid respectively.[16] Examples of acidic and basic CSFs are shown in Figure 3. There is some debate over the identity of the basic groups, though the acidic groups on carbon surfaces are well-known.[16-21]

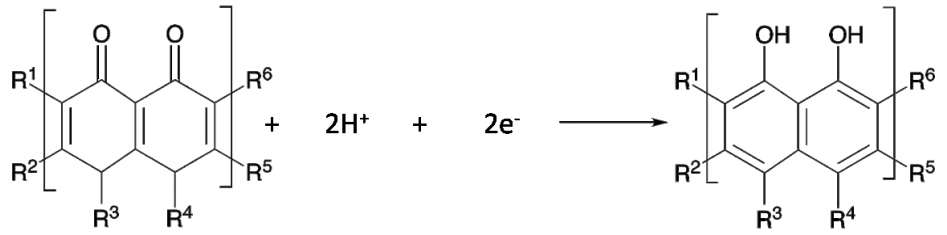

(R1)

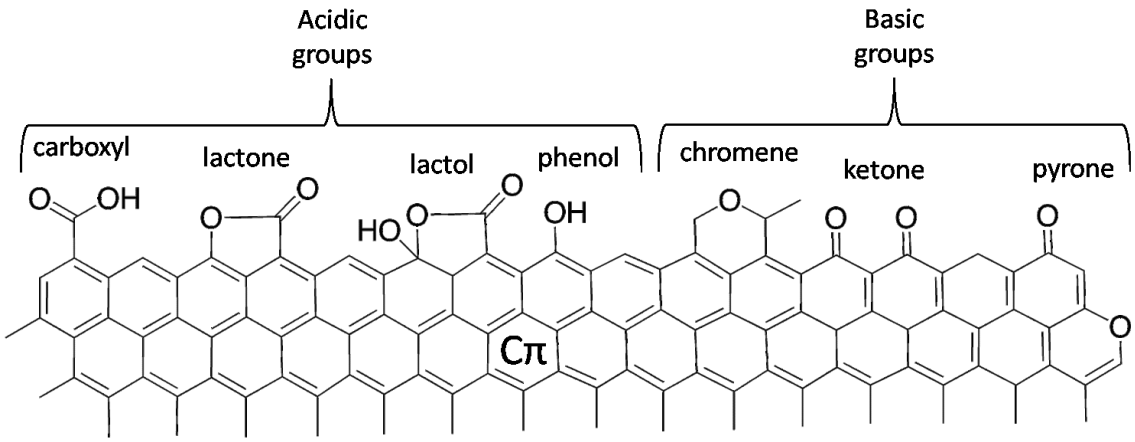

Figure 3. Possible acidic and basic carbon surface functionalities (modified from reference [21]).

Activation methods can be used to intentionally form surface groups on carbon to initiate pseudocapacitance. Carbon can be chemically treated, for example with nitric acid[22] or hydrogen peroxide,[23, 24] or it can be treated with ozone,[25] or with oxygen while heating.[14, 26] Electrochemical treatments can also be used to oxidize the surface of carbon electrodes through potentiostatic polarization in various electrolytes, for example NaOH,[27] $HClO_4$,[27] $NaNO_3$,[28] Na_2SO_4[28] and H_2SO_4.[27-29]

2.3 Spectroscopy

Spectroscopy is an instrumental technique that uses electromagnetic radiation and tracks changes in a sample as a function of frequency. The fundamentals of the spectroscopic techniques used in this thesis are outlined: Ultraviolet-Visible-Near-Infrared (UV-Vis-NIR) spectroscopy, Fourier Transform Infrared (FTIR) spectroscopy, X-ray Photoelectron Spectroscopy (XPS), X-ray Absorption Spectroscopy (XAS), and Photoacoustic Spectroscopy (PAS).

2.3.1 Ultraviolet-Visible-Near-Infrared Spectroscopy

Ultraviolet-Visible-Near-Infrared (UV-Vis-NIR) spectrometers are typically used in transmission mode, to measure liquids and gases; however, reflectance mode is also possible for the analysis of solids. In this research, both transmission and reflectance UV-Vis-NIR spectroscopy were used. The instrumental setups for transmission and reflection modes are shown in Figure 4a and Figure 4b respectively, and are based on the Cary 5000 UV-Vis-NIR Spectrophotometer by Varian, Inc. The extra mirrors and the integration sphere in Figure 4b are part of the diffuse reflectance

accessory, DRA 2500. The spectrum is displayed as absorbance, percent transmittance (%T) or percent reflectance vs. wavelength.

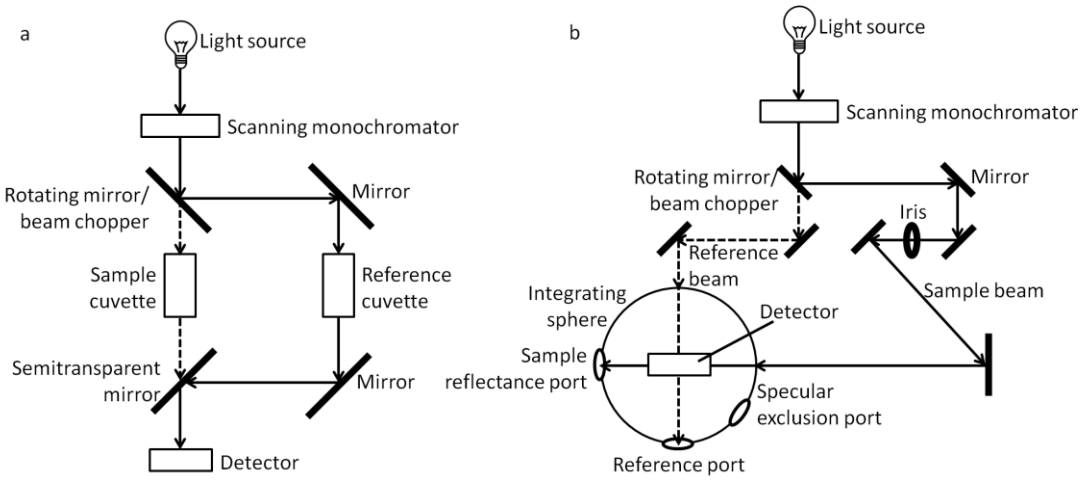

Figure 4. Instrumental setup of a UV-Vis-NIR spectrometer in a) transmission mode (modified from reference [30]) and b) reflectance mode (modified from the Cary 5000 Diffuse Reflectance Accessory (external) manual).

The integration sphere of the DRA 2500 accessory is designed to collect all scattered light and to direct it to the detector and therefore it is painted completely white on the inside using Spectralon, a highly-reflective thermoplastic resin, so that none of the light is absorbed by the sphere.[31] There are two types of reflected light off a sample: specular and diffuse. Specular is the reflection in which the angle of reflection is equal to the angle of the incident light about the normal, whereas diffuse reflection is the light that is scattered at all other angles by the sample. In this research, diffuse reflectance was studied.

2.3.2 Fourier Transform Infrared Spectroscopy

Used in this work are transmission Fourier Transform Infrared (FTIR) spectroscopy and Attenuated Total Reflectance Fourier Transform Infrared (ATR-FTIR) spectroscopy. ATR was initially called Internal Reflection Spectroscopy, and was developed by Harrick and coworkers.[32, 32-37] ATR works, as the name suggests, through reflectance, but differs from diffuse reflectance in which light hits the sample directly. In an ATR setup, the sample is held in contact with an internal reflection element (Figure 5), which is a crystal of a material such as germanium[38-40] or diamond (used in the present research). Radiation is propagated through this element, coming in contact with the sample while doing so to a sample depth a fraction of the incident light wavelength, on the order of micrometres.[32, 33, 33] The material of the internal reflection element is chosen so that its refractive index is higher than that of the sample, and the angle of incident light into the element is larger than the critical angle;[32, 33, 39] thus, the light is not lost to the sample, and the light reflected from the sample is directed from the crystal to the detector. The IR light excites the surface atoms and the spectra collected resemble those obtained in transmission FTIR.[32] The main advantage to ATR is the small amount of sample preparation. Liquid, solid or powder samples can all be used, and simply need to come into contact with the internal reflection element.[33] As in transmission FTIR, the instrument is a single-beam instrument, and background scans are collected to subtract the effect of atmospheric gas from the spectra.

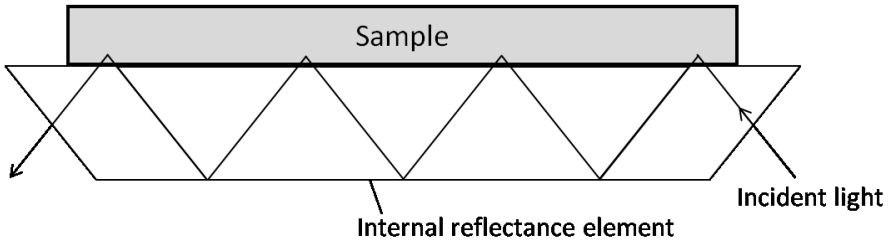

Figure 5. Total internal reflection at the interface of an ATR internal reflection element and a sample.

2.3.3 X-ray Photoelectron and X-ray Absorption Spectroscopy

X-rays can also be used to study surface composition of materials. In X-ray Photoelectron Spectroscopy (XPS), radiation is focused on the sample and causes a core level electron to be ejected from the sample surface as a photoelectron (see Figure 6). XPS usually requires ultra high vacuum conditions,[41] and for this reason solid samples are typically studied. The kinetic energy ($E_{kinetic}$) of the ejected electron is detected and converted to binding energy of the ejected electron ($E_{binding}$) for the spectra, which are plotted as the number of emitted electrons (which can be thought of as signal intensity) with respect to the binding energy:

$$E_{kinetic} = hv - E_{binding} - \varphi \quad (3)$$

where hv is the energy of the incident radiation and φ is the work function (the energy required to remove an electron from a sample into vacuum) that is associated with the particular sample.[42] Various x-ray sources can be used, for example Al Kα, Mg Kα or synchrotron radiation; Al Kα and synchrotron sources were both used in this research. Al Kα has a discreet line energy of 1486.6 eV and a line width of 0.85 eV,[42] and the resulting x-rays have a penetration depth of about 20 Å.[41] Conversely, synchrotron radiation is tunable, utilizing a monochromator to select an appropriate energy for a

particular sample. The excitation energy should be higher than the binding energies expected for the elements in the sample, so that the electrons can become excited enough to be ejected.

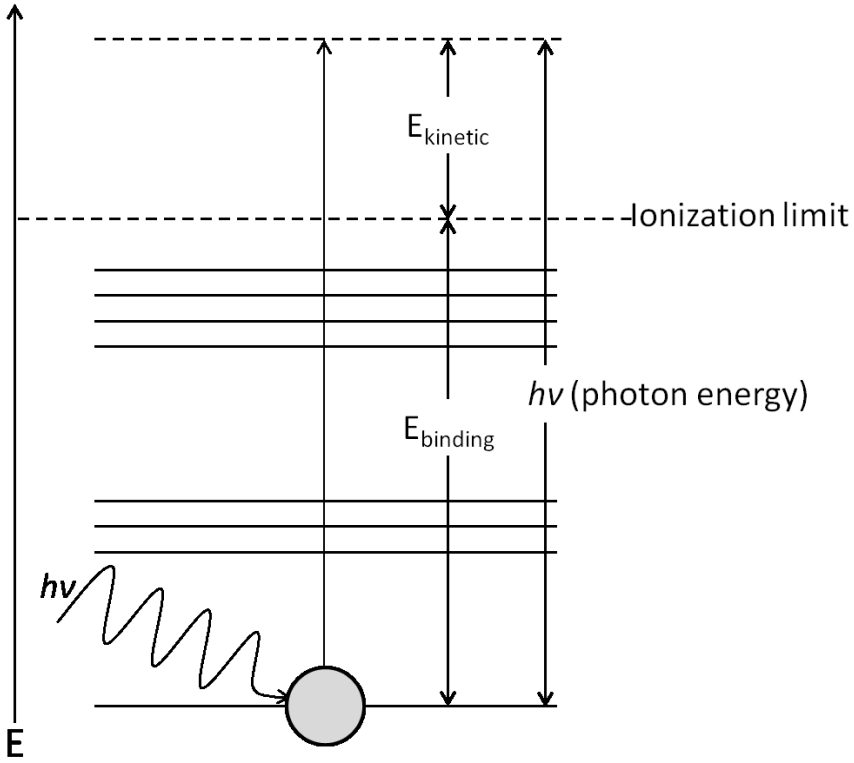

Figure 6. Principle of electron excitation (modified from reference [43]).

In an XPS spectrum, the binding energy location of a peak or group of peaks indicates the presence of a particular element, and these energies vary by atomic core level. For example, the carbon 1s peak is located around a binding energy of 285 eV, and the oxygen 1s peak around a binding energy of 535 eV.[44] These core level peaks are made up of smaller peaks; the chemical shifts of those peaks in terms of binding energy distance from the pure element indicate the chemical environments of that element in

the sample.[43] For example, a peak corresponding to an oxide group on carbon would have a specific chemical shift from the graphitic peak.

Depth profiling can also be achieved using the XPS technique, to determine whether species are only present on the surface or are present throughout the bulk of the material as well.[41, 45, 46] Depth profiling is most commonly performed destructively through ion etching, which is done using argon ion bombardment to sputter away the surface atoms of the sample so that underlying layers or bulk structure can be seen using typical XPS analysis.[44]

X-ray Absorption Spectroscopy (XAS) is similar to other absorption spectroscopy techniques, in that the radiation energy hitting the sample is scanned throughout a range, compared to XPS where the excitation energy is kept constant. In XAS, the incident x-ray energy is scanned and once the x-ray energy reaches a level high enough to excite core level electrons to an unoccupied molecular orbital, there is a sharp increase in intensity in the spectrum (plotted as intensity vs. photon energy), which in the spectra collected in this research is called the K-edge.[47] It is termed the K-edge as it refers to electrons in the K-shell of the atoms in the sample. The K-edge for carbon, for example, occurs around 285 eV. The region approximately 30 eV above the K-edge is termed Near Edge X-ray Absorption Fine Structure (NEXAFS). NEXAFS, used in this research, was designed to detect molecules, mainly those with low atomic numbers, bound to surfaces: hydrogen, carbon, oxygen, nitrogen and fluorine.[48]

Since XPS and XAS used in this research must be performed in a vacuum, they must be *ex situ* techniques, meaning that changes in a sample due to a specific experiment, for example electrochemistry, must be examined by comparing spectra of

the sample before and after the experiment, but not during. Oxygen-containing groups are particularly studied on electrodes, as oxygen is present in aqueous electrolytes and so could adsorb onto or react with the electrode surface.[41]

2.3.4 Photoacoustic Spectroscopy

The concept behind photoacoustic spectroscopy (PAS) was developed by Alexander Graham Bell; he discovered that a beam of chopped light being shone on a thin sample produces sound.[49] The acoustic signal is produced by infrared radiation coming into contact with the sample, which creates heat due to vibrational-thermal relaxation processes, which in turn cause the pressure of the gas in the photoacoustic cell to vary, resulting in the acoustic signal.[50] An acoustic detector such as a microphone or a piezoelectric device in the cell records the intensity of the acoustic response as a function of wavelength of the light. The spectra are obtained by taking the ratio of the generated signal to the signal from a strongly absorbing reference material, such as carbon black.[51] The spectra tend to correspond qualitatively with typical optical absorption spectra in terms of peak location with respect to wavenumber.[49]

The main advantage of PAS is that it can be performed on samples of any phase. The other benefits of PAS are that it is non-destructive and that scattered light is not an issue.[49] Additionally, there is very little sample preparation, and samples do not need to be ground or have a flat surface.[51] The signal to noise ratio is low,[51] however, which is a distinct disadvantage when trying to determine CSFs which are low in concentration, as in this thesis.

2.3.5 Spectroelectrochemistry

Spectroelectrochemical techniques are methods which combine spectroscopy with electrochemistry, to observe changes in species during electrochemistry *in situ*, i.e. performing electrochemistry in a spectrometer to collect spectra during electrochemical experiments. Several spectroscopic techniques have been realized *in situ* with electrochemistry, but the one most commonly used is the easiest to set up: UV-Vis-NIR spectroscopy.[52] Optically transparent electrodes (OTEs), such as mesh or minigrid electrodes,[52, 53] or conductive thin films on an optically transparent substrate (typically indium tin oxide (ITO)), are commonly used in spectroelectrochemistry,[54] and can be used in conventional spectrometer setups.

2.4 Polymer Electrodes

Polymers are commonly-used electrode materials for ECs. Polymers have attractive mechanical properties, and some of them are conductive and electroactive, or even pseudocapacitive. When a conducting polymer is oxidized, it is positively charged, and when it is reduced, it is negatively charged. During charging and discharging of a polymer electrode, couterions diffuse into and out of the polymer film to balance the charge.[55] Through this diffusion of ions into the polymer, charge builds throughout the entire volume of the electrode instead of being restricted to the electrode/electrolyte interface of carbon electrodes, and so higher energy densities can be attained than for carbon electrodes.[56, 57]

One of the polymers studied the most extensively in the literature is polyaniline (PANI), which is one of the electroactive polymers studied here. The structure of PANI

in its different forms is shown in Figure 7: the fully reduced form of PANI is leucoemeraldine, the partially oxidized form is emeraldine, and the fully oxidized form is pernigraniline. The CV of PANI has oxidation peaks at ca. 0.2 V due to the transformation of leucoemeraldine to emeraldine,[58-61] at ca. 0.5 V from the formation of degradation products,[58, 62, 63] and at ca. 0.8 V due to the transformation of emeraldine to pernigraniline,[58, 60, 61] all vs. Ag/AgCl (ca. 0.4 V, 0.7 V, 1.0 V vs. SHE). The degradation products may include quinones, which could form due to the presence of water, breaking up the PANI chain and replacing the nitrogen atoms with oxygen.[62] The CV shows reversible behaviour.[13]

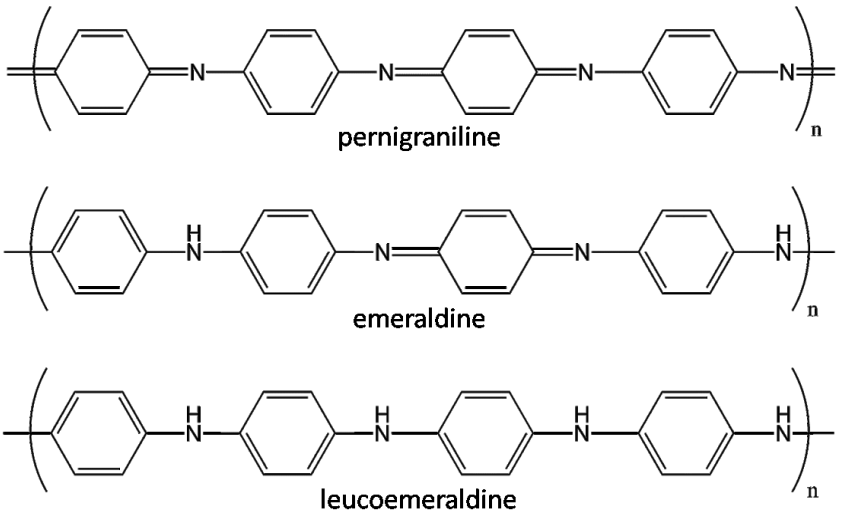

Figure 7. Chemical structures of polyaniline.

Polypyrrole (PPy) is also studied often in literature for its conductive properties. The PPy structure is shown in Figure 8. The reversibility of PPy is not as established in literature as PANI, and the reversibility seems to vary depending on conditions such as

potential window, sweep rate and electrolyte; literature studies discuss irreversible,[64, 64, 65] and reversible behaviour.[64-67]

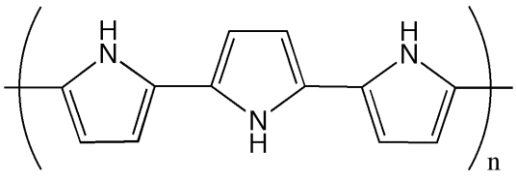

Figure 8. Chemical structure of polypyrrole.

Electrochemical polymerization, or electropolymerization, is most commonly carried out through anodic oxidation of monomers.[55, 56] The method used in this research for electrodeposition of polymers onto electrode substrates is cyclic voltammetry. In the cyclic voltammetric method, the increase in current in each cycle is a direct measure of the growth of a polymer.[55]

2.5 Literature Review

A review of the literature on the subjects covered in this thesis is summarized. The purpose of this review is to highlight previous studies on the topics researched, to compare with the discoveries made in this work.

2.5.1 Carbon Characterization

For many applications it is helpful or necessary to determine the identity of functional groups present on the carbon surface. The uses of carbon do not only include electrodes[41, 68] for devices such as ECs,[14, 28, 69-71] but also coal,[72] tires for vehicles, printer

ink, water purifiers,[73] etc. To resolve how to characterize the carbon in this thesis, a literature search was conducted of carbon studies in general and was not limited to carbon used as electrodes. Carbon has been characterized by a number of different techniques; see Table 1 for a summary of these, including techniques already described in this chapter in addition to Temperature Programmed Desorption (TPD) and Diffuse Reflectance Infrared Fourier Transform Spectroscopy (DRIFTS). TPD can be used to verify the presence of oxide groups; with heating, loss of mass can be attributed to the expulsion of CO or CO_2 groups, where CO can correspond to the desorption of quinones, hydroquinones, and phenols, and CO_2 can correspond to the desorption of carboxylic acids, carboxylic anhydrides and lactones.[74] DRIFTS works in the same way as UV-Vis-NIR diffuse reflectance spectroscopy, using IR radiation rather than UV-Vis-NIR light. It is common practice to use methods such as spectroscopic techniques to identify CSFs, though more than one characterization technique is often used to support deductions. The Boehm titration, for example, is often used to complement spectroscopic techniques,[18, 75, 76] as is TPD.[14, 25, 74, 77-80] The current section describes briefly some carbon characterization studies.

Table 1. Summary of techniques for CSF identification from literature.

Technique	Type	References
Boehm Titration	Chemical technique	16-18, 25, 69, 74, 75, 81-8574
TPD	Thermal technique	14, 25, 74, 77-80, 86
XPS	Spectroscopic technique using x-rays	14, 25, 68, 74, 76, 83, 87-89
Transmission FTIR	Spectroscopic technique using infrared radiation through transmission	8, 73, 74, 81-83, 90-97
ATR-FTIR	Spectroscopic technique using infrared radiation through total reflectance	38-40, 73, 87, 93, 98, 99
DRIFTS	Spectroscopic technique using infrared radiation through diffuse reflectance	73, 86, 100
PAS	Spectroscopic technique using infrared radiation through acoustics	73, 101-104
Cyclic Voltammetry	Electrochemical method	69, 76, 83, 96
UV-Vis-NIR	Spectroscopic technique using ultraviolet,	96, 105
Diffuse Reflectance	visible and near-infrared radiation through diffuse reflectance	96, 105

Examples of functional groups identified using FTIR techniques in the literature are summarized in Table 2. Although FTIR is widely used on carbon samples, there are problems associated with it when used in transmission mode. Carbon is strongly absorbing and is also prone to light scattering;[39] therefore the success of transmission FTIR is dependent on the type of carbon used [100] and the carbon sample needs to be ground very fine.[90] To avoid the scattering and absorbing issues, either DRIFTS[100] or ATR-FTIR[38, 39, 87, 93, 98, 99] can be used, which take advantage of the light scattering of carbon. PAS is not a commonly-used spectroscopic technique, but it has been used on carbon in some studies.[73, 101-104] Low et al., obtained PAS spectra containing peaks that occurred at the same wavenumber as in transmission FTIR.[102] Rockley et al. studied the surface of carbon black by comparing different FTIR spectroscopic methods: transmission, ATR, DRIFTS and PAS.[73] PAS had a different spectrum from the rest, though transmission, ATR and DRIFTS had similar spectra. The difference in the PAS

spectrum was attributed to the type of detector. The authors found that all the techniques aside from PAS have issues with reproducibility. It has been said that ATR is less sensitive than transmission FTIR.[91]

Table 2. Relevant carbon peaks in FTIR identified in literature.

Wavenumber (cm^{-1})	Assignment	Reference
3600-3200	O-H stretch (surface hydroxyl groups and chemisorbed water)	74, 83, 93, 95
3000-2800	C-H stretch (hydrocarbons)	74, 95
1775-1675	C=O stretch (carboxylic, ester, lactonic, anhydride groups)	83, 86, 106
1675-1550	C=O stretch (quinone, enol, cyclic β-ketones/ion-radical groups)	83, 86
1670-1500	C=C stretch	83, 86, 106
1600-1500	O-H bend	83
1560-1500	C=O stretch (conjugated systems: diketones, keto-esters, keto-enols)	83, 93
1580-1520	N-O asymmetric stretch	96
1490-1390	N-O symmetric stretch	96
1480-1340	O-H bend	81
1400-1000	C-O stretch (COOH or aromatic ether)	81, 83, 86, 92, 94, 106
1050-1000	Phenyl ring vibration	96
900-750	C-H out-of-plane bending (aromatic)	96

Characterization by XPS has often been used to study carbon samples subjected to chemical or electrochemical treatments. Examples of chemical shifts in XPS of carbon and oxygen found in literature studies are summarized in Table 3 and Table 4, respectively. XPS has been used to study different forms of carbon, including carbon fibres,[88, 89] glassy carbon,[68] and carbon powder.[83]

Table 3. Relevant XPS chemical shifts in the C 1s peak identified in literature.

Shift from graphitic peak (eV)	Assignment	Reference
-2	Carbidic carbon	[74]
0	C=C, C-H	[14, 74, 83, 88, 89]
1.6-2.0	C-OH, C-O-C≡, C-O-R	[14, 74, 83, 88]
2	C=O or quinone-type groups	[88, 89]
3-4	C=O	[14, 74, 83]
4-5	COOR	[14, 74, 83, 86, 88, 89]
6	π-π* shake-up satellite	[74, 83]
6-7.5	plasmon processes	[83, 88, 89]

Table 4. Relevant XPS binding energies in the O 1s peak identified in literature.

Binding Energy (eV)	Assignment	Reference
530-531.5	C=O	[74, 83, 88]
532.5-533.5	C-OH, C-O-C	[74, 83, 88]
534	COOH	[83]
535-536	Chemisorbed oxygen/water	[74, 83]

NEXAFS is rarely used to examine carbon, presumably because of the lack of availability of synchrotron radiation, and that adequate alternative techniques are readily available. It seems that when NEXAFS is used to study carbon it is not applied to simple carbon samples, but rather more complex samples such as carbon nanotubes[107, 108] or polymers.[109] Rarely are there examples of NEXAFS studies of graphitic-type carbons.[48, 110] Relevant assignments in carbon NEXAFS from literature are shown in Table 5, which are used to identify groups in XAS spectra in Section 4.3.2.

Table 5. Relevant chemical shifts in NEXAFS identified in literature.

Binding Energy (eV)	Assignment	Reference
284-285	$1s \rightarrow \pi^*_{C=C}$	[109, 111, 112]
287	$1s \rightarrow \pi^*_{C-OH}$	[111, 112]
287-288	$1s \rightarrow \pi^*_{C-H}$	[112]
288-289	$1s \rightarrow \pi^*_{C=O}$	[107, 109, 112]
285-290	$1s \rightarrow \pi^*_{C=C/C=O}$	[109]
290-291	$1s \rightarrow \sigma^*_{C-O}$	[107]
292-294, 302-304	$1s \rightarrow \sigma^*$(ring)	[107]

Others[69, 76, 83, 96] have used electrochemistry to study different forms of carbon. Hsieh and Teng oxidized carbon samples to determine how the degree of oxidation would affect the electrochemical double-layer of carbon fabric.[14] Through a combination of electrochemistry, TPD and XPS, they determined that the longer the oxidation time and the more the oxidation, the larger number of carbonyl or quinone groups were formed, which increased the capacitance through pseudocapacitance.[14]

Clearly, there are many chemical, spectroscopic and electrochemical techniques that have been used to characterize carbon samples. The purpose of the information presented here was to highlight the various possibilities of characterizing carbon samples and electrodes, which methods had potential to successfully yield information on the carbon samples studied in this thesis, and possible difficulties that could have arisen. In the future, the spectroscopic technique which worked best can be used to develop a spectroelectrochemical method to study changes in electrochemistry on the carbon cloth *in situ*.

2.5.2 Boehm Titration Methodology

The Boehm titration is frequently used as a chemical method to identify specific oxygen surface groups on carbon materials.[16-18, 20, 80, 84, 85, 113, 114] The principle of the Boehm titration is explained in the experimental chapter (Chapter 3.3) and in Chapter 5, in which the standardization of the method is described. Although the Boehm titration is widely used, explicit methodology has not been specified and certain titration steps vary between research groups. Reference is typically made to Boehm's papers[17, 18] but his procedure is often not followed precisely. The lack of standardization makes it

difficult to compare literature results. Some of the factors that vary are the ratio of carbon to reaction base, the length of time that samples are agitated, the method of CO_2 expulsion from the solutions, and the method of titration endpoint determination. Boehm suggests that at least 10% of reaction base should react with the carbon sample,[16] but this is not commonly referred to in literature. Agitation can come in the form of shaking,[113, 115-117] stirring[71, 118, 119] or sonication.[69, 120] CO_2 expulsion may be accomplished through boiling (or refluxing)[16-18, 20] or degassing with an inert gas during reaction and titration,[80, 121] conducting the titration in an inert atmosphere in a glove box,[114] or subtracting the value of a blank titration (no carbon) from the results.[114, 121] In terms of endpoint determination for the titrations, commonly used methods include colour indicators (such as phenolphthalein, methyl red and methylene blue), "one-point" pH measurements (where the titration is carried out until a pH value of "7" is reached) or potentiometric measurement throughout the titration for the production of a titration curve.

2.5.3 Pseudocapacitive Polymer Electrodes

There have been many studies done on various polymers for use in ECs. The focus here will be on polymers exclusively, though there have also been composites made of polymers with carbon, including carbon nanotubes,[6, 122-124] glassy carbon,[125] carbon powders[126-129] and even carbon fabric.[130, 131] These hybrid materials are designed to combine the different characteristics of each individual material, combining the high energy of a conducting polymer, with the stability and high power of the carbon

electrodes.[132] Many examples of copolymers exist as well; the focus here is the copolymer of polyaniline (PANI) with polypyrrole (PPy).

PANI can be formed chemically,[133-135] or by electrochemically depositing aniline onto a substrate potentiostatically[58, 133, 136, 137] or galvanostatically.[138] Spectroelectrochemistry of PANI has been conducted by depositing PANI on OTEs and utilizing UV-Vis spectroelectrochemistry,[136, 137] NIR spectroelectrochemistry,[61] or Electron Spin Resonance-UV-Vis spectrocyclovoltammetry.[139]

PPy can also be formed chemically,[64, 140, 141] galvanostatically[66, 137, 142-144] or potentiostatically.[136] OTEs were employed to study PPy with UV-Vis transmission spectroelectrochemistry,[67, 136, 137] UV-Vis reflection spectroelectrochemistry[66] and *in situ* Electron Paramagnetic Resonance/UV-Vis spectroelectrochemistry.[65]

The copolymer of PANI and PPy has been made potentiostatically by coating one polymer followed by the polymerization of the other and studied by FTIR spectra, thermogravimetric analysis, CVs, and scanning electron microscopy micrographs.[145] It has also been made through electrocopolymerization, i.e. electropolymerizing with both monomers simultaneously, either potentiostatically[146-148] or galvanostatically.[146] Spectroscopic methods were used for characterization in some cases,[147, 148] whereas cyclic voltammetry was used in other studies. It was often found based on these CVs that the properties of the copolymer were dependent on the ratio of the monomers.[146, 148, 149] Chemical polymerization was also used to form the copolymer of PANI and PPy,[150-155] characterized using FTIR and scanning electron microscopy.[151, 156] In one study the copolymer was made specifically for EC electrodes.[10, 152-154]

PANI, PPy and their copolymer have been polymerized in different ways, both chemically and electrochemically. Many of the studies utilize spectroscopy to characterize the resulting polymers, and although spectroelectrochemistry has been used to characterize the homopolymers of PANI and PPy, no studies have characterized the copolymer using spectroelectrochemistry. As part of this thesis, the copolymer was formed by electrochemical cycling – a method not seen in the referenced literature – and with spectroelectrochemistry.

Chapter 3 Experimental Methods

3.1 Electrochemistry

3.1.1 Carbon Electrodes for Spectroscopic Studies in UV-Vis-NIR and FTIR Spectroscopy

To identify CSFs on carbon electrodes using spectroscopy, different carbons were used as the working electrode in electrochemical treatments: Spectracarb 2225 carbon cloth (Engineered Fibers Tech., LLC), and graphite, mesoporous and glassy carbon powders (Sigma Aldrich). Carbon cloth electrodes were circular, 10 mm in diameter, with a mass of ca. 10 mg. These were held in a Teflon Swagelok tube fitting and were in electrical contact with platinum wire through a piece of platinum mesh as a current collector. A silicone gasket was used to keep the platinum mesh and the cloth in place. The platinum wire was connected to a nickel wire, enclosed in a glass tube. The glass tube was sealed with either beeswax or silicone to prevent electrolyte from leaking into the tube and corroding the nickel. Powders were also mounted in a Teflon Swagelok tube fitting and were in electrical contact with platinum wire, but platinum disks were used instead of mesh current collectors. Each powder electrode also had a barrier made of three layers of Kimwipes between the carbon and electrolyte to keep the powder contained in the Swagelok. Graphite and glassy carbon powder electrodes had masses of ca. 200 mg, whereas mesoporous carbon powder electrodes were ca. 90 mg. Counter electrodes were made from large pieces, ca. 7 × 4 cm, of Spectracarb 2225 carbon cloth with masses ca. 0.35 g, woven onto either platinum or gold wire.

Electrochemistry was performed on a Princeton Applied Research VMP3 multipotentiostat with EC-Lab software. The potential of the working electrodes were cycled between fixed limits (described below) with respect to a Standard Hydrogen

Electrode (SHE) at a sweep rate of 1.00 mV/s in a two- or three-compartment, three-electrode cell using carbon cloth as a counter electrode. This process will in future be denoted as electrochemical or potential cycling. The electrolyte solution was 1.0 M H_2SO_4 prepared from concentrated H_2SO_4 (Sigma Aldrich, 99.999% pure) and 18 MΩ water. Nitrogen was bubbled through the compartment(s) containing the counter and working electrodes to remove O_2 from electrolyte. Hydrogen was bubbled through the reference compartment, which was connected to the working electrode compartment by a Luggin capillary, to ensure that the reference electrode was at 1 atm H_2, a requirement for the SHE (to prevent its potential from shifting). All electrodes were cycled to steady-state, after which no more changes in size or shape in the cyclic voltammogram occurred. For Spectracarb 2225 carbon cloth, this took ca. 300 cycles from 0.00 to 1.00 V and back to 0.00 V vs. SHE. Hydrogen evolution occurs below 0.00 V, and above 1.00 V an irreversible oxidation reaction occurs on the carbon to destroy the electrode. The carbon powder electrodes for examination using spectroscopy were electrochemically cycled in different potential windows: graphite from 0.00 to 1.30 V for nine cycles, mesoporous carbon from 0.00 to 1.00 V for four cycles, and glassy carbon powder from 0.00 to 1.00 V vs. SHE for 14 cycles. The powder electrodes did not show changes after the first cycle, but were cycled the number of times listed to ensure that they were at steady-state. The upper potential limit of cycling was chosen based on the carbon, low enough that the electrode did not get destroyed due to a reaction similar to that in the carbon cloth. All experiments were performed at room temperature.

3.1.2 Carbon Electrodes for Spectroscopic Studies at the Canadian Light Source

Spectracarb 2225 carbon cloth, Black Pearls 2000 carbon powder (Cabot Corporation) and ELIT carbon powder (ELIT Co.) were all studied using X-ray Photoelectron Spectroscopy (XPS) and X-Ray Absorption Spectroscopy (XAS). Electrochemistry was done on a Princeton Applied Research VMP3 multipotentiostat with EC-Lab software. The samples run in XPS were Spectracarb 2225 cloth (ca. 10 mg): untreated cloth, cloth soaked in 1.0 M H_2SO_4 electrolyte, an electrode cycled between 0.00 and 1.00 V vs. SHE at 1.00 mV/s for two cycles, an electrode cycled for one day, an electrode cycled for two days, an electrode cycled for one week, and three electrodes each cycled for one week and removed from the electrochemical cell while holding at different potentials vs. SHE (0.00 V, 0.50 V and 1.00 V). In each case the electrolyte was 1.0 M H_2SO_4. Only the electrodes that had cycled for one week had reached steady-state.

The samples for XAS included the ones examined in XPS, as well as ELIT and Black Pearls 2000 carbon powders: ELIT powder untreated, soaked in 18 MΩ water for two weeks and an electrode (ca. 80 mg) electrochemically cycled between 0.00 and 1.00 V at 1.00 mV/s for three cycles; and Black Pearls 2000 untreated, soaked in 18 MΩ water for two weeks and an electrode (ca. 20 mg) cycled from 0.00 to 1.00 V at 1.00 mV/s for one day. Electrolyte was consistently 1.0 M H_2SO_4.

Three of the Spectracarb 2225 carbon cloth samples used in XPS and XAS were also examined using Photoacoustic Spectroscopy (PAS): untreated carbon cloth, the carbon cloth electrode that had been cycled for two days, and the electrode that had been cycled for one week.

3.1.3 Carbon Cloth Electrodes for Study in the Boehm Titration

Spectracarb 2225 carbon cloth working electrodes examined using the Boehm titration each had a mass of ca. 200 mg and were approximately 2 × 8 cm in size. These were too large to fit into a Swagelok tube fitting and were simply woven onto a platinum wire. Like the smaller carbon cloth electrodes, the platinum wire was connected to a nickel wire and enclosed in a glass tube sealed with either beeswax or silicone, to prevent corrosion of the nickel by electrolyte. The electrodes were electrochemically cycled from 0.00 to 1.00 V vs. SHE at 1.00 mV/s in 1.0 M H_2SO_4 for different lengths of time: one day, two days, four days, and one week. The instrument performing the cyclic voltammetry was either a Princeton Applied Research VMP3 multipotentiostat with EC-Lab software or a WaveNow USB potentiostat/galvanostat by Pine Research Instrumentation.

3.1.4 Polymer Electrodes

Polymer films were formed on metal electrodes using electropolymerization methods. Initial trials involved polymerizing polyaniline (PANI) onto a gold wire by electrodeposition, with the gold as a working electrode, a SHE as a reference and platinised platinum mesh as counter electrode in a three-compartment, three-electrode cell with 1.0 M H_2SO_4 electrolyte, ca. 100 mL. The gold wire was cleaned by cycling from -0.05 to 1.70 V vs. SHE at a sweep rate of 1000 mV/s for approximately five minutes in 1.0 M H_2SO_4. Following this, ca. 1 mL aniline monomer (Sigma-Aldrich, 99.5%) was injected into the electrolyte solution. Electrochemical cycling to polymerize the PANI was compared in two different potential windows: 0.00 to 1.50 V

and 0.00 to 1.30 V vs. SHE. In subsequent trials, PANI was polymerized from 0.00 to 1.30 V vs. SHE at 100 mV/s for 20 cycles. Reversibility of the film was then tested by using different potential windows, from 0.00 to 0.20 V, 0.00 to 0.30 V, 0.00 to 0.40 V, and so on, until the full window of 0.00 to 1.30 V vs. SHE was completed.

Further trials were performed in a smaller three-compartment, three-electrode cell, using ca. 10 mL electrolyte, composed of 1.0 M H_2SO_4 with 1.0 M KCl (Fisher Scientific, ACS reagent) as a supporting electrolyte. The reference was 1.0 M KCl Ag/AgCl, and the KCl in the electrolyte was present to ensure that the reference did not shift if the frit of the reference electrode compartment was leaky enough to have electrolyte seep into it. The potential of the Ag/AgCl reference electrode is +0.22 V vs. SHE. The counter electrode was platinized platinum mesh, ca. 5 × 15 mm. The monomers aniline and pyrrole (Sigma-Aldrich, 98%) were purified by running through an alumina column, composed of a Pasteur pipette packed with alumina powder. When not in use, aniline was stored in dark and pyrrole in a refrigerator. PANI and polypyrrole (PPy) were polymerized individually on a 5 × 5 mm platinum mesh working electrode (Sigma-Aldrich, 100 mesh, 99.9%) by adding 10 μL of the desired monomer (aniline or pyrrole) to the electrolyte (therefore ca. 0.01 M monomer concentration) and performing continuous cyclic voltammetry. PANI was cycled from -0.20 to 1.10 V vs. Ag/AgCl at 100 mV/s. It was cycled for 350 cycles to observe the change in CV shape with continuous electropolymerization. PPy was polymerized by cycling from -0.27 to either 1.48 V or to 1.10 V at 100 mV/s for 20 cycles.

PANI and PPy were polymerized together in a copolymer by adding various amounts of each of their respective monomers to the electrolyte and cycling, or by

polymerizing one after the other. Two trials of polymerizing ca. 0.01 M aniline with ca. 0.01 M pyrrole were done by electrochemically cycling together, one from -0.20 to 1.10 V and the other from -0.27 to 1.48 V vs. Ag/AgCl at 100 mV/s for 20 cycles. Electrocopolymerization was also done using 0.01 M aniline and 0.005 M pyrrole and cycling from -0.20 to 1.10 V vs. Ag/AgCl at 100 mV/s for 20 cycles. Other copolymerization strategies included polymerizing one polymer after the other. Aniline was polymerized by completing twenty cycles from -0.20 to 1.10 V followed by adding pyrrole and cycling 10-20 times, using ca. 0.005 M aniline and ca. 0.005 M pyrrole, or by cycling five times and using ca. 0.01 M aniline followed by 20 cycles using ca. 0.02 M pyrrole. The steps were then reversed, and copolymerization began with 0.005 M pyrrole being polymerized with 20 cycles followed by the addition of 0.005 M aniline and cycling from -0.20 to 1.10 V vs. Ag/AgCl. This last technique was done again polymerizing PPy in five cycles using 0.002 M pyrrole, followed by the addition of 0.01 M aniline and cycling for 20 cycles. In the cases where the initial polymer was cycled for five cycles, the electrochemical cell was cleaned out after the initial polymerization and before the addition of the second monomer to ensure that the polymerization of the initial polymer would not dominate the copolymerization. Subsequently the reversibility of the last copolymer, of polymerizing PANI after five cycles of PPy, was tested through different potential windows, from -0.20 to -0.10 V, -0.20 to 0.00 V and so on, until the full window of -0.20 to 1.10 V vs. Ag/AgCl at 100 mV/s was covered.

Between polymerization trials, the electrochemical cell was cleaned using concentrated H_2SO_4. The working electrode was cleaned by burning off the polymer using a propane flame, rinsing with concentrated H_2SO_4 and then sonicating in 18 MΩ

water for 5 min. The reference and counter electrodes were cleaned of possible monomer contamination by rinsing with acetone and 18 MΩ water. Prior to each polymerization, the Pt mesh was cleaned by cycling from -0.27 to 1.48 V vs. Ag/AgCl at 1000 mV/s for approximately five minutes (which corresponds to -0.05 to 1.70 V vs. SHE) followed by cycling at 100 mV/s for about two minutes to ensure that there was no polymer remaining from the previous polymerization trial. Spectroelectrochemistry was performed on polymer electrodes as well, outlined in Section 3.2.1.3.

3.2 Spectroscopy

3.2.1 Ultraviolet-Visible-Near-Infrared Spectroscopy

To study carbon surfaces using UV-Vis-NIR spectroscopy, the instrument used was a Cary 5000 UV-Vis-NIR Spectrophotometer by Varian, Inc. The software used was Cary WinUV: Varian UV Scan Application Version 3.00(339). The spectrophotometer is a double-beam instrument, with beams for reference and sample. The wavelength range is 175-3300 nm and measurements were taken every 1.0 nm for 0.1 s at a rate of 600 nm/min. A tungsten halogen source provides the visible range, and a deuterium arc lamp is used in the UV range. A R928 photomultiplier tube is used as detector in the UV-Vis range, and lead sulphide photocell is the detector in the NIR range. Transmission mode was used on samples in solution and for spectroelectrochemistry of polymers, and both transmission and reflectance techniques were used to examine solid carbon samples.

3.2.1.1 Transmission Spectroscopy

Carbon powders were examined by UV-Vis-NIR spectroscopy by enclosing them in clear tape. The samples were made by dusting just enough powder onto the tape to create a thin film visible to the naked eye. The absorbance range used for these measurements was 3300 to 175 nm, and a spectrum of tape containing no carbon was obtained and subtracted from the spectra of powders in the tape. The samples were held in a transmission cell called the Omni Cell (Specac Ltd.). The powders studied in this manner were graphite, mesoporous, glassy, as well as a graphite electrode that had been electrochemically cycled between 0.00 and 1.30 V vs. SHE at 1.00 mV/s in 1.0 M H_2SO_4 (see Section 3.1.1 for electrochemistry). The windows used were CaF_2 (transmission range 100-1000 nm). The Omni Cell is a demountable cell that is designed to create thin layers of liquids for spectra measured in transmission spectroscopy. A schematic of the Omni Cell is shown in Figure 9.

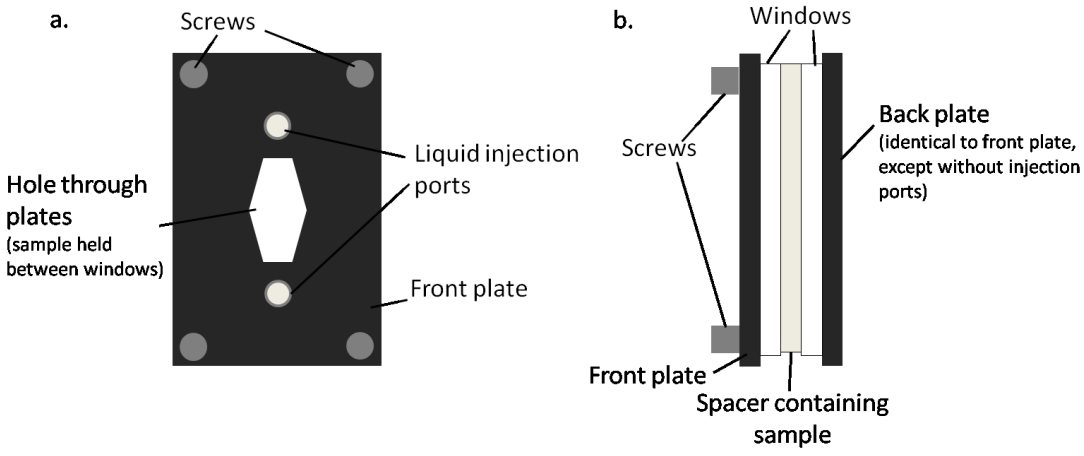

Figure 9. Schematic of Omni Cell: a. front view; and b. side view.

3.2.1.2 Diffuse Reflectance Spectroscopy

A diffuse reflectance accessory, DRA 2500, was used in the spectrophotometer to measure diffuse reflectance of carbon samples. Mirrors were aligned by hand using white light to adjust the location of the reference and the sample beams to ensure that they hit their respective targets. A small spot kit was used so that the sample beam had a diameter small enough to cover the small sample sizes used; due to the small masses of carbon required for electrodes, when packed in a powder cell (powder cell for external DRA, Varian, Inc.) they covered a spot approximately 5-10 mm in diameter. The key piece of the small spot kit is an iris, a hole through which the sample light beam passes. The diameter of the iris can be changed to decrease the spot size of the sample beam. Here the sample beam was reduced to a ca. 1 × 1 mm spot on the sample, whereas without the iris the spot is ca. 1 × 30 mm. Wire mesh was placed in front of the reference beam before it entered the integrating sphere to decrease the amount of light from the reference beam and therefore increase the signal-to-noise ratio; using the full reference beam, also approximately 1 × 30 mm, creates too much noise to obtain any usable spectra when the sample beam is reduced by the small spot kit.

The UV-Vis-NIR spectra of various carbon cloth and powder samples, held in a powder cell, were measured. Spectracarb 2225 cloth samples examined, each ca. 10 mg, included untreated cloth, cloth soaked in 18 MΩ water, soaked in 1.0 M H_2SO_4 electrolyte, and soaked in 1.0 M NaOH. The soaked samples were dried in an oven at ca. 80 °C for two days. The treatment of these samples was carried out by Bryanna Wood. Graphite, mesoporous carbon, and glassy carbon powders were all measured as well as electrode samples of each of these that had been electrochemically cycled at 1.00

mV/s in 1.0 M H_2SO_4; see Section 3.1.1 for electrochemical details. Each of these electrodes was rinsed with ca. 20 mL 18 MΩ water and dried in a desiccator for several days. Electrodes were prepared and electrochemical experiments were performed by Jennifer Black. Untreated ELIT carbon powder samples were also examined.

A zero/baseline correction was used; the so-called "zero" collected a spectrum when the sample beam was blocked, giving 0%T, and a Spectralon reflectance standard (Labsphere, Inc.) was used to collect a 100%T baseline. Diffuse reflectance data were collected from 2500 to 200 nm. In the near-IR region energy (the gain required to set the signal of the reference beam to an internal reference value) was fixed at 150.00, whereas in the UV-Vis region the spectral bandwidth was fixed at 4.00 nm; these two parameters gave the greatest signal-to-noise ratio.

3.2.1.3 Spectroelectrochemistry of Polymers

Polymers were also studied using transmission UV-Vis-NIR spectroscopy. For *in situ* measurements of the polymer electrodes, the spectroelectrochemical cell was a quartz cuvette with a 1-cm path length. The instruments used were a Varian Cary 5000 UV-Vis-NIR Spectrophotometer using Cary WinUV software (Scan and Kinetics programs), and a Model 1200A Electrochemical Analyzer from CH Instruments. The working electrode was Pt mesh, the reference electrode was a Ag/AgCl, and the counter electrode was a platinised Pt mesh; these are the same electrodes described in Section 3.1.4, with the exception that the working electrode was made up of two layers of 5 × 5 mm mesh behind each other in the light path, to allow for a larger polymer volume for the sample beam from the spectrometer to pass through. The electrolyte was 1.0 M

H_2SO_4 with 1.0 M KCl supporting electrolyte and also contained one of the monomers. The aniline-containing electrolyte was 0.1 M aniline, whereas the pyrrole electrolyte was 0.01 M. Polymerization was performed by electrochemically cycling from -0.20 to 1.10 V vs. Ag/AgCl (+0.22 V vs. SHE) at 100 mV/s, while UV-Vis-NIR scans were taken every few cycles, from 1500 to 200 nm. PANI and PPy were studied by spectroelectrochemistry, as well as the copolymer. The copolymer was made by polymerizing aniline after initial polymerization of PPy: PPy was formed on the working electrode by ten cycles of -0.20 to 1.10 V vs. Ag/AgCl at 100 mV/s in the electrolyte containing pyrrole, the cuvette was cleaned with concentrated H_2SO_4, the electrolyte was replaced with the aniline-containing electrolyte, and then polymerization was done by continuous electrochemical cycling using the same potential window and sweep rate. Additionally, spectroscopic scans were taken while "holding" polymers at various potentials, and the reverse was done as well, measuring absorbance at various discreet wavelengths while performing linear sweep voltammetry from -0.20 to 1.10 V vs. Ag/AgCl. This was done to determine whether the varying forms of the polymers at different potentials could be observed in UV-Vis-NIR spectra. Due to software limitations, the hold experiments were not true holds: linear sweep voltammetry was performed by ramping from the initial potential at 0.0001 V/s. At the end of the spectrum collection the change in potential was about 0.015 V. The holding potentials for PANI were -0.20, 0.00, 0.25, 0.50, 0.80, and 1.00 V, for PPy -0.20, 0.10, 0.40, 0.70, and 1.00 V, and for the copolymer -0.20, 0.00, 0.25, 0.45, 0.70, and 1.00 V vs. Ag/AgCl. These potentials were chosen so that they were relatively evenly spaced while taking enough spectra to get a clear idea of the trend with potential; fewer spectra

were collected for PPy as it cannot be seen to change colour visually and not much change in the spectra was expected. The held wavelengths varied depending on the features of the spectra so that peaks were measured, which on the PANI film were 240, 400, 590, 1150 and 1360 nm, for PPy were 200, 220, 300, 445, 700, 960, 1250 and 1400 nm, and for the copolymer were 217, 300, 450, 700, 1050 and 1366 nm. For all spectroscopic measurements, water was used as the baseline and electrolyte containing the appropriate monomer was the reference.

3.2.2 Fourier Transform Infrared Spectroscopy

3.2.2.1 Transmission Spectroscopy

The instrument used was a Perkin Elmer Spectrum 100 FTIR spectrometer with a mid-IR source and a $LiTaO_3$ detector. Powder samples such as graphite, mesoporous, glassy and ELIT carbons, both untreated samples and some that had been electrodes, were examined. The electrodes, the same used in Section 3.2.1.2, had previously been electrochemically cycled in 1.0 M H_2SO_4 at 1.00 mV/s. Graphite was cycled for nine cycles between 0.00 and 1.30 V, mesoporous carbon was cycled for four cycles between 0.00 and 1.00 V, and glassy carbon powder was cycled for 14 cycles between 0.00 and 1.00 V vs. SHE. The transmission spectra of H_2SO_4 electrolytes of different concentrations were also measured: 0.01 M, 0.1M and 1.0 M. Spectra of water were collected as well for comparison. Typically 4 scans were collected at a scan speed of 0.2 cm/s and a resolution of 4 cm^{-1}.

Two different windows were used in the sample holders: CsI windows (transmission range 200-40000 cm^{-1}) and CaF_2 (transmission range 1000-100000 cm^{-1}). The CsI windows were used only for carbon powder samples, by making a thin film, as

they dissolve in aqueous solution. The CaF_2 windows were used in the Omni Cell (see Figure 9) for the liquid samples. A Teflon spacer (0.05, 0.2 or 0.5 mm) was used in between the windows to contain the liquids.

3.2.2.2 Attenuated Total Reflectance Spectroscopy

Attenuated Total Reflectance (ATR)-FTIR was performed in the Faculty of Dentistry at Dalhousie University by Christopher Felix. A diamond internal reflection element was used. Nitrogen was pumped through the system to expel any water vapour present; the background was air. The resolution of collected scans was 4 cm^{-1} and 400 scans were collected for each sample.

Samples included Spectracarb 2225 carbon cloth, glassy carbon plate, as well as some carbon powders: graphite, mesoporous, glassy and ELIT. Samples of graphite, mesoporous and glassy powders that had been electrodes, the same used in UV-Vis-NIR (Section 3.2.1.2) and FTIR transmission (Section 3.2.2.1), were also examined, using their respective untreated samples as background spectra.

3.2.3 X-ray Spectroscopy

X-ray Photoelectron Spectroscopy (XPS) was carried out at two different locations: the Department of Physics at Dalhousie University, by Dr. Zeynel Bayindir and the Canadian Light Source (CLS) in Saskatoon, Saskatchewan (XPS and XAS spectra of the sample cycled for one week and removed from the electrochemical cell while holding at and 1.00 V vs. SHE were collected by Tom Regier later than the rest of

the samples, because of instrumental problems during the beam time allotted at the CLS).

At Dalhousie University several untreated carbon samples were measured: Spectracarb 2225 carbon cloth and Spectracarb 2050A carbon paper, glassy carbon plate, as well as ELIT, graphite, mesoporous and glassy carbon powders. The system used was a Thermo Scientific Multilab 3000 instrument (Thermo Fisher Scientific Inc.). Al Kα radiation was used (photon energy 1486.6 eV) with pass energy 50 eV. The analyzer was in a constant energy mode and the lens mode was 600 μm. Samples were measured under a vacuum level of 2×10^{-9} Torr. Depth profiling was also done here, by etching using argon ion bombardment to remove a layer of ca. 20 nm. An untreated carbon cloth sample and a carbon cloth electrode that had been electrochemically cycled for one week (0.00 to 1.00 V vs. SHE at 1.0 mV/s in 1.0 M H_2SO_4) were examined before and after etching. Analysis of spectra was done with Advantage Version 3.99 by Dr. Zeynel Bayindir.

XPS was also performed at the CLS at the High Resolution Spherical Grating Monochromator (SGM) Beamline, where the x-ray source was a 45 mm planar undulator, the spot size used was 1000 × 100 μm and resolution (E/ΔE) was greater than 5000.

For XPS, the samples run were Spectracarb 2225 cloth (see Section 3.1.2 for electrochemical details on electrodes): untreated cloth, cloth soaked in 1.0 M H_2SO_4 electrolyte, an electrode cycled for two cycles, an electrode cycled for one day, an electrode cycled for two days, an electrode cycled for one week, and three electrodes each cycled for one week and removed from the electrochemical cell while holding at

different potentials vs. SHE: 0.00 V, 0.50 V and 1.00 V. All samples with the exception of the untreated cloth were rinsed thoroughly with at least 100 mL of 18 MΩ water through a suction filtration system followed by soaking in 18 MΩ water for two weeks, followed by another round of rinsing. All samples were dried at ca. 80 ºC for 24 h in air with the exception of the sample that had been soaked in electrolyte followed by soaking in water, which was vacuum dried for 30 min. The one vacuum-dried sample was an experiment to test whether drying method affects surface chemistry. Unfortunately, due to time constraints at the CLS, the sample treated the same way but oven-dried was not examined. Samples were held in place on a copper sample holder by taping down the edges with carbon tape. A Scienta SES100 photoelectron spectrometer was used. The excitation energy was 700 eV and the exit slit was 50 μm. The vacuum level drawn for collection was 1×10^{-9} Torr. The oxygen peaks were scanned at a kinetic energy range of 150 to 170 eV in 100 meV steps; the carbon peaks were scanned from 400 to 414 eV in 50 meV steps; sulfur peaks, scanned to confirm that no residual electrolyte was present, were scanned from 500 to 550 eV in 500 meV steps. Peak fitting was done using Casa XPS Version 2.3.12. Normalization of peaks was done using WinXAS Version 3.11 for comparison of spectra.

X-ray Absorption Spectroscopy (XAS) was also performed at the CLS, at a different endstation also on the SGM Beamline, in the NEXAFS region. The samples examined included the same samples analyzed using XPS at the CLS, as well as six carbon powder samples of ELIT and Black Pearls 2000: ELIT powder untreated, soaked in 18 MΩ water for two weeks and an electrode electrochemically cycled for three cycles; and Black Pearls 2000 untreated, soaked in 18 MΩ water for two weeks and an

electrode cycled for one day (see Section 3.1.2 for electrochemical details). The electrodes were rinsed and soaked in 18 MΩ water and dried in the same manner as the samples for XPS. Cloth samples were held in place on a copper sample holder by taping down the edges with carbon tape. Powder samples were prepared by forming slurries with 18 MΩ water which were then dropped onto gold-plated metal squares adhered to the copper sample holder with carbon tape and left to air-dry for approximately 1 h. Carbon peaks for each sample were scanned with an energy range of 275 to 325 eV in 0.1 eV steps, and oxygen peaks from 520 to 580 eV in 0.25 eV steps. The exit slit height was 25 μm. The vacuum level drawn was 5×10^{-8} Torr. Total electron yield was measured by monitoring the drain current through the samples using a Keithley 6485 picoammeter. The spectra were normalized for comparison by setting the background at low energy to 0.0, and the background at high energy to 1.0.

3.2.4 Photoacoustic Spectroscopy

Photoacoustic spectroscopy (PAS) was performed at the Far-Infrared Beamline of the CLS by Dr. Brant Billinghurst. Three samples of Spectracarb 2225 cloth were analyzed using PAS: untreated cloth, an electrode that had been electrochemically cycled for one day in 1.0 M H_2SO_4, and an electrode that had been cycled for one week (three of the same electrodes used in Section 3.2.3). The buffer gas was helium; the window material and the beamsplitter were both KBr. The resolution of the scans was 4 cm^{-1} and 256 scans were collected.

3.3 Boehm Titration

3.3.1 Boehm Titration General Procedure for Identification of Acidic Carbon Surface Functionalities

The general titration procedure was carried out based on Boehm's method.[16] A known mass of carbon was added to 50.00 mL of one of three reaction bases of 0.05 M concentration: $NaHCO_3$ (Sigma, 99.5%), Na_2CO_3 (Anachemia, ACS Reagent) and NaOH (Sigma-Aldrich, 99.998%) in 18 MΩ water. The samples were agitated by shaking for 24 h and then filtered to remove the carbon, and 10.00-mL aliquots were taken by pipette from the samples. The aliquots of the reaction base $NaHCO_3$ were then acidified by the addition of 20.00 mL of 0.05 M HCl (Sigma Aldrich, 99.999% in 18 MΩ water). The aliquots of the reaction base Na_2CO_3 were acidified by the addition of 30.00 mL of 0.05 M HCl, to ensure complete neutralization of the base, which requires two protons, vs. the one proton required by the NaOH and $NaHCO_3$ reaction bases. The acidified solutions were then back-titrated with 0.05 M NaOH (titrator base), while being stirred with a magnetic stirrer. The aliquots of the NaOH reaction base were titrated using two different methods: 1) the aliquot was acidified by the addition of 20.00 mL of 0.05 M HCl and the sample was back-titrated with 0.05 M NaOH; or 2) the aliquot was titrated directly with 0.05 M HCl (titrator acid). The bases used in the titration that are intended to react with the acidic surface functionalities ($NaHCO_3$, Na_2CO_3 and NaOH) are denoted as reaction bases, and the base used for titration is denoted as the titrator base. The direct titration of NaOH with HCl is denoted as $NaOH^{direct}$. Basic groups were identified by performing the opposite: 50.00 mL of 0.05 M HCl was reacted with the carbon, 10.00-mL aliquots were basified with 20.00 mL of 0.05 M NaOH, and a back-titration was performed using standardized HCl. Fresh

solutions were used to limit the amount of CO_2 permeating through polyethylene storage bottles and dissolving into the reagents. In all cases, CO_2 was removed from solution immediately before the titration, using the various methods described below. All titrations were carried out at room temperature.

Blank samples, containing no carbon, were run with each reaction base to test the quality of various CO_2 removal techniques. Carbon samples of Black Pearls 2000 (Cabot Corporation) and Spectracarb 2225 carbon cloth, were also tested using the final standardized method. Black Pearls 2000 samples, ca. 1.5 g, were used to verify the standardized procedure, while Spectracarb 2225 samples were tested using ca. 0.8 g. Both untreated carbon cloth and carbon cloth electrodes were examined, and basic groups were measured on a sample that had been soaked in electrolyte for 24 h without performance of electrochemistry. The samples of cloth electrodes were made up of four electrodes of ca. 0.2 g each. The cloth electrodes were electrochemically cycled for different lengths of time: one day, two days, four days, and one week (see Section 3.1.3 for electrochemical details). Since it takes one week for Spectracarb 2225 electrodes to reach steady-state, shorter times were chosen to observe the development of or changes in CSFs up until the steady-state is reached. All of the carbon cloth electrodes, as well as the sample soaked in electrolyte without cycling, were rinsed with at least 200 mL of 18 MΩ water, soaked for one week in 18 MΩ water followed by rinsing, soaked for another week in 18 MΩ water, and finishing with a final round of rinsing with 18 MΩ water. This washing procedure was followed to ensure that no electrolyte was left in the samples, which, being acid, would affect the Boehm titration results. Samples were dried prior to the titration procedure at 100°C for 24 h in air. CO_2 was removed by

degassing for 2 h with N_2 bubbling. Potentiometric back-titrations were performed while continually degassing the titrands with N_2.

3.3.2 Endpoint Determination

To examine which method of endpoint determination was most precise and accurate, titrations were done using a pH electrode/meter and colour indicators separately and simultaneously. The potentiometric examinations were done as a "one-point" endpoint determination where the titration was carried out until a pH of 7.0 was measured, at which point the titration volume was noted. As well, full potentiometric titrations, i.e. titration curves, were carried out and the endpoint was determined either from inspection of the curve using an endpoint of pH 7.0 or from the first derivative of the pH-volume plot. The indicators used were methyl red (Fluka) and phenolphthalein. Methyl red was used in basic samples titrated with HCl, and phenolphthalein was used in acidic samples titrated with NaOH.

3.3.3 Standardization of Solutions

To ensure a correct NaOH concentration was used in the calculation of the CSFs, all NaOH solutions were standardized, since solid NaOH is hygroscopic and solutions made with NaOH pellets are less concentrated than what is first assumed. Dried (1 h at 100°C in air) potassium hydrogen phthalate (KHP) (Sigma Aldrich, 99.95%) (stored in a desiccator) was the primary standard used to standardize NaOH. A mass of ca. 0.2 g of KHP, measured to 0.01 mg, was used as the titrand in each titration and was dissolved in ca. 40 mL of 18 MΩ water, making a solution containing ca. 0.001 mol KHP. This

mass was chosen as it resulted in the amount of titrant used to be about 80% of the 25-mL burette, as is usually required in analytical titrations; therefore, ca. 20 mL of the 0.05 M NaOH solution (0.001 mol) was used to titrate the KHP solution. Since a titration curve showed that KHP is a weak acid, with an endpoint of ca. 8.6, phenolphthalein is a good choice of indicator. No more than 2 drops of phenolphthalein per 40 mL were added to avoid a bias. The standardized NaOH was then used as a titrant in the standardization titration of the HCl solution to an endpoint of pH 7.0, conducted using a pH electrode and meter. 20.00 mL of 0.05 M HCl was neutralized by ca. 20 mL of standardized NaOH.

3.3.4 CO_2 Expulsion Methods

To determine the best method of CO_2 expulsion, blank samples (i.e. no carbon present) were used in the titrations. This removes the variation that may arise due to differences in CSFs, carbon wettability or carbon provenance. In addition, the use of blanks makes the amount of base reacted (and therefore the amount of carbon surface functionality) expected to be zero. Consequently, a bias can be easily seen, when the amount of base reacted is not zero.

3.3.4.1 Degasification with N_2 or Ar

Studies on the effect of N_2 and Ar degasification (sparging) on CO_2 removal were conducted on blank solutions, where no carbon was used. Many of the titrations were carried out by Kim Thériault. These solutions were a mixture of 10.00 mL of reaction base and the appropriate volume of HCl to achieve the volume of a typical

Boehm titration aliquot (as per Section 3.3.1). Samples were contained in 40-mL glass vials utilizing polytetrafluoroethylene (PTFE)/silicone septum lids. The inert gas, either N_2 or Ar, was bubbled into the vial through a needle submerged in the solution, and another needle was positioned in the vial head space for use as an exhaust. Bubble size was ca. 1 mm in diameter. Bubbling rate was less than 1 mL/min; ca. 2-3 bubbles/s. Small bubbles were desired due to the high surface area to volume ratio.[157] The time of degasification was varied from 0 to 24 h, to test the minimum time required for CO_2 removal. The mass of the sample was taken before and after degasification to detect any mass change due to bubbling of the inert gas.

After degasification, the acidified aliquots were transferred to a beaker that had been purged with the inert gas and covered with Parafilm. This was done to prevent introduction of environmental CO_2 into the sample. Each sample was then titrated with 0.05 M NaOH (or HCl for the direct titration of NaOH). With some samples, the degasification was continued throughout the titration by bubbling the aliquot. During the titration, a seal of Parafilm was maintained around both the electrode and the burette tip. Each experiment was carried out in triplicate. The endpoint was determined using a pH meter (SympHony, VWR) with a posi-pHIo electrode (VWR).

3.3.4.2 Use of a N_2-filled Glove Box

Blank titrations, using blank, acidified aliquots of each reaction base (as in Section 3.3.4.1), were performed in a glove box filled with N_2, with and without degasification prior to titration, using potentiometric endpoint detection. When degasification was done, it was by bubbling the aliquot with N_2 for 1 h in the glove box.

Mass changes due to degasification were determined by taking the mass prior to and after degassing.

3.3.4.3 CO_2 Removal through Heating and Refluxing

To examine the effects of heat on CO_2 removal two methods were used, performed by Anthony Tarasuk. In the first method, blank aliquots were made in small sample vials for each reaction base and acidified (as in Section 3.3.4.1). The vials were sealed except for a needle passing through the septum in the vial lid to act as an exhaust. The samples were heated at 80 °C on a hot plate for 30 min, then sealed and left to cool to room temperature before titrating. Each of the three replicate samples was weighed before heating and after cooling to determine the mass loss due to evaporation.

In the second method, the sample preparation was carried out as above for heating, but the solutions were placed in 50-mL round bottom flasks. By employing a water-cooled condenser that was open to the atmosphere, the samples were refluxed using a hot water bath at 100 °C for 30 min and then sealed and left to cool to room temperature. The aliquots were weighed before heating and after cooling to determine the mass change, and again after being transferred to a small sealed beaker for titration. Three replicate samples were carried out for each reaction base.

There were also experiments done to test heating in open rather than closed vials. Firstly an acidified blank $NaHCO_3$ aliquot (10.00 mL of 0.05 M $NaHCO_3$ with 20.00 mL 0.05 M HCl) was heated in an open flask at ca. 80 °C for 2 h, left to cool to room temperature for a few hours while covered, and titrated with NaOH. Another acidified blank $NaHCO_3$ aliquot, 50.00 mL $NaHCO_3$ and 100.00 mL HCl, both 0.05 M, was

heated for 30 min at 80 °C. 10-mL aliquots from this solution were taken every 5 min, covered and left to cool for 1 h, and pH was measured to determine whether HCl was leaving solution during heating. Then was tested how both heating and degassing with N_2 would affect CO_2 removal. An acidified blank $NaHCO_3$ aliquot was heated in an open flask at ca. 80 °C for 15 min or for 30 min, covered and left to cool, followed by titration with NaOH. N_2 was bubbled through the aliquot solution during titration.

3.3.5 Calculations

The equations used to determine the quantity of carbon surface functionalities depends on the titration method: back-titration or direct titration. For a back-titration, amounts of the acidic groups on carbon were determined by:

$$[HCl]V_{HCl} = [NaOH]V_{NaOH} + \left(\frac{n_{HCl}}{n_B}[B]V_B - n_{CSF}\right)\frac{V_a}{V_B} \quad (4)$$

$$n_{CSF} = \frac{n_{HCl}}{n_B}[B]V_B - ([HCl]V_{HCl} - [NaOH]V_{NaOH})\frac{V_B}{V_a} \quad (5)$$

where $[B]$ and V_B are the concentration and volume of the reaction base mixed with the carbon, providing the number of moles of reaction base that was available to the carbon surface for reaction with the surface functionalities. n_{CSF} denotes the moles of CSFs on the surface of the carbon that reacted with the base during the mixing step. V_a is the volume of the aliquot taken from the V_B, and $[HCl]$ and V_{HCl} are the concentration and volume of the acid added to the aliquot taken from the original sample. This gives the number of moles of acid added to the aliquot, and available for reaction with the remaining reaction base. The remaining moles of acid are then determined through the titration using $[NaOH]$ and V_{NaOH}, the concentration and volume of the titrant in the back-titration. Thus, through the knowledge of the remaining moles of acid, leading to

the amount of reaction base remaining after reaction, and by difference (knowing the total amount of reaction base available initially) the amount of base reacted with the CSFs, the CSFs can be quantified. These equations are based on the calculations from Chen and Wu [23] but modified to take the molar ratio of acid to base $\left(\frac{n_{HCl}}{n_B}\right)$ into account to allow for monoprotic vs. diprotic reaction bases.

When NaOH is used in the Boehm titration and is directly titrated with HCl, the following equation is used:

$$n_{CSF} = [B]V_B - [HCl]V_{HCl}\frac{V_B}{V_a} \tag{6}$$

with a similar description of the reaction calculations as above.

For a back-titration using HCl, the following equation is used:

$$n_{CSF} = \frac{n_{NaOH}}{n_B}[A]V_A - ([NaOH]V_{NaOH} - [HCl]V_{HCl})\frac{V_A}{V_a} \tag{7}$$

where $[A]$ and V_A are the concentration and volume of the HCl reacted with basic groups on the carbon, V_a is the volume of the aliquot taken from the V_A, [NaOH] and V_{NaOH} are the concentration and volume of the base added to the aliquot, and $[HCl]$ and V_{HCl} are the concentration and volume of the titrant in the back-titration.

The quantity of the different possible surface groups are calculated through the difference in the calculated amount of surface functionality reacted (n_{CSF}). NaOH reacts with all acidic surface groups (carboxylic acids, lactones/lactols, phenols), and will therefore have a n_{CSF} that includes all of these groups. Na_2CO_3 reacts with carboxyl and lactonic groups and the difference between the n_{CSF} measured with NaOH and the n_{CSF} measured with Na_2CO_3 will denote the number of phenols on the surface. Similarly, since $NaHCO_3$ reacts only with carboxylic groups, the difference between Na_2CO_3 and

$NaHCO_3$ are the number of lactonic groups. The number of carboxylic acid groups are found directly from the $NaHCO_3$ reacted. HCl reacts with all basic surface groups. For blank solutions, without carbon, n_{CSF} should be equal to zero since there is no carbon present and therefore no carbon surface functionalities to react with the reaction base. For carbon samples, the n_{CSF} calculated is divided by mass to determine the amount of CSFs per gram of sample.

Chapter 4 Carbon Surface Functionalities Determined by Spectroscopy

The goal of this project was to examine CSFs on carbon electrodes using spectroscopy. Several different spectroscopic methods are available for use on surfaces, as discussed in Section 2.5.1. This chapter describes the studies undertaken to examine surfaces of carbon electrodes using different spectroscopy techniques.

4.1 UV-Vis-NIR Spectroscopy

Transmission mode and reflectance mode UV-Vis-NIR spectroscopy were used for the study of carbon samples. There was thought to be potential for reflectance spectroscopy to be employed for *in situ* electrochemical measurements on non-optically transparent carbon cloth electrodes.

4.1.1 Transmission Spectroscopy

Transmission measurements were performed on carbon powder samples enclosed in the Omni Cell as described in Section 3.2.1.1; spectra are shown in Figure 10. The samples examined were graphite, a graphite electrode (electrochemically cycled in 1.0 M H_2SO_4, see Section 3.1.1 for electrochemical details), mesoporous carbon powder and glassy carbon powder. The glitch at 800 nm is due to a change in detector, filter and grating in the instrument. All the spectra contain a peak at 200 nm, which could possibly be from a C-O or a C=O n-π^* transition, or an aromatic π-π^* transition[158] of the basal plane, and is strongest in mesoporous carbon. The peaks around 2300 and 2700 nm could be due to O-H vibrations from water,[158, 159] likely from

atmospheric water given the weakness of the peak in the spectra other than the graphite electrode, where the O-H could be from water adsorbed to the surface after rinsing the electrode. These assignments are assumptions based on liquid and gaseous samples; therefore, other techniques should be used in addition to support these results, as will be seen further in this chapter.

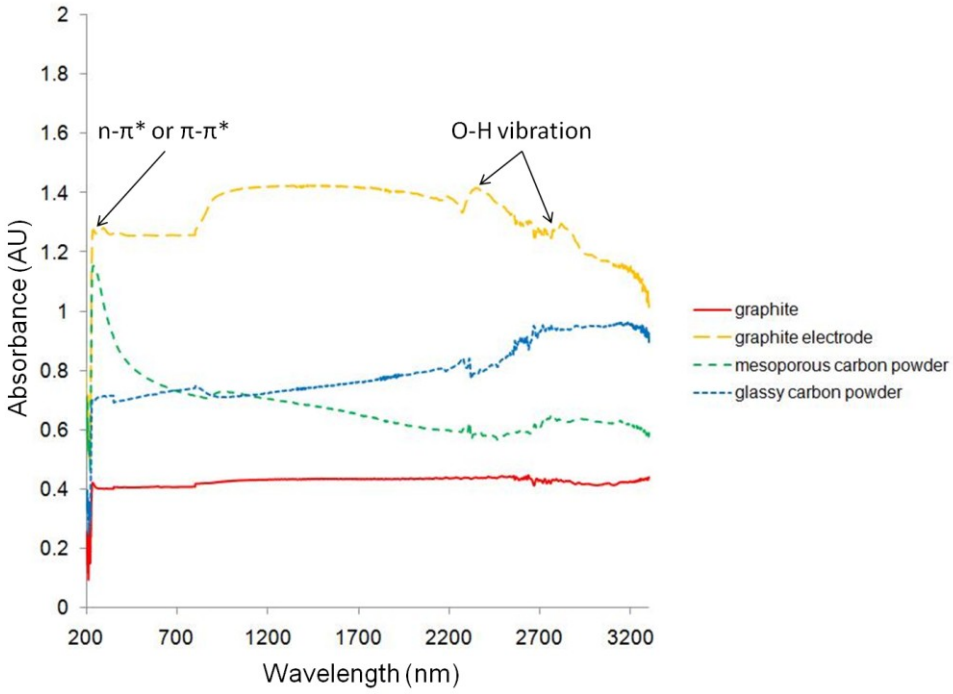

Figure 10. UV-Vis-NIR transmission spectra of carbon powders using the Omni Cell.

4.1.2 Diffuse Reflectance Spectroscopy

It was thought that an *in situ* spectroelectrochemical cell could be built for use in examining carbon electrodes in UV-Vis-NIR reflectance spectroscopy, so UV-Vis-NIR spectroscopy on carbon samples was attempted using reflectance mode. A powder cell was obtained and the reflectance measurements were collected on carbon powder and

cloth samples without electrolyte initially. A description of the setup and parameters of the instrument and of the samples is in Section 3.2.1.2. The carbon powders examined were graphite, glassy carbon, mesoporous carbon and ELIT carbon, spectra in Figure 11. Untreated samples of each of these were studied, as well as electrodes of graphite, glassy carbon powder and mesoporous carbon. The electrodes were cycled in 1.0 M H_2SO_4 at 1.0 mV/s (see Section 3.1.1 for electrochemical details). The four carbon cloth samples were: untreated, soaked in deionized water, soaked in 1.0 M H_2SO_4, and soaked in 1.0 M NaOH, spectra in Figure 12. The spectra were plotted in absorbance (converted from percent reflectance by the Cary software) so that peak location can be compared to other spectroscopic techniques using absorbance or %T (as is done with DRIFTS spectra of carbon samples[73, 86, 100]). All spectra are noisy in the NIR region. Energy of the reference beam relative to an internal reference can be varied in the NIR region to reduce the noise, and the spectra shown here gave the best result; since it continued to be noisy, the analysis of the spectra will exclude the NIR region. The spectra of the carbon powder samples, except for the ELIT powder, exhibit a very broad peak around 350 nm. Transitions in this region are typically n-π^*,[158] possibly from an oxygen-containing species. All except the mesoporous carbon powder have a peak around 200 nm, which could be due to carbon-oxygen bond transitions, or due to aromaticity of the basal plane.[158]

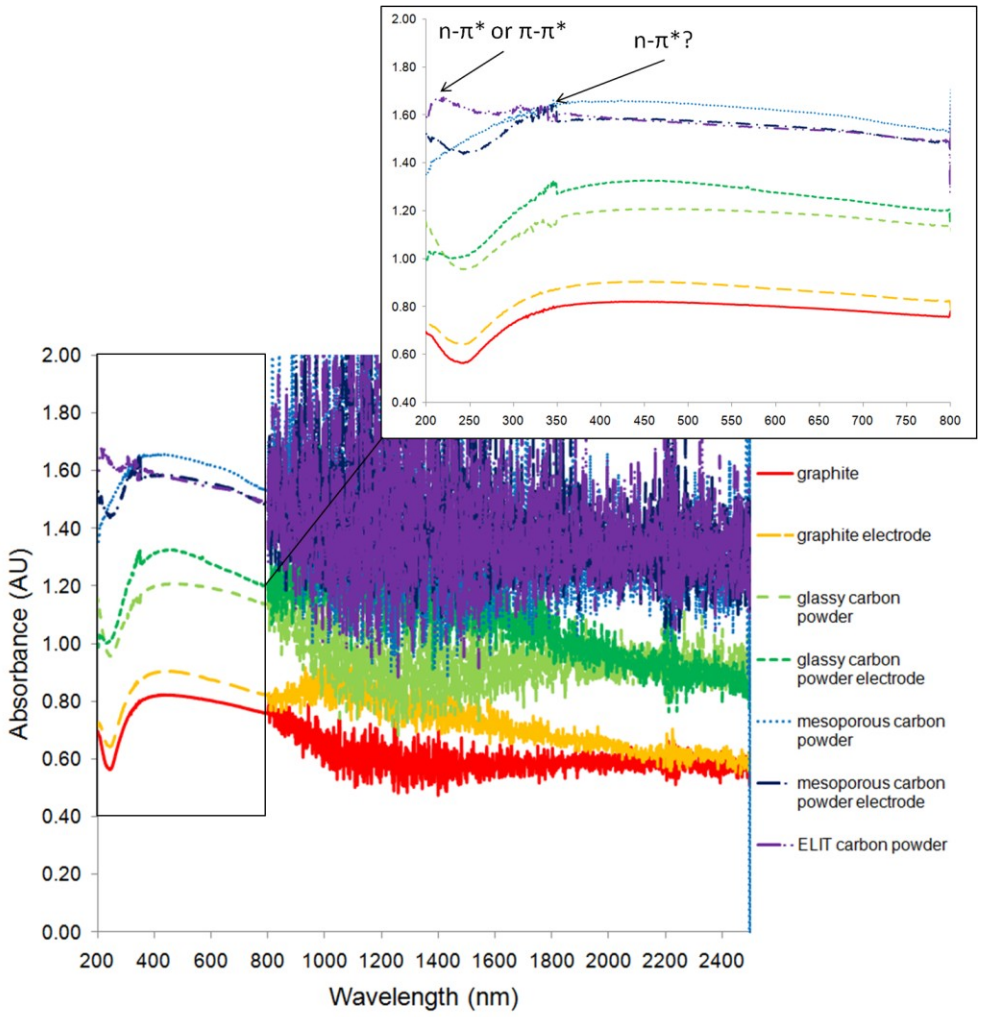

Figure 11. UV-Vis-NIR diffuse reflectance spectra of carbon powders.

The spectra for the cloth samples also exhibit the peak at 350 nm in all samples with the exception of the sample that had been soaked in 1.0 M NaOH. The untreated cloth and the sample that had been soaked in water have the peak at 200 nm, which is not present in the samples soaked in acid or base. Perhaps the acid and base destroyed the bond causing the peak at 200 nm, which may have been a carbon-oxygen bond.

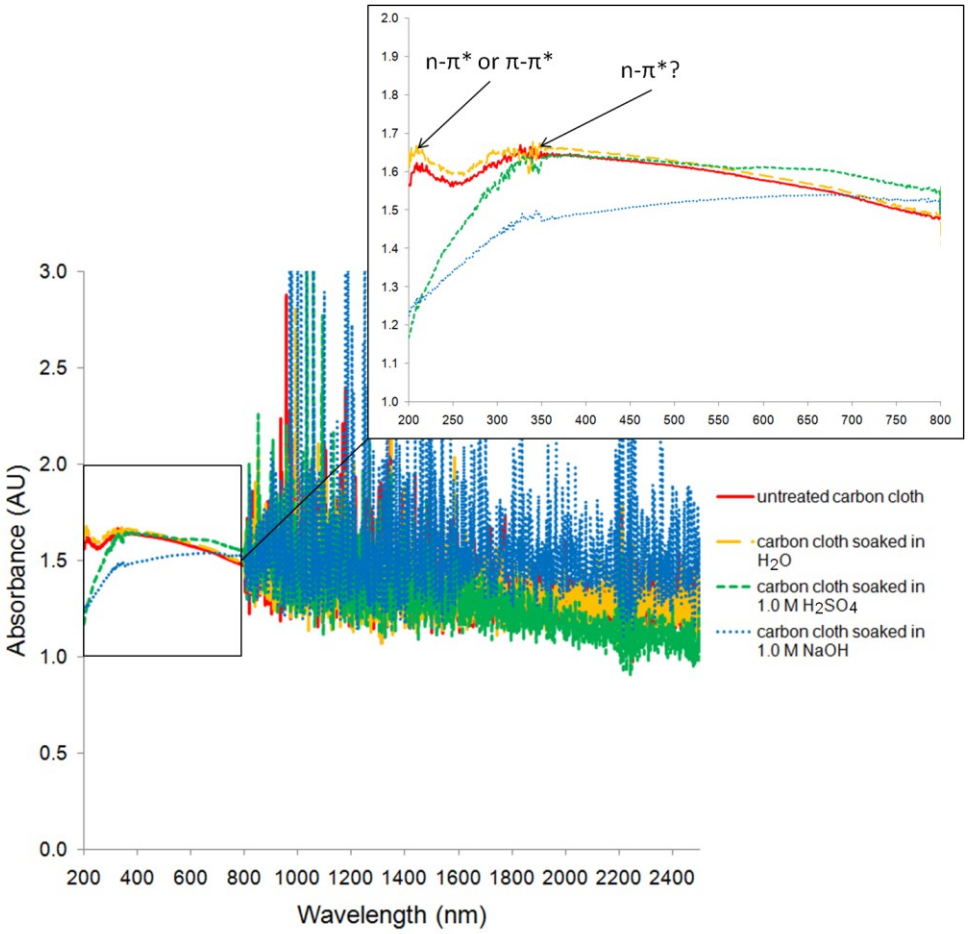

Figure 12. UV-Vis-NIR diffuse reflectance spectra of carbon cloth samples.

UV-Vis-NIR spectra in transmission and reflectance mode were both used to obtain spectra on solid carbon samples, but the resulting spectra did not provide concrete information on CSFs; as solid carbon samples are not typically studied using UV-Vis, the identities of the peaks in the spectra analyzed here were speculative based on liquid and gaseous samples. It is not surprising that distinct peaks corresponding to CSFs did not appear, however, as the expected CSFs on carbon solids (e.g. C=O, C-O, C-OH) absorb as well-defined peaks in the mid-IR range. Hence, this method was no longer

used to study CSFs on carbon electrodes and efforts to characterize the carbon were shifted to other spectroscopic techniques.

4.2 Fourier Transform Infrared Spectroscopy

Two different methods of FTIR spectroscopy were employed: transmission and ATR. The advantage to FTIR spectroscopy over UV-Vis-NIR spectroscopy described in the previous section is that expected CSFs absorb in the mid-IR range. The goal was to observe changes in these CSFs due to electrochemistry. Experimental details are in Section 3.2.2.

4.2.1 Transmission Spectroscopy

As was discussed in Section 2.5.1, carbon has often been characterized using transmission FTIR, though there are difficulties associated with it, such as the fact that carbon tends to scatter light. Despite the potential issues, transmission FTIR was used to try to identify CSFs on carbon powder samples. The objective was again to perform electrochemistry *in situ* with spectroscopy on carbon electrodes, but before that was attempted, carbon samples and electrolytes were tested separately to ensure that the FTIR spectroscopy would work in an *in situ* situation. This section describes the use of transmission FTIR, where only carbon powders were used.

The carbon samples examined were untreated and electrode samples of graphite, glassy carbon powder and mesoporous carbon powder, as well as an untreated sample of ELIT carbon powder. The samples were prepared by forming a thin powder film between CsI transmission plates. All the electrodes were electrochemically cycled in

1.0 M H_2SO_4, details in Section 3.1.1. The identities of the peaks discussed here are based on the peaks summarized from literature studies in Table 2 in Section 2.5.1, unless otherwise referenced. The resulting spectra from the untreated samples are shown in Figure 13. The spectra for these powders have very broad peaks of low percent transmittance (%T). The background level varies between samples because the thickness of the powder thin films is not reproducible, causing light to be transmitted through the samples to varying degrees. A peak due to –OH stretching, in the 3200 to 3600 cm^{-1} range, is detectable in all the spectra. While this peak could be due to a CSF, the possibility that it is due to adsorbed water from the atmosphere cannot be excluded, since the instrument was not purged with an inert gas. The spectrum for graphite has a peak at 2800 cm^{-1} from C-H stretching, a peak at 1400 cm^{-1} due to –OH bend, and at 1000 cm^{-1}, from a C-O stretch which could be from an ether group. Glassy carbon powder, aside from the –OH stretch, has barely-detectable peaks at 1600 and 1300 cm^{-1} in its spectrum. The 1600 cm^{-1} peak can be attributed to a C=O stretch, a C=C stretch or a –OH bend. Since C=O should be seen as a very strong, sharp peak,[160] it is more likely that the peak is due to the –OH bend or the C=C stretch. The peak at 1300 cm^{-1} could be due to a C-O stretch. The spectrum for mesoporous carbon powder has very broad regions of decreased %T, which could be due to an overlap of peaks such as –OH stretching, C-O stretching, C=C stretching, C-H stretching (2800 to 3000 cm^{-1}), etc. There was a slight fluctuation around 2300 cm^{-1}, which could be due to CO_2[161] either from the atmosphere or adsorbed onto the sample. The spectrum for ELIT carbon powder has again the –OH stretching peak, as well as the C-H stretching peak at 2900 cm^{-1}. There is also a peak at 2500 cm^{-1}, which could be from a triple bond or possibly a

nitrogen group,[160] a peak at 1600 cm^{-1} which could be from C=O stretching, C=C stretching or –OH bending, and peaks at 1200 and 1100 cm^{-1} which could be from C-O stretching. In all samples but the glassy carbon powder, there are some minor peaks in the wavelength region lower than 900 cm^{-1}, which represent C-H bending in aromatic compounds.

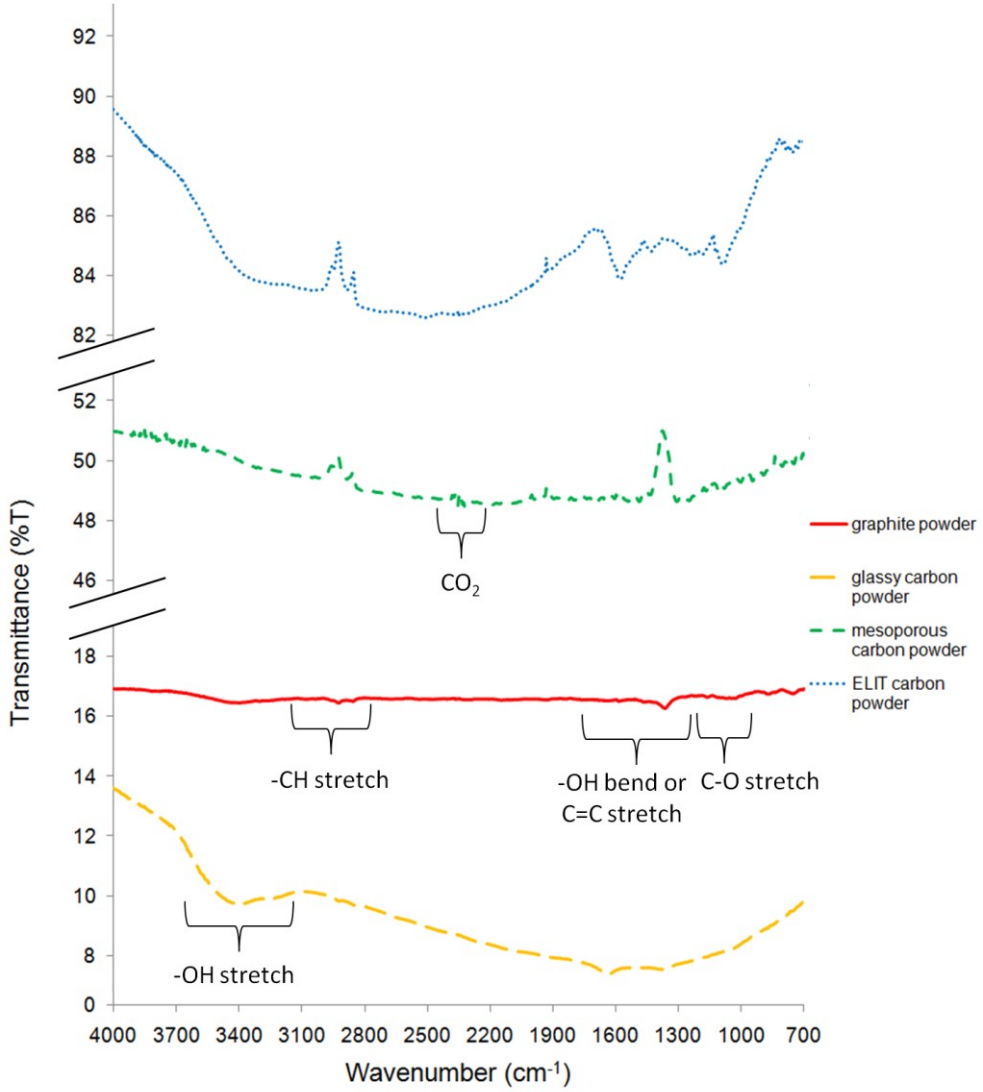

Figure 13. Transmission FTIR spectra of untreated carbon samples.

Figure 14 shows the transmission FTIR spectra for the powder electrodes of graphite, glassy carbon powder and mesoporous carbon powder. As with the untreated samples, the spectrum for each of these has the peak that represents –OH stretching. Each spectrum also has the small peak at 2300 cm^{-1} corresponding to CO_2. The graphite and glassy carbon powder electrodes have similar spectra with a small peak at 2900 cm^{-1} representing a C-H stretch, and small broad peaks in the range where C=C stretching occurs, 1700 to 1500 cm^{-1}. They also have small peaks where C-O stretching peaks occur, at wavelengths from 1400 to 1000 cm^{-1}. This region could also be exhibiting stretching peaks from S=O bonds,[160] due to residual electrolyte in the sample. The –OH stretching peak at 3400 cm^{-1} in the mesoporous carbon electrode spectrum is strong compared to the –OH peak in the other two spectra, suggesting a C-OH group rather than –OH adsorbed to the surface. This spectrum also exhibits peaks from 1300 to 1000 cm^{-1} which could again be for the C-O stretch due to ether, or from S=O stretching.

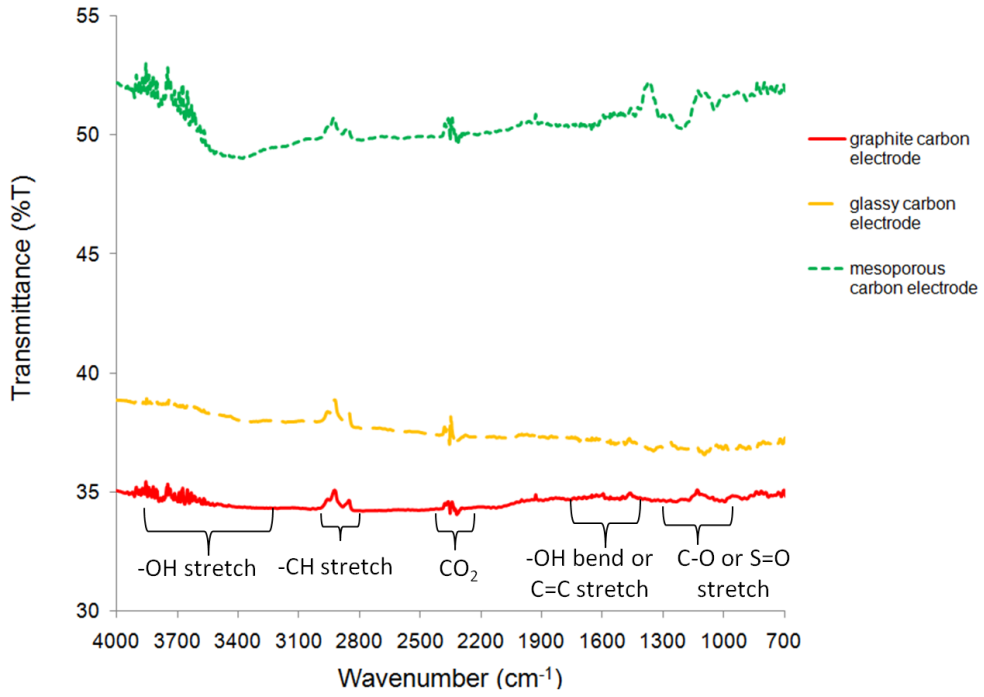

Figure 14. Transmission FTIR spectra of carbon powder electrodes.

Although surface groups could not be easily seen on carbon powders using FTIR spectroscopy due to small peak intensities, some CSFs can be suspected. Every spectrum contained peaks due to C-O stretching and –OH stretching, which could suggest CSFs such as ethers and phenols. The peak due to C=O stretching was only seen in spectra from untreated glassy carbon powder and ELIT carbon powders, suggesting a carbonyl group or quinone. It could also be part of a lactonic or a carboxylic group. Unfortunately, changes due to electrochemistry were not seen, either because there were no changes to be seen, or because changes in peaks in the spectra were too weak to be seen.

Testing of electrolyte was carried out as another step in developing spectroelectrochemistry in transmission FTIR spectroscopy. For the transmission FTIR spectroscopy method to be *in situ*, the thin-layer spectroscopy cell, the Omni Cell,

would be used containing both electrolyte and a carbon powder electrode. Therefore, electrolyte was tested in the Omni Cell to obtain a background for future spectra containing sample in electrolyte. All results shown in the current section are from samples contained in the Omni Cell using CaF_2 windows.

Issues arose in the collection of electrolyte spectra, in that the electrolyte solution in a 0.5-mm spacer absorbed too strongly for the instrument and the spectra went off scale, less than 0%T, which is seen in the spectrum of 1.0 M H_2SO_4, the electrolyte used throughout this research (Figure 15). Different sizes of spacers (0.2 and 0.05 mm) were used to try and shorten the pathlength of the sample beam through the sample, thus increasing the %T of the 1.0 M H_2SO_4 electrolyte, seen in Figure 15. Using the 0.05-mm spacer did increase the %T, but the largest peaks continued to go off-scale. The spectrum contains a broad peak from 3700 to 2600 cm^{-1} due to –OH stretching, a peak around 2200 cm^{-1} possibly due to CO_2,[161] around 1700-1600 cm^{-1} due to –OH bending, and from 1300 to 1000 cm^{-1} due to stretching of S=O bonds.[160] To try and increase the %T even further, a lower concentration, 0.1 M H_2SO_4, was used in the Omni Cell with the smallest, 0.05-mm spacer. This spectrum, in Figure 16, is not much improved over the spectrum of higher concentration. Spectra for an even lower concentration of electrolyte, 0.01 M H_2SO_4, was used as well, in 0.5- and 0.05-mm spacers, are also in Figure 16. Since again no significant improvement was seen at the lowest concentration, water itself was examined in the 0.5- and 0.05-mm spacers, shown in Figure 17. The spectra for 0.01 M electrolyte and water do not have the S=O stretching peaks, but the rest of the peaks are the same as at higher electrolyte concentrations.

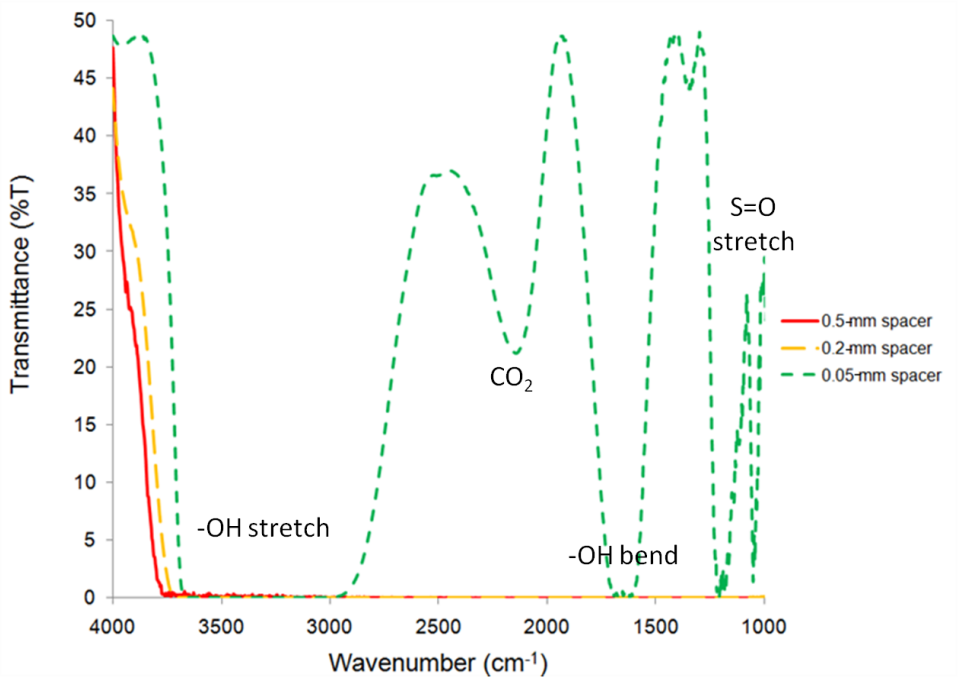

Figure 15. Transmission FTIR spectra of 1.0 M H_2SO_4 in different-sized spacers in the Omni Cell.

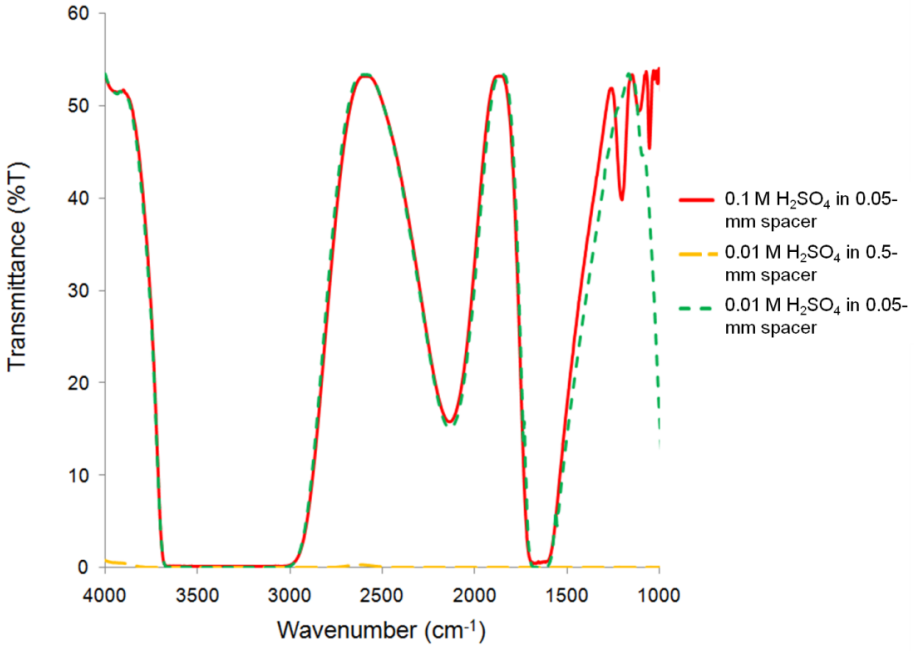

Figure 16. Transmission FTIR spectra of 0.1 M H_2SO_4 in a 0.05-mm spacer and 0.01 M H_2SO_4 in 0.5-mm and 0.05-mm spacers in the Omni Cell.

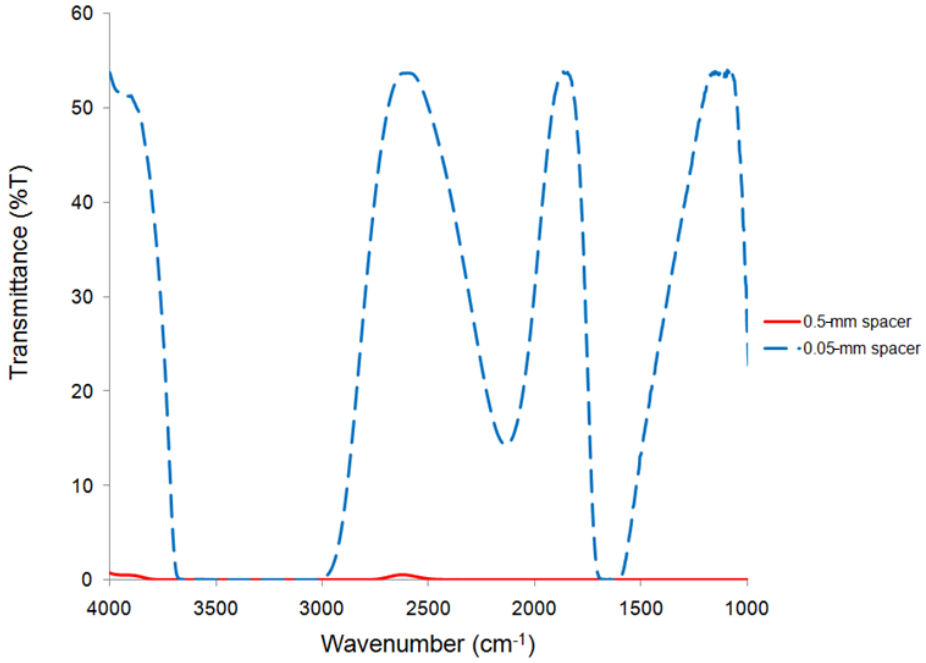

Figure 17. Transmission FTIR spectra of H_2O in different sized spacers in the Omni Cell.

Regardless of electrolyte concentration, the best spectra were obtained when using the smallest amount of solution, i.e. using the 0.05-mm spacer. It is possible to perform electrochemistry in an electrolyte volume as low as contained in the 0.05-mm spacer. However, if spectroelectrochemistry were to be done at this level, a spectroelectrochemical cell would have to be designed and built, as the Omni Cell in its current form cannot accommodate electrodes. Before spending the time to develop the cell, other types of spectroscopy were explored to ensure that the most appropriate spectroscopic technique to characterize the carbon cloth was being employed. Additionally, the peaks in the spectra of the electrolyte would prevent CSFs on carbon electrodes surfaces from being seen. For instance, the –OH stretching of the aqueous

solution would likely dominate over –OH from the carbon, –OH bending occurs in the same region as C=O, and S=O stretching peaks occur in the same region as the C-O stretch.

Thus far, FTIR spectroscopy has not been particularly enlightening on the subject of CSFs on carbon electrodes. Transmission spectroscopy yielded some information on possible oxides on carbon samples, but the peaks were very small and difficult to identify. The strong IR absorption of aqueous electrolyte prevented the development of a spectroelectrochemical method of observing changes in CSFs on carbon electrodes *in situ* during electrochemical experiments. Transmission FTIR spectroscopy was therefore abandoned for this project, but there is promise for future experiments if a non-aqueous electrolyte is used.

4.2.2 Attenuated Total Reflectance Spectroscopy

Attenuated Total Reflectance (ATR) cannot perform *in situ* electrochemistry coupled with spectroscopy for carbon electrodes; the sample light beam propagates through the reflection element and hits the sample, which is in direct contact with the element. If an electrochemical cell were to be coupled with ATR, electrolyte would be required between the electrode sample and the reflection element, causing electrolyte to be detected rather than the electrode. Nonetheless, ATR was employed to examine carbon samples and carbon electrodes, so that perhaps some information on the development of CSFs could be collected *ex situ*. ATR was thought to yield more informative spectra compared to transmission FTIR, as ATR is not affected by the

scattering nature of carbon. Additionally, carbon cloth and a glassy carbon plate could be examined through reflectance.

Spectra of untreated carbon samples of Spectracarb 2225 carbon cloth and glassy carbon plate are shown in Figure 18, and spectra of graphite, glassy carbon, mesoporous carbon and ELIT carbon powders are shown in Figure 19. Spectra were plotted as %T vs. wavenumbers to be comparable to transmission FTIR spectra. The spectra presented here tend to have sloping backgrounds. This is caused by the change in penetration depth of the incident light into the sample, which is inversely proportional to the wavenumber, resulting in smaller penetration depth and higher %T at high wavenumbers.[98] Peaks were identified based on peaks from literature in Table 2.

The spectrum from the carbon cloth (Figure 18) has peaks at 3300 cm^{-1} from –OH stretching and at 2700 cm^{-1} from the C-H stretch. Because the instrument was purged with nitrogen, it is likely that the –OH is not due to water from the atmosphere but is a CSF. There is also a peak at 2300 cm^{-1}, perhaps due to CO_2.[161] The spectrum from the glassy carbon plate also exhibits the –OH stretching peak around 3300 cm^{-1}. The peaks at 1100 and 900 cm^{-1} correspond to C-O stretching due to ether. The spectra of the untreated powder samples are in Figure 19. Each spectrum has the 2700 cm^{-1} peak due to C-H stretching, and a very slight peak at 2300 cm^{-1} from CO_2. The CO_2 could have been from adsorption onto the carbon surfaces from the atmosphere. There is a very broad, low-intensity peak around 3200 cm^{-1} in the spectra for graphite and for ELIT carbon powder corresponding to the –OH stretch. ELIT has additional peaks around 1600 cm^{-1} for the –OH bend or C=C stretch, and around 1000 cm^{-1} from C-O

stretching. These spectra, like the spectra from transmission FTIR spectroscopy, had peaks of very low intensity, making identification difficult.

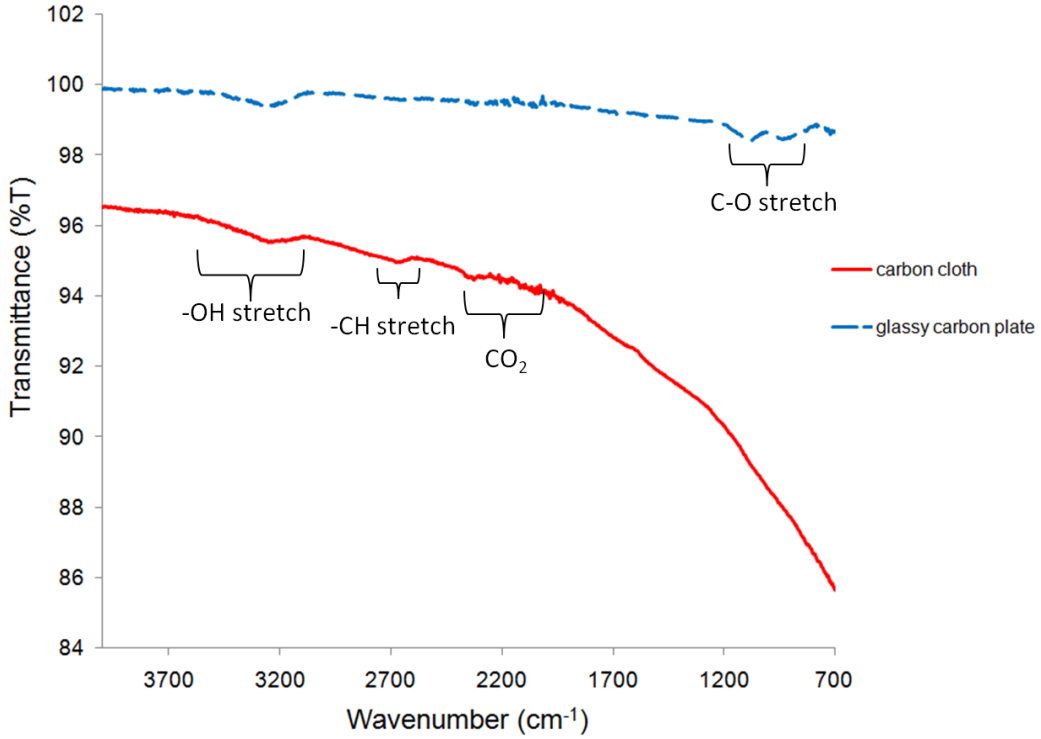

Figure 18. ATR spectrum of untreated carbon cloth and glassy carbon plate.

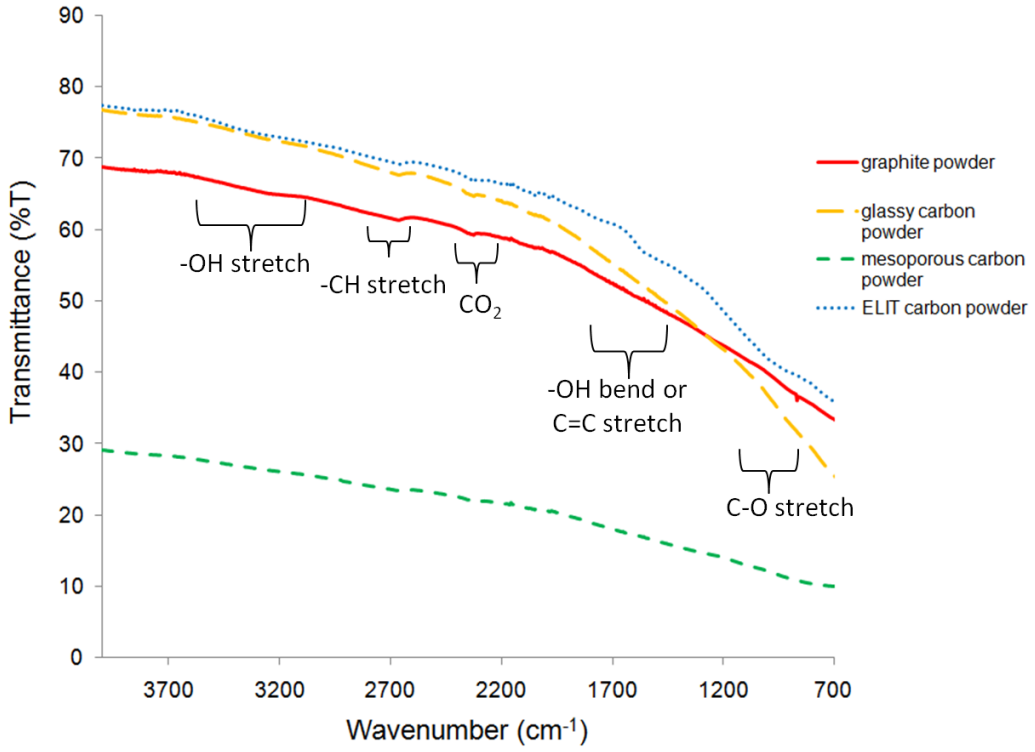

Figure 19. ATR spectra of untreated carbon powders.

Carbon electrodes were examined after their electrochemistry was completed (Section 3.1.1 for electrochemistry) to identify changes in CSFs using ATR spectroscopy. Spectra from electrode samples of graphite, glassy carbon powder and mesoporous carbon powder are shown in Figure 20. The background for each of these electrode spectra was the corresponding untreated sample. The spectra are similar to the spectra from electrolytes in transmission FTIR (Section 4.2.1), with peaks around 3400 cm^{-1} (–OH stretch), 1700 cm^{-1} (-OH bend), 1100 cm^{-1} (S=O stretch), and 1000 and 900 cm^{-1} (also S=O stretching vibrations).[160] This suggests that the peaks seen in the ATR spectra are due to residual electrolyte trapped in the samples, rather than due to functional groups on the carbon samples. If there are functional groups that formed with

electrochemical cycling, they are blended with the peaks from the electrolyte: the –OH bend and C=O stretch are at similar wavenumbers (1700 to 1500 cm^{-1}) as the S=O and C-O stretches (1400 to 1000 cm^{-1}).

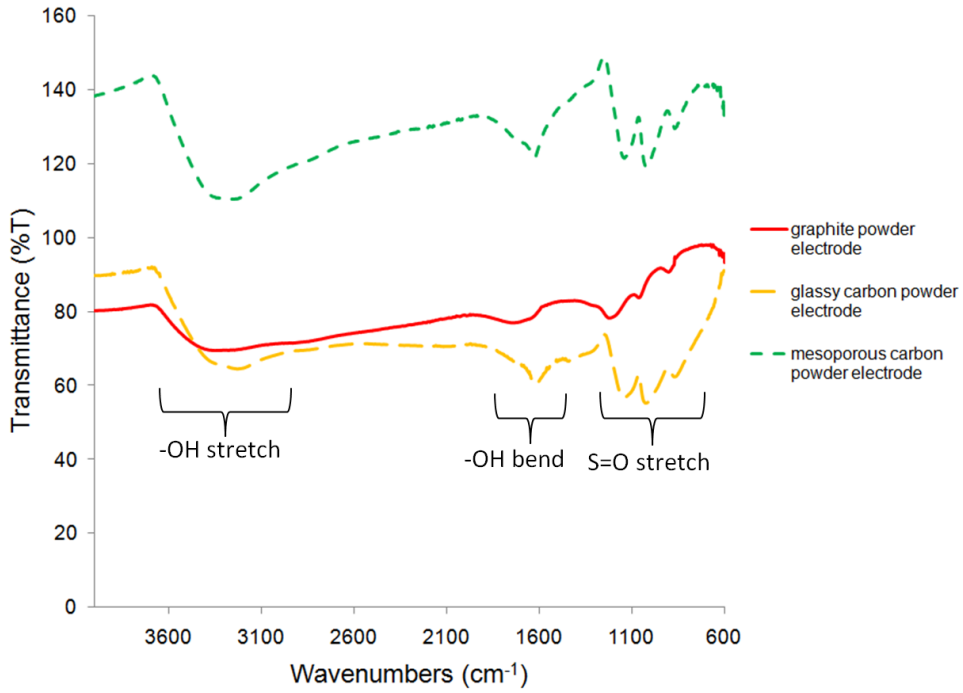

Figure 20. ATR spectra of carbon powder electrodes.

Overall, FTIR spectroscopy gave some insight on CSFs on carbon electrodes, in that many of them contain –OH and C-O groups, possibly from ether and phenols. However, differences between untreated and electrode samples were not positively identified. At this point, it was not possible to perform spectroelectrochemistry using FTIR spectroscopy.

4.3 X-ray Spectroscopy

X-ray spectroscopic techniques were performed both at Dalhousie University and at the Canadian Light Source (CLS). Since x-ray spectroscopy used in this research must be performed in a vacuum, electrochemistry cannot be performed in the instrument, thus eliminating the opportunity to accomplish *in situ* experiments on carbon electrodes with electrochemistry and x-ray spectroscopy. However, x-ray techniques are more sensitive than the techniques utilized in the previous sections, UV-Vis-NIR (Section 4.1) and FTIR spectroscopy (Section 4.2), and therefore more likely to identify CSFs on carbon samples *ex situ*. Both XPS and XAS were performed; experimental details in Section 3.2.3.

4.3.1 X-ray Photoelectron Spectroscopy

XPS at Dalhousie University was performed and analyzed by Dr. Zeynel Bayindir. Untreated samples of carbon cloth, glassy carbon plate, graphite, glassy carbon powder, mesoporous carbon powder and ELIT carbon powder were fitted with peaks of oxygen-containing CSFs as shown in A 1 to A 12 in Appendix A.1 (figures courtesy of Dr. Bayindir). The identity and percent by area of the peaks used to fit the spectra are summarized in Table 6 and Table 7 for the C1s spectrum and the O1s spectrum, respectively. The ELIT carbon powder had more complex spectra than the other samples and is summarized separately in Table 8. Each sample had a peak corresponding to the C-O-C,C-OH group, corresponding to ether or a phenol, both of which were also seen in FTIR spectra in Section 4.2.1 and 4.2.2. From the O1s peak, graphite and mesoporous carbon powder also had a C=O group. This was not seen in

FTIR; either the peak was not intense enough to be seen, or each particular sample has slightly different surface characteristics. All the samples except the mesoporous carbon powder had a peaks attributed to C-O-C=O, which could be from a lactonic group. ELIT carbon powder had multiple peaks for the C1s spectrum. The ELIT peaks at binding energies higher than 293 eV could be attributed to the presence of potassium. The spectrum for ELIT also contained the most features in the FTIR spectra, suggesting a complex surface structure.

Table 6. Percent by area of peaks fitting the C1s XPS spectra of various carbon samples.

	Peak Area (%)		
Sample	**C-C, C-H**	**C-O-C, C-OH**	**π-π***
Carbon cloth	53.80	36.30	9.90
Glassy carbon plate	62.60	33.40	0.00
Graphite powder	57.56	32.95	9.49
Glassy carbon powder	62.94	30.73	6.33
Mesoporous carbon powder	52.75	38.34	8.91

Table 7. Percent by area of peaks fitting the O1s XPS spectra of various carbon samples.

	Peak Area (%)		
Sample	**C=O**	**C-O-C, C-OH**	**C-O-C=O**
Carbon cloth	0.00	64.10	35.90
Glassy carbon plate	0.00	58.90	41.10
Graphite powder	39.38	43.82	16.80
Glassy carbon powder	0.00	81.68	18.32
Mesoporous carbon powder	64.07	35.93	0.00

Table 8. Peaks seen in fitting the XPS spectra of ELIT carbon powder.

Peak	Binding Energy (eV)	Peak Area (%)
C-C, C-H	285	69.1
C-O-C=O	286.76	15.9
O-C=O	288.75	9.2
π-π*	290.79	5.8
K 2p3/2	293.44	49.5
K 2p1/2	296.26	23.9
(unknown)	294.86	20.8
(unknown)	297.78	5.8
C-O-C=O	531.83	58.6
O-C=O	533.62	27.7
H_2O,O_{2ads}	534.97	13.7

Depth profiling of carbon cloth samples, one untreated and one electrode electrochemically cycled to steady-state, was carried out by etching. The atomic percents of carbon and oxygen before and after etching are shown in Table 9. In both cases, the atomic percent of carbon increased and oxygen decreased with etching, indicating that the oxide groups determined in the XPS spectra were principally surface groups and were not prominent in the bulk structure. Additionally, the atomic percent of oxygen is higher before etching in the electrode than the untreated sample, suggesting that electrochemical cycling does form oxygen-containing CSFs on the electrode.

Table 9. Depth profiling of untreated Spectracarb 2225 carbon cloth and a carbon cloth electrode.

	Atomic Percent (%)	
Sample (carbon cloth)	Carbon	Oxygen
Untreated carbon, before etching	91	9
Untreated carbon, after etching	97	3
Cycled to steady-state, before etching	84	16
Cycled to steady-state, after etching	98	2

XPS spectra were collected at the CLS on samples of Spectracarb 2225 carbon cloth treated in different ways. One sample was untreated, one was soaked in electrolyte without having electrochemistry performed on it, and the rest of the samples were electrodes which had undergone different electrochemical treatments. As mentioned in Section 3.1.1, carbon cloth electrodes reach steady-state after one week of electrochemical cycling from 0.0 to 1.0 V vs. SHE at 1.0 mV/s in 1.0 M H_2SO_4. During this cycling procedure, quinone groups are known to be formed; however, it is possible that different CSFs could be formed or changed during electrochemical cycling as well, and at different rates. Thus, samples cycled for different lengths of time were studied. Additionally, three of the electrode samples were cycled for one week and were removed from the electrochemical cell while holding at different potentials: ca. 0.0 V, 0.5 V and 1.0 V to compare CSFs present at different potentials.

Two different analyses were completed: spectra were normalized and sample spectra were directly compared between samples, and the spectra were fitted with peaks of oxygen-containing CSFs to determine relative amounts of CSFs in each sample.

The peak around a binding energy of 285 eV is the graphitic peak. The C1s spectra showing different potential cycling times were shifted and normalized in Figure 21 so that this peak, which appears in every carbon sample, is the same height and at the same binding energy, which allows for a visual comparison of the samples. The peaks at higher binding energies than 285 eV are due to carbon-oxygen bonds. The peaks in this region are highest in intensity in the sample that was soaked in electrolyte and the sample that was cycled the longest, to steady-state. It seems based on this that exposure to electrolyte for one week, from either simply soaking in electrolyte or from potential

cycling increases the amount of CSFs formed on the surface of the carbon. A comparison of the electrodes cycled for one week and removed at different potentials is shown in Figure 22. The trend in this plot shows increasing oxide groups with increasing potential; however, the electrode that was not held at a particular potential when removed had the highest intensity of oxide groups. More in-depth analysis of the peaks in the spectra is discussed below.

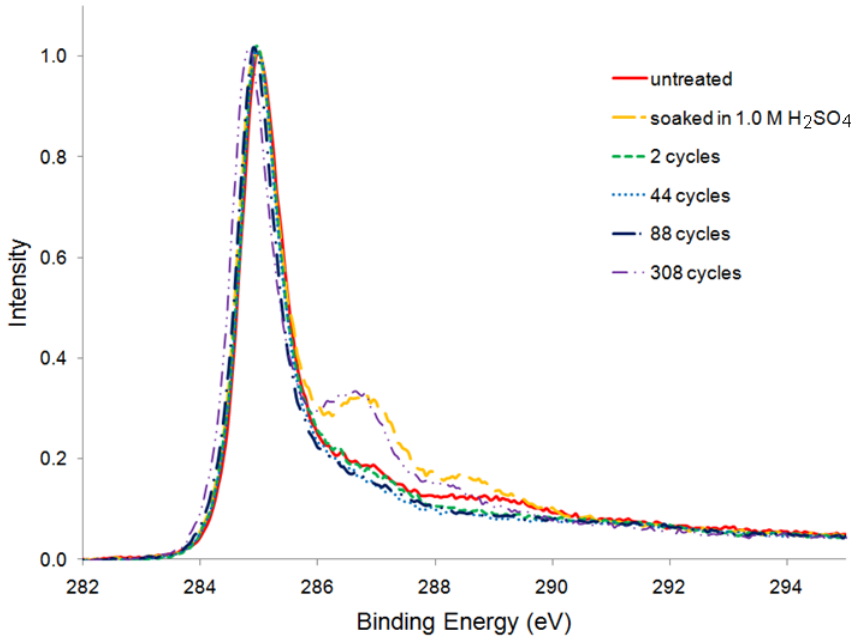

Figure 21. Normalized XPS C1s spectra of Spectracarb 2225 carbon cloth electrochemically cycled for different lengths of time.

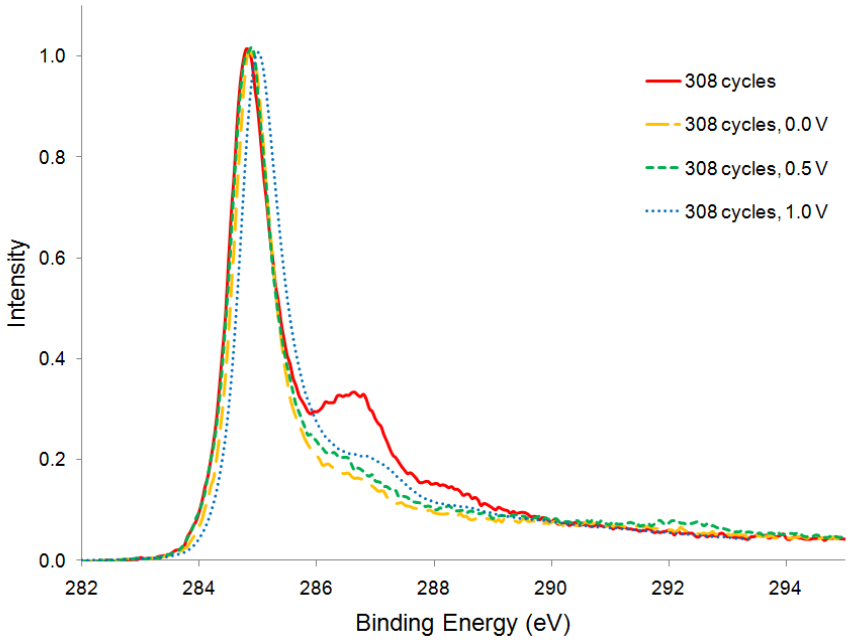

Figure 22. Normalized XPS C1s spectra of Spectracarb 2225 carbon cloth electrochemically cycled for one week and removed at different potentials.

The C1s and O1s spectra were fitted using Casa XPS software as shown in Figure 23. These are representative spectra; the rest of the spectra are similar and are contained in Appendix A.1. Peak identities were based on literature studies summarized in Table 3 and Table 4 in Section 2.5.1. The peak at 285 eV is the so-called "graphitic" peak, the peak at 287 eV corresponds to C-O-C or C-OH, 289 eV is related to O-C=O or HO-C=O, and 291 is the peak for π-π* (the transition of an electron from a bonding to an anti-bonding orbital). There is a peak in the spectrum of the untreated carbon cloth sample not present in the rest of the samples, which may be due to plasmon resonance. Plasmon resonance is caused by electron oscillations and is expected to disappear with the formation of CSFs,[89, 162] which it did. From the fitted O1s spectra, the three peaks present in all samples from lowest to highest binding energy are: C-O-C,C-OH; O-C=O,HO-C=O; H_2O,O_{2ads}.

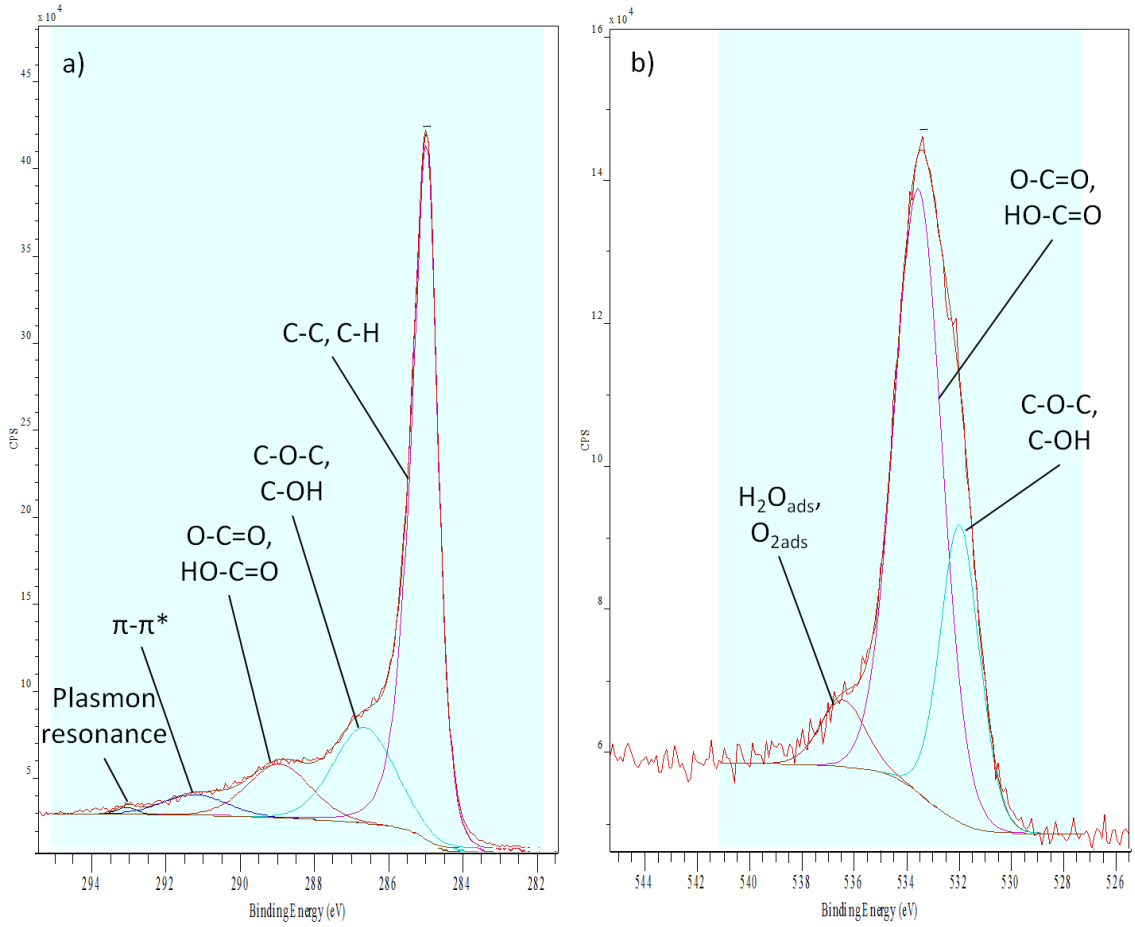

Figure 23. Fitted XPS spectra of untreated Spectracarb 2225 carbon cloth: a) C1s spectrum and b) O1s spectrum.

Table 10 and Table 11 summarize the percent areas of peaks used to fit the C1s and the O1s XPS spectra, respectively (percents provided by the CasaXPS software). All compounds contain the C-C, C-H peak (typically called the 'graphitic' peak) in the C1s spectrum. Conducting samples cause this peak to be asymmetric.[163] Since carbon cloth is conducting, which is why it is used as an electrode, this peak was fit with an asymmetric Gaussian-Lorentzian function and a Shirley background. The C-O-C, C-OH peak represents either an ether group or an alcohol. From Table 10, this peak is most dominant in the sample soaked in 1.0 M H_2SO_4, the electrode cycled to steady-state, and

the sample cycled to steady-state but extracted at a potential of 1.0 V. The O-C=O, HO-C=O peak could represent an ester or a carboxylic acid, or a lactonic group. This peak is strongest in the sample soaked in H_2SO_4, the electrode cycled to steady-state, and the untreated cloth sample. A trend based on cycling time cannot be determined based on the peak area percentages, as the percentages fluctuate until one week is reached. The samples removed at different potentials were analyzed to determine whether different CSFs are present at different potentials. From Table 10 the C-O-C, C-OH peak is most prominent in the sample removed at 1.0 V followed by 0.0 V. The O-C=O, HO-C=O peak is most prominent in the sample removed at 0.5 V on the anodic scan. A lactonic group could be formed upon oxidizing the sample, but changes form at high and low potentials. The most oxidation, however, is seen in the electrode not removed at a particular potential, from Figure 22, Table 10 and Table 11.

Table 10. Percent by area of peaks fitting the C1s XPS spectra of Spectracarb 2225 carbon cloth.

Sample Treatment	Peak Area (%)				
	C-C, C-H	C-O-C, C-OH	O-C=O, HO-C=O	π-π*	Plasmon
Untreated	60	22	12	5	1
Soaked in 1.0 M H_2SO_4 one week then DI	53	29	14	4	0
Electrode: 2 cycles	68	16	10	6	0
Electrode: 1 day	63	22	8	6	0
Electrode: 2 days	66	19	9	6	0
Electrode: 1 week	54	29	13	4	0
Electrode: 1 week, taken out at 0.0 V	64	20	9	6	0
Electrode: 1 week, taken out at 0.5 V	66	14	11	6	0
Electrode: 1 week, taken out at 1.0 V	64	23	9	4	0

In the O1s spectra, all of the samples contain the same peaks: C-O-C, C-OH, which could be an ether group or an alcohol; O-C=O, HO-C=O, which could be an ester/carboxylic acid group, or a lactonic group; and adsorbed water or oxygen. From Table 11 the sample treated with H_2SO_4 and the electrode cycled to steady-state have the strongest adsorbed water/oxygen peak. The other samples have similar peak percentages for this peak. Water and oxygen must adsorb from the atmosphere to varying degrees; it is also possible that drying processes are not consistently efficient to remove water adsorbed onto the carbon surface during rinsing and soaking. As with the C1s peak, trends based on peak area percentages cannot be determined.

Table 11. Percent by area of peaks fitting the O1s XPS spectra of Spectracarb 2225 carbon cloth.

	Peak Area (%)		
Treatment	**C-O-C, C-OH**	**O-C=O, HO-C=O**	**H_2O, O_{2ads}**
Untreated	27	66	7
Soaked in 1.0 M H_2SO_4 one week then DI	30	51	19
Electrode: 2 cycles	19	74	7
Electrode: 1 day	24	69	7
Electrode: 2 days	30	62	8
Electrode: 1 week	17	68	15
Electrode: 1 week, taken out at 0.0 V	23	69	8
Electrode: 1 week, taken out at 0.5 V	28	64	7
Electrode: 1 week, taken out at 1.0 V	14	78	8

Based on both the C1s and the O1s spectra, the sample that was soaked in electrolyte but without any electrochemistry performed, as well as the same that was cycled to steady-state, have the highest formation of CSFs, based both on the direct comparison of the spectra in Figure 21 and on data in Table 10 and Table 11. Aside from this observation, no trend of CSF development with length of electrochemical cycling time or with potential was found. XPS fitting is subjective; the number and widths of the peaks is determined by the user. Therefore, quantitative analysis is difficult to carry out reliably. However, potential CSFs have been identified (ether, phenol, carboxylic acid, lactonic groups), and can be compared with other identification and quantification techniques, such as the Boehm titration in Chapter 6.

4.3.2 X-ray Absorption Spectroscopy

XAS was performed at the CLS as a complementary x-ray technique to XPS. Oxygen-containing CSFs contribute to peaks in the K-edge C1s spectrum. As with XPS, the chemical shifts of these peaks can be used to indicate which CSFs are present in a sample. Samples of the carbon powders ELIT and Black Pearls 2000 were examined using XAS in addition to the same Spectracarb 2225 carbon cloth samples studied using XPS in Section 4.3.1.

The spectra from the carbon samples, Spectracarb 2225 carbon cloth, ELIT carbon, and Black Pearls 2000, were normalized for visual comparison. Spectra were all normalized for the low-energy baseline, below 282 eV, to 0 and high-energy baseline, above 324 eV, to 1. The peak at the lowest binding energy, around 285-286 eV, is the graphitic peak, as in the XPS analysis. Each sample has this peak. There is a region following this peak of lower intensity; depending on the sample, this region contains either one, two, or even three peaks. The region following this at higher energy increases in intensity once again, which corresponds to the $1s \rightarrow \sigma^*$ transition of the ring. The region of lower intensity, between 286 and 291 eV, is where any indication of CSFs would occur, and as a result it is this region that is discussed here. The identities of the peaks are based on the summary in Section 2.5.1, Table 5.

Every spectrum for the carbon cloth, shown in Figure 24 and Figure 25, contains a strong peak at 289 eV. This peak corresponds to the $1s \rightarrow \pi^*_{C=O}$ transition (288 to 289 eV). This peak could indicate the presence of CSFs such as carbonyl or quinone, and possibly carboxyl or lactonic groups, which contain the C=O bond. The peak at 290 eV is due to the $1s \rightarrow \sigma^*_{C-O}$ transition (290 to 291 eV). It is only present in the electrodes. It corresponds to an ether group but could also suggest CSFs that contain the C-O bond

such as lactonic groups. Since it is not present in the samples without electrochemistry, it is likely due to a CSF that formed due to electrochemical cycling. The peak seems to increase in intensity with cycling time, which supports the idea that the CSF is formed with cycling (this will be discussed in more depth and will be compared to CV and Boehm titration data in Chapter 6). There is a difference between the spectra removed at different potentials (Figure 25). The entire region between 286 and 291 eV decreased with increasing potential. Because the baseline of this region is not the same between samples, it is difficult to compare peak heights. However, it can be said that the C-O peak increased significantly at 1.0 V. This suggests that there is an electroactive CSF formed with potential cycling that is oxidized between 0.5 and 1.0 V, likely the same one contributing to the C-O peak increase with cycling time.

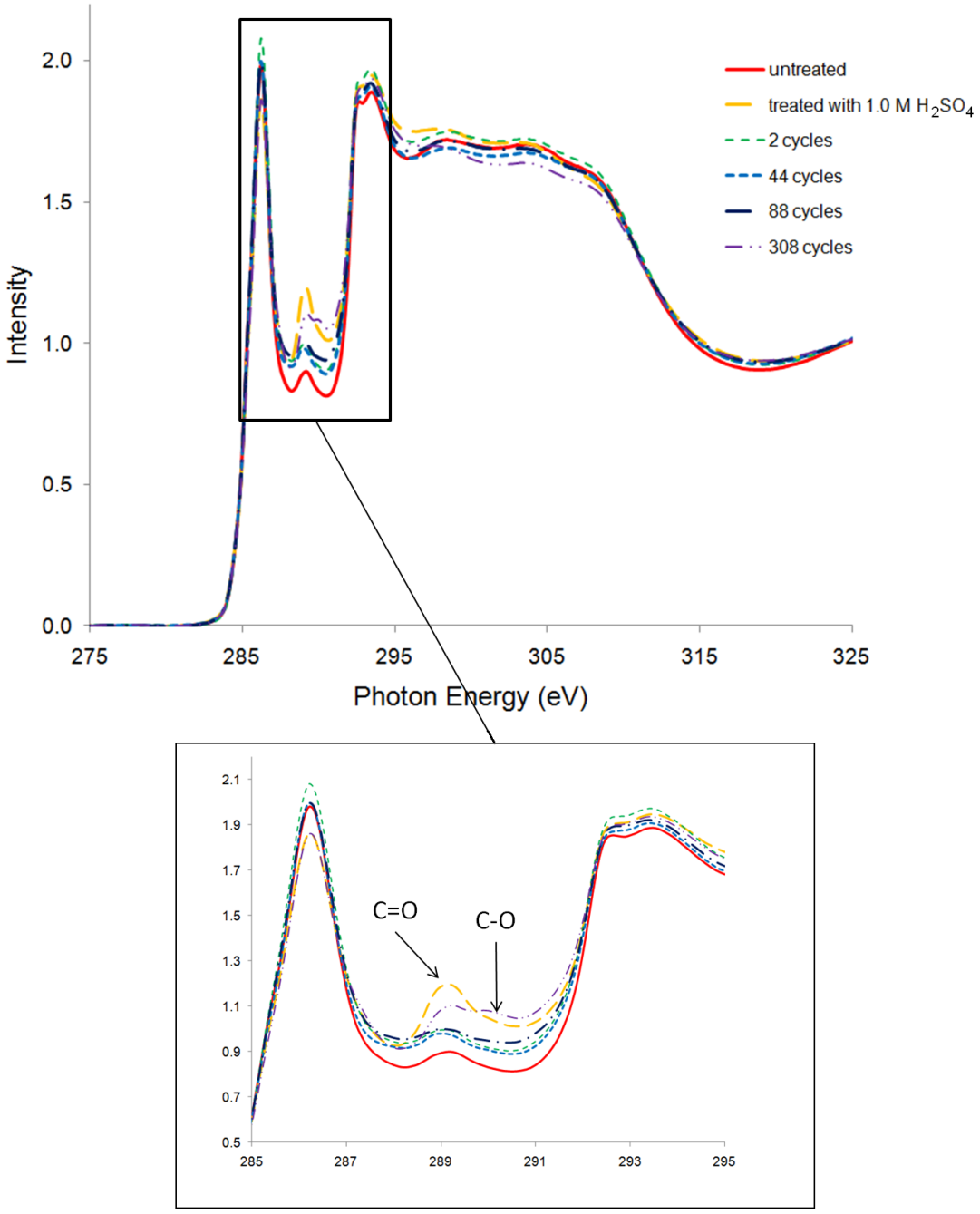

Figure 24. Normalized XAS C K-edge spectra of Spectracarb 2225 carbon cloth samples electrochemically cycled for different lengths of time.

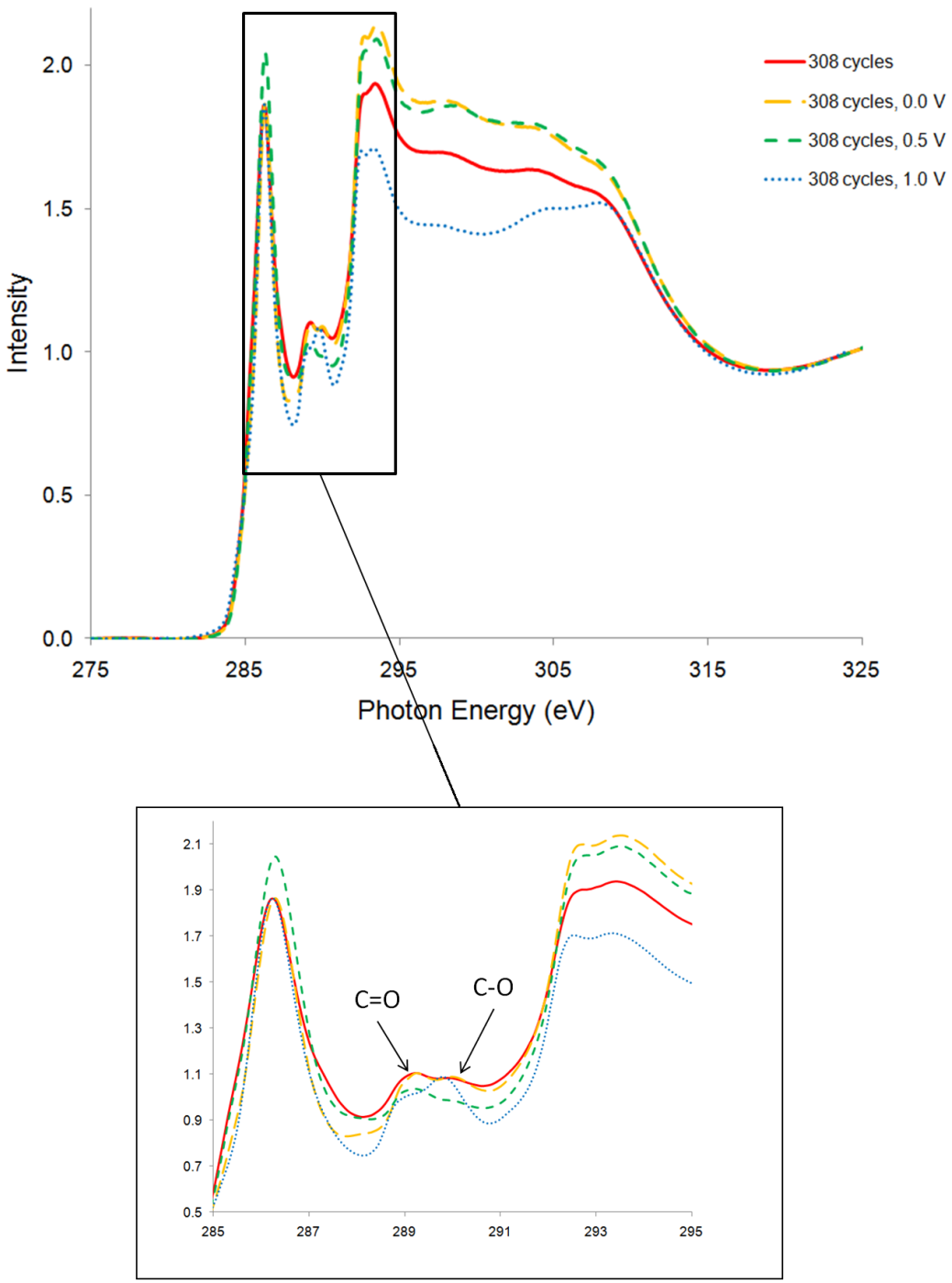

Figure 25. Normalized XAS C K-edge spectra of Spectracarb 2225 carbon cloth samples electrochemically cycled and removed at different potentials.

The spectra for ELIT carbon powder (untreated, soaked in water, and electrochemically cycled for three cycles, Figure 26) each contain the peak at 289 eV likely corresponding to the C=O bond (refer to Table 5). This could be from quinone groups, which are electroactive and likely the cause of the pseudocapacitive peak in the CV for ELIT at ca. 0.6 to 0.7 V vs. SHE (Figure 27). There is a peak at 291 eV present only in the spectrum for the untreated ELIT sample that could be caused by the C-O bond, but it disappears with treatment in water or with electrochemical cycling. Perhaps this peak is due to a surface group weakly adsorbed to the untreated sample surface. A peak at 288 eV of low intensity is present in the untreated sample and very slightly in the sample treated with water, and also disappears with electrochemical cycling. There is a possibility that this is due to a C-OH bond, indicating a phenolic group, which is destroyed with electrochemical treatment, though the disappearance of an acidic surface oxide with electrochemical cycling has not been seen in literature studies. The region above 291 eV is due to ring transitions (from Table 5). The untreated sample as well as the one soaked in water exhibit sharp peaks in their spectra, whereas the peaks are diminished significantly in the spectrum of the electrode. It could be that electrochemical cycling destroys the ring structure of the electrode.

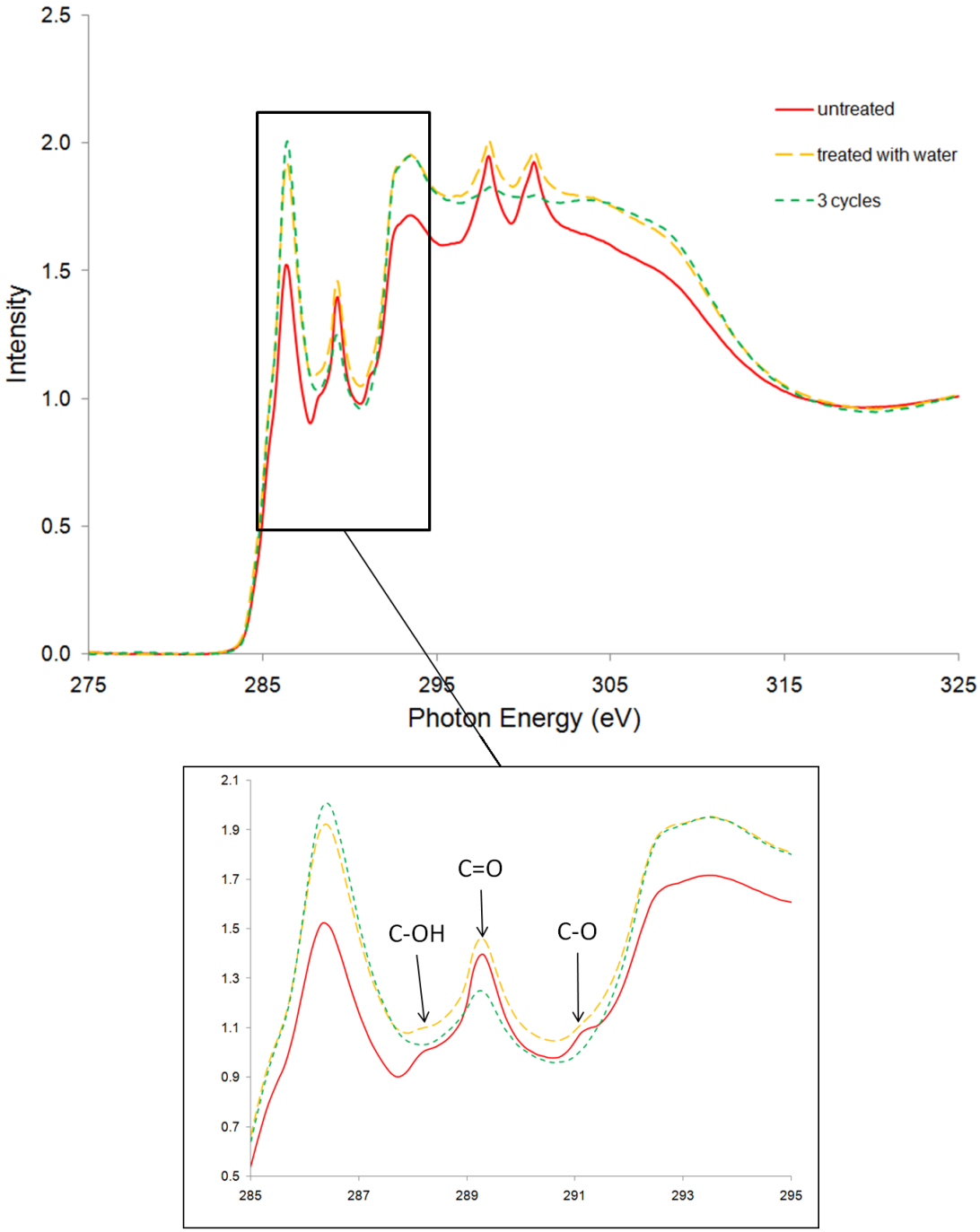

Figure 26. Normalized XAS C K-edge spectra of ELIT carbon powder.

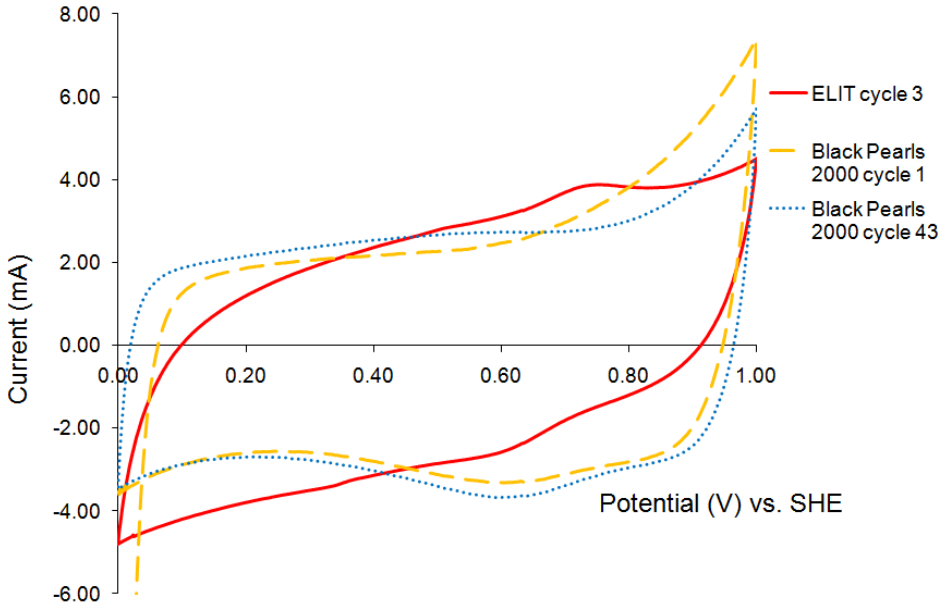

Figure 27. CVs of ELIT and Black Pearls 2000 carbon powder electrodes examined using XAS.

The spectra from all of the Black Pearls 2000 carbon powder samples, Figure 28, include the peak around 289 eV, for C=O, which could be due to a carbonyl or quinone group, or another CSF that contains the C=O bond such as lactones. This could correspond to the pseudocapacitive peak seen in the CV for Black Pearls 2000 at ca. 0.6 V vs. SHE (Figure 27), that increased with potential cycling but was present already in the first cycle, which could mean that it was already present on the surface before cycling. As with the ELIT samples, there is a peak corresponding to C-O at 291 eV present only in the untreated sample, and a peaks corresponding to C-OH at 288 eV present in the untreated sample and only slightly in the sample soaked in water. It could be that some CSFs formed during the carbon processing are weakly adsorbed to the carbon surface and consequently get destroyed when the samples are treated.

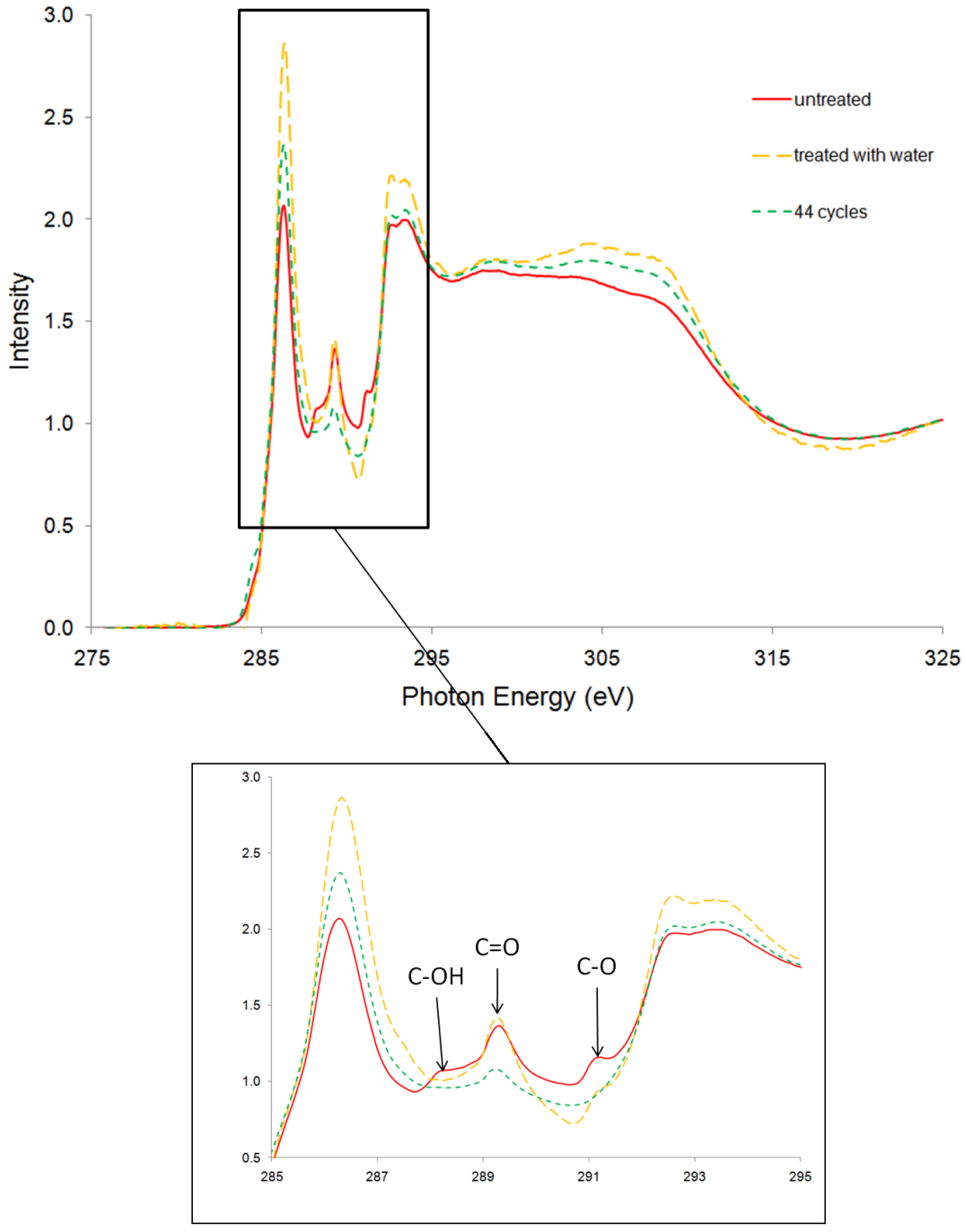

Figure 28. Normalized XAS C K-edge spectra of Black Pearls 2000 carbon powder.

Every spectrum shown from XAS contains the peak indicating a C=O bond. This could be from a lactonic group, which is a support of the results from XPS (and

from Boehm titration, Chapter 6). The C-O bond is affected by electrochemical cycling in different ways depending on the carbon; in carbon cloth this peak is only present on electrodes, and in ELIT and Black Pearls 2000 it disappears with electrochemistry. The suspected C-OH bond is only present in the untreated carbon powders, which means that it could be a weakly-adsorbed group that is desorbed with treatment in aqueous solution.

4.4 Photoacoustic Spectroscopy

Photoacoustic spectroscopy (PAS) is often used for solid samples, including carbon samples. PAS was used to gain information on the surface of carbon prior to and after electrochemistry. The instrument at the CLS was used by Dr. Brent Billinghurst to obtain spectra of carbon cloth samples using carbon black as a reference. The resulting spectra of untreated carbon cloth, an electrode that had been electrochemically cycled for one day, and an electrode cycled for one week are shown in Figure 29. The untreated sample spectrum contains a broad peak from 4000 to 3000 cm^{-1} due to an –OH group, and some very small and broad peaks in the 1300 to 1200 cm^{-1} range, perhaps from C-O stretching. There is also some noise at 1600 to 1500 cm^{-1}, perhaps due to –OH bending. The spectra from electrochemically cycled electrodes appear similar to the spectrum of the untreated sample, though their peaks are even less pronounced. The peaks seen in the PAS spectra are too small to be conclusive evidence of CSFs. The low intensity of peaks could be that the CSFs did not form on the outer surface but in the pores of the electrode, perhaps near the pore mouth, and the chopping speed of the light was not slow enough to allow light to reach the pores.[164] Conversely, it could be that the CSFs were in such low concentration as to not be significantly detected through PAS.

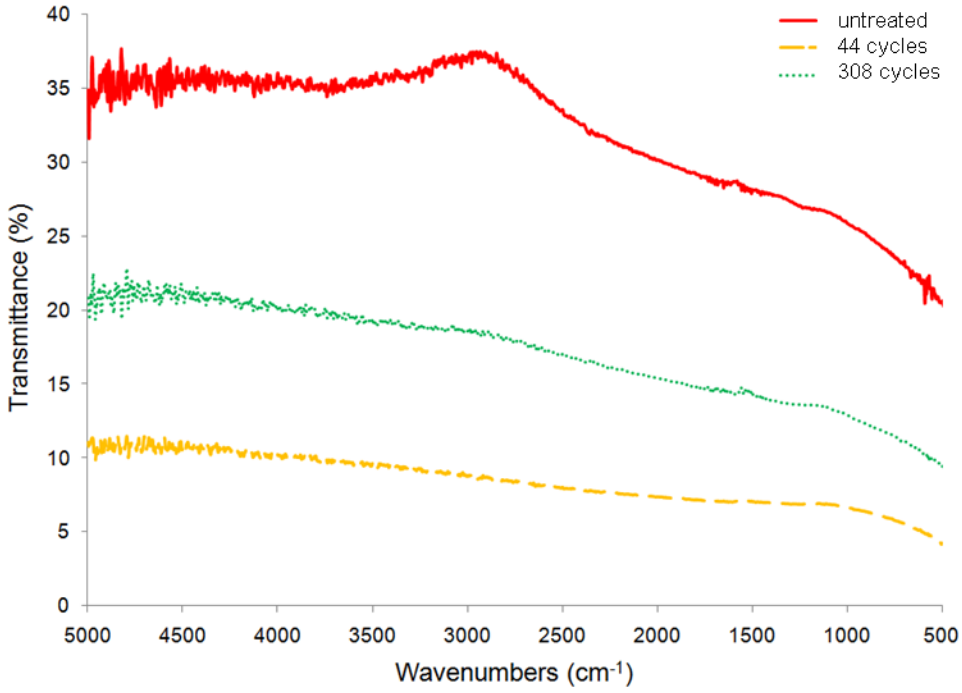

Figure 29. PAS spectra of Spectracarb 2225 carbon cloth samples.

4.5 Conclusions

UV-Vis-NIR spectroscopy yielded spectra from carbon samples that could not be used to identify CSFs. Transmission FTIR, ATR-FTIR and PAS yielded spectra with low-intensity peaks suggesting surface oxide groups on various forms of carbon samples and electrodes, though changes to CSFs due to electrochemistry could not be determined definitively. The x-ray techniques, XPS and XAS, were able to easily detect surface oxygen groups on samples of carbon that were untreated, treated chemically or electrochemically. XPS spectra showed the same surface groups on all carbon cloth samples. Quantitative characterization using XPS is considered to be subjective and it is recommended that quantitative studies be left to chemical techniques such as the Boehm

titration. XAS spectra suggested a CSF containing a C-O bond formed on carbon cloth with electrochemical cycling. Powders examined using XAS appeared to have CSFs that electrochemical cycling caused to disappear. *In situ* spectroscopy measurements with electrochemical cycling could not be accomplished on carbon electrodes by any of the spectroscopic techniques studied here.

Chapter 5 Standardization of the Boehm Titration

As mentioned in Section 2.5.1, the Boehm titration is a common chemical technique for studying surface oxide groups on carbon. It works on the theory that bases of different strengths react with different acidic CSFs on carbon samples. $NaHCO_3$ neutralizes carboxylic CSFs, Na_2CO_3 neutralizes carboxylic and lactonic groups, and NaOH neutralizes carboxylic, lactonic and phenolic CSFs. Carbon samples are agitated with these bases, aliquots from the supernatant solutions are taken, and back-titrations performed on the acidified aliquots to determine the amount of CSFs reacted with each base. Through subtraction the moles of each type of CSFs per gram of sample, n_{CSF}, of each type are determined. In the current research, the reason for using the Boehm titration was as a complementary technique to spectroscopy. However, when searching for the procedure in the literature, discrepancies were found in the methodology. The differences in carrying out the Boehm titration are outlined in Section 2.5.2. So that results found could be compared to results in the literature, it was decided that the method should be standardized. The two factors undertaken were titration endpoint determination and removal of CO_2 effects on titration. Part of this project was published as "Standardization of the Boehm titration. Part I. CO_2 expulsion and endpoint determination." by Sarah L. Goertzen, Kim D. Thériault, Alicia M. Oickle, Anthony C. Tarasuk and Heather A. Andreas in Carbon in 2010, volume 48, page 1252-1261.

5.1 Endpoint Determination

To ascertain the optimal method for endpoint determination, colour indicators and a pH electrode and meter were used for strong acid (HCl)-strong base (NaOH)

titrations, whose equivalence point occurs at pH 7.00. Boehm suggests using an indicator mixture of methyl red and methylene blue.[16] The methylene blue is added to make the endpoint easier to observe compared to the typical yellow (alkali) to red (acidic) transition of the methyl red: with the added methylene blue, a green to purple transition is visible with a grey-coloured endpoint. However, this indicator mixture is rarely used, and therefore the more commonly used indicators were examined in this study: phenolphthalein with a basic titrant,[115, 118, 166-169] and methyl red with an acidic titrant.[115, 168, 170-173]

Strong acid-strong base titrations of HCl and NaOH were carried out to evaluate endpoints determined by indicators compared to endpoints determined by a pH meter. When HCl was titrated with NaOH, relative standard deviation (RSD) values, based on three replicates, of the titrant volume used for neutralization were 0.19% and 0.06% for phenolphthalein and a pH electrode, respectively (data in Appendix A.2, Tables A 29 and A 30). When NaOH was titrated with HCl, RSD values of 0.79% for methyl red and 1.3% using a pH electrode were obtained from three replicates (data in Appendix A.2, Tables A 31 and A 32). The low RSD values for all these endpoint detection methods suggest that either colour indicators or a pH electrode would provide precise enough measurements to be used in these titrations. Nevertheless, these results do not indicate the accuracy of the measurements. For instance, the RSD values obtained from colour indicator endpoints show that reproducible results are possible based on human observation of colour changes, but since observation is subjective, results could change drastically depending on the experimentalist. Additionally, the endpoints of the colour indicators are not at a pH of 7.0, as desired for the strong acid-strong base titrations used

in the Boehm titration. Conversely, potentiometric endpoint determination, with the use of a pH meter, allows for an objective endpoint determination, rather than subjective, and can result in endpoints at a pH of 7.0. Another option for endpoint determination is to use the first derivative of the titration curve. On the first derivative plot, the location on the x-axis of the highest intensity corresponds to the location on the x-axis of the titration curve with the steepest slope (the inflection point), which is the equivalence point. It must be determined how the volume differences which result from these endpoint differences affect the amounts of CSFs calculated (n_{CSF} from Equation 5 in Section 3.3.5).

As an example, Figure 30 shows the titration curve of a blank acidified aliquot of $NaHCO_3$ titrated with NaOH (with the effect of CO_2 removed by degassing with N_2 for 1 h in a N_2-filled glove box prior to titration), which should have a calculated n_{CSF} of 0 µmol. The first derivative shows that the equivalence point occurs at a n_{CSF} of 5 µmol. By inspection of this titration curve, phenolphthalein would suggest a n_{CSF} of 8 µmol (pH 8.9), methyl red a n_{CSF} of 1 µmol, (pH 5.9) and a pH meter of 4 µmol (pH 7.0). All of these values are small compared to the typical Boehm titration n_{CSF} values of 50-2000 µmol/g,[18, 79] (often for 0.5-1 g[79, 80, 84, 113]), and so any of these endpoint detection methods are appropriate for the Boehm titration.

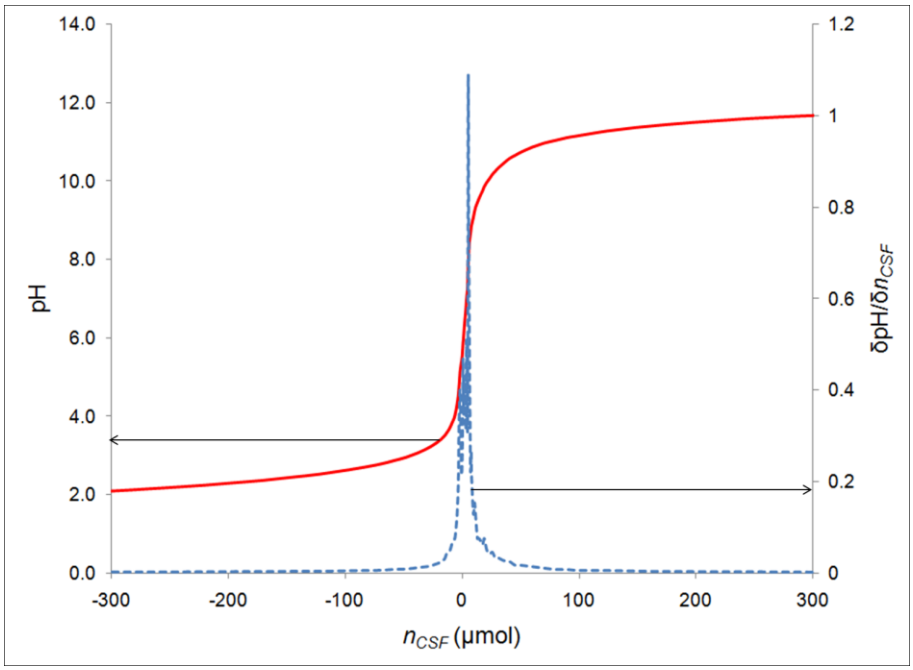

Figure 30. Titration curve (solid) and first derivative of the titration curve (dashed) of a back-titration of a blank acidified $NaHCO_3$ aliquot with the effect of CO_2 removed.

It should be noted, however, that error in all endpoint determination methods can occur. Endpoints based on colour indicators are subject to interpretation, and pH electrodes can have error as well; they are calibrated based on a specific temperature, but the room temperature is often not exactly what is programmed into the pH meter and can fluctuate throughout the time it takes to perform a titration. The aliquot may also become hotter than expected during the titration due to the stir plate heating up.

The important consequence of the previous discussion is that all of these endpoint detection methods, whether colour indicator, one-point pH 7.0 measurements, or first derivative of the titration curve, give the same results in the Boehm titration since neither the accuracy nor the precision is greatly influenced by the different methods. The endpoint detection method should, nevertheless, still be reported and

error ranges should be included in reported values to aid in the comparison between relatively close values.

5.2 Removal of the Effect of CO_2

The predicted Boehm titration curves for both the back-titration, where the acidified aliquots are titrated with NaOH, and direct titration, where the NaOH aliquot is directly titrated with HCl, are expected to be typical monoprotic acid titration curves, with an endpoint of pH 7.0. However, as is well known, the dissolution of CO_2 into an aqueous solution, even permeating through polyethylene storage bottles, causes the pH of the solution to shift [30]. The effect of this in the current titrations is the appearance of a second inflection point marking two endpoints (at ca. pHs of 4 and 8), for example 1.0 h of bubbling N_2 through a Na_2CO_3 in Figure 31 b and f, in the blank acidified aliquots that have not been sufficiently degassed. As gaseous CO_2 enters solution, it dissolves as in Reaction 2:[30]

$CO_2\,(g) \leftrightharpoons CO_2\,(aq)$ pK = 1.463 R2

and the dissolved CO_2 reacts with water to form carbonic acid, which then becomes bicarbonate (Reaction 3 and 4[30]):

$CO_2 + H_2O \leftrightharpoons H_2CO_3\,(aq)$ pK = 2.699 R3

$H_2CO_3\,(g) \leftrightharpoons HCO_3^- + H^+\,(aq)$ $pK_a = 6.352$ R4

The presence of the two inflection points in the titration curve may have a significant impact on the calculated n_{CSF}, particularly if the experimentalist is using a one-point potentiometric endpoint detection or colour indicators, as a pH of 7.0 is reached at a larger titrant volume in the titration resulting in a falsely high endpoint

volume, and leading to a falsely large calculated amount of surface functionality; for instance, a measured increase in volume of ca. 0.1 mL corresponds to a false increase in n_{CSF} of ca. 25 μmol (n_{CSF} being calculated using Equation 5, assuming a blank titration with V_B 50.00 mL, V_a 10.00 mL, V_{HCl} 20.00 mL where all concentrations are 0.05 M). Clearly it is imperative that the CO_2 be removed before the titration, particularly for carbon samples with CSFs in the range of only 50-100 μmol/g of CSFs. In the present standardization, methods studied for the removal of the effect of CO_2 on the titration results were: the use of blanks, sparging with an inert gas, performing the titration in a glove box filled with inert gas, heating and refluxing.

5.2.1 Removal of the Effect of CO_2 through the Use of Non-Degassed "Blanks"

Often in the literature, the effect of CO_2 is removed from non-degassed samples by the subtraction of calculated blank results from the calculated carbon samples results, without any experimental CO_2 removal process.[23, 97, 114, 116, 167, 174-177] Thus, the effectiveness of this subtraction method was examined. For this method to be valid, the effect of CO_2 in the non-degassed solutions, as measured by the n_{CSF} of the base reacted, must be consistent. There should be little to no variation in the amount of base reacted between these samples, otherwise, the results would vary depending on the particular blank sample used. Hence, the n_{CSF} was determined from three identical samples of non-degassed blank aliquots of each reaction base, in order to determine the reproducibility, tabulated in Table 12 (using Equation 5 for $NaHCO_3$ and Na_2CO_3, and Equation 6 for NaOH). The aliquots of $NaHCO_3$ and Na_2CO_3 were acidified before back-titration, and the NaOH aliquots were titrated directly (denoted as $NaOH^{direct}$). Since these are blanks, no carbon is used, and therefore the expected value for the n_{CSF}

with no effect of CO_2 is 0 µmol. The clearly non-zero value of n_{CSF} in each result in Table 12, in some cases positive, in some cases negative, suggests that there is an effect of CO_2 in solution, and that it is not consistent between samples.

Table 12. Calculated n_{CSF} of non-degassed blank aliquots.

	n_{CSF} (µmol) as determined by		
Sample #	$NaHCO_3$	Na_2CO_3	$NaOH^{direct}$
1	-30	14	4
2	-4	22	-5
3	32	52	21

Typically, when this type of blank subtraction method is used to remove the n_{CSF} bias caused by CO_2 in solution, only one blank measurement is taken.[23, 97, 114, 116, 167, 174-177] However, as can be seen by the numbers shown above, which vary between -30 and 52 µmol, the effect of CO_2 is inconsistent. Consequently, the n_{CSF} results that would be calculated for a real carbon sample would vary, leading to erroneously high or low results depending on the particular blank sample. As has been mentioned, n_{CSF} values typically calculated for the Boehm titration can range anywhere from 50 to 2000 µmol/g.[18, 79] Perhaps the variation due to CO_2 seen here would not affect carbons containing CSFs numbering on the larger end of this scale, but it puts CSFs amounts on the lower end greatly into question. For instance, if CO_2 had a particularly significant effect on a blank, but had little effect on the titration curve of the sample itself, after the subtraction of the blank the results may suggest a complete lack of CSFs on that sample, though the CSFs may in fact be present.

The average n_{CSF} reacted of these non-degassed blanks is seen in Table 13, with an efficacy comparison of all the CO_2 removal methods. From the standard deviation

(SD) given for the data of the non-degassed blanks, as well as the previous discussion of the unpredictability of the effect of CO_2, it can be seen that the blank subtraction method is unreliable, in particular for use on carbon samples with low concentration of CSFs. For that reason, it is recommended that the blank subtraction method not be used during CSF quantification using the Boehm titration.

Table 13. Comparison of average calculated n_{CSF} neutralized by each reaction base to determine the effectiveness of each CO_2 removal, based on three replicates.

Titration	n_{CSF} ± SD (µmol)			
	$NaHCO_3$	**Na_2CO_3**	**NaOH**	**$NaOH^{direct}$**
Non-degassed	-1 ± 25	29 ± 20	--	7 ± 13
N_2 Prior (2 h)	-5 ± 3	-23 ± 23	2 ± 20	35 ± 42
N_2 Prior and During	1 ± 1	11 ± 1	-4 ± 2	--
In N_2-filled Glove Box	13 ± 33	14 ± 17	-1 ± 1	10 ± 6
N_2 Prior to Titration in Glove Box	-8 ± 1	-2 ± 1	-15 ± 1	12 ± 2
Heating	24 ± 16	-13 ± 8	-40 ± 26	--
Reflux	3 ± 17	57 ± 19	-8 ± 23	--

SD denotes standard deviation based on three replicates
-- denotes a measurement not carried out

5.2.2 Effect of Degasification Time

It is well known that dissolved gases (e.g. CO_2 and O_2) can be removed from solution through sparging with an inert gas, such as N_2 or Ar. However, there is no information available for the length of bubbling time required for effective CO_2 removal from the Boehm titration. Figure 31 shows the potentiometric titration curves for sample blanks (no carbon) for each of the reaction bases with different degasification times. In Figure 31a-d, pH is plotted vs. the calculated n_{CSF} rather than vs. titrant volume so that the effectiveness of CO_2 removal can more easily be compared (as this way they can all be compared to 0 µmol, which is what the n_{CSF} should be at the endpoint of the blank samples). Figure 31e shows the titration curve for the direct

titration of NaOH vs. the volume of titrant added, simply to illustrate the difference in shape of the titration curve itself compared to the back-titrations: it is reversed, beginning at a high pH and decreasing with added titrant. For clarity, a dotted line is shown on each figure which shows where a pH of 7 falls on the curve. Figure 31f shows a comparison of the first derivative of two of the Na_2CO_3 blank aliquot titration curves with varying degrees of CO_2 removal.

The minimum degasification time required to completely remove the effect of dissolved CO_2 by sparging with an inert gas was examined, and is shown in Figure 31 for blank acidified aliquots of each reaction base. Since there was no significant difference in degasification time between N_2 and Ar, only the N_2 results are shown. As the degasification time increases, less evidence of dissolved CO_2 is seen as the second endpoint begins to disappear, and the calculated n_{CSF} gets closer to 0 μmol. For the titrations based on blank samples of the $NaHCO_3$ reaction base a minimum of 1.5 h of degasification is required to completely remove the effects of CO_2 (Figure 31a). 2 h of degasification is required for the blank samples of Na_2CO_3 (Figure 31b).

For NaOH, both direct titrations and back-titrations were tested. A back-titration of a blank acidified NaOH aliquot after degassing for 2 h is shown in Figure 31c. The effects of CO_2 were not completely removed, and so the acidified NaOH aliquot was degassed with N_2 for 2 h prior to titration, and the degassing through the aliquot was maintained during the titration (Figure 31c). This was carried out for both the direct and the back-titration of NaOH, the former shown in Figure 31d. It was seen that CO_2 effects were removed from the back-titration curve of the blank acidified NaOH aliquot by 2 h of degassing with N_2 prior to titration, followed by continuous degasification

during the back-titration. However, in the direct titration of the NaOH aliquots, the most often used Boehm titration for the NaOH reaction base, even 24 h of degasification does not completely remove the CO_2, as evidenced by the second endpoint (Figure 31d). This suggests that for the complete removal of the effects of CO_2 a back-titration should be carried out with the NaOH samples as with the other reaction bases. Since degasification in the back-titration takes place in an acidified solution, where the CO_2 exists as dissolved CO_2, the effects of CO_2 can be easily removed through this degasification of a back-titration.

The result of the number of inflection points on the titration curves is seen on first derivative plots, for example Figure 31f from titration curves for 1.0 h and 2.0 h of degassing the Na_2CO_3 aliquots; the one inflection point for 2.0 h bubbling in Figure 31b corresponds to one equivalence point. Accordingly, the optimum conditions for the removal of CO_2 effects are 2 h of degasification of the titration sample with an inert gas prior to titration followed immediately by a back-titration in which the sample is degassed throughout. Though it seems that degassing during titration is not required for $NaHCO_3$ and Na_2CO_3 the same conditions are suggested for consistency.

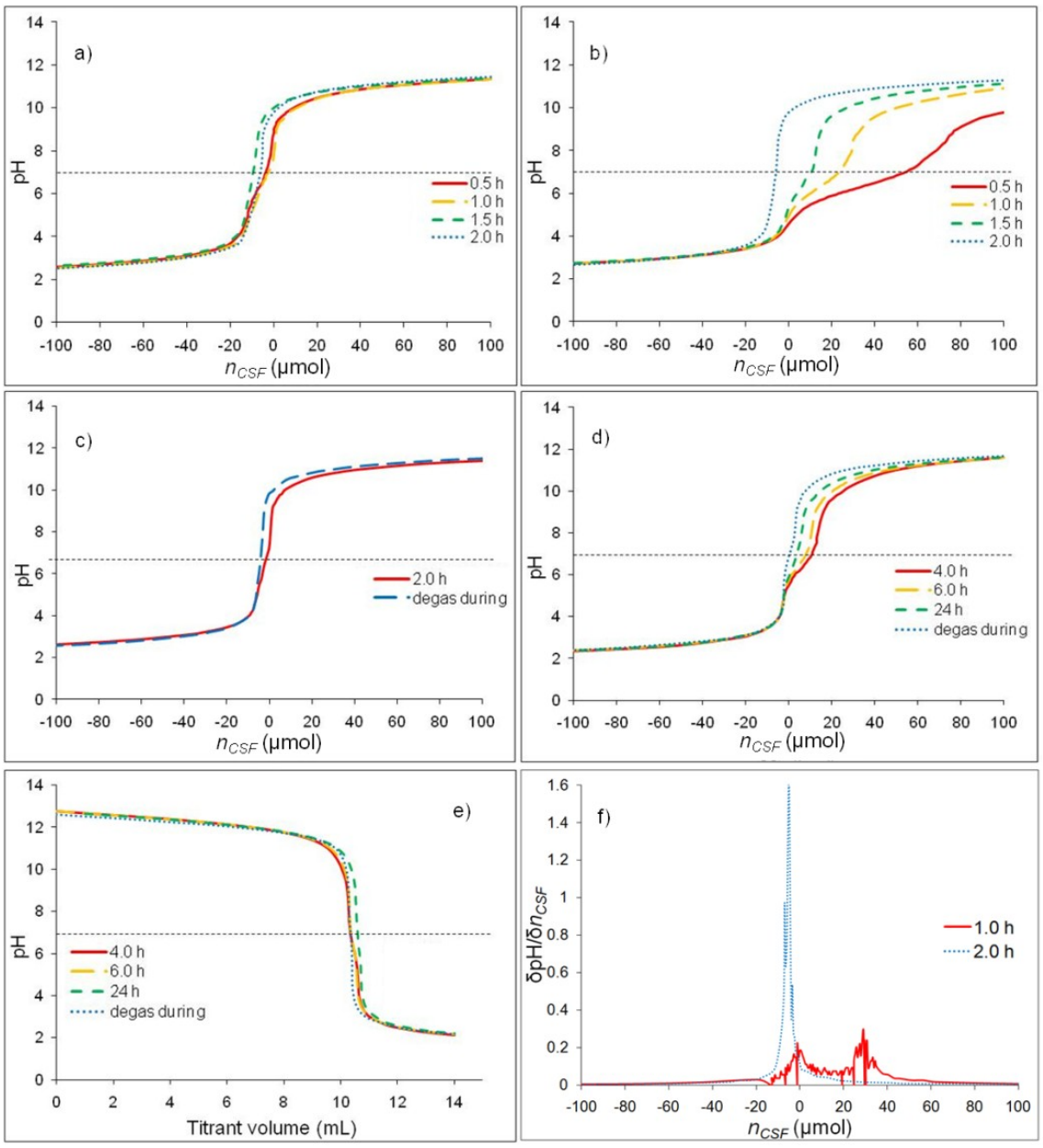

Figure 31. Titration curves (plotted vs. amount of n_{CSF}) for blank acidified aliquots of the reaction bases: a) $NaHCO_3$; b) Na_2CO_3; c) NaOH back-titration; d) NaOH direct titration; and e) titration curve for NaOH direct titration plotted vs. titrant volume; and f) first derivative plot for titration curves of Na_2CO_3. Different times of degasification of acidified aliquot prior to or during titration are noted in the legends.

Endpoints determined from three identical titrations for each reaction base using the different degassing methods were used to calculate the average n_{CSF} reacted and the

SD of the three replicates (Table 13). Since these samples are blank, containing no carbon, and therefore no CSFs, it is expected that no base should have reacted, giving a result of 0 µmol of n_{CSF}. The aliquots that were degassed with N_2 for 2 h before titration but not degassed during titration are denoted as "N_2 Prior". The aliquots degassed with N_2 prior to (2 h) as well as during the titration are denoted as "N_2 Prior and During". The positive values for n_{CSF} could be due to a small amount of CO_2 remaining in the sample, or CO_2 being introduced to the titrand from the titrant during titration. A negative n_{CSF} may suggest HCl evaporation from the titrated sample during degassing. The large SD suggests that there is great variability in the efficacy of CO_2 removal in these aliquots without the additional continuous bubbling during titration step. In all, the n_{CSF} values calculated in Table 13 using the two CO_2 removal methods outlined here support the conclusions drawn from Figure 31 that bubbling the aliquot for two hours prior to titration combined with bubbling during the titration is the optimal method of CO_2 removal using degasification with an inert gas, and that simply degassing for 2 h prior to titration is not sufficient.

5.2.3 Removal of the Effect of CO_2 through Titration in a N_2-Filled Glove Box

Blank back-titrations were performed in a N_2-filled glove box to determine whether titrations done in an inert atmosphere would remove the effect of CO_2. The titrations were either simply performed in the glove box without any additional CO_2 removal or they were done after 1 h of bubbling the aliquots with N_2 inside the glove box.

From the data shown in Table 13, it can be seen that doing the titration in a N_2-filled glove box (with no bubbling), denoted as "In N_2-filled Glove Box", is not necessarily an acceptable method to remove effects of CO_2. Both the direct titration and back-titration of blank NaOH aliquots result in n_{CSF} values close to 0 μmol (10 ± 6 μmol and -1 ± 1 μmol, respectively). However, the n_{CSF} values calculated from titrations of blank acidified aliquots of $NaHCO_3$ (13 ± 33 μmol) and Na_2CO_3 (14 ± 17 μmol) are positive, indicating the continued presence of CO_2, and with large standard deviation values.

The magnitude of the standard deviations themselves suggest that CO_2 is still present in aliquots in varying amounts in the glove box when they are not actively degassed, likely because N_2 is not actually being forced into the aliquot. The standard deviations are much lower if the acidified aliquot is degassed with N_2 in the glove box prior to titration; the n_{CSF} values are -8 ± 1 μmol for $NaHCO_3$ aliquots and -2 ± 1 μmol for Na_2CO_3. The small negative bias for the sample bubbled for 1 h in the glove box may be from a small degree of preferential HCl loss from the acidified aliquot solutions.

It is interesting to note that the calculated n_{CSF} of the direct titration of NaOH aliquots is not greatly affected by whether the aliquots are degassed beforehand; the n_{CSF} with the degassing step is 12 ± 2 μmol compared to 10 ± 6 μmol of the non-degassed direct titration in the glove box. The 1 h degassing of the acidified aliquots does, however, result in a larger negative value of n_{CSF} (-15 ± 1 μmol) for the back-titration of the blank acidified aliquots of NaOH compared to no degassing in the glove box (-1 ± 1 μmol). Perhaps for this reaction base, simply performing the back-titration in a glove

box is sufficient to remove the effect of CO_2, whereas excess degassing of the aliquot begins to remove some of the HCl as well as the CO_2.

Despite the positive and negative biases seen, this method may be sufficient to remove the effect of CO_2. Potentiometric titration curves, such as that seen in Figure 32, show that simply leaving the aliquot open under the inert atmosphere (no direct degasification with N_2) was sufficient to remove the effect of CO_2 since only one inflection point is in evidence. This indicates that performing the Boehm titration in a glove box is a good method; however, this method is more complex and more expensive (in terms of the purchase of a glove box and the volume of inert gas used) than the bubbling regime proposed earlier (Section 5.2.2).

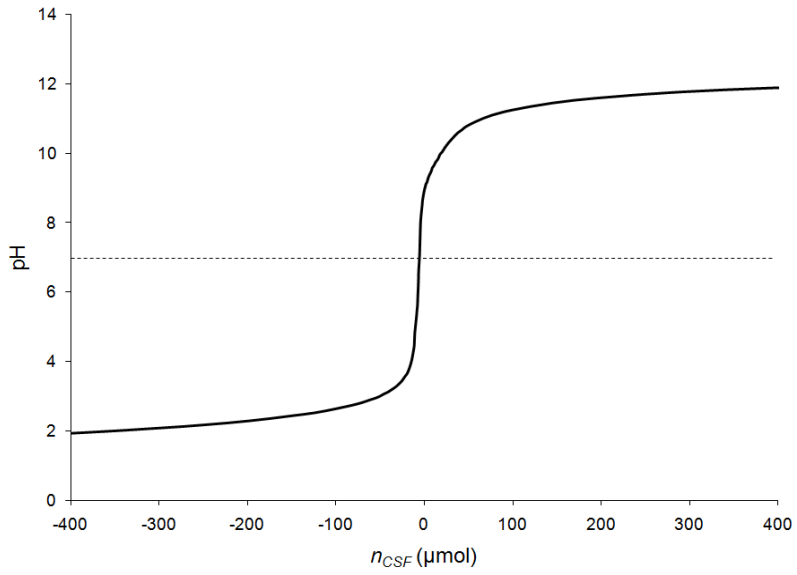

Figure 32. Back-titration of a blank acidified $NaHCO_3$ aliquot in a N_2-filled glove box. The dotted line shows where pH 7 occurs.

5.2.4 Removal of the Effect of CO_2 through Heating and Refluxing

In the papers where Boehm discussed CO_2 removal, he suggests that heating of the acidified aliquots is sufficient to remove the CO_2 from solution.[16, 18, 20] To determine the effectiveness of heating samples to remove CO_2, blanks were heated and cooled, and then back-titrated to a potentiometric endpoint of pH 7.0. The n_{CSF} calculated based on three titrations of blank, acidified aliquots heated in a vented vial (denoted as "Heating") or refluxed under an open, water cooled condenser (denoted as "Reflux") are shown in Table 13. In this table it can be seen that heating of the blank acidified aliquots in a vented vial results in a large positive bias in the $NaHCO_3$ results, and negative biases in the Na_2CO_3 and NaOH results (suggesting CO_2 and HCl expulsion), as well as a large standard deviation with all reaction bases.

The large positive bias with the $NaHCO_3$ reaction base suggests that heating may not be sufficient to remove the CO_2. This is confirmed in Figure 33a by the two inflection points in the titration curve and the two peaks in the first derivative plots, as would be expected for the diprotic titration of carbonic acid from dissolved CO_2. This residual CO_2 may have been trapped in the head space of the flask during heating and dissolved back into solution during cooling, and the large standard deviation is likely due to the variability of the quantity of trapped CO_2. However, the concern with heating in an open flask is that a significant amount of the acidified aliquot will be lost due to evaporation. This evaporation may lead to a negative bias, as HCl evaporates from solution with the water. In fact, the HCl evaporation may have occurred in the vented flasks of the Na_2CO_3 and the NaOH aliquots, as they resulted in negative n_{CSF} values

(-13 ± 8 µmol and -40 ± 26 µmol, respectively). It is possible that HCl evaporation in $NaHCO_3$ occurred as well, but the CO_2 in the vial headspace overwhelmed the HCl loss. Perhaps the re-dissolution of CO_2 didn't occur in the Na_2CO_3 and NaOH aliquots because they were not sealed as well, meaning both CO_2 and HCl escaped from the vial.

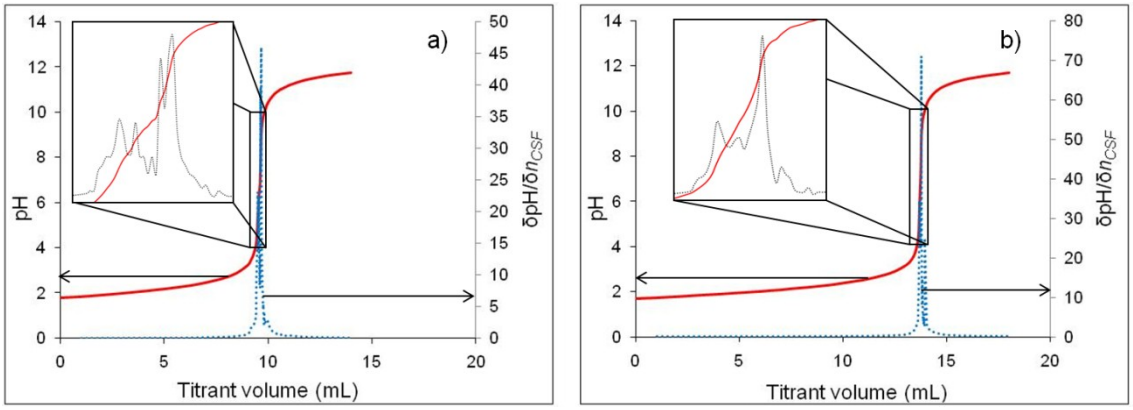

Figure 33. Titration curve (solid) and first derivative of titration curve (dotted) of $NaHCO_3$ blank aliquot after removal of CO_2 through a) heating method and b) refluxing method.

When an acidified blank $NaHCO_3$ aliquot in an open flask was heated to 80 °C for 2 h, with N_2 bubbling through solution, a negative bias of -12 µmol was seen, suggesting that HCl was leaving solution during this heating step. HCl leaving solution while heating could be the cause of the negative biases in the Na_2CO_3 and NaOH results when heated, and the variability in amount of HCl evaporated may be the cause for the large standard deviations seen with these samples.

30 min of heating a blank acidified $NaHCO_3$ aliquot at ca. 80 ºC while bubbling with N_2 in an open vial was, however, sufficient to remove the effect of CO_2 on the titration curve, which is a significantly shorter time than simply degassing with N_2 (Section 5.2.2). 15 min of heating prior to titration was insufficient to remove CO_2,

even with the bubbling of N_2 during titration. Figure 34 includes the titration curves for both 15 and 30 min heating while degassing. A negative bias of -7 µmol was evidenced from the titration that had 30 min of degasification preceding it, likely from a small amount of HCl evaporation, though not enough to affect n_{CSF} values of real samples with carbon. However, a significant volume loss was seen, ca. 30% of the aliquot, which makes the pH measurements difficult as only a very small volume remains after heating when the typical 10 mL aliquot volume is used. Upscaling the aliquot volume to account for this would mean using significantly more carbon in a real sample, and often amounts of samples are limited, making this impractical.

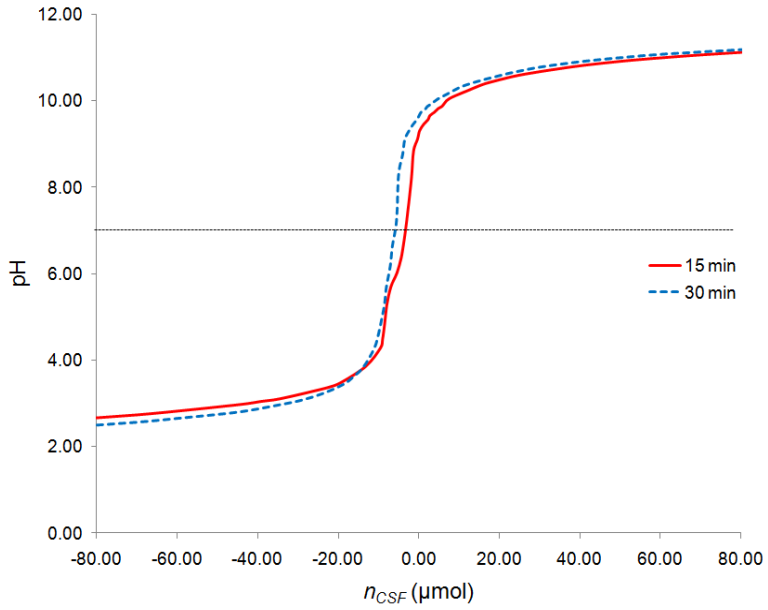

Figure 34. Titration curve of an acidified blank $NaHCO_3$ aliquot subjected to N_2 bubbling during titration and heating prior to titration for 15 min (solid) and 30 min (dashed).

The results discussed show that merely heating the solutions is not a consistent method for the removal of CO_2. Heating may also cause a loss of HCl from the

acidified aliquots leading to a negative bias in the results. It seems that heating, depending on the heating logistics and the sample, either is insufficient to remove CO_2 from aliquots, or it removes HCl as well as CO_2. This unpredictability, in addition to the large standard deviations in the n_{CSF} values, makes this CO_2 removal method inadequate for use in the Boehm titration.

Two inflection points are also seen in the titration curves with the aliquots which were refluxed (see Figure 33b), showing that refluxing the samples may not be sufficient to remove CO_2 effects, and this may be the reason for the large positive bias seen in the Na_2CO_3 results in Table 13. Although there is no evident bias in the data in Table 13 for refluxing of the acidified aliquots of $NaHCO_3$ and NaOH (3 ± 17 μmol and -8 ± 23 μmol, respectively), this is because of the large standard deviations which result from this method. It is likely that these large standard deviations can be explained by the large mass changes experienced during the refluxing. A mass gain (ca. 3 g) was recorded for refluxed samples, unlike the slight mass loss for bubbling and the large mass loss for heating. The unexpected mass gain may be attributed to high air humidity experienced in the geographic region in which these experiments were conducted, which may result in extra water condensing from the air as it touches the cool reflux condenser and adding to the solution contained in the round-bottom flask. This water may introduce CO_2 or impurities into the sample and, since water content in the air varies substantially by the day and region, it is a difficult parameter to control.

With the positive and negative biases and the large variation in the heated and refluxed samples, it is suggested that neither heating nor refluxing the acidified aliquots from the Boehm titration is a reproducible CO_2 removal method, and should not be used.

Additionally, the titration curves in Figure 33 showed that the effect of CO_2 was removed neither by heating nor by refluxing. Heating in combination with degassing with N_2 was successful in removing the effect of CO_2 on the titration, as seen in Figure 34, but resulted in such a large loss of solution as to be difficult to titrate with the aliquot volumes used in the present research.

5.3 Experiments with Carbon

The Boehm titration was carried out on samples of Black Pearls 2000 carbon powder, with CO_2 removal by degassing for 2 h with N_2 prior to titration, with saturation of the aliquots with N_2 during titration, to ensure that this standardization method will work in practice. As expected, the amounts of CSFs on this carbon, shown in Table 14, are all positive, indicating that the surface functionalities noted in the table are present on the carbon surface. The standard deviations are based on triplicate measurements and suggest that this method of CO_2 removal is adequate for samples containing carbon and result in precise data. Although the standard deviations are larger than the blanks using the same method of CO_2 removal, this is due to the variability in the amount of CSFs expected between real samples. Titration curves (Figure 35) performed on these samples using carbon showed no evidence of CO_2, confirming that this degassing procedure is sufficient to remove the CO_2 from solution.

Table 14. Moles of carbon surface functionalities on Black Pearls 2000 carbon, as determined through the Boehm titration using standardized method of CO_2 removal by degassing prior to and during the titration with N_2, and of endpoint determination by a one-point potentiometric measurement.

Functional Groups	n_{CSF} (µmol/g) ± SD
Phenolic	59 ± 14
Lactonic	54 ± 14
Carboxylic	18 ± 5

SD denotes standard deviation based on three replicates

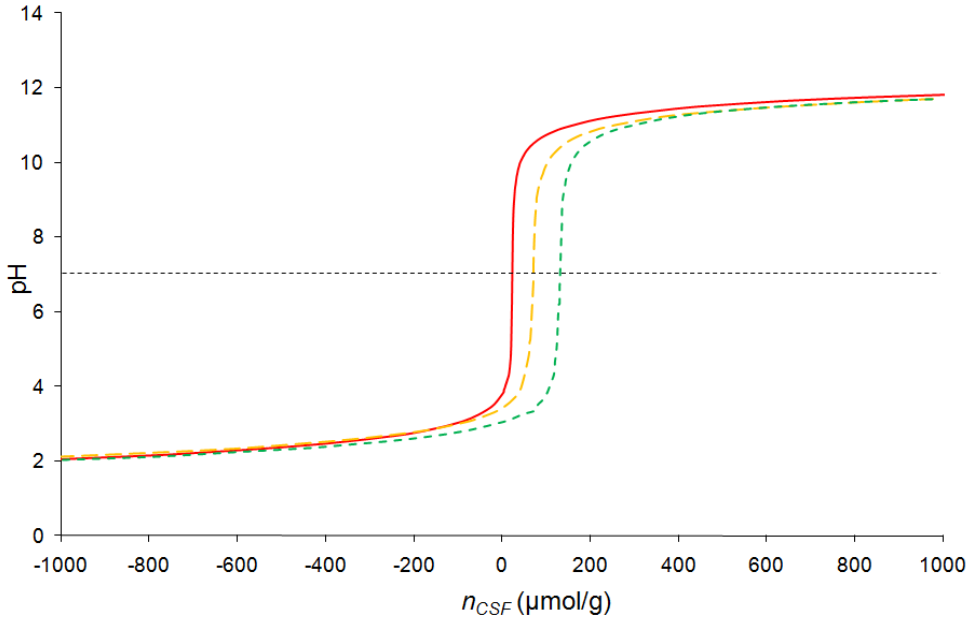

Figure 35. Titration curves of aliquots from Black Pearls 2000 carbon samples reacted with: $NaHCO_3$ (solid); Na_2CO_3 (long dashes); and NaOH (short dashes).

Chapter 6 Carbon Surface Functionalities Determined by the Boehm Titration

Chemical methods are often utilized along with spectroscopic techniques to study carbon samples, as discussed in Section 2.5.1. In this research the Boehm titration was used to complement the spectroscopy employed to identify CSFs on carbon surfaces, and was performed on samples of carbon cloth electrodes to determine how CSFs develop or change during electrochemical cycling. This was done using the method standardized in Chapter 5.

It is known that quinone groups form on carbon cloth with potential cycling[7-9] and there is a redox peak on the CV that corresponds to this. However, no information about other CSFs can be observed based on the CV; no peaks other than the quinone peak are present, or they are hidden by the domination of the quinone peak. Consequently, the Boehm titration was employed to examine the CSFs on electrodes cycled (from 0.0 to 1.0 V vs. SHE at 1.0 mV/s in 1.0 M H_2SO_4, refer to Section 3.1.3 for electrochemical details), for different lengths of time as well as an untreated cloth sample and a cloth sample that had been soaked in electrolyte for one day but not cycled.

Due to the limited amount of Spectracarb 2225 carbon cloth available, the electrolyte-soaked sample was tested for basic groups only, to determine the effect of the acidic electrolyte itself (with no potential cycling) on the basic CSFs such as quinone. Additionally, there was the concern that the reaction base for the Boehm titration could react with residual acidic electrolyte in the electrode pores, and it is not possible to differentiate between base reacting with the acidic groups and base reacting with electrolyte. Results from basic groups on carbon would then be more reliable than

the amounts of acidic groups, leading to the decision to use the remaining cloth available for basic group determination.

Figure 36 is a set of representative CVs, where one cycle from each day is shown for 7 days of continuous electrochemical cycling. The arrows indicate the progression of the cycles, with the peak around 1.0 V decreasing in current and the peak at 0.4-0.7 V increasing in current. The increase in current on the latter peak corresponds to the development of quinone on the surface of the carbon electrode.[7-9, 27]

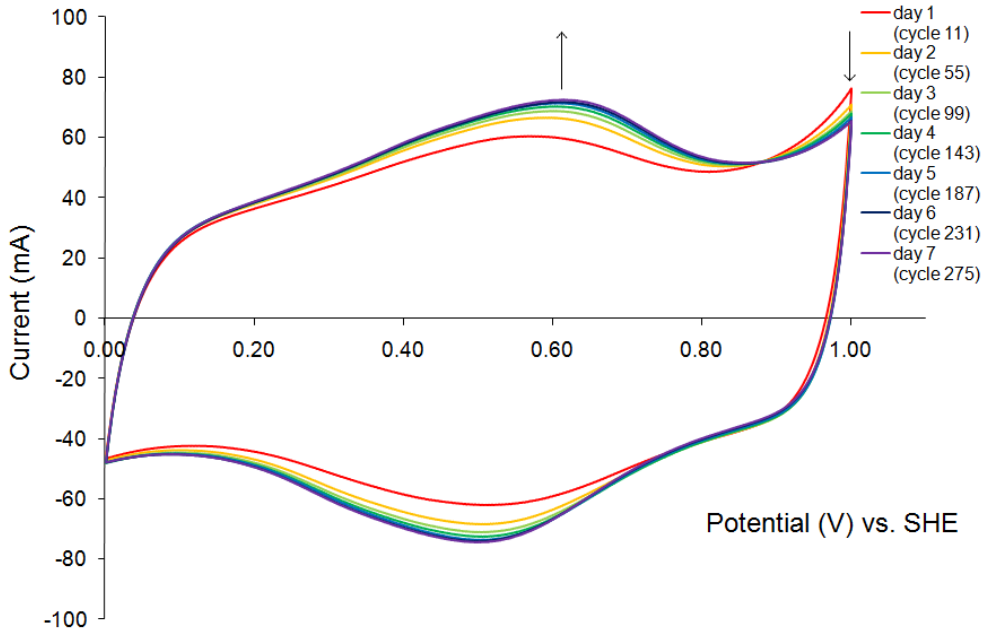

Figure 36. Representative CVs of a Spectracarb 2225 carbon cloth electrode (0.2106 g) for examination in the Boehm titration, as electrochemically cycled continuously from 0.0 to 1.0 V vs. SHE at 1.0 mV/s in 1.0 M H_2SO_4.

Boehm titrations were done in triplicate for each sample. Each sample was made up of four ca. 0.2-g Spectracarb 2225 carbon cloth samples. The electrode samples and the electrolyte-soaked sample were rinsed and soaked with deionized water to remove

electrolyte, and dried in an oven. Refer to Section 3.1.3 for details. The amounts of functional groups on the carbon cloth samples, denoted n_{CSF}, that were neutralized by each reaction base or acid are summarized in Table 15 in terms of micromoles per gram of sample. The calculated amounts of specific CSFs, including carboxylic, lactonic, phenolic and basic groups, are shown in Table 16. The calculations for n_{CSF} are outlined in Section 3.3.5.

Table 15. Average amounts of functional groups on Spectracarb 2225 carbon cloth based on the Boehm titration.

Time of electrochemical cycling (days)	n_{CSF} ± SD (µmol/g)			
	Reacted with $NaHCO_3$	**Reacted with Na_2CO_3**	**Reacted with NaOH**	**Reacted with HCl**
Not cycled	-29 ± 4	203 ± 16	189 ± 3	384 ± 9
1	56 ± 3	318 ± 11	533 ± 9	333 ± 7
2	84 ± 4	413 ± 10	509 ± 18	322 ± 2
4	128 ± 9	438 ± 19	607 ± 4	307 ± 1
7	90 ±10	371 ± 21	704 ± 12	369 ± 5
Not cycled, soaked in electrolyte	--	--	--	139 ± 5

SD denotes standard deviation based on three replicates
-- denotes a measurement not carried out

Table 16. Summary of average amounts of acidic and basic groups on Spectracarb 2225 carbon cloth calculated based on the Boehm titration.

Time of electrochemical cycling (days)	n_{CSF} ± SD (µmol/g)			
	Carboxylic groups	Lactonic groups	Phenolic groups	Basic groups
Not cycled	-29 ± 4	232 ± 17	-13 ± 17	384 ± 9
1	56 ± 3	263 ± 11	215 ±14	333 ± 7
2	84 ± 4	329 ± 11	95 ± 21	322 ± 2
4	128 ± 9	310 ± 21	169 ± 20	307 ±11
7	90 ± 10	280 ± 23	338 ± 24	369 ± 5
Not cycled, soaked in electrolyte	--	--	--	139 ± 5

SD denotes standard deviation based on three replicates
-- denotes a measurement not carried out

Uncertainty calculations were completed assuming random error only, ignoring systematic errors such as bias in the analytical balance and the pH meter, and were calculated using partial derivatives approximations. Partial derivatives were taken for each term in the n_{CSF} equation (Equation 6) and then the terms were combined to propagate the error in each n_{CSF} value calculated. The issue with the Boehm titration for this carbon is that since the values are small, in the µmol/g range, uncertainties become large in comparison to the results. In this case, the factors taken into account in the uncertainty calculations were uncertainties in measuring implements such as volumetric flasks, pipettes, the burette, and the analytical balance.

The uncertainty for each implement is shown in Table 17. The values before averaging with uncertainties are summarized in A 33 in Appendix A.3, while the averaged values with uncertainties for groups reacted with each base, as well as for each specific CSF, are summarized in Tables A 34 and A 35 also in Appendix A.3. For $NaHCO_3$, the uncertainty is on the order of 70 to 90 µmol/g, for Na_2CO_3 from 120 to

140 μmol/g, for NaOH 20 to 30 μmol/g, and for HCl from 15 to 30 μmol/g. Since these are done in triplicate and averaged and subtracted to calculate the different CSFs, once averaging and subtraction occurred the uncertainty values increased to 120 to 160 μmol/g for carboxylic groups, 230 to 280 μmol/g for lactonic groups, 200 to 250 μmol/g for phenolic groups and 40 to 55 μmol/g for basic groups. The solutions of NaOH and HCl were standardized, but the concentrations of the weak acids, $NaHCO_3$ and Na_2CO_3, were calculated based on their measured values of mass and volume; it is the error in the volumetric flasks in which these two solutions were made that cause the high uncertainty values in the n_{CSF} calculated for these two reaction bases. Since the amounts of specific acidic groups are based on subtractions of the number of groups reacted with each base, the high uncertainties are factored into the subtraction calculations, affecting results for each of the three acidic CSFs. Nonetheless, the trends observed in the data presented here will be discussed.

Table 17. Uncertainty values for measurement devices used in the Boehm titration.

Measurement device	Uncertainty
analytical balance	0.02 mg
10.00-mL pipette	0.02 mL
20.00-mL pipette	0.03 mL
50.00-mL pipette	0.05 mL
25.00-mL burette	0.01 mL
500-mL volumetric flask	0.2 mL

With electrochemical cycling, there is an increase in the overall number of acidic CSFs as determined by the Boehm titration (averaged in Table 16). The number of functionalities reacting with NaOH, which neutralizes all the acidic groups studied here, increased as the cycling time increased: the amount of acidic groups before cycling was

189 μmol/g, and reached 704 μmol/g after one week of continuous cycling. Because of the high uncertainties and the fluctuation in the results from the specific acidic CSFs, i.e. carboxylic, lactonic and phenolic groups, it is difficult to determine how each CSF is changing. However, within the first 24 h of cycling, the amount of each acidic CSF increased with electrochemical cycling compared to the uncycled samples: carboxylic groups increased from less than zero to 56 μmol/g with one day of cycling, lactonic groups increased from 232 to 263 μmol/g with one day of cycling, and phenolic groups increased from less than zero to 215 μmol/g after one day.

Some trends can be seen in the formation and depletion of acidic CSFs. The amount of carboxylic groups, for example, increased during four days of electrochemical cycling and then decreased to seven days. The amount of lactonic groups increased during two days of cycling, then decreased. The amount of phenolic groups increased immediately with one day of cycling, decreased with two days, and began to increase again following that. The data presented in Table 16 are average values, but these trends hold for the individual values calculated before averaging as well. From the possible trends seen in the n_{CSF} results calculated, electrochemistry can be said to affect acidic CSFs. If these trends are valid, the fluctuation of the different acidic CSFs with cycling time suggests that electrochemical cycling not only causes CSFs to form, but may cause depletion of CSFs as well, or cause oxides to change from one form to another.

As for the basic groups, these seem to be depleted with potential cycling. The trend for these is also seen in Table 16. However, the lowest value of all the basic groups, 139 μmol/g, was found for the sample that was treated with 1.0 M H_2SO_4

electrolyte for one day without electrochemistry of any kind being performed. Perhaps there are basic groups adsorbed on the surface of the carbon cloth that desorb in electrolyte, as the uncycled carbon sample had 384 μmol/g CSFs, much higher than the sample soaked in electrolyte. If this is the case, then there must be different basic groups that form immediately on the carbon surface with electrochemical cycling but deplete with further cycling. One to four days of cycling had decreasing n_{CSF} values (333, 322 and 307 μmol/g for one day, two days and four days of cycling, respectively) which were lower than the n_{CSF} of the untreated sample, but were still higher than the sample soaked without electrochemistry. The other option is that the sample soaked in electrolyte was simply erroneous.

The exception to the depletion trend with potential cycling is the electrode that was cycled for the longest amount of time, seven days, which had 369 μmol/g of basic CSFs, nearly as much as the untreated sample. Since this is the only cycled electrode sample to not fit with the trend, it may simply be an outlier. Nonetheless, it is possible that there are different basic groups being formed and destroyed simultaneously during electrochemical cycling. This is possible, given the debate over which groups are in fact basic, and so the basic groups present in the carbon samples studied here could be any or a combination of chromenes, ketones or pyrones.[16-20] Conceivably, all of these could be present and affected by electrolyte, electrochemical cycling, or both. Unfortunately, it is not possible to perform an analogous Boehm titration to differentiate between basic CSFs.

The pseudocapacitive quinone peak in the CV for carbon cloth (Figure 36, ca. 0.5 to 0.7 V vs. SHE) increases with amount of cycling. It is possible that there are

other electroactive CSFs that have pseudocapacitive peaks somewhere in the CV, but do not exhibit an intense or a sharp enough peak to be noticed explicitly. The quinone peak is broad, and the potential range where the current increases with cycling time extends from 0.10 to 0.90 V vs. SHE, almost the entire potential window. Some of the current increase, particularly at potentials relatively far away from the most intense portion of the peak, could in fact be due to CSFs other than quinone.

In general, the amount of acidic groups increases with amount of cycling, and so it could be acidic CSFs that contribute to the overall increase in current and therefore capacitance (which is directly proportional to current). Basic CSFs showed a general decrease in amount based on the Boehm titration (aside from the sample electrochemically cycled for seven days). There is a tail on the carbon cloth CV at 1.0 V vs. SHE that decreases with cycling, which could be caused by the depletion of basic CSFs on the surface of the carbon electrode. Further study should be done to determine whether the CSFs identified with the Boehm titration are electroactive and can be seen for certain in the CV.

The overall trends seen, the increase in acidic groups and the decrease in basic groups with continuous cycling, can be compared to previous studies of surface groups on carbon. Electrochemical cycling has been seen to oxidize carbon electrode surfaces.[29, 178, 179] Many studies oxidizing carbon have seen, based on the Boehm titration, an increase in the surface concentration of acidic groups,[79, 80, 84, 165, 180-182] and a decrease in the concentration of basic groups[79, 80, 84, 165] (unless oxidation treatment occurred at high temperature, which was not the case in electrochemical cycling, where basic groups increased[16, 75]).

The apparent trends in CSF changes with electrochemical cycling on the surface of the carbon cloth samples determined by the Boehm titration can also be compared to Section 4.3, where CSFs were identified by x-ray spectroscopy. All the samples that were subjected to the Boehm titration were also examined using XPS and XAS except for the electrode cycled for four days. Additional samples studied by XPS and XAS but not the Boehm titration will not be discussed here. In XPS, peaks corresponding to the ester/phenol (C-O-C,C-OH) group and the carboxylic acid/lactone (O-C=O,HO-C=O) group were present in all samples. The ester/phenol peak, which could correspond to phenolic CSFs, was the most populated in the carbon cloth sample that was electrochemically cycled for one week. This is based on the % area of the peaks fitted in the C1s spectrum. Results from the Boehm titration also suggest that the one week-cycled sample had the highest amount of phenols compared to the samples electrochemically cycled for shorter periods of time. The carboxylic acid/lactone peak in XPS was also the most populated in the XPS sample cycled for one week.

Like the results from the Boehm titration, the XPS results presented above suggest that acidic CSFs increase with cycling time. However, the XPS results do not have the trend itself showing the increase with cycling. Instead, there is a fluctuation in the amounts of acidic groups between all samples cycled less than one week.

The conclusions made here for the XPS results are based on peak fitting and ratios; it is possible that the discrepancy between XPS and Boehm titration results is due to the subjectivity of this type of XPS analysis. For instance, if one of the peaks used to fit the XPS spectrum was made slightly wider than that peak in the spectra of the other samples, then the other peaks used to fit that particular spectrum would become slightly

narrower in the fitting process, affecting the area ratios of all the peaks fitted in that spectrum. As was seen in Table 10 in Section 4.3.1, many of the percent areas of the peaks used to fit spectra are very similar between samples. Thus, a slight change in the fitting process could affect the outcome of this supposedly quantitative analysis. Additionally, the possibility exists that issues in the performance of the Boehm titration could affect results as well. For example, if the reaction base had not fully reacted with the carbon sample before removal of aliquots for titration, or if CO_2 was not properly removed from the titrant before the titration, there could be bias manifested in the calculated results.

A comparison of Boehm titration results with XAS is qualitative only, as quantitative analysis was not carried out. From XAS, it was determined that all the samples contained the C=O peak, which is a group present in all the possible basic CSFs. Since basic CSFs are present in all the samples tested in the Boehm titration, these results agree. Conversely, the C-O bond was only present in XAS spectra for the electrode samples. All the acidic CSFs suggested here contain the C-O bond, but the Boehm titration results suggest that both carboxylic and phenolic groups are not present before electrochemical cycling, as seen in Table 16. Since the C-O peak in the XAS spectra is also only formed on samples that had been electrochemically cycled, this peak is likely due to one or both of carboxylic acid or phenolic groups. The C-O could also represent a C-OH; it could be that the apparent phenolic groups are quinone groups in their reduced form. Since the number of phenolic groups was seen by the Boehm titration to increase with electrochemical cycling, as do quinone groups, it could be that the phenols are related to quinone and caused the current increase in the CV.

Although there are large uncertainties associated with the results shown here, if precision can be improved the Boehm titration can be a suitable method to determine CSFs and to compare with the findings from spectroscopic techniques. The results here showed that acidic CSFs are formed by electrochemical cycling, whereas basic groups are generally depleted. The increase in current over the majority of the potential window with electrochemical cycling can be attributed to the formation of acidic CSFs, including carboxylic acids, phenols and possibly the reduced form of quinone, whereas the peak at the high end of the potential window (1.0 V vs. SHE) could be from basic groups on the surface of the carbon that deplete with continuous potential cycling.

Chapter 7 Polymer Electrodes

As discussed in Section 2.4, polymers can be used as EC electrodes. Polyaniline (PANI) was studied first in this project, principally as it has been widely studied in the literature and its CV is well-known. To combine two polymers is common, in order to combine the properties of each material. For example, the PANI CV exhibits peaks at specific potentials for its redox reactions. Combining another polymer with PANI could cause a capacitance increase in potential regions of the CV where PANI does not have peaks. Polypyrrole (PPy) was chosen, as it has also been much studied. Recently, as mentioned in Section 2.5.3, the copolymer of PANI and PPy has been made for EC application specifically. However, these particular copolymers were made chemically. Other studies combining PANI and PPy used potentiostatic or galvanostatic polymerization. Additionally, both of the polymers PANI and PPy have been studied using spectroelectrochemistry; the copolymer, however, has not. The overall object of this thesis was to perform spectroelectrochemistry on EC electrodes. The goal for this project, then, was to achieve polymerization of both the homopolymers and the copolymer through electrochemical cycling, and to obtain UV-Vis-NIR spectra while doing so.

7.1 Polyaniline

Initially, PANI was polymerized electrochemically through cyclic voltammetry on a gold wire (see Section 3.1.4), to ensure that the polymer could be developed this way and that the resulting CVs would compare with literature studies. Typically cycling of PANI is done from a potential of 0.00 V vs. SHE (-0.22 V vs. Ag/AgCl) to a potential

of ca. 1.00 to 1.20 V vs. SHE (0.78 V to 0.98 V vs. Ag/AgCl).[13, 55, 58, 60, 183] To observe what would change in the CV of PANI if it was cycled to higher potentials, it was first cycled from 0.00 to 1.60 V (-0.22 to 1.38 V vs. Ag/AgCl), and then 0.00 to 1.30 V (-0.22 to 1.08 V vs. Ag/AgCl) using non-purified aniline monomer in a large three-compartment electrochemical cell containing ca. 100 mL of 1.0 M H_2SO_4 electrolyte, using a SHE reference electrode and platinised platinum mesh as a counter electrode.

The difference between these two CVs can be seen in Figure 37. It seemed that oxygen evolution began around a potential of 1.40 V vs. SHE. The process of gas evolution destroys the electrode, and is therefore undesirable. The more limited potential window was adequate, its peaks corresponding with those in the literature. The polymer film builds with cycling, with a corresponding increase in current,[55] as seen in Figure 38. The polymer could also be seen visually on the wire: at low potential the polymer was pale green, which darkened as potential increased to become black.

The shape of the CV is similar to what is seen in literature.[55, 183] The peaks in the CV correspond to three redox couples, from low to high potential: the transformation between leucoemeraldine and emeraldine, ca. 0.2 to 0.4 V vs. SHE (0.0 to 0.2 V Ag/AgCl),[58-61] to degradation products, ca. 0.6 to 0.8 V vs. SHE (0.4 to 0.6 V vs. Ag/AgCl),[58, 62, 63] and to the transformation between emeraldine and pernigraniline, ca. 0.8 to 1.0 V vs. SHE (0.6 to 0.8 V vs. Ag/AgCl).[58, 60, 61] Different potential windows within the 0.00 to 1.30 V range are shown in Figure 39; the varying current is due to the continued polymerization of PANI from remaining aniline monomer in the electrolyte. This figure displays the reversibility of the CV by its mirror-image shape about the x-axis, and the vertical lines upon switching to the reverse potential. Reversibility is one

of the key characteristics of ECs, and is important for regeneration of the electrode so that it can be used many times (see Section 2.1).

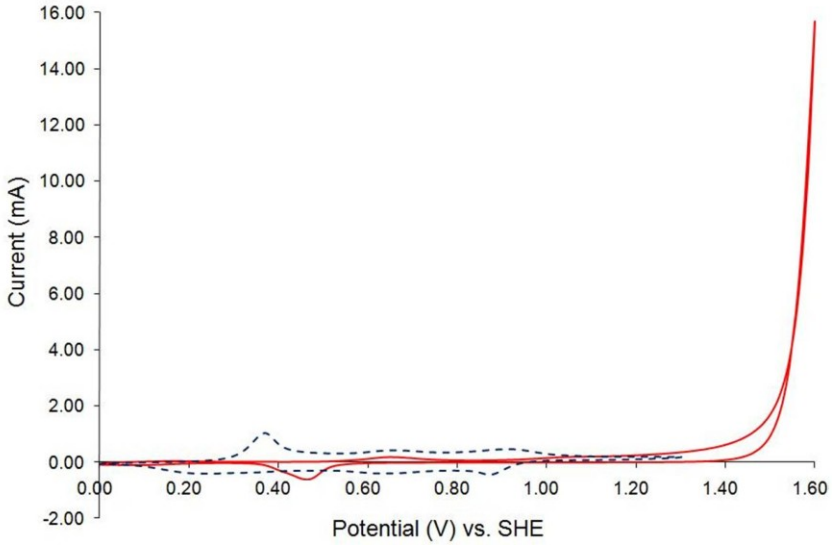

Figure 37. Comparison of potential windows for PANI polymerized on Au wire by electrochemical cycling at 100 mV/s in 1.0 M H_2SO_4 containing aniline monomer, from 0.00 to 1.60 V vs. SHE (solid) and from 0.00 to 1.30 V vs. SHE (dashed).

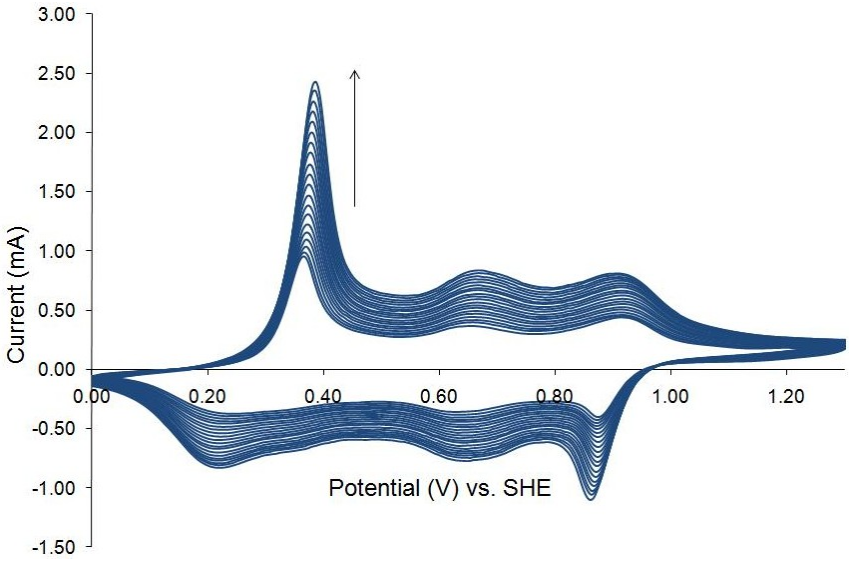

Figure 38. Electropolymerization of PANI on Au wire by electrochemically cycling at 100 mV/s from 0.00 to 1.30 V vs. SHE in 1.0 M H_2SO_4 containing aniline monomer (cycles 3-20). The arrow shows the direction of current change with increasing number of cycles.

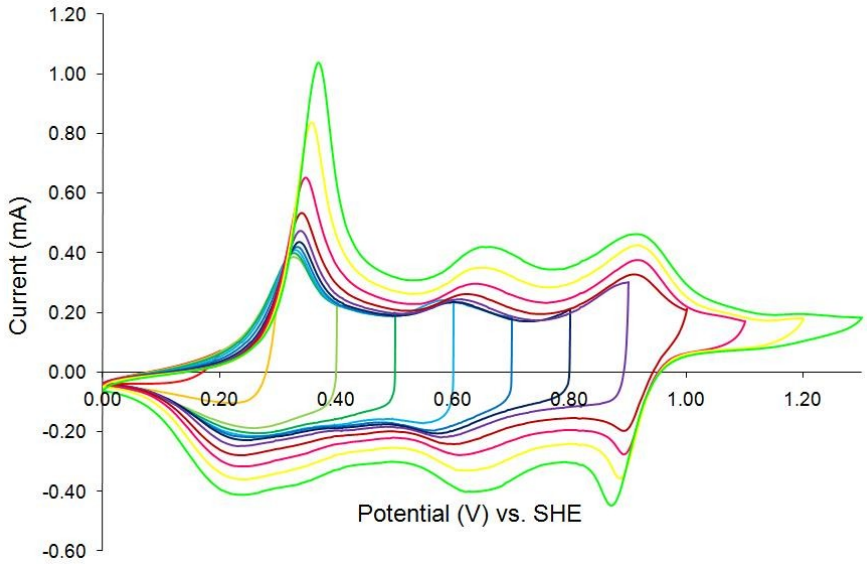

Figure 39. Various potential windows for PANI electrochemically cycled on Au wire, in 1.0 M H_2SO_4 containing aniline monomer at 100 mV/s.

For spectroelectrochemistry, the electrochemical cell would be a UV-Vis-NIR cuvette containing ca. 2-3 mL electrolyte, and no reference compartment for the SHE. Consequently, a Ag/AgCl reference electrode was used, which has a potential of +0.22 V vs. SHE and the working electrode was changed from a gold wire to a platinum mesh, which would be required as the optically transparent electrode for spectroscopy measurements. Before spectroelectrochemistry was attempted, a small three-compartment electrochemical cell containing 10 mL of electrolyte was used with the above electrodes, and with a counter electrode of platinised platinum mesh as before. PANI was developed on the working electrode again using cyclic voltammetry with electrolyte containing the monomer, this time purified, from -0.20 to 1.10 V vs. Ag/AgCl (0.02 to 1.32 V vs. SHE; values were rounded to the nearest 0.1 V for these experiments), as seen in Figure 40. The CVs are similar here as on gold, with three main oxidation and reduction peaks; however, there is an additional peak in the 0.4 to

0.6 V range. This double peak has been seen in the literature.[58, 63, 184] The peak at the lower potential of this double peak was explained to be possibly from quinone,[58] but the second peak was not explained. The region in general is said to be due to the formation of degradation products, as mentioned previously. Perhaps the separation of peaks seen here, compared to the polymerization of PANI on gold, is due to the use of a purified monomer, causing the peaks to be better resolved.

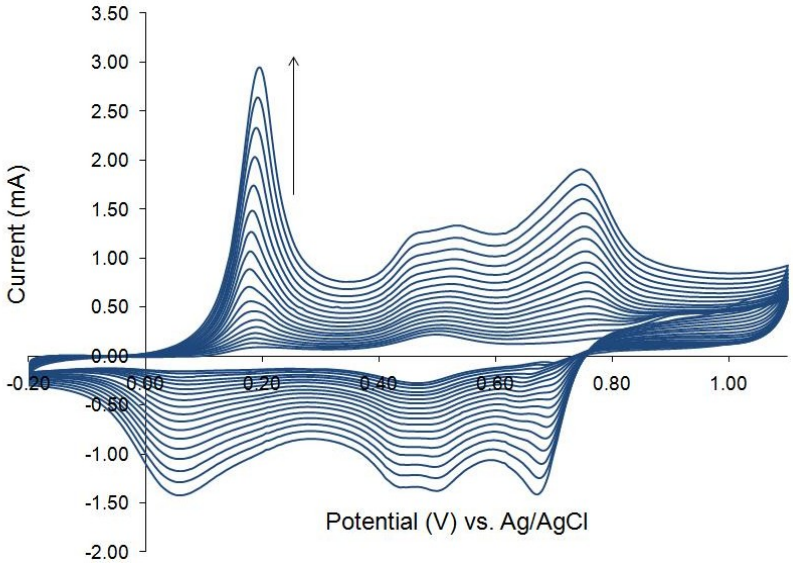

Figure 40. Electropolymerization of PANI on Pt mesh at 100 mV/s in 1.0 M H_2SO_4 containing aniline monomer (cycles 3-20).

Continuous cycling was performed with aniline in the electrolyte to determine how long the film would form and continue to be reversible, seen in Figure 41. By cycle 75, the peaks from the transformation between the oxidation forms of PANI had decreased and the peaks from degradation products increased, which agrees with the literature.[62] By cycle 221 the peaks present had shifted in potential significantly, becoming more irreversible. It seems based on the CVs seen here that 20 cycles are

enough to form a PANI polymer yielding a CV with clearly isolated peaks without becoming irreversible.

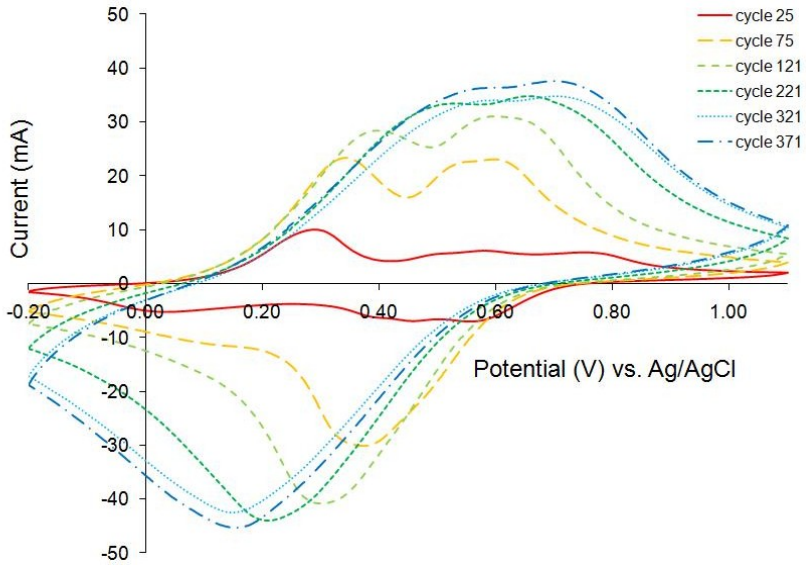

Figure 41. Continuous electropolymerization of PANI on Pt mesh at 100 mV/s in 1.0 M H_2SO_4 containing aniline monomer.

Electropolymerization was also performed *in situ* in a UV-Vis-NIR cuvette to observe changes in the spectrum during film formation, using the same potential window of -0.20 to 1.1 V vs. Ag/AgCl (0.02 to 1.32 V vs. SHE) (setup explained in Section 3.2.1.3). The progression of the polymerization can be seen in the CVs shown in Figure 42. The three main peaks seen in previous PANI CVs (Figure 38) are seen again here; however, the two peaks associated with transformation of the forms of PANI (ca. 0.2 and 0.7 V vs. Ag/AgCl) are much smaller in size than the peak due to degradation products (ca. 0.5 V vs. Ag/AgCl), whereas in the previous CVs the degradation peaks were small. Although the aniline concentration used was the same as in the electrochemical cell used previously, there are fewer aniline molecules in the

cuvette. For this reason, it could be that there is less polymerization of PANI. Additionally, it has been said that the degradation peaks in PANI CVs are from oxidation from water in aqueous electrolyte.[58] It was not possible to fit tubing into the cuvette to degas the solution to purge it of oxygen, so it may be that dissolved oxygen in solution contained in the cuvette exerted a large influence on the CV because of the small volume in addition to the oxygen from water. The decrease in PANI polymerization with the increase in oxidation due to dissolved oxygen could account for the change in the relative intensities of the peaks. Additionally, there is a peak at -0.2 to 0.0 V vs. Ag/AgCl that corresponds to the underpotential deposition peak for adsorbed hydrogen on platinum (Hupd),[185] which indicates that the platinum is exposed, suggesting a porous film formation.

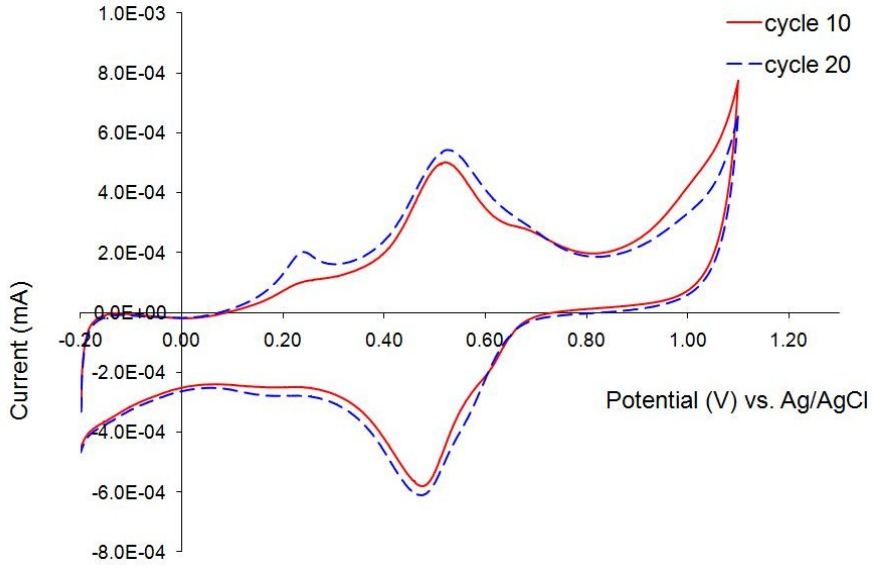

Figure 42. Electropolymerization of PANI on Pt mesh at 100 mV/s in 1.0 M H_2SO_4 containing aniline monomer during UV-Vis-NIR spectroscopy.

Figure 43 shows UV-Vis-NIR spectra collected during the polymerization. The region from 650 to 1300 nm has very little change in absorbance after the initial increase from the first electropolymerization cycle, but the UV and 1350 to 1400 nm regions show a consistent increase in absorbance throughout the cycling process. That the absorbance increases with amount of electropolymerization suggests that the film is forming on the platinum mesh,[61] increasingly absorbing the light as the polymer increases in thickness. The peaks in the UV region, from 200 to 300 nm, have been seen in literature[129, 186] and may be due to molecular conjugation of the polymer.[129] The peak around 350 nm can be attributed to a π-π^* transition in the benzenoid rings of the structure,[60, 128, 186-188] and the peaks around 450, 600 and 800 nm are caused by polaron band transitions.[60, 128, 129, 133, 187, 188] In the NIR region, the peaks from 900 to 1000 nm may be due to O-H overtone vibrations from water, the peak around 1150 nm is from the C-H aromatic overtone vibration and 1360 nm may be due to a C-H combination vibration.[189]

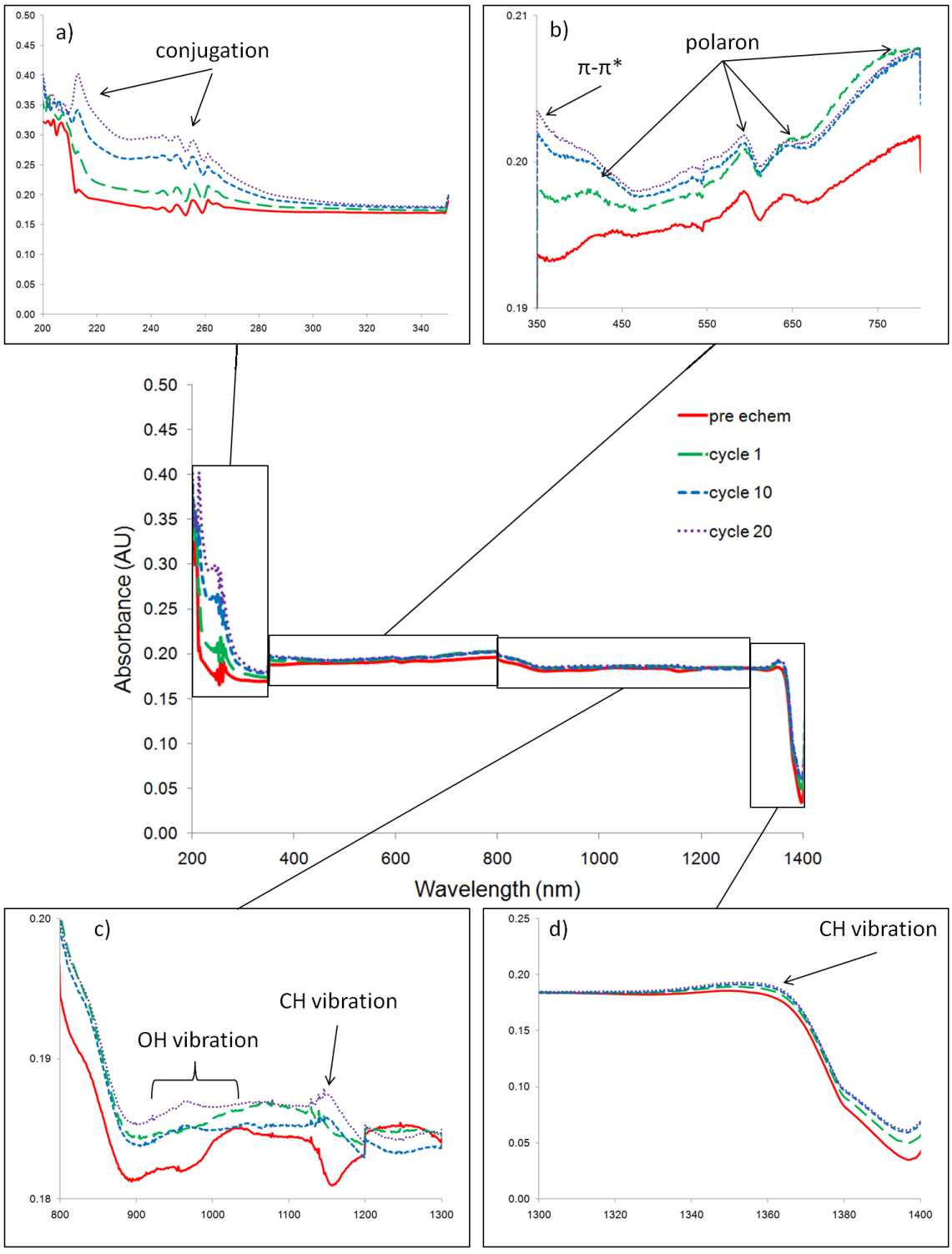

Figure 43. UV-Vis-NIR spectra before ("pre echem") and during electropolymerization of PANI (after cycles 1, 10 and 20), with insets a) 200 to 350 nm; b) 350 to 800 nm; c) 800 to 1300 nm; and d) 1300 to 1400 nm.

PANI can be seen with the naked eye to change colour as potential increases. Spectra were collected while holding at certain potentials after PANI was formed, shown in Figure 44, to see whether this colour change could be seen in the absorbance spectrum. Since PANI has three different oxidation forms at different potentials (for this study, leucoemeraldine from -0.2 to 0.2 V, emeraldine from 0.2 to 0.8 V and pernigraniline from 0.8 to 1.1 V vs. Ag/AgCl), it could be that the difference in spectra was due to changes in absorbing properties of the different oxidized forms of PANI. Given the identities of the peaks in the spectra, the peak locations would not be expected to change significantly, but there is a general increase in absorbance with increasing potential in the UV and visible regions, which can be particularly seen at the highest potentials of 0.80 and 1.00 V vs. Ag/AgCl. This has been seen before in the visible range[133] and can be explained by the more PANI is oxidized, the darker it gets and the more light is absorbed. In the NIR region the spectra change in absorbance only slightly.

To further explore this, absorbance at specific wavelengths was collected as potential increased, shown in Figure 45. In general, the absorbance did not change with potential, except for a slight increase in the absorbance of the wavelengths in the visible range (400 and 590 nm). Again, since PANI is seen to darken to black as potential increases, this likely accounts for the absorbance increase in this region. The biggest change can be seen in the absorbance collected at 240 nm, which decreased from -0.2 to 0.4 V vs. Ag/AgCl, followed by a period of increasing absorbance up to 1.1 V. It could be that degradation products appeared at the potential of the lowest region of absorbance, breaking up the molecular conjugation that is manifested in the UV region.

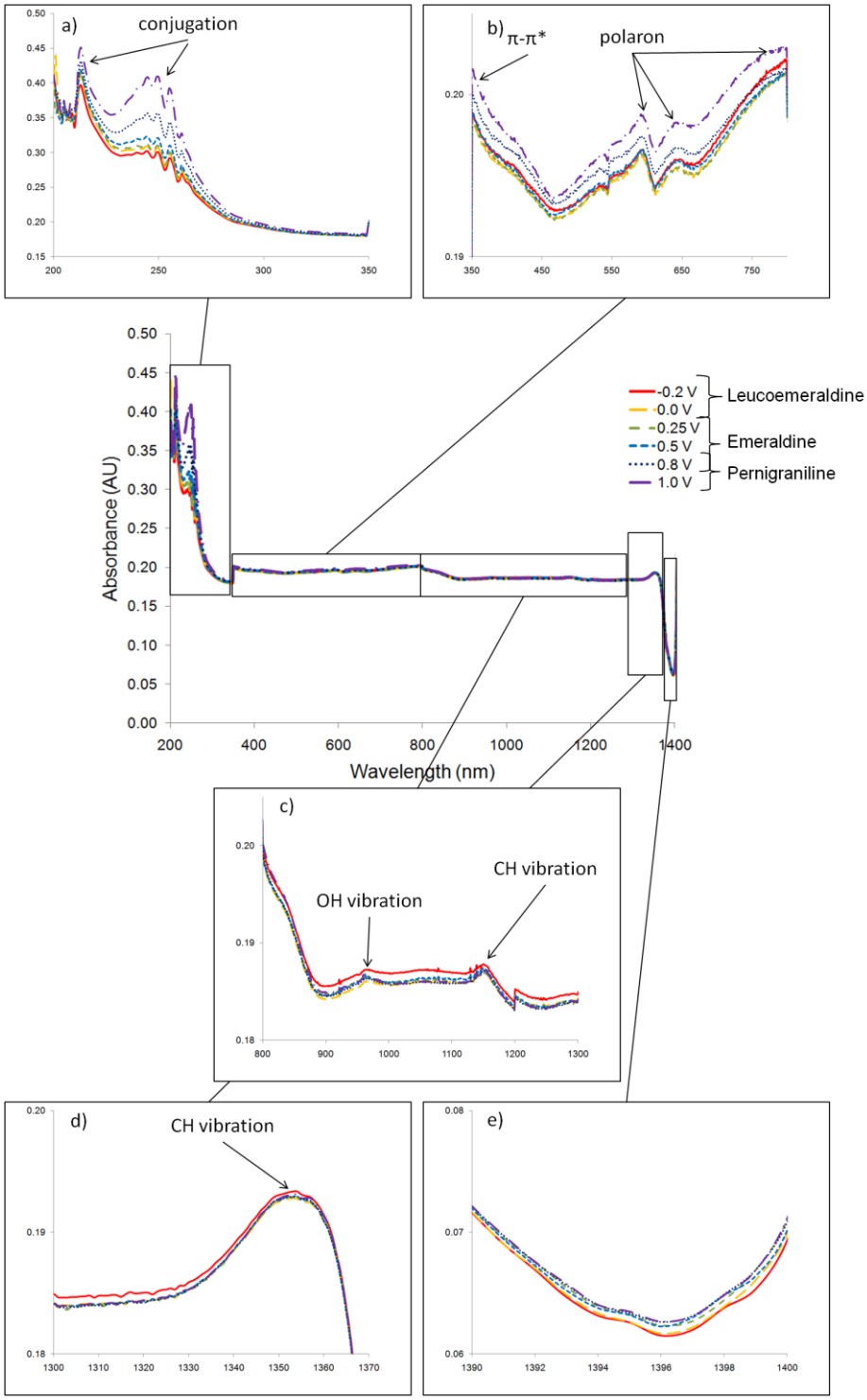

Figure 44. UV-Vis-NIR spectra of PANI while holding at different potentials vs. Ag/AgCl with insets a) 200 to 350 nm; b) 350 to 800 nm; c) 800 to 1300 nm; d) 1300 to 1370 nm; and e) 1370 to 1400 nm.

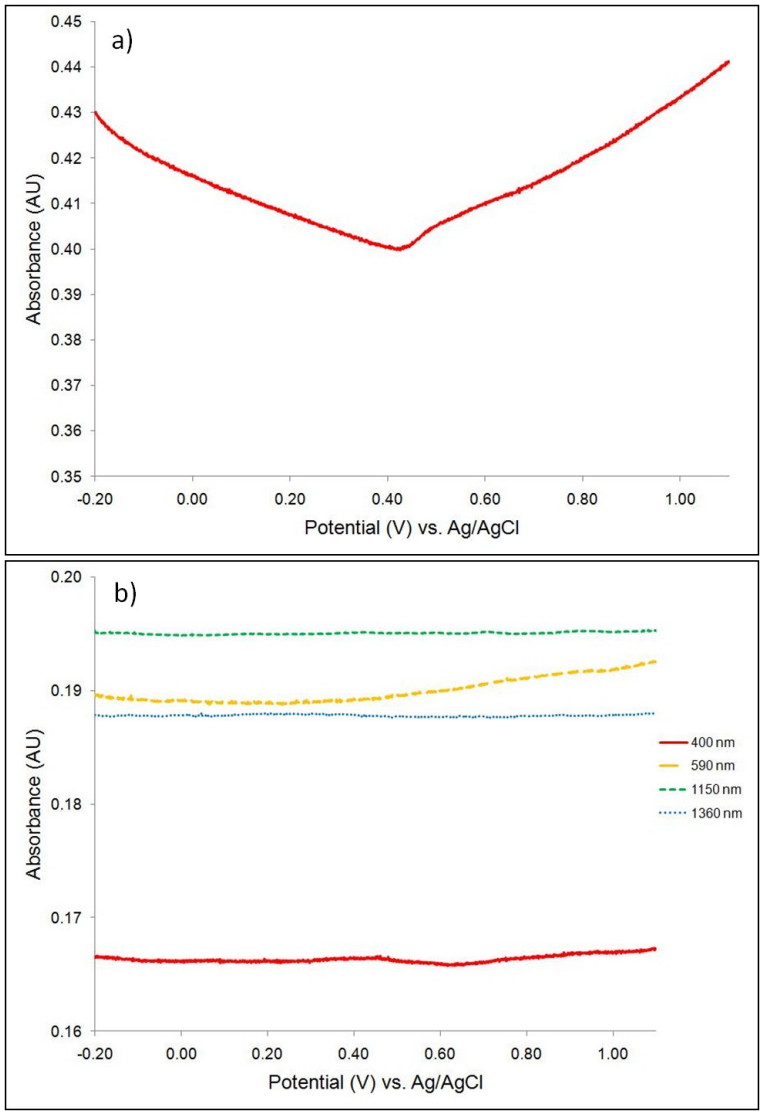

Figure 45. Absorbance measurements on PANI during linear potential sweep from -0.20 to 1.10 V vs. Ag/AgCl at a) 240 nm and b) wavelengths in the visible and NIR range.

The polymerization of PANI was achieved through electrochemical cycling from -0.2 to 1.1 V vs. Ag/AgCl (0.0 to 1.3 V vs. SHE), and the CV matched what has been seen in literature. The spectroelectrochemical experiment was successful as well, and UV-Vis-NIR spectra showed that the polymer formed with potential cycling by an

increase in absorbance with an increase in cycling time. Collecting spectra while holding the potential of the polymer constant, as well as measuring absorbance at specific wavelengths while scanning the potential, showed that in general, the more PANI is oxidized the more light is absorbed by the polymer.

7.2 Polypyrrole

As with PANI, PPy electropolymerization was done on platinum mesh in a small three-compartment electrochemical cell (10 mL of electrolyte) in preparation for spectroelectrochemistry, using the same electrode materials (experimental details in Seciton 3.1.4). Since PPy CVs vary in the literature,[64, 65, 67, 141, 144, 156, 190, 191] a wide potential window was tried initially, from -0.27 to 1.48 V vs. Ag/AgCl (-0.05 to 1.70 V vs. SHE) to observe the CV for the conditions used here. The electropolymerization using this potential window is seen in Figure 46, and the CV looks irreversible (i.e. it is not a mirror image about the x-axis). The arrows show the direction of the current change with cycling; the CV tilts from a horizontal shape to a diagonal shape with cycling, and has an irreversible oxidation peak. This agrees with the statement made in the literature review of PPy in Section 2.5.3, that irreversible oxidation of PPy occurs at high potentials.[62, 64, 65]

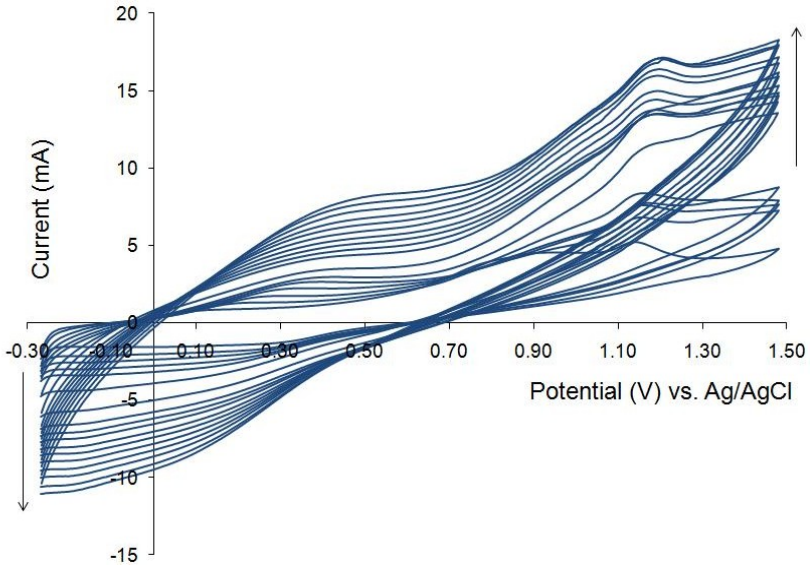

Figure 46. Electropolymerization of PPy on Pt mesh at 100 mV/s in 1.0 M H_2SO_4 containing pyrrole monomer, full potential window (cycles 4-20).

Electropolymerization was also done using a smaller potential window, cycling from -0.27 to 1.10 V vs. Ag/AgCl, to match the upper potential limit used for PANI, as the copolymer of these two polymers will be formed in the next study (Section 7.3). The electropolymerization is shown in Figure 47, and the CV shape is similar to two shown previously.[156, 190] In both potential windows the film could be seen forming as a black film on the platinum working electrode. In the smaller potential window the CV exhibits the same tilt to diagonal, indicative of resistance. It could be that as PPy forms, it becomes thick, making it difficult for ions to diffuse into pores – or through the film, depending on the polymer structure – during charging and discharging. Since the goal of the polymer project was to form the PANI/PPy copolymer, and as discussed above, the PANI polymerization cannot go to a potential higher than 1.1 V vs. Ag/AgCl (1.3 V vs. SHE), the potential window use for PPy was kept restricted to the potential window of PANI. The broad peak from 0.3 to 0.6 V vs. Ag/AgCl is due to oxidation of the ring

in the PPy structure by water.[64] Oxidation in PPy occurs on one of the ring carbon atoms until eventually at high enough oxidation C=O bond is formed.[64]

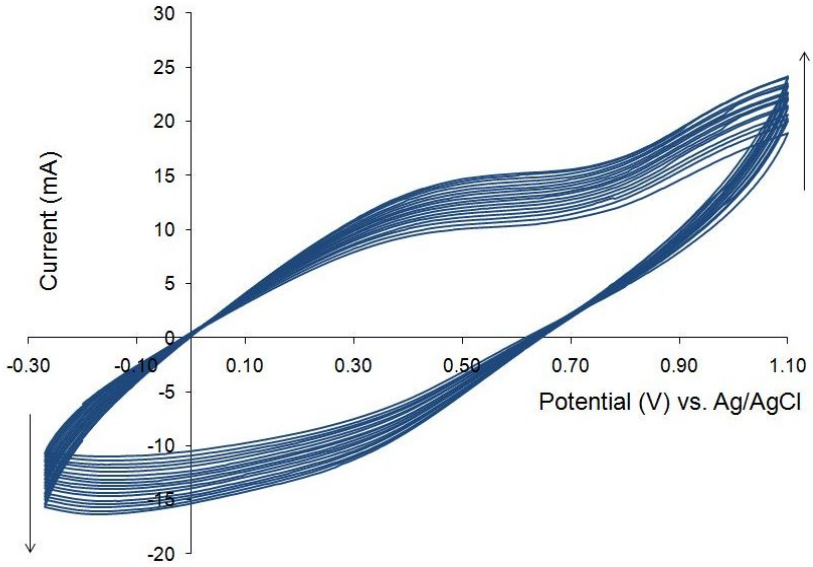

Figure 47. Electropolymerization of PPy on Pt mesh at 100 mV/s in 1.0 M H_2SO_4 containing pyrrole monomer in smaller potential window (cycles 4-20).

PPy electropolymerization was also performed along with UV-Vis-NIR in a cuvette (see Section 3.2.1.3 for experimental details). The polymerization CVs can be seen in Figure 48 to be different from the previous PPy CVs. The broad peak around 0.4 V vs. Ag/AgCl due to ring oxidation is missing, whereas there is a peak around -0.1 V that has appeared in this CV, characteristic of the Hupd peak for platinum[185], again suggesting a porous film. The peak from 0.8 to 1.1 V may be due to Pt oxidation; however, since it is broad, it seems that the oxidation is slow, which could be due to polymer film buildup.

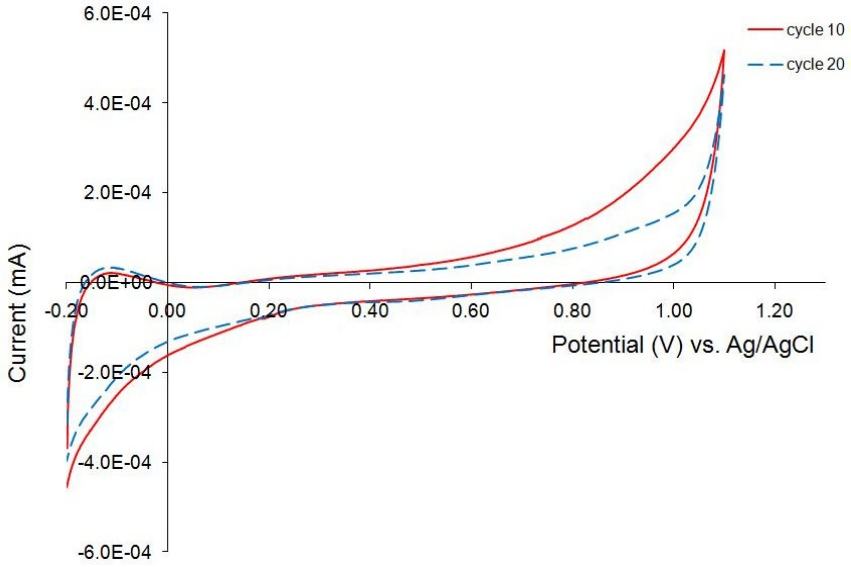

Figure 48. Electropolymerization of PPy on Pt mesh at 100 mV/s in 1.0 M H_2SO_4 containing pyrrole monomer during UV-Vis-NIR spectroscopy.

Figure 49 shows the spectra collected during the PPy polymerization. That the absorbance increased by the end of the electrochemical cycling time suggests a PPy film building on the platinum mesh, despite not seeing PPy peaks in the CV. Most notably there is a peak at 450 nm that increases drastically with polymerization. This presumably corresponds to the peak reported in the literature present anywhere from 400 to 600 nm,[66, 67, 136, 148] and is attributed to the high-energy polaron transition.[67, 136] The peak around 850 nm could be due to oxidation of the pyrrole ring,[192] and the peak around 970 nm can be attributed to a stretching overtone of O-H from water.[189] The peak around 1150 nm could be due to a C=O stretching vibration,[189] caused by oxidation of the pyrrole ring at high potentials.[64] The C-H vibration occurred around 1360 nm like in PANI, with the addition of a second C-H overtone vibration around 1390 nm. Aside from the steady increase of the 450 nm peak, the absorbance level seemed to decrease

slightly as cycling time increased, until the last cycle. Additionally, the spectra exhibit the same shape as the spectrum taken of the electrochemical cell prior to electrochemical cycling, except for the peaks at 450 and 1150 nm, which only appeared with cycling, and there are peaks in the UV region associated with the pyrrole monomer[158] that decrease after 20 electropolymerization cycles. It could be that the monomer in solution exerted an influence over most of the spectra except for the peaks at 450 and 1150 nm, and the monomer concentration decreased as cycling progressed and the polymer formed. By cycle 20, the PPy had become thick enough to dominate the spectrum and absorbance increased.

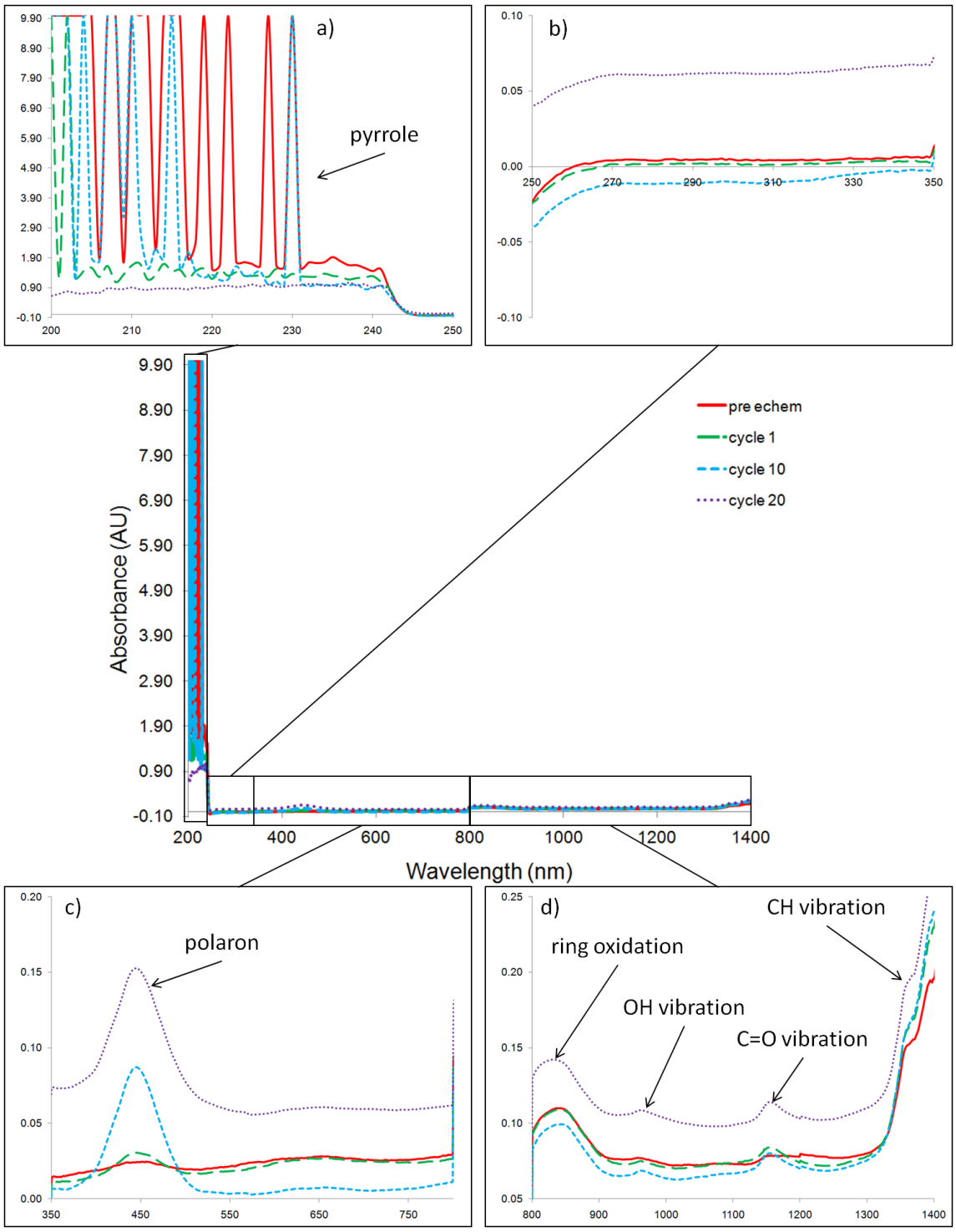

Figure 49. UV-Vis-NIR spectra taken before ("pre echem") and during electropolymerization of PPy (after cycles 1, 10, 20) with insets a) 200 to 250 nm; b) 250 to 350 nm; c) 350 to 800 nm; and d) 800 to 1400 nm.

Spectra were also collected while holding at various potentials, shown in Figure 50. The visible and NIR regions both increased in absorbance at increased potentials, perhaps due to darkening of the film with oxidation as was seen with PANI. Absorbance in the UV region did not exhibit such a trend. From 250 to 350 nm the absorbance increased with potential except at -0.20 V, where the absorbance was at a level between the spectra for 0.40 V and 0.70 V vs. Ag/AgCl. There also seemed to be some process affecting the region from 200 to 250 nm, particularly at 0.4 and 0.7 V, though the identity of this process is unknown (typically spectra in literature studies did not go to a lower wavelength than 300 nm). There are C-O and C=O transitions that occur in this region, and so it can be hypothesized that the peaks in the UV region were due to oxidation of the polymer, associated with the peak around 0.4 V seen in the CV of Figure 47.

A study of the absorbance at specific wavelengths while scanning the potential of the polymer is shown in Figure 51. In general, the absorbance remained constant with some minor fluctuations throughout the visible and NIR ranges. However, the potential did seem to influence the absorbance in the UV region significantly, as was also seen in Figure 50.

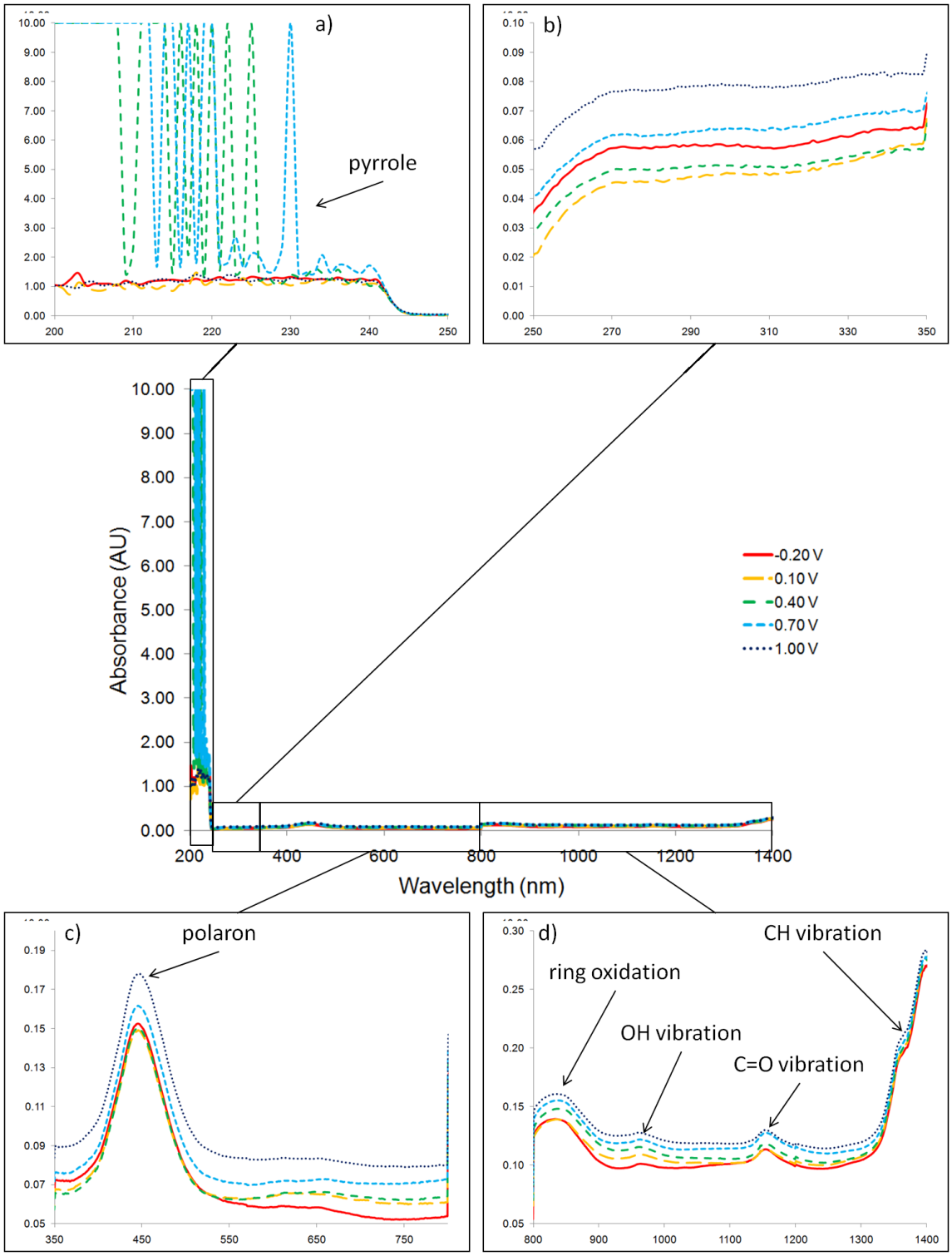

Figure 50. UV-Vis-NIR spectra of PPy while holding at different potentials vs. Ag/AgCl with insets a) 200 to 250 nm; b) 250 to 350 nm; c) 350 to 800 nm; and d) 800 to 1400 nm.

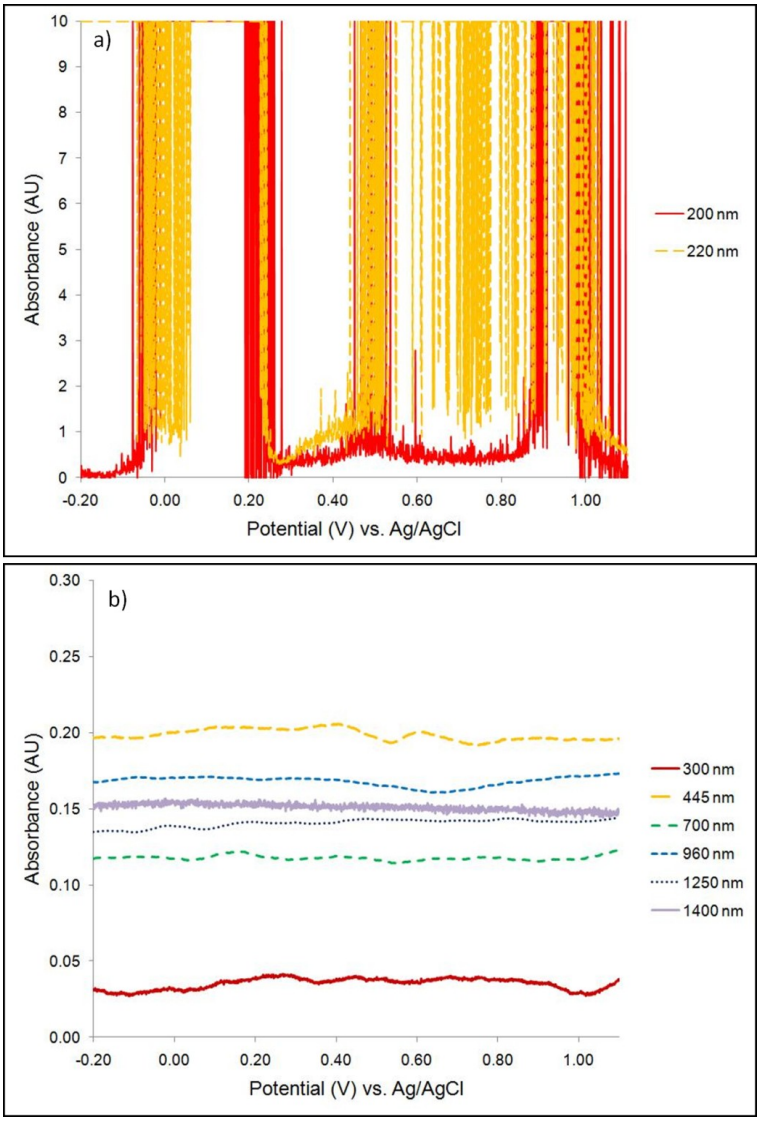

Figure 51. Absorbance measurements on PPy during linear potential sweep from -0.20 to 1.10 V vs. Ag/AgCl at a) UV wavelengths and b) wavelengths in the visible and NIR range.

PPy was successfully formed by electrochemical cycling, both in a standard electrochemical cell and in a small cell for spectroelectrochemistry. UV-Vis-NIR spectra supported the formation of the polymer by characteristic peaks. Spectra obtained while holding potential and the measurement of absorbance while scanning

potential showed the change in the absorbance characteristics of PPy based on potential, where low potentials in particular caused a fluctuation of absorbance in the UV region.

7.3 Copolymer of Polyaniline and Polypyrrole

One of the goals of studying polymers here was to polymerize the copolymer of PANI and PPy, which has recently been discussed as an electrode material for ECs, and to perform spectroelectrochemistry, specifically collecting UV-Vis-NIR spectra during electropolymerization. Ideally, the copolymer obtained would have increased capacitance overall compared to the PANI homopolymer.

Before spectroelectrochemistry was attempted, different methods of forming the copolymer were compared, all variations of electropolymerization using cyclic voltammetry; this technique was chosen as it was not found to be used previously (experimental details in Section 3.1.4). Firstly, electrocopolymerization (simultaneous electropolymerization of both polymers) was tried in the small, 10-mL electrochemical cell, using both monomers in approximately equal concentrations, 0.01 M, in the 1.0 M H_2SO_4. Two potential windows were used, the same as with PPy: -0.27 to 1.48 V vs. Ag/AgCl (-0.05 to 1.70 V vs. SHE), and -0.27 to 1.10 V vs. Ag/AgCl (-0.05 to 1.32 V vs. SHE). The resultant CVs from this deposition method are shown in Figure 52 and compared with CVs for PANI and PPy. Since the electrocopolymerization in the wider window seemed to be dominated by pyrrole, given the irreversible behaviour also seen for the electropolymerization of PPy, the smaller window was tried. It was thought that since this is restricted to the maximum potential used in the electropolymerization of PANI, PANI would have no risk of being destroyed due to gas evolution and would

have some influence on the CV. Unfortunately, the CV within this smaller window was also dominated by PPy. Since the goal was to increase overall capacitance in the copolymer compared to PANI, which would be seen in the CV as an increase in current in the regions where PANI did not have redox peaks, this electrocopolymerization method, using equal amounts of both monomers, was deemed inappropriate.

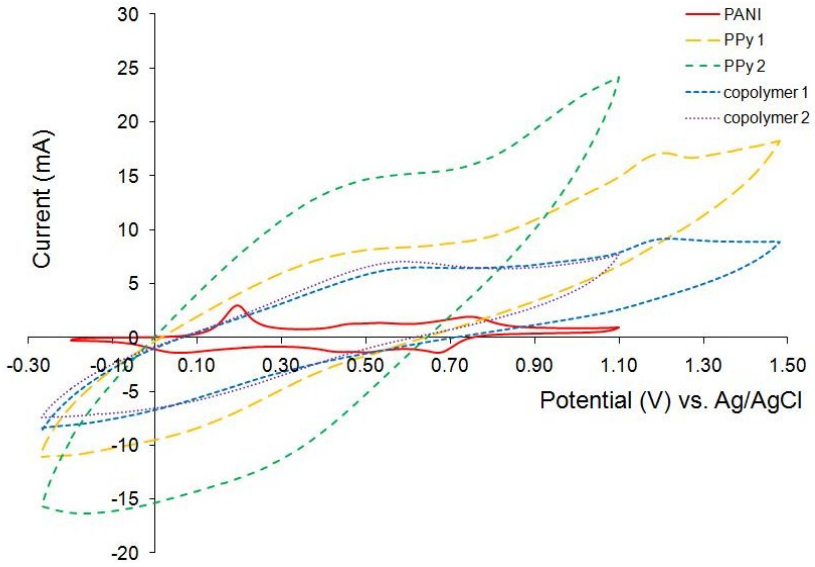

Figure 52. Comparison of electrocopolymerization of PANI and PPy on Pt mesh at 100 mV/s in 1.0 M H_2SO_4 with equal concentrations of aniline and pyrrole with PANI and PPy CVs (cycle 20 for each polymer).

It is not known whether the PPy polymer here formed a film or a porous layer, but if it formed a film, then it may be possible to form a PANI layer on top of PPy, and if it formed a porous layer, then PANI may diffuse into the pores. To study this, aniline was added to electrolyte (for a concentration of 0.01 M) after PPy had polymerized for 20 cycles (from 0.01 M pyrrole), and cycling was resumed using the potential window used earlier for PANI (-0.20 to 1.10 V vs. Ag/AgCl) resulting in Figure 53. As electropolymerization progressed, the current decreased and the CV became more

horizontal. Since capacitance is directly proportional to current, the capacitance was also decreasing. With the CV shape becoming more horizontal, the resistance may have been decreasing as well. This could suggest that PANI did not form on top of PPy but either reacted with PPy to form a new material, or that PANI diffused into the pores of PPy, which made the polymer less resistive but decreasing the current.

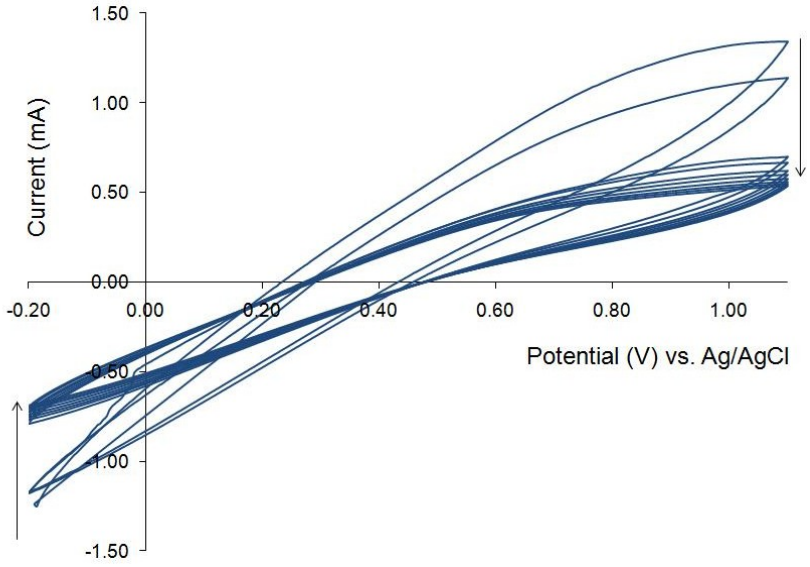

Figure 53. Electropolymerization of PANI on previously-polymerized PPy on Pt mesh at 100 mV/s in 1.0 M H_2SO_4 (cycles 1-20).

Next, PPy was polymerized over PANI that had been electropolymerized for 20 cycles, again using monomer concentrations of 0.01 M and a potential window of -0.20 to 1.10 V vs. Ag/AgCl: the CV of the PPy part of the electropolymerization is shown in Figure 54. This time current increased on the anodic scan, above 0.0 V, and on the cathodic scan between 0.5 and -0.2 V vs. Ag/AgCl; this region in fact resulted in close to a constant current. This CV, though better than the CVs from the previous two methods for forming the copolymer, still does not show significant improvements over

PANI alone, as it is still not reversible for most of the potential range, and has a diagonal slant like PPy. The CV can give insight into the nature of the PANI layer, however. The shape of the peak around a potential of 0.80 V vs. Ag/AgCl in the first cycle is characteristic of diffusion.[193] This suggests that the PANI layer is porous, and that pyrrole diffused into the PANI pores.

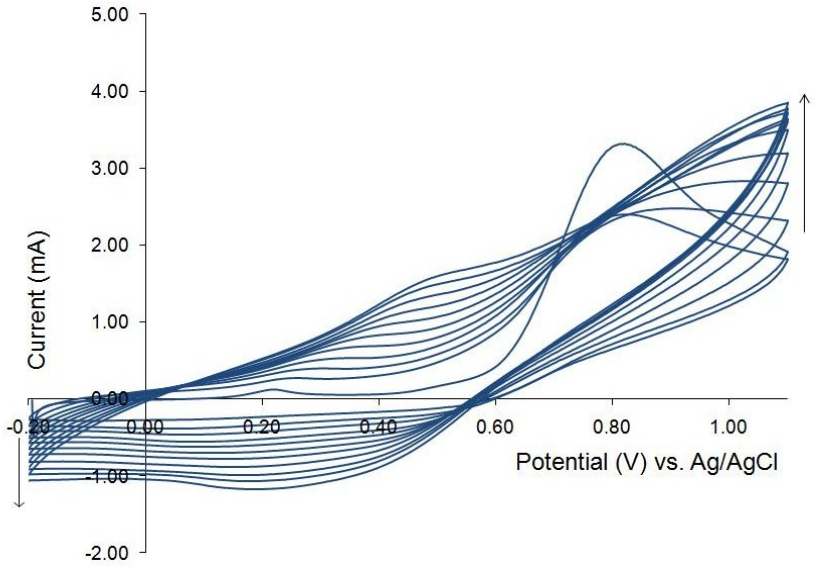

Figure 54. Electropolymerization of PPy on fully-polymerized PANI on Pt mesh at 100 mV/s in 1.0 M H_2SO_4 (cycles 1-20).

The previous copolymerizations had been done with equal concentrations of the two monomers. Since PPy had been dominating the CVs, electrocopolymerization was also carried out using a 2:1 ratio of aniline to pyrrole. Figure 55 shows the CV using again the same potential window as used previously for PANI (-0.20 to 1.10 V vs. Ag/AgCl). The slanting of the CV with cycling suggests that the film becomes more resistive as it forms, and less reversible. This could suggest a continued dominance of

PPy, if PPy forms a solid film whereas PANI forms a porous film. This copolymer continues to not be reversible enough to be used as an EC electrode.

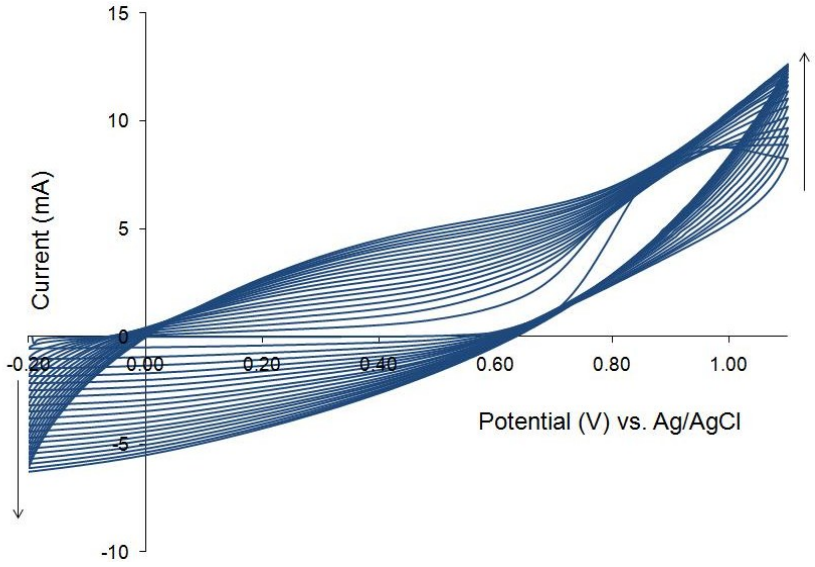

Figure 55. Electrocopolymerization of PANI and PPy on Pt mesh at 100 mV/s with a 2:1 ratio of aniline to pyrrole in 1.0 M H_2SO_4 (cycles 1-20).

Electropolymerization was attempted by depositing one polymer after only a few electrochemical cycles of the other monomer's polymerization, thus beginning to build the base of a film but not of any significant thickness before the addition of the other monomer. Figure 56 and Figure 57 show the electropolymerization CVs of the copolymer formed from pyrrole added after PANI electropolymerization and from aniline added after PPy electropolymerization, respectively. A 5:1 ratio by concentration of aniline to pyrrole was used, to try to increase the dominance of PANI in the CVs.

Because there is a consistent increase in current in the CV, the electropolymerization of pyrrole on the PANI film did seem to accomplish the

polymerization of the copolymer; however, the CV continues to have the slanted PPy shape, suggesting irreversibility and dominance of PPy. On the other hand, the CV of the polymerization of aniline over PPy has closer to a constant current over the potential window, and in turn a steady capacitance. It is also less tilted and seemingly reversible, based on the vertical lines when the potential direction is switched (see Figure 58). The CV shape is also similar to the copolymer CVs in the literature,[150, 156, 194] in terms of peak location as well as the broadness of the peaks, though those CVs were not cycled to as high a potential as the one presented here. This copolymer is not reversible in all regions of the CV, but from about 0.2 to 0.7 V vs. Ag/AgCl (0.4 to 0.9 V vs. SHE). The peaks that can be seen correspond to the same locations as the PANI CV. However, instead of sharp peaks as seen with PANI solely, these peaks are broad, suggesting that there are other reactions that occurred than the ones associated with PANI.

Constant capacitance was the goal for the copolymer, as is desired for EC electrodes. This seems to have been achieved by the electropolymerization of PANI after PPy, though in a restricted potential window of 0.2 to 0.7 V vs. Ag/AgCl (0.4 to 0.9 V vs. SHE). This is the first time that this has been accomplished utilizing electrochemical cycling.

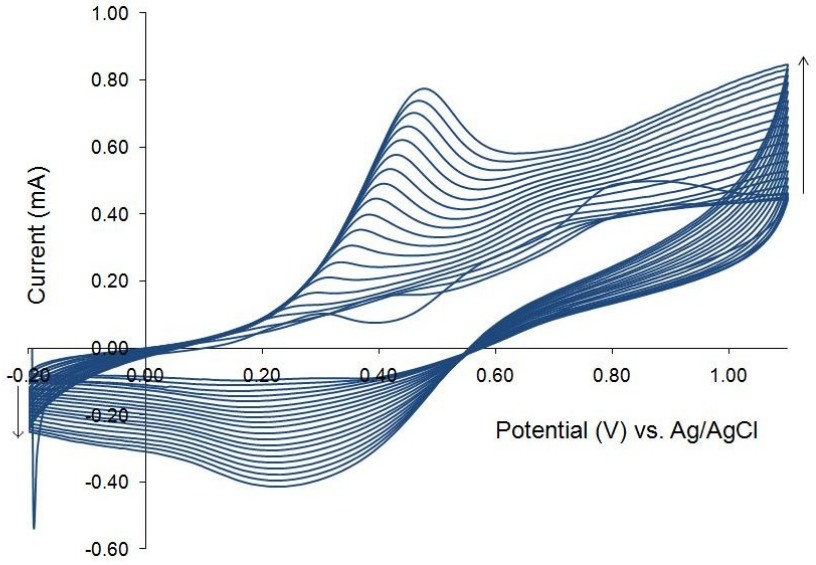

Figure 56. Copolymer electropolymerization at 100 mV/s by adding pyrrole after 5 cycles of PANI on Pt mesh in 1.0 M H_2SO_4 with a 5:1 ratio of aniline to pyrrole (cycles 1-20).

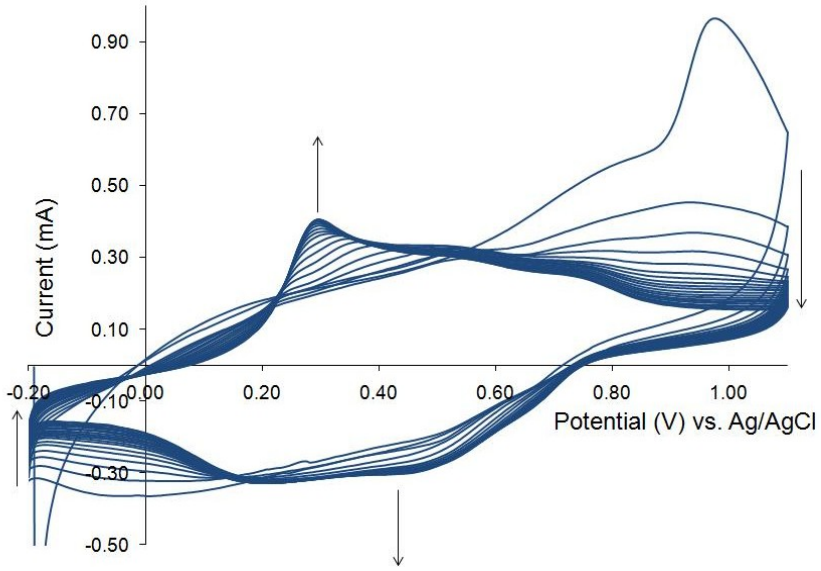

Figure 57. Copolymer electropolymerization at 100 mV/s by adding aniline after 5 cycles of PPy on Pt mesh in 1.0 M H_2SO_4 with a 5:1 ratio of aniline to pyrrole (cycles 1-20).

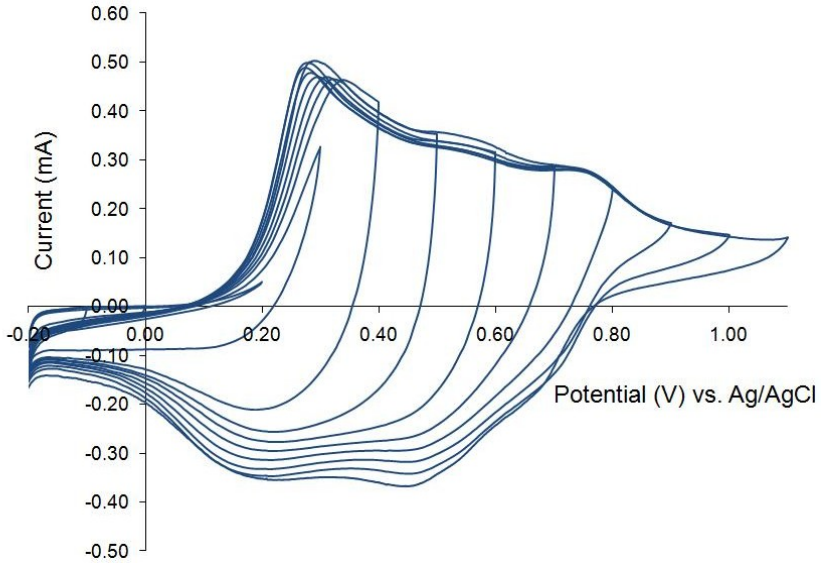

Figure 58. Various potential windows of copolymer of PANI on PPy on Pt mesh with a 5:1 ratio of aniline to pyrrole in 1.0 M H_2SO_4 at 100 mV/s.

The electropolymerization method of cycling -0.20 to 1.10 V vs. Ag/AgCl five times with 0.002 M pyrrole followed by continuous cycling with 0.01 M aniline yielded the most reversible CV with the most constant capacitance of the copolymer of PANI and PPy. Therefore, it was a method similar to this chosen for UV-Vis-NIR spectroelectrochemistry. The electropolymerization method during spectroscopy was to cycle from -0.20 to 1.10 V vs. Ag/AgCl with 0.01 M pyrrole followed by continuous cycling with 0.1 M aniline (specifics in Section 3.2.1.3). The PPy polymerization was carried out for ten cycles instead of five as a 10:1 ratio of aniline to pyrrole was used rather than the 5:1 ratio previously (to be more consistent with literature[148]).

Figure 59 shows the CVs obtained from the electropolymerization of the copolymer after adding aniline, which was added after building the PPy layer. The CV shape is similar to Figure 57, indicating that the electropolymerization of the copolymer in the spectroelectrochemical cell was successful: the current increased at a constant

rate, indicating polymer formation, and the peaks are located at approximately the same potentials as the previous copolymer. However, there is a slight shift in the peak locations to higher potentials. The Hupd peak at -0.1 V that appeared in the previous spectroelectrochemical CVs appeared here as well, and the sharp current increase at 1.1 V appears to be oxygen evolution. The presence of the platinum Hupd peak suggests that the polymer forming was porous as well as thin, based on the small increase in current with potential cycling.

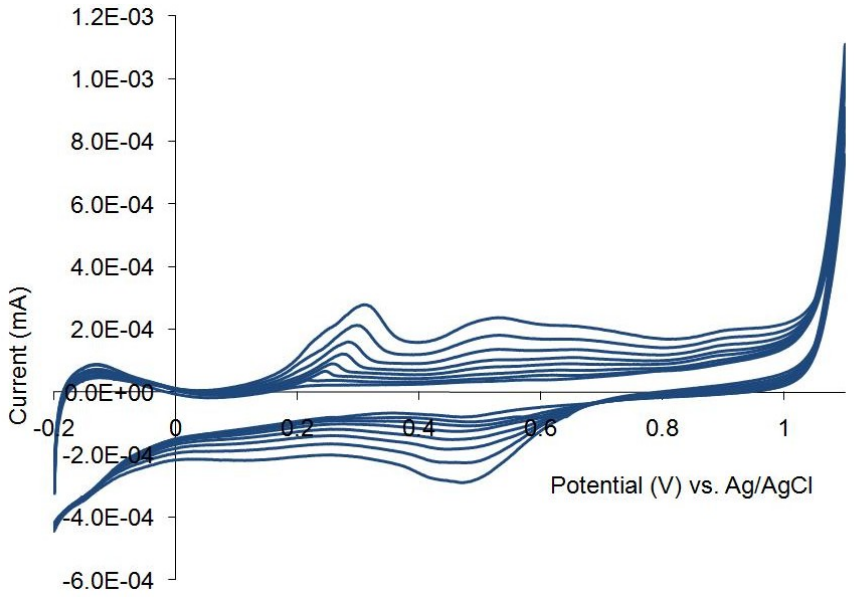

Figure 59. Electropolymerization of PANI after polymerizing PPy at 100 mV/s in 1.0 M H_2SO_4 during UV-Vis-NIR spectroscopy (every 5 cycles from 5 to 40).

UV-Vis-NIR spectroscopy was performed during the electropolymerization. Spectra are shown in Figure 60 for every ten cycles during the electropolymerization of PANI after PPy was deposited. Absorbance of the spectra increases overall as cycling progresses, which is evidence that the film is building on the platinum mesh. The most prominent peak in the spectrum for the copolymer is at 450 nm, which was present in

the UV-Vis-NIR spectrum for PPy but did not appear in the UV-Vis-NIR spectrum for PANI. The presence of this peak suggests the continued occurrence of PPy in the copolymer, likely still at the surface of the copolymer as a porous film for PANI to diffuse into.

The UV region is different than the spectra for both homopolymers; it has two separate regions of absorbance plateaus, whereas in the PANI spectrum this region was sloped, and in the PPy spectrum there was a constant (though noisy) plateau from 200 to 250 nm and then the absorbance decreased at higher wavelengths. That the spectrum in this region is different than either PPy and PANI suggests that neither one is dominating completely, supporting the successful formation of the copolymer.

Most of the spectrum for the copolymer is a plateau with small, broad peaks like the spectra of the homopolymers, but there is another region of note from 1300 to 1400 nm, exhibiting peaks due to C-H combination vibrations. This region contains a double peak at ca. 1360 and 1390 nm (1360 nm higher in absorbance than 1390 nm), whereas in the PANI spectrum there is a peak at 1360 nm and a valley at 1390 nm, and in the PPy spectrum a double peak (1360 nm lower in absorbance than 1390 nm). This feature of the copolymer spectrum also suggests a combination of both polymers.

What is more difficult to determine is how the copolymer was formed in terms of the interaction between PANI and PPy. Because the spectrum of the copolymer has features of both PANI and PPy, it likely had blocks of both of these polymers in its formation. It could be that the copolymer was made up of two discreet layers of PPy and PANI, and this is why the spectrum seems to be a simple addition of both individual spectra, or, it could also be that PANI molecules diffused into the pores of PPy.

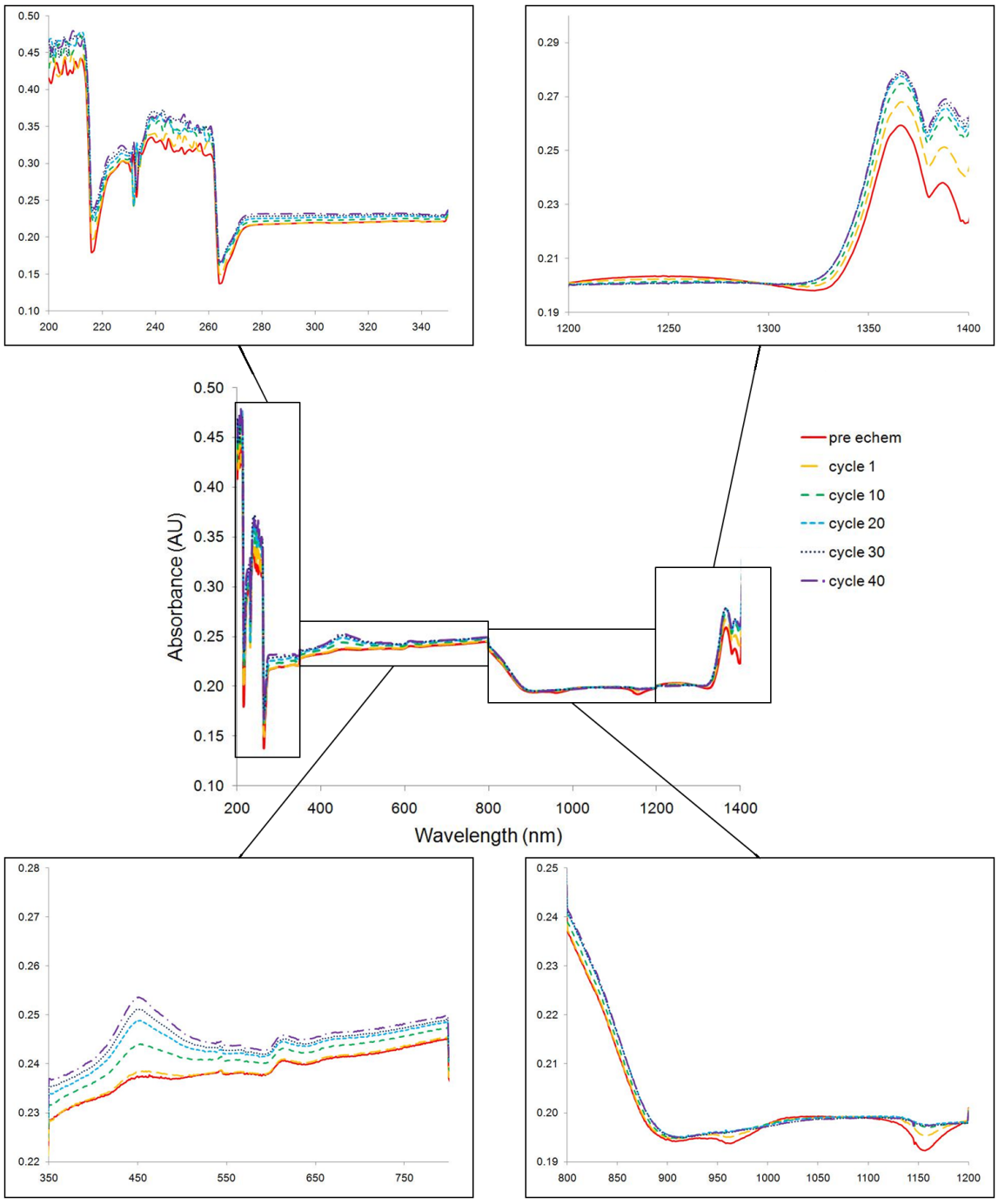

Figure 60. UV-Vis-NIR spectra taken after the polymerization of PPy, before ("pre echem") and during electropolymerization of the copolymer of PANI and PPy (after cycles 1, 10, 20, 30, 40) with insets a) 200 to 350 nm; b) 350 to 800 nm; c) 800 to 1200 nm; and d) 1200 to 1400 nm.

Spectra collected while holding at specific potentials, Figure 61, are very similar regardless of potential, except for the highest potentials of 0.7 V and 1.0 V vs. Ag/AgCl. At these two potentials there was an increase in absorbance for most of the spectrum, from 200 to 1200 nm at 0.7 V, and for the entire spectrum at 1.0 V. This increase with increasing potential was seen for both homopolymers as well, mainly in the UV range for PANI, and in the visible range for PPy. It could be that the significant increase in absorbance over the entire spectrum for the copolymer is due to accelerated film formation, which is plausible based on the fact that typically when the polymers studied here are formed potentiostatically, they are held at high oxidizing potentials.[58, 133, 136, 137, 148, 195]

Potential scans were also performed while measuring absorbance at particular wavelengths (Figure 62). When sweeping the potential, the absorbance did not change significantly except for the wavelengths in the UV region. Apparently the large jump to higher absorbance values occurs with a potential hold at high potential, and not when the potential is swept across a range from low to high, which suggests that the copolymer may have increased formation only potentiostatically at high potentials due to the oxidized forms of the polymer.

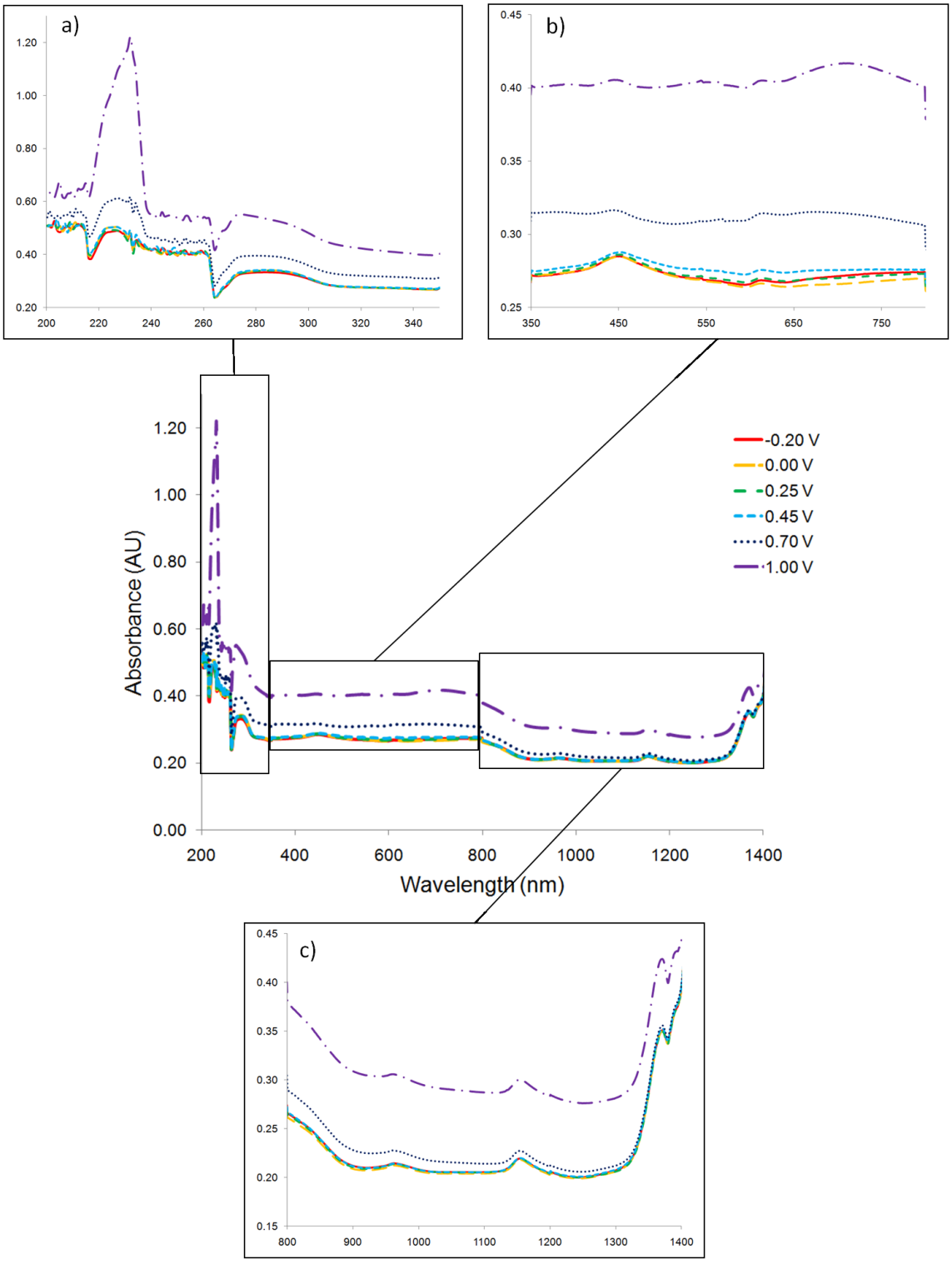

Figure 61. UV-Vis-NIR spectra while holding potential vs. Ag/AgCl on the copolymer of PANI and PPy, with insets a) 200 to 350 nm; b) 350 to 800 nm; and c) 800 to 1400 nm.

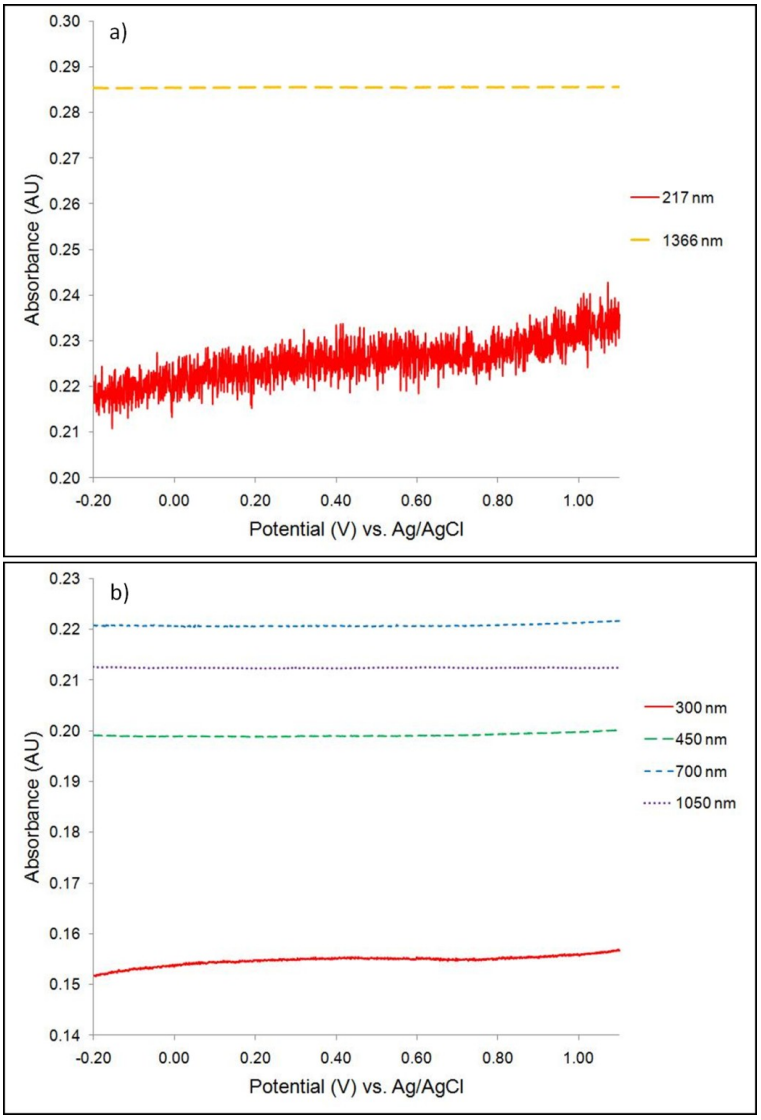

Figure 62. Absorbance change at different wavelengths during linear potential sweep from -0.2 to 1.1 V vs. Ag/AgCl on copolymer.

A copolymer of PANI and PPy was successfully formed for the first time by electrochemical cycling. The most reversible copolymer was formed by electropolymerizing PPy followed by the electropolymerization of PANI using potential cycling. The copolymer was successfully formed *in situ* in a UV-Vis-NIR spectroscopic cell while polymerizing with potential cycling. The spectra obtained while holding

potential and the measurement of absorbance while scanning potential showed increased absorbance of the copolymer at high potentials, particularly when holding at high potential.

7.4 Conclusions

Electropolymerization of PANI, PPy, and their copolymer was achieved through electrochemical cycling. By polymerizing PANI after PPy, a copolymer was formed with reversibility and a limited potential region of near-constant capacitance, which is desired for EC electrodes. Spectroelectrochemical experiments of each of the three polymers were successfully performed. Collecting UV-Vis-NIR spectra during electropolymerization aided in proving the successful electropolymerizations by increasing absorbance with electrochemical cycling time, and collecting spectra while holding potentials of the polymers constant and measuring absorbance while scanning the potential range was used to observe changes in absorbing properties of the polymers with change in potential, namely increasing absorption of light with oxidation.

Chapter 8 Conclusions

8.1 Thesis Summary

Spectroelectrochemistry is a useful way to gain information on how electrochemistry affects EC electrodes during experimentation. Through this research, the available and working techniques to identify CSFs on carbon electrodes were identified, though an *in situ* method remains to be developed. One of the initial goals of this research project was to determine the changes in CSFs on carbon electrodes caused by electrochemistry. Ultimately the observation of these changes *in situ* is desired. The first step in these proceedings was to solve how to identify these CSFs, and to do this, various spectroscopic techniques as well as the Boehm titration were studied. The background and previous work carried out on this topic, as well as the topic of polymer electrodes, was outlined in Chapter 2. All experimental procedures performed in this research were detailed in Chapter 3.

The spectroscopic studies of CSFs on carbon samples and carbon electrodes were described in Chapter 4. UV-Vis-NIR spectroscopy was deemed unsuitable for CSF detection principally because likely CSFs (e.g. C=O, C-O, C-OH) absorb in the mid-IR range. It was determined that transmission FTIR will not be able to handle *in situ* electrochemistry in aqueous electrolyte, because the spectrum of the electrolyte exhibits strong peaks that dominate over carbon peaks. Spectra on carbon samples were obtained using transmission FTIR, ATR and PAS techniques, but the peaks in the spectra were very weak, making determination of possible functionalities difficult. X-ray spectroscopic methods, XPS and XAS, were sensitive enough to detect CSFs on carbon samples and electrodes *ex situ*. All the XPS spectra for carbon cloth had peaks

suggesting the presence of surface oxides such as ether, phenolic, carboxylic acids and lactonic groups. The XAS spectra showed the appearance of the C-O group on carbon cloth electrodes with electrochemical cycling, suggesting that electrochemical treatment affects carbon surface chemistry by forming surface groups, possibly lactonic groups. XAS spectra for ELIT and Black Pearls 2000 had peaks that disappeared with soaking in water and electrochemical cycling, suggesting adsorbed CSFs that desorbed with treatment in aqueous solutions. All the samples had the C=O peak in the spectra, suggesting carbonyl or quinone groups. While further research needs to be undertaken to ascertain positively the effects of electrochemistry on electrode surfaces, the methods that should be used to carry out this research are, as determined by this research, XPS, XAS, and the standardized Boehm titration.

Since XPS and XAS are subjective in their interpretation, in terms of peak fitting and quantification, often in literature these methods are employed in addition to another means of identifying CSFs on carbon samples and electrodes. The Boehm titration is a commonly-used complementary technique to spectroscopy, and is not difficult to perform. However, the methodology in the literature is inconsistent, and consequently standardization of the Boehm titration was carried out in this project, in particular the methods for titration endpoint determination and removal of the effects of dissolved CO_2 in solution, outlined in Chapter 5. In Chapter 6 the Boehm titration was carried out using the standardized method on carbon cloth electrodes: findings suggested that while acidic surface functional groups increase with electrochemical cycling, basic groups generally decrease with cycling, which agrees with literature studies.[79, 80, 165] The increase in current over most of the potential window in the CV for carbon cloth could

correspond to the formation of acidic CSFs with electrochemical cycling, while the decrease at 1.0 V vs. SHE in the CV could be due to the decrease in basic groups. This presence of carboxylic, lactonic and phenolic CSFs determined by the Boehm titration was also seen in XPS.

Although electrochemistry on carbon electrodes has not yet been accomplished *in situ* with a CSF measurement technique, spectroelectrochemistry of polymer electrodes was achieved. Chapter 7 described the electropolymerization of PANI and PPy, and how a copolymer of PANI and PPy as a possible EC material was formed and its formation followed *in situ* by employing transmission UV-Vis-NIR spectroscopy, which had not previously been done with this copolymer. Polymerization of the copolymer of PANI and PPy as a potential electrode material for ECs was not only achieved by electrochemical cycling but was studied during electropolymerization through spectroelectrochemical measurements, neither of which had been previously done in literature. Overall, the research completed included the initial stages to studying carbon electrodes and polymer electrodes using analytical, non-electrochemistry techniques in conjunction with electrochemistry. Now that the groundwork has been laid, these projects can continue to allow more in-depth research.

8.2 Future Work

The initial experiments have been completed on the projects covered throughout this research, and further experiments that can be carried out are to use the techniques established to gain results on different types of samples. For the project involving spectroscopy on carbon electrodes, it was found that x-ray techniques yielded the best

information on carbon electrodes and the CSFs present. To further understand the effect of electrochemistry on carbon electrodes, x-ray spectra for electrodes that have been treated by different electrochemical experiments than have been studied here. For example, the effect of electrochemical cycling using varying parameters such as potential windows, cycling time and sweep rates on CSF formation can now be studied. It was shown that *in situ* measurements would not work in FTIR due to the strongly absorbing aqueous electrolytes. In the future, therefore, non-aqueous electrolytes can be studied for possible use in spectroelectrochemistry on electrodes for ECs. Work will also go into determining which surface groups on the carbon electrodes are electroactive.

The Boehm titration was standardized and employed to identify CSFs on carbon samples and electrodes. The method did accomplish the detection of different CSFs on the samples, and in the future replicates and samples treated with varied electrochemistry can be examined using this technique and compared to XPS and XAS.

Spectroelectrochemistry of the copolymer formed with PANI and PPy was accomplished, but it is not known precisely how the copolymer deposits. It could be that PANI polymerized after PPy polymerization diffuses into pores, or that they form layers of solid films; there are a number of possibilities which must be studied. Methods of forming the copolymer should also be explored, including varying parameters in the electropolymerization process such as sweep rate and polymerization time.

References

(1) Burke, A. *Electrochim. Acta* **2007***, 53*, 1083-1091.

(2) Winter, M.; Brodd, R. J. *Chem. Rev.* **2005***, 105*, 1021-1021.

(3) Conway, B. E. In *Electrochemical Supercapacitors;* Kluwer Academic: New York, 1999.

(4) Conway, B. E. *J. Electrochem. Soc.* **1991***, 138*, 1539-1548.

(5) Conway, B. E.; Pell, W. G. *Journal of Solid State Electrochemistry* **2003***, 7*, 637-644.

(6) Frackowiak, E. *Physical Chemistry Chemical Physics* **2007***, 9*, 1774-1785.

(7) Garten, V. A.; Weiss, D. E. *Aust. J. Chem.* **1955***, 8*, 68-95.

(8) Hallum, J. V.; Drushel, H. V. *J. Phys. Chem.* **1958***, 62*, 110-117.

(9) Drushel, H. V.; Hallum, J. V. *J. Phys. Chem.* **1959***, 62*, 1502-1505.

(10) Palaniappan, S.; Sydulu, S. B.; Srinivas, P. *J. Appl. Polym. Sci.* **2010***, 115*, 1695-1701.

(11) Kolb, D. M. *Surf. Sci.* **2002***, 500*, 722-740.

(12) Bockris, J. O.; Reddy, A. K. N.; Gamboa-Aldeco, M. In *Modern Electrochemistry;* Kluwer Academic: New York, 2000; Vol. 2A: Fundamentals of Electrodics.

(13) Conway, B. E.; Birss, V.; Wojtowicz, J. *J. Power Sources* **1997***, 66*, 1-14.

(14) Hsieh, C.; Teng, H. *Carbon; Carbon* **2002***, 40*, 667-674.

(15) Kotz, R.; Carlen, M. *Electrochim. Acta* **2000***, 45*, 2483-2498.

(16) Boehm, H. In *Surface Chemical Characterization of Carbons from Adsorption Studies;* Eduardo J. Bottani, Juan M.D. Tascón, Eds.; Adsorption by Carbons; Elsevier: Amsterdam, 2008; pp 301-327.

(17) Boehm, H. P. In *Chemical Identification of Surface Groups;* D.D. Eley,Herman Pines and Paul B.Weisz, Ed.; Advances in Catalysis; Academic Press: 1966; Vol. Volume 16, pp 179-274.

(18) Boehm, H. P. *Carbon* **1994***, 32*, 759-769.

(19) Lahaye, J. *Fuel* **1998***, 77*, 543-547.

(20) Boehm, H. P. *World Carbon; World of Carbon* **2001***, 1*, 141-178.

(21) Montes-Morán, M. A.; Suárez, D.; Menéndez, J. A.; Fuente, E. *Carbon* **2004***, 42*, 1219-1225.

(22) Noh, J. S.; Schwarz, J. A. *Carbon; Carbon* **1990***, 28*, 675-682.

(23) Chen, J. P.; Wu, S. *Langmuir* **2004***, 20*, 2233-2242.

(24) Gomez-Serrano, V.; Acedo-Ramos, M.; Lopez-Peinado, A. J.; Valenzuela-Calahorro, C. *Fuel* **1994***, 73*, 387-395.

(25) Valdes, H.; Sanchez-Polo, M.; Rivera-Utrilla, J.; Zaror, C. A. *Langmuir* **2002***, 18*, 2111-2116.

(26) Braun, A.; Bartsch, M.; Merlo, O.; Schnyder, B.; Schaffner, B.; Kotz, R.; Haas, O.; Wokaun, A. *Carbon; Carbon* **2003***, 41*, 759-765.

(27) Dekanski, A.; Stevanovic, J.; Stevanovic, R.; Nikolic, B. Z.; Jovanovic, V. M. *Carbon; Carbon* **2001***, 39*, 1195-1205.

(28) Hu, C.; Wang, C. *J. Power Sources* **2004***, 125*, 299-308.

(29) Thiagarajan, S.; Tsai, T.; Chen, S. *Biosensors and Bioelectronics* **2009***, 24*, 2712-2715.

(30) Harris, D. C. In *Quantitative Chemical Analysis;* W.H. Freeman and Company: New York, 2003.

(31) Weckhuysen, B. M. *In-Situ Spectrosc.Catal.; In-Situ Spectroscopy of Catalysts* **2004**, 255-270.

(32) Harrick, N. J.; Riederman, N. H. *Spectrochimica Acta* **1965***, 21*, 2135-2139.

(33) Harrick, N. J. In *Internal Reflection Spectroscopy.* Section Title: Spectra and Other Optical Properties; John Wiley & Sons: New York, 1967, pp 327.

(34) Harrick, N. J. *Ann. N. Y. Acad. Sci.* **1963***, 101*, 928-959.

(35) Harrick, N. J. *J. Phys. Chem.* **1960***, 64*, 1110-1114.

(36) Harrick, N. J. *Phys. Rev. Lett.* **1960***, 4*, 224-226.

(37) Harrick, N. J. *Phys.Rev.; Physical Review* **1956***, 101*, 491-492.

(38) Mattson, J. S.; Lee, L.; Mark, H. B.; Weber, W. J. *Journal of Colloid and Interface Science* **1970***, 33*, 284-293.

(39) Mattson, J. S.; Mark, H. B. *Journal of Colloid and Interface Science* **1969***, 31*, 131-144.

(40) Mattson, J. S.; Mark, H. B., Jr.; Weber, W. J.,Jr *Anal. Chem.* **1969***, 41*, 355-358.

(41) Koetz, R. *NATO ASI Ser., Ser.C; NATO ASI Series, Series C: Mathematical and Physical Sciences* **1990***, 320*, 409-438.

(42) Riviere, J. C. In *Practical Surface Analysis by Auger and X-ray Photoelectron Spectroscopy;* Briggs, D., Seah, M. P., Eds.; John Wiley & Sons: New York, 1983.

(43) Engel, T.; Reid, P. In *Physical Chemistry;* Benjamin Cummings: San Francisco, 2006.

(44) Ghosh, P. K. In *Introduction to Photoelectron Spectroscopy;* Elving, P. J., Winefordner, J. D. and Kolthoff, I. M., Eds.; Chemical Analysis; John Wiley & Sons: New York, 1983; Vol. 67.

(45) Seah, M. P.; Briggs, D. In *Practical Surface Analysis by Auger and X-ray Photoelectron Spectroscopy;* Briggs, D., Seah, M. P., Eds.; John Wiley & Sons: New York, 1983.

(46) Hofmann, S. In *Practical Surface Analysis by Auger and X-ray Photoelectron Spectroscopy;* Briggs, D., Seah, M. P., Eds.; John Wiley & Sons: New York, 1983.

(47) Fornasini, P. *Chim. Ind. (Milan)* **2000***, 82*, 177-182.

(48) Stohr, J. In *NEXAFS Spectroscopy, Springer Series in Surface Science;* Springer-Verlag: Berlin, 1996; Vol. 25.

(49) Rosencwaig, A.; Gersho, A. *J. Appl. Phys.* **1976***, 47*, 64-69.

(50) Gerson, D. J.; Wong, J. S.; Casper, J. M. *Am.Lab.(Fairfield, Conn.); American Laboratory (Shelton, CT, United States)* **1984***, 16*, 63-4, 66, 69-71.

(51) Ryczkowski, J. *Catal. Today* **2007***, 124*, 11-20.

(52) Alessio, E.; Daff, S.; Elliot, M.; Iengo, E.; Jack, L. A.; Macnamara, K. G.; Pratt, J. M.; Yellowlees, L. J. *Trends Mol.Electrochem.; Trends in Molecular Electrochemistry* **2004**, 339-381.

(53) MacGregor, S. A.; McInnes, E.; Sorbie, R. J.; Yellowlees, L. J. *NATO ASI Ser. , Ser. C* **1993***, 385*, 503-517.

(54) Plieth, W.; Wilson, G. S.; De La Fe, C. G. *Pure and Applied Chemistry* **1998***, 70*, 1395-1414.

(55) Heinze, J. *Top. Curr. Chem.* **1990***, 152*, 1-47.

(56) Rudge, A.; Davey, J.; Raistrick, I.; Gottesfeld, S.; Ferraris, J. P. *J. Power Sources* **1994***, 47*, 89-107.

(57) Frackowiak, E.; Beguin, F. *Carbon* **2001***, 39*, 937-950.

(58) Hu, C.; Lin, J. *Electrochim. Acta* **2002***, 47*, 4055-4067.

(59) Ali Shah, A.; Holze, R. *Electrochim. Acta* **2006***, 52*, 1374-1382.

(60) Shah, A. A.; Holze, R. *Electrochim. Acta* **2008***, 53*, 4642-4653.

(61) Abd-Elwahed, A.; Holze, R. *Russ. J. Electrochem.* **2003***, 39*, 391-396.

(62) Pud, A. A. *Synth. Met.* **1994***, 66*, 1-18.

(63) Arsov, L. D.; Plieth, W.; Kossmehl, G. *J. Solid State Electrochem.* **1998***, 2*, 355-361.

(64) Schlenoff, J. B.; Xu, H. *J. Electrochem. Soc.* **1992***, 139*, 2397-2401.

(65) Rapta, P.; Neudeck, A.; Petr, A.; Dunsch, L. *J. Chem. Soc. , Faraday Trans.* **1998***, 94*, 3625-3630.

(66) Otero, T. F.; Bengoechea, M. *Langmuir* **1999***, 15*, 1323-1327.

(67) Arjomandi, J.; Holze, R. *J. Solid State Electrochem.* **2006***, 11*, 1093-1100.

(68) Zhao, Q.; Zhang, Z.; Bao, L.; Pang, D. *Electrochem.Commun.; Electrochemistry Communications* **2008***, 10*, 181-185.

(69) Kim, C.; Pyun, S.; Shin, H. *J. Electrochem. Soc.* **2002***, 149*, A93-A98.

(70) Kim, Y.; Ito, Y.; Tadai, K.; Mitani, T.; Kim, U.; Kim, H.; Cho, B. *Appl. Phys. Lett.* **2005***, 87*, 234106/1-234106/3.

(71) Kim, Y.; Mitani, T. *J. Power Sources* **2006***, 158*, 1517-1522.

(72) Painter, P.; Starsinic, M.; Coleman, M. In *In Determination of functional groups in coal by Fourier transform interferometry.* Section Title: Fossil Fuels, Derivatives, and Related Products; 1985; Vol. 4, pp 169-241.

(73) Rockley, M. G.; Ratcliffe, A. E.; Davis, D. M.; Woodard, M. K. *Appl. Spectrosc.* **1984**, *38*, 553-556.

(74) Biniak, S.; Szymanski, G.; Siedlewski, J.; Swiatkowski, A. *Carbon; Carbon* **1997**, *35*, 1799-1810.

(75) Seredych, M.; Bandosz, T. J. *Energy Fuels* **2008**, *22*, 850-859.

(76) Lowde, D. R.; Williams, J. O.; Attwood, P. A.; Bird, R. J.; McNicol, B. D.; Short, R. T. *J.Chem.Soc., Faraday Trans.1; Journal of the Chemical Society, Faraday Transactions 1: Physical Chemistry in Condensed Phases* **1979**, *75*, 2312-2324.

(77) Boehm, H. P. *High Temp.- High Pressures; High Temperatures - High Pressures* **1990**, *22*, 275-288.

(78) Boehm, H. P. *Carbon* **2002**, *40*, 145-149.

(79) Salame, I. I.; Bagreev, A.; Bandosz, T. J. *J Phys Chem B* **1999**, *103*, 3877-3884.

(80) Salame, I. I.; Bandosz, T. J. *J. Colloid Interface Sci.* **2001**, *240*, 252-258.

(81) Ishizaki, C.; Martí, I. *Carbon* **1981**, *19*, 409-412.

(82) Kazimierczak, J.; Biniak, S.; Swiatkowski, A.; Radeke, K. H. *J. Chem. Soc. , Faraday Trans.* **1991**, *87*, 3557-3561.

(83) Swiatkowski, A.; Pakula, M.; Biniak, S.; Walczyk, M. *Carbon; Carbon* **2004**, *42*, 3057-3069.

(84) Bandosz, T. J.; Jagiello, J.; Schwarz, J. A. *Anal. Chem.* **1992**, *64*, 891-895.

(85) Boehm, H. P.; Heck, W.; Sappok, R.; Diehl, E. *Angewandte Chemie-International Edition* **1964**, *3*, 669-&.

(86) Zhuang, Q.; Kyotani, T.; Tomita, A. *Energy Fuels* **1994**, *8*, 714-718.

(87) Marsh, H.; Foord, A. D.; Mattson, J. S.; Thomas, J. M.; Evans, E. L. *J. Colloid Interface Sci.* **1974**, *49*, 368-382.

(88) Kozlowski, C.; Sherwood, P. M. A. *J. Chem. Soc. , Faraday Trans. 1* **1985**, *81*, 2745-56, 1 plate.

(89) Kozlowski, C.; Sherwood, P. M. A. *J.Chem.Soc., Faraday Trans.1; Journal of the Chemical Society, Faraday Transactions 1: Physical Chemistry in Condensed Phases* **1984**, *80*, 2099-107, 4 plates.

(90) Friedel, R. A.; Carlson, G. L. *Fuel* **1972***, 51*, 194-198.

(91) Friedel, R. A.; Hofer, L. J. E. *J. Phys. Chem.* **1970***, 74*, 2921-2922.

(92) O'Reilly, J. M.; Mosher, R. A. *Carbon* **1983***, 21*, 47-51.

(93) Papirer, E.; Guyon, E.; Perol, N. *Carbon* **1978***, 16*, 133-140.

(94) Studebaker, M. L.; Rinehart, R. W. *Carbon* **1972***, 10*, 328-328.

(95) Mawhinney, D. B.; Rossin, J. A.; Gerhart, K.; Yates, J. T.,Jr *Langmuir* **1999***, 15*, 4617-4621.

(96) Pandurangappa, M.; Ramakrishnappa, T. *J.Solid State Electrochem.; Journal of Solid State Electrochemistry* **2008***, 12*, 1411-1419.

(97) Barton, S. S. *Colloid Polym. Sci.* **1986***, 264*, 176-181.

(98) Sellitti, C.; Koenig, J. L.; Ishida, H. *Carbon; Carbon* **1990***, 28*, 221-228.

(99) Thomasson, J.; Coin, C.; Kahraman, H.; Fredericks, P. M. *Fuel* **2000***, 79*, 685-691.

(100) Fanning, P. E.; Vannice, M. A. *Carbon; Carbon* **1993***, 31*, 721-730.

(101) Low, M. J. D.; Parodi, G. A. *Spectrosc.Lett.; Spectroscopy Letters* **1980***, 13*, 663-669.

(102) Low, M. J. D.; Parodi, G. A. *Appl. Spectrosc.* **1980***, 34*, 76-80.

(103) Bennett, C. A., Jr.; Patty, R. R. *J.Photoacoust.; Journal of Photoacoustics* **1982***, 1*, 237-250.

(104) Ryczkowski, J.; Pasieczna, S.; Figueiredo, J. L.; Pereira, M. F. R.; Borowiecki, T. *J. Phys. IV* **2004***, 117*, 57-62.

(105) Pandurangappa, M.; Ramakrishnappa, T.; Compton, R. G. *Int.J.Electrochem.Sci.; International Journal of Electrochemical Science* **2008***, 3*, 1218-1235.

(106) Meldrum, B. J.; Rochester, C. H. *J. Chem. Soc. , Faraday Trans.* **1990***, 86*, 2997-3002.

(107) Kuznetsova, A.; Popova, I.; Yates, J. T., Jr.; Bronikowski, M. J.; Huffman, C. B.; Liu, J.; Smalley, R. E.; Hwu, H. H.; Chen, J. G. *J. Am. Chem. Soc.* **2001***, 123*, 10699-10704.

(108) Tran, N. H.; Wilson, M. A.; Milev, A. S.; Bartlett, J. R.; Lamb, R. N.; Martin, D.; Kannangara, G. S. K. *Adv. Colloid Interface Sci.* **2009***, 145*, 23-41.

(109) Dhez, O.; Ade, H.; Urquhart, S. G. *J. Electron Spectrosc. Relat. Phenom.* **2003***, 128*, 85-96.

(110) Zou, Y.; Feng, X. S.; Tang, J. C. In *In Theoretical analysis of carbon K-edge NEXAFS spectra of graphitelike film and related material.* Section Title: Optical, Electron, and Mass Spectroscopy and Other Related Properties; 1994, pp 124-129.

(111) Braun, A. *J. Environ. Monit.* **2005***, 7*, 1059-1065.

(112) Solomon, D.; Lehmann, J.; Kinyangi, J.; Liang, B.; Heymann, K.; Dathe, L.; Hanley, K.; Wirick, S.; Jacobsen, C. *Soil Sci. Soc. Am. J.* **2009***, 73*, 1817-1830.

(113) Seredych, M.; Hulicova-Jurcakova, D.; Lu, G. Q.; Bandosz, T. J. *Carbon* **2008***, 46*, 1475-1488.

(114) Guo, Y.; Rockstraw, D. A. *Microporous Mesoporous Mater.; Microporous and Mesoporous Materials* **2007***, 100*, 12-19.

(115) Kato, Y.; Machida, M.; Tatsumoto, H. *J. Colloid Interface Sci.* **2008***, 322*, 394-398.

(116) Tennant, M. F.; Mazyck, D. W. *Carbon* **2007***, 45*, 858-864.

(117) Mestre, A. S.; Pires, J.; Nogueira, J. M. F.; Carvalho, A. P. *Carbon* **2007***, 45*, 1979-1988.

(118) Hermans, S.; Diverchy, C.; Demoulin, O.; Dubois, V.; Gaigneaux, E. M.; Devillers, M. *J. Catal.* **2006***, 243*, 239-251.

(119) Feng, X.; Dementev, N.; Feng, W.; Vidic, R.; Borguet, E. *Carbon* **2006***, 44*, 1203-1209.

(120) Gonzalez-Guerrero, A. B.; Mendoza, E.; Pellicer, E.; Alsina, F.; Fernandez-Sanchez, C.; Lechuga, L. M. *Chem. Phys. Lett.* **2008***, 462*, 256-259.

(121) Barton, S. S.; Dacey, J. R.; Evans, M. J. B. *Colloid Polym. Sci.* **1982***, 260*, 726-731.

(122) Peng, C.; Zhang, S.; Jewell, D.; Chen, G. Z. *Prog. Nat. Sci.* **2008***, 18*, 777-788.

(123) Zhang, J.; Kong, L.; Wang, B.; Luo, Y.; Kang, L. *Synth. Met.* **2009***, 159*, 260-266.

(124) Xiao, Q.; Zhou, X. *Electrochim. Acta* **2003***, 48*, 575-580.

(125) Vijayan, M.; Krishnan, V. *Electroanalysis* **1995***, 7*, 197-198.

(126) Chen, W.; Wen, T. *J. Power Sources* **2003***, 117*, 273-282.

(127) Xing, W.; Yuan, X.; Zhuo, S.; Huang, C. *Polym. Adv. Technol.* **2009***, 20*, 1179-1182.

(128) Konwer, S.; Pokhrel, B.; Dolui, S. K. *J. Appl. Polym. Sci.* **2010***, 116*, 1138-1145.

(129) Wang, H.; Hao, Q.; Yang, X.; Lu, L.; Wang, X. *ACS Appl. Mater. Interfaces* **2010***, 2*, 821-828.

(130) Sivakumar, C.; Nian, J.; Teng, H. *J. Power Sources* **2005***, 144*, 295-301.

(131) Jurewicz, K.; Frackowiak, E. *Mol. Phys. Rep.* **2000***, 27*, 38-45.

(132) Suppes, G. M.; Deore, B. A.; Freund, M. S. *Langmuir* **2008***, 24*, 1064-1069.

(133) Qasim, H.; Sadek, A. Z.; Arsat, R.; Wlodarski, W.; Belski, I.; Kaner, R. B.; Kalantar-zadeh, K. *Proc. SPIE* **2008***, 6800*, 680012/1-680012/8.

(134) Sbaite, P.; Huerta-Vilca, D.; Barbero, C.; Miras, M. C.; Motheo, A. J. *Eur. Polym. J.* **2004***, 40*, 1445-1450.

(135) Huang, J.; Kaner, R. B. *Angew Chem Int Ed Engl* **2004***, 43*, 5817-5821.

(136) Zotti, G.; Schlavon, G. *Synth. Met.* **1989***, 30*, 151-158.

(137) Lippe, J.; Holze, R. *Mol. Cryst. Liq. Cryst.* **1991***, 208*, 99-108.

(138) Li, G.; Feng, Z.; Zhong, J.; Wang, Z.; Tong, Y. *Macromolecules (Washington, DC, U. S.)* **2010***, 43*, 2178-2183.

(139) Neudeck, A.; Petr, A.; Dunsch, L. *Synth. Met.* **1999***, 107*, 143-158.

(140) Myers, R. E. *J. Electron. Mater.* **1986***, 15*, 61-69.

(141) Qi, Z.; Pickup, P. G. *Chem. Mater.* **1997***, 9*, 2934-2939.

(142) Komura, T.; Usui, T.; Takahasi, K. *Bull. Chem. Soc. Jpn.* **1995***, 68*, 1129-1135.

(143) Komura, T.; Usui, T.; Takahasi, K. *Bull. Chem. Soc. Jpn.* **1995***, 68*, 3391-3396.

(144) Hallik, A.; Alumaa, A.; Tamm, J.; Sammelselg, V.; Vaeaertnou, M.; Jaenes, A.; Lust, E. *Synth. Met.* **2006***, 156*, 488-494.

(145) Sari, B.; Talu, M. *Synth. Met.* **1998***, 94*, 221-227.

(146) Koleli, F.; Dudukcu, M.; Arslan, Y. *Turk. J. Chem.* **2000***, 24*, 333-341.

(147) Iroh, J. O.; Levine, K. *J. Power Sources* **2003***, 117*, 267-272.

(148) Hussain, A. M. P.; Kumar, A. *Indian J. Phys.* **2008***, 82*, 349-356.

(149) Branzoi, V.; Pilan, L.; Gautieri, A.; Pruna, A.; Ionita, M. *Sci. Bull. - Univ. "Politeh. " Bucharest, Ser. B* **2007***, 69*, 21-34.

(150) Zhang, A.; Wang, L.; Zhang, L.; Zhang, Y. *J. Appl. Polym. Sci.* **2010***, 115*, 1881-1885.

(151) Stejskal, J.; Trchova, M.; Ananieva, I. A.; Janca, J.; Prokes, J.; Fedorova, S.; Sapurina, I. *Synth. Met.* **2004***, 146*, 29-36.

(152) Li, X.; Zhang, X.; Li, H. *J. Appl. Polym. Sci.* **2001***, 81*, 3002-3007.

(153) Zhou, C.; Han, J.; Song, G.; Guo, R. *J. Polym. Sci. , Part A: Polym. Chem.* **2008***, 46*, 3563-3572.

(154) Kim, J. W.; Cho, C. H.; Liu, F.; Choi, H. J.; Joo, J. *Synth. Met.* **2003***, 135-136*, 17-18.

(155) Prasannan, A.; Somanathan, N.; Hong, P.; Chuang, W. *Mater. Chem. Phys.* **2009***, 116*, 406-414.

(156) Xu, P.; Han, X. J.; Wang, C.; Zhang, B.; Wang, H. -. *Synth. Met.* **2009***, 159*, 430-434.

(157) Burns, S. E.; Yiacoumi, S.; Tsouris, C. *Sep. Purif. Technol.* **1997***, 11*, 221-232.

(158) Silverstein, R. M.; Bassler, G. C.; Morrill, T. C. In *Spectrometric Identification of Organic Compounds;* John Wiley & Sons, Inc.: United States of America, 1981.

(159) Robinson, J. W.; Skelly Frame, E. M.; Frame, G. M. In *Chapter 4: Infrared Spectroscopy;* Undergraduate Instrument Analysis; CRC Press: United States of America, 2005; pp 213-315.

(160) Silverstein, R. M.; Webster, F. X.; Kiemle, D. J. In *Spectrometric Identification of Organic Compounds;* John Wiley & Sons, Inc.: United States of America, 2005.

(161) Givan, A.; Loewenschuss, A.; Nielsen, C. J. *J. Mol. Struct.* **2002***, 604*, 147-157.

(162) Proctor, A.; Sherwood, P. M. A. *Journal of Electron Spectroscopy and Related Phenomena* **1982**, *27*, 39-56.

(163) Doniach, S.; Sunjic, M. *J. Phys. C* **1970**, *3*, 285-291.

(164) Ball, D. W. *Spectroscopy (Duluth, MN, U. S.)* **2006**, *21*, 14-16.

(165) Salame, I. I.; Bandosz, T. J. *Langmuir* **1999**, *15*, 587-593.

(166) Zhang, N.; Wang, L.; Liu, H.; Cai, Q. *Surf Interface Anal* **2008**, *40*, 1190-1194.

(167) Meng, G.; Li, A.; Yang, W.; Liu, F.; Yang, X.; Zhang, Q. *Eur. Polym. J.* **2007**, *43*, 2732-2737.

(168) Machida, M.; Mochimaru, T.; Tatsumoto, H. *Carbon* **2006**, *44*, 2681-2688.

(169) El-Sheikh, A. H.; Newman, A. P.; Al-Daffaee, H. K.; Phull, S.; Cresswell, N. *J. Anal. Appl. Pyrolysis* **2004**, *71*, 151-164.

(170) Kalpakli, Y. K.; Koyuncu, I. *Ann. Chim. (Rome, Italy)* **2007**, *97*, 1291-1302.

(171) Otowa, T.; Nojima, Y.; Miyazaki, T. *Carbon* **1997**, *35*, 1315-1319.

(172) Beker, U. G.; Malik, D. J.; Strelko, V., Jr.; Streat, M. *Chem. Eng. Commun.* **2003**, *190*, 610-629.

(173) Strelko, V., Jr.; Malik, D. J. *J. Colloid Interface Sci.* **2002**, *250*, 213-220.

(174) Duman, G.; Onal, Y.; Okutucu, C.; Onenc, S.; Yanik, J. *Energy Fuels* **2009**, *23*, 2197-2204.

(175) de Mesquita, J. P.; Martelli, P. B.; Gorgulho, H. d. F. *J. Braz. Chem. Soc.* **2006**, *17*, 1133-1143.

(176) Zhao, N.; Wei, N.; Li, J.; Qiao, Z.; Cui, J.; He, F. *Chem. Eng. J. (Amsterdam, Neth.)* **2005**, *115*, 133-138.

(177) Dastgheib, S. A.; Rockstraw, D. A. *Carbon* **2001**, *39*, 1849-1855.

(178) Momma, T.; Liu, X.; Osaka, T.; Ushio, Y.; Sawada, Y. *J. Power Sources* **1996**, *60*, 249-253.

(179) Grcev, T. P.; Cvetkovska, M. V.; Obradovic, T. B. **1997**, *62*, 157-164.

(180) Bandosz, T. J. *J. Colloid Interface Sci.* **2002**, *246*, 1-20.

(181) Bandosz, T. J.; JagieÅ‚Å‚o, J.; Schwarz, J. A.; Krzyzanowski, A. *Langmuir* **1996**, *12*, 6480-6486.

(182) Bandosz, T. J.; Jagiello, J.; Schwarz, J. A. *Langmuir* **1993**, *9*, 2518-2522.

(183) Yano, J.; Hirayama, H.; Harima, Y.; Kitani, A. *J. Electrochem. Soc.* **2010**, *157*, B506-B511.

(184) Palaniappan, S.; Manisankar, P. *Polym. Int.* **2010**, *59*, 456-462.

(185) Sawyer, D. T.; Sobkowiak, A.; Roberts, J. L. J. In *Chapter 5: Electrochemical Cells and Instrumentation.* Electrochemistry for Chemists; John Wiley: New York, 1995; pp 170-248.

(186) Kinyanjui, J. M.; Hanks, J.; Hatchett, D. W.; Smith, A.; Josowicz, M. *J. Electrochem. Soc.* **2004**, *151*, D113-D120.

(187) Weng, S.; Lin, Z.; Chen, L.; Zhou, J. *Electrochim. Acta* **2010**, *55*, 2727-2733.

(188) Yue, J.; Epstein, A. J. *J. Am. Chem. Soc.* **1990**, *112*, 2800-2801.

(189) Shenk, J. S.; Workman, J. J. J.; Westerhaus, M. O. In *Application of NIR Spectroscopy to Agricultural Products;* Burns, D. A., Ciurczak, E. W., Eds.; Handbook of Near-Infrared Analysis; CRC Press, Taylor & Francis Group: United States of America, 2008; pp 347-386.

(190) Li, N.; Shan, D.; Shi, C.; Xue, H. *J Appl Polym Sci* **2009**, *112*, 1070-1075.

(191) Branzoi, V.; Pilan, L.; Branzoi, F.; Anghel, C. *Mol. Cryst. Liq. Cryst.* **2006**, *447*, 319-340.

(192) Yakushi, K.; Lauchlan, L. J.; Clarke, T. C.; Street, G. B. *J. Chem. Phys.* **1983**, *79*, 4774-4778.

(193) Bard, A. J.; Faulkner, L. R. In *Electrochemical Methods: Fundamentals and Applications;* John Wiley & Sons: United States of America, 2001, pp 833.

(194) Mi, H.; Zhang, X.; Ye, X.; Yang, S. *J. Power Sources* **2008**, *176*, 403-409.

(195) Iroh, J. O.; Zhu, Y.; Shah, K.; Levine, K.; Rajagopalan, R.; Uyar, T.; Donley, M.; Mantz, R.; Johnson, J.; Voevodin, N. N.; Balbyshev, V. N.; Khramov, A. N. *Prog. Org. Coat.* **2003**, *47*, 365-375.

Appendix

A.1 XPS Spectra

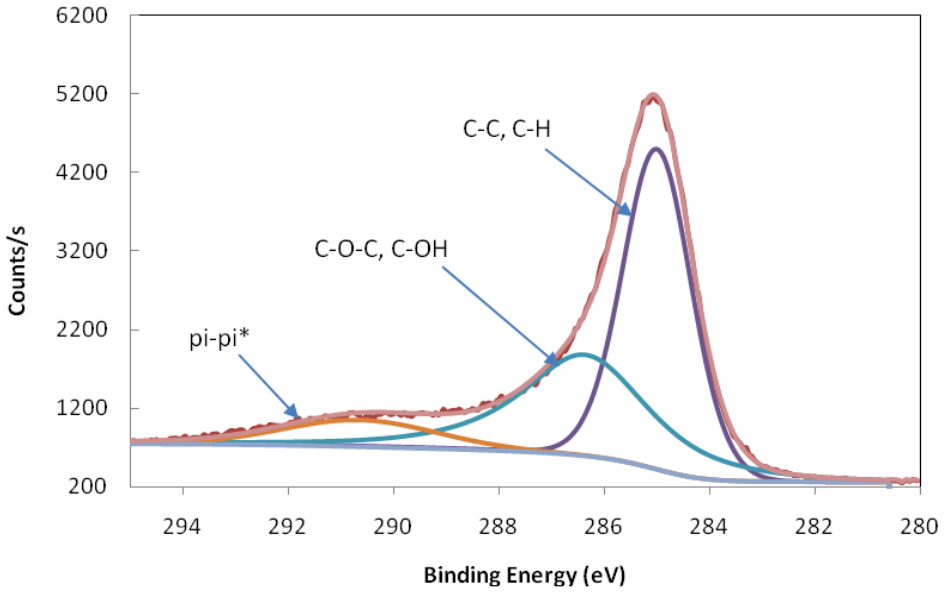

A 1. Fitted C1s XPS spectrum of Spectracarb 2225 carbon cloth performed at Dalhousie University.

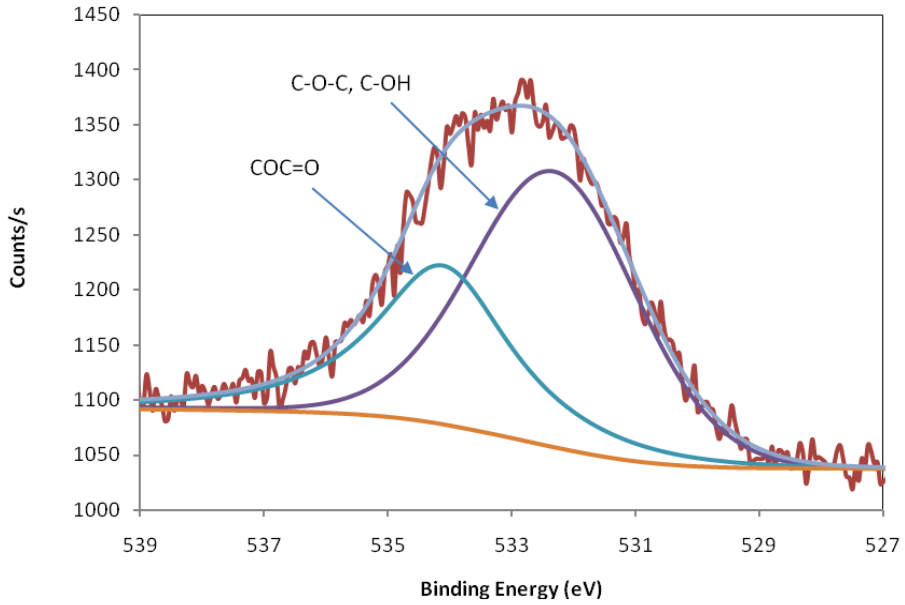

A 2. Fitted O1s XPS spectrum of Spectracarb 2225 carbon cloth performed at Dalhousie University.

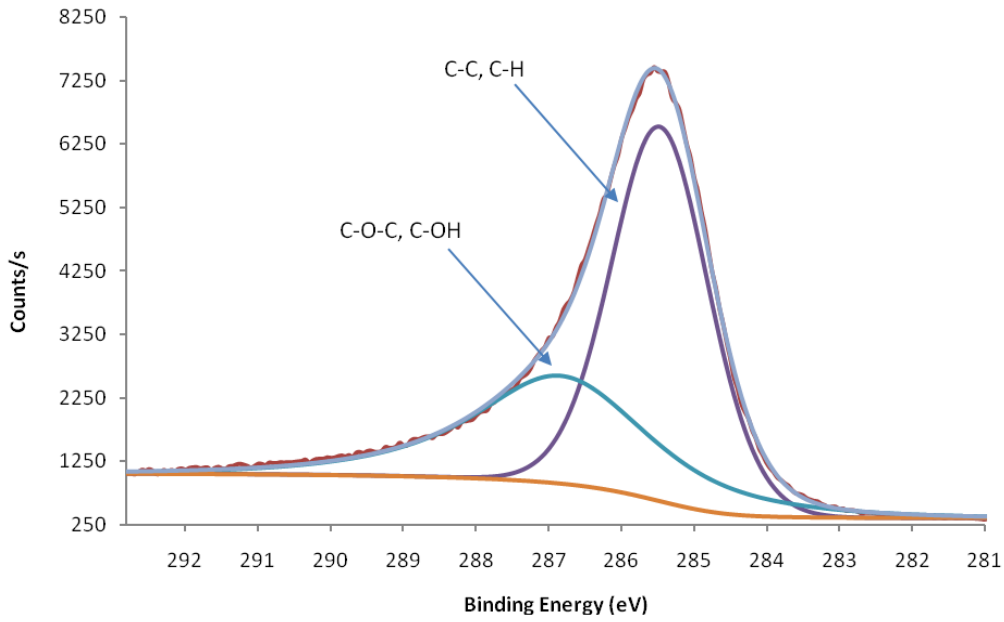

A 3. Fitted C1s XPS spectrum of glassy carbon plate performed at Dalhousie University.

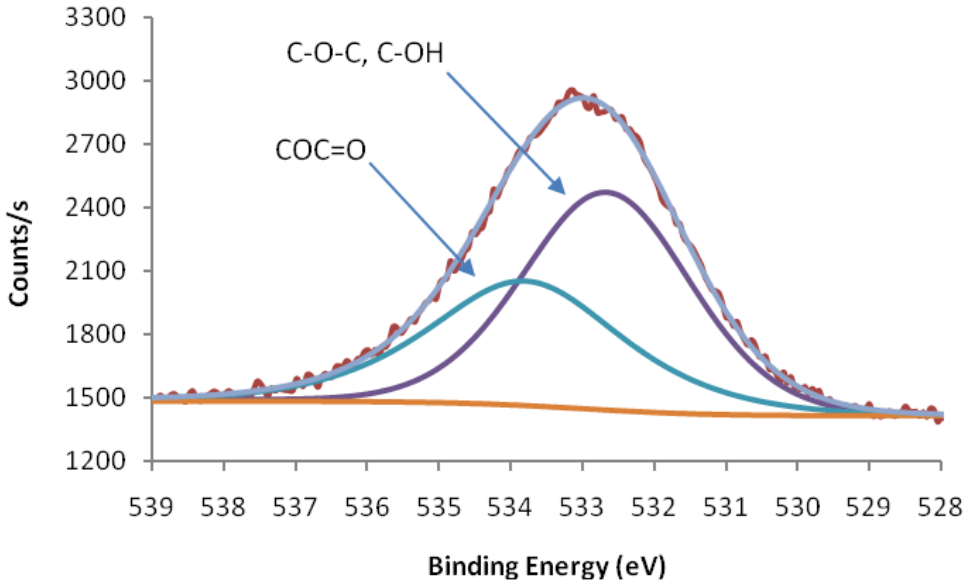

A 4. Fitted O1s XPS spectrum of glassy carbon plate performed at Dalhousie University.

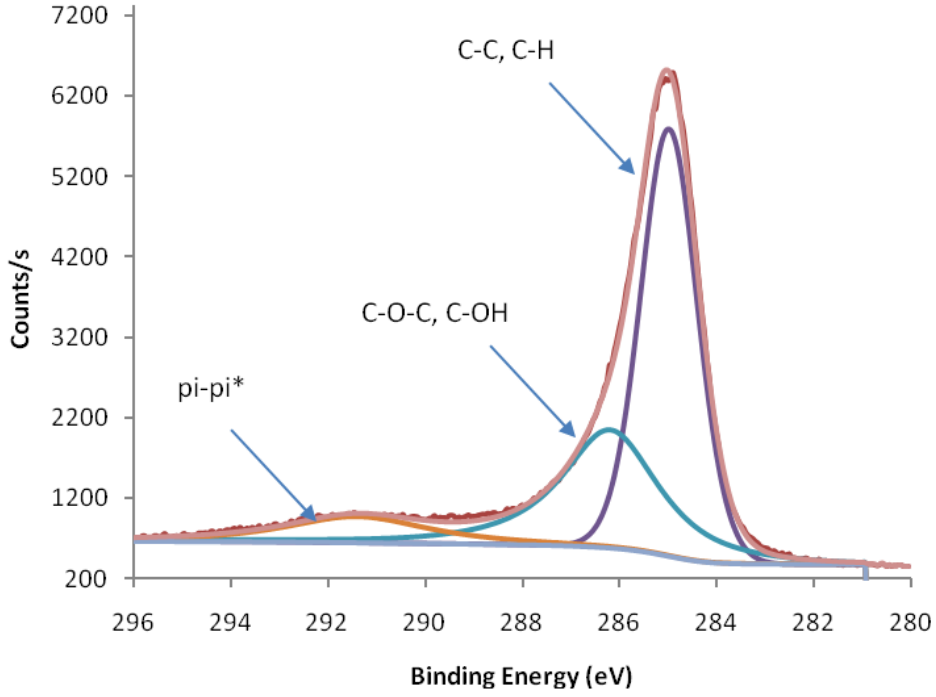

A 5. Fitted C1s XPS spectrum of graphite powder performed at Dalhousie University.

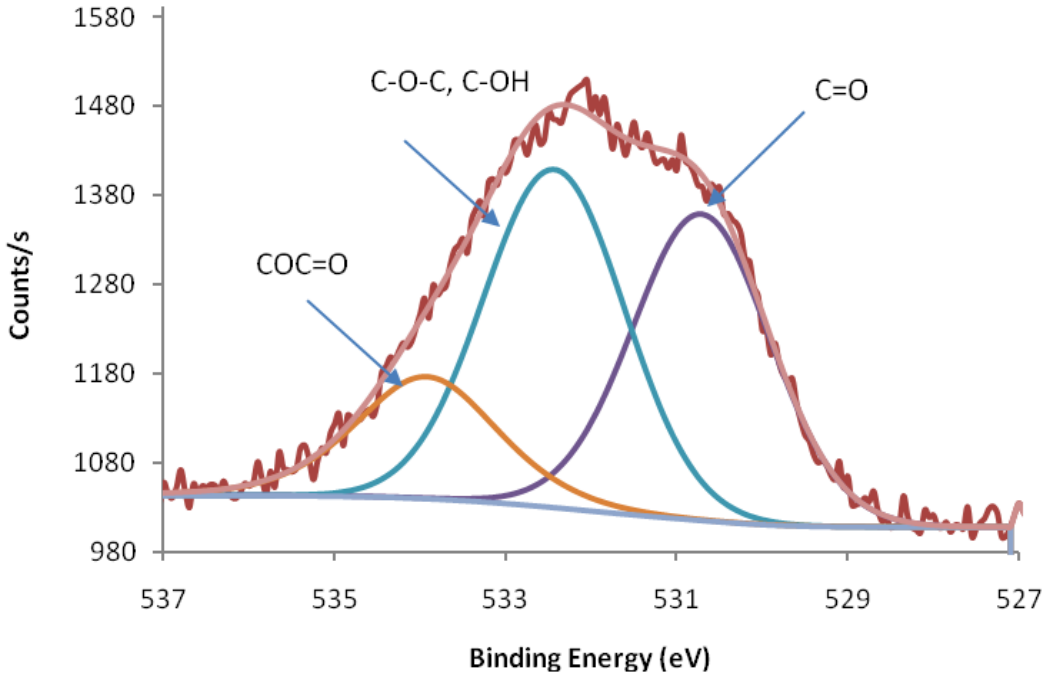

A 6. Fitted O1s XPS spectrum of graphite powder performed at Dalhousie University.

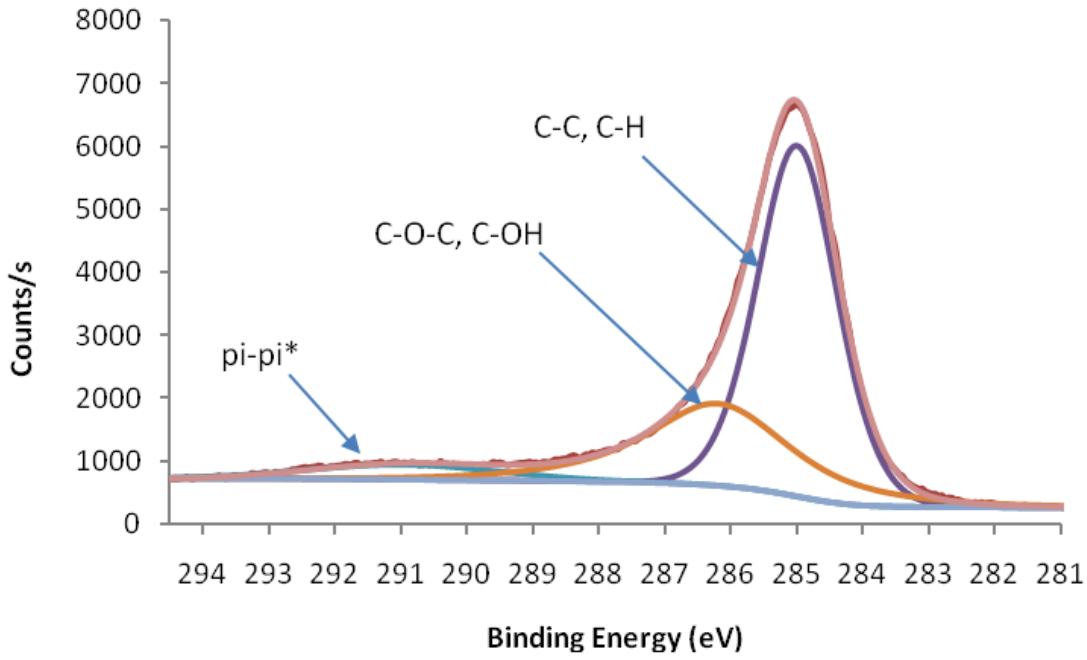

A 7. Fitted C1s XPS spectrum of glassy carbon powder performed at Dalhousie University.

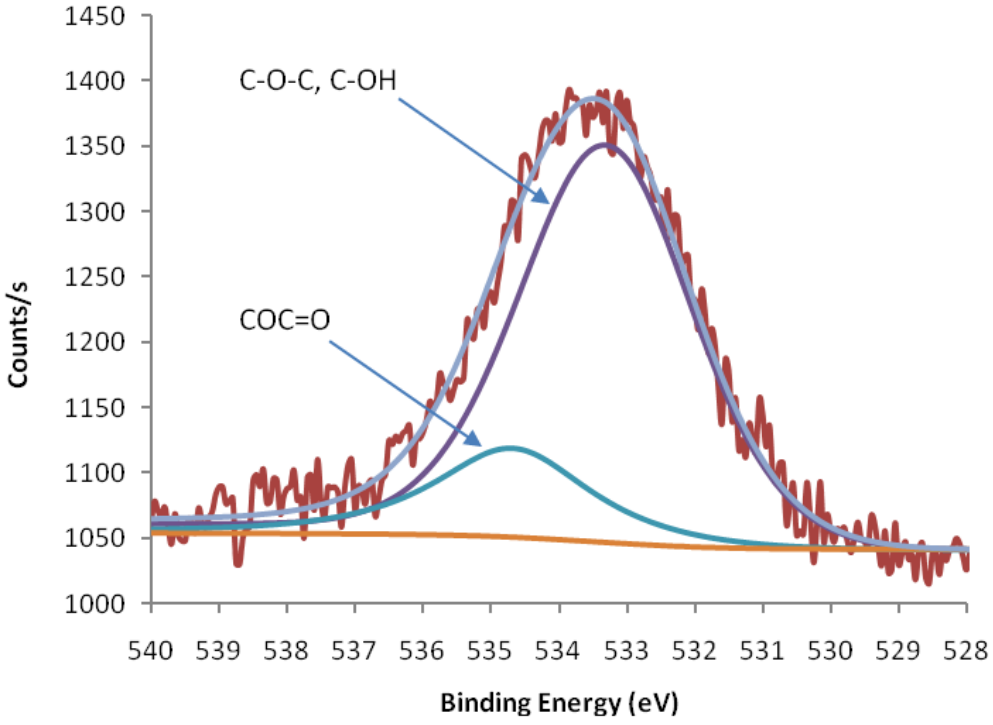

A 8. Fitted O1s XPS spectrum of glassy carbon powder performed at Dalhousie University.

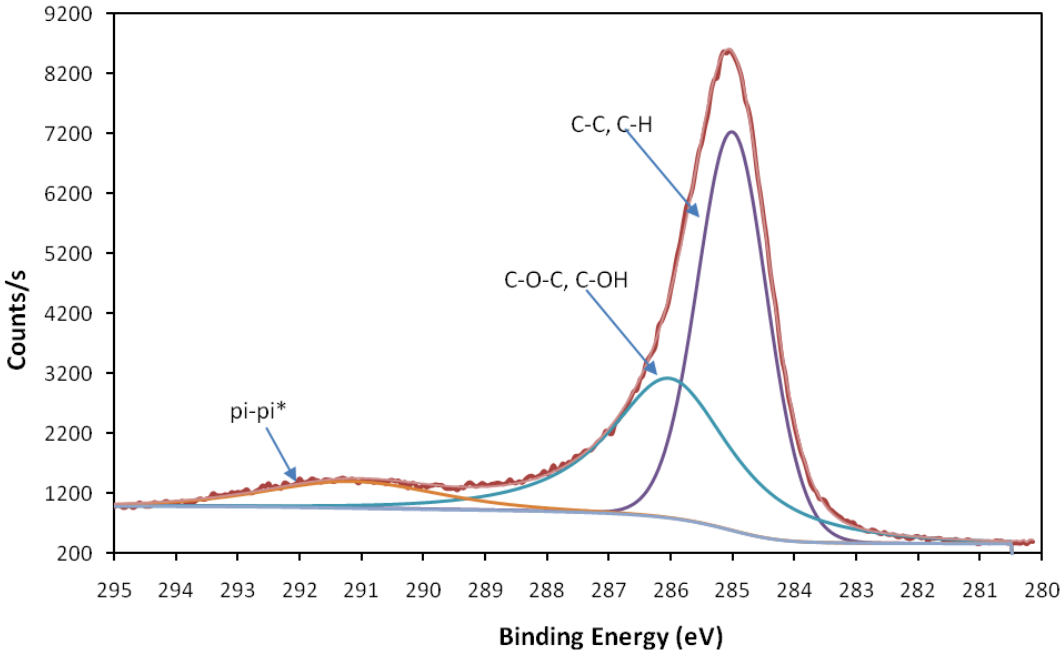

A 9. Fitted C1s XPS spectrum of mesoporous carbon powder performed at Dalhousie University.

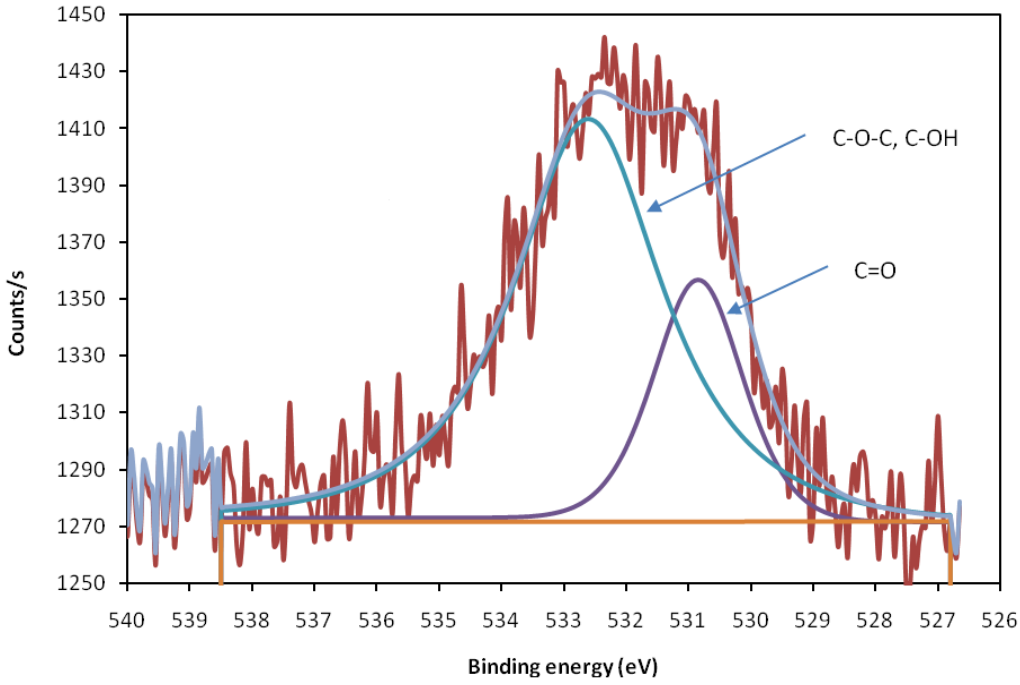

A 10. Fitted O1s XPS spectrum of mesoporous carbon powder performed at Dalhousie University.

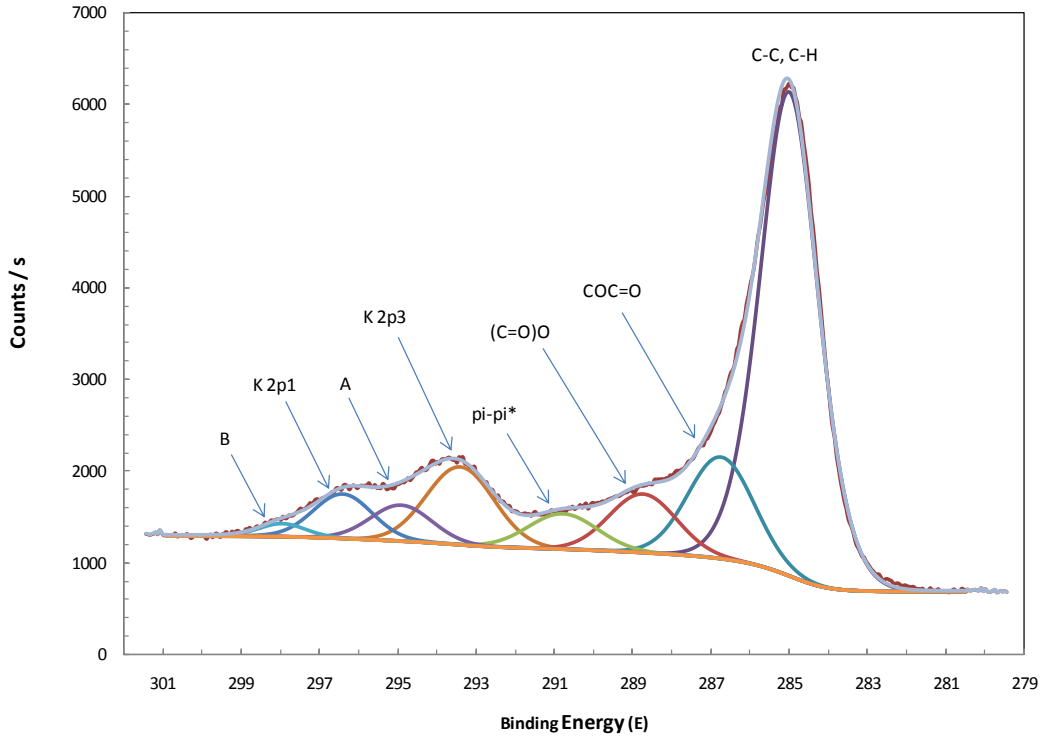

A 11. Fitted C1s XPS spectrum of ELIT carbon powder performed at Dalhousie University.

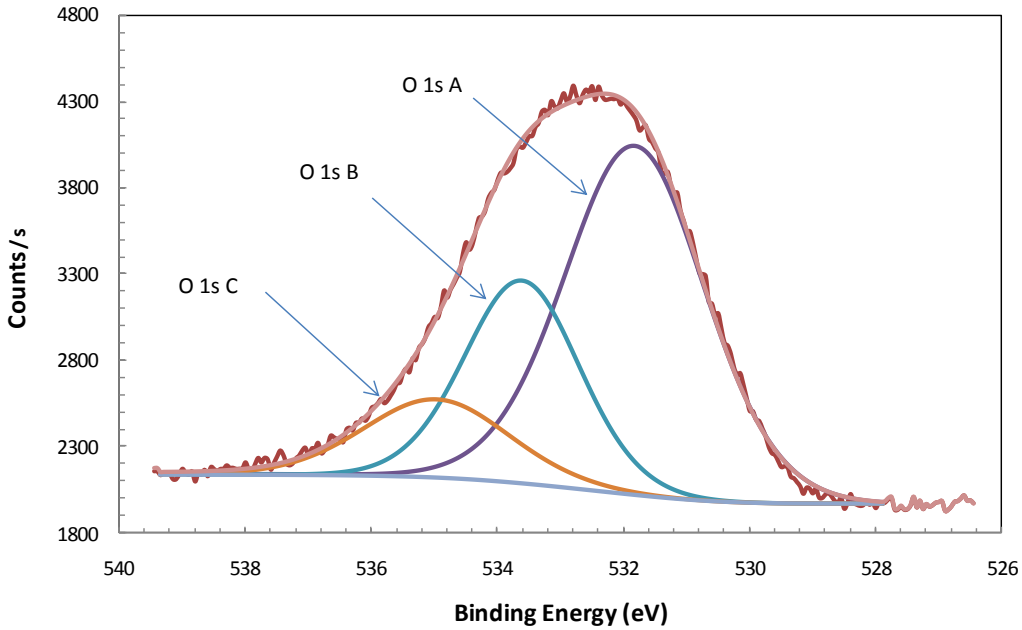

A 12. Fitted O1s XPS spectrum of ELIT carbon powder performed at Dalhousie University.

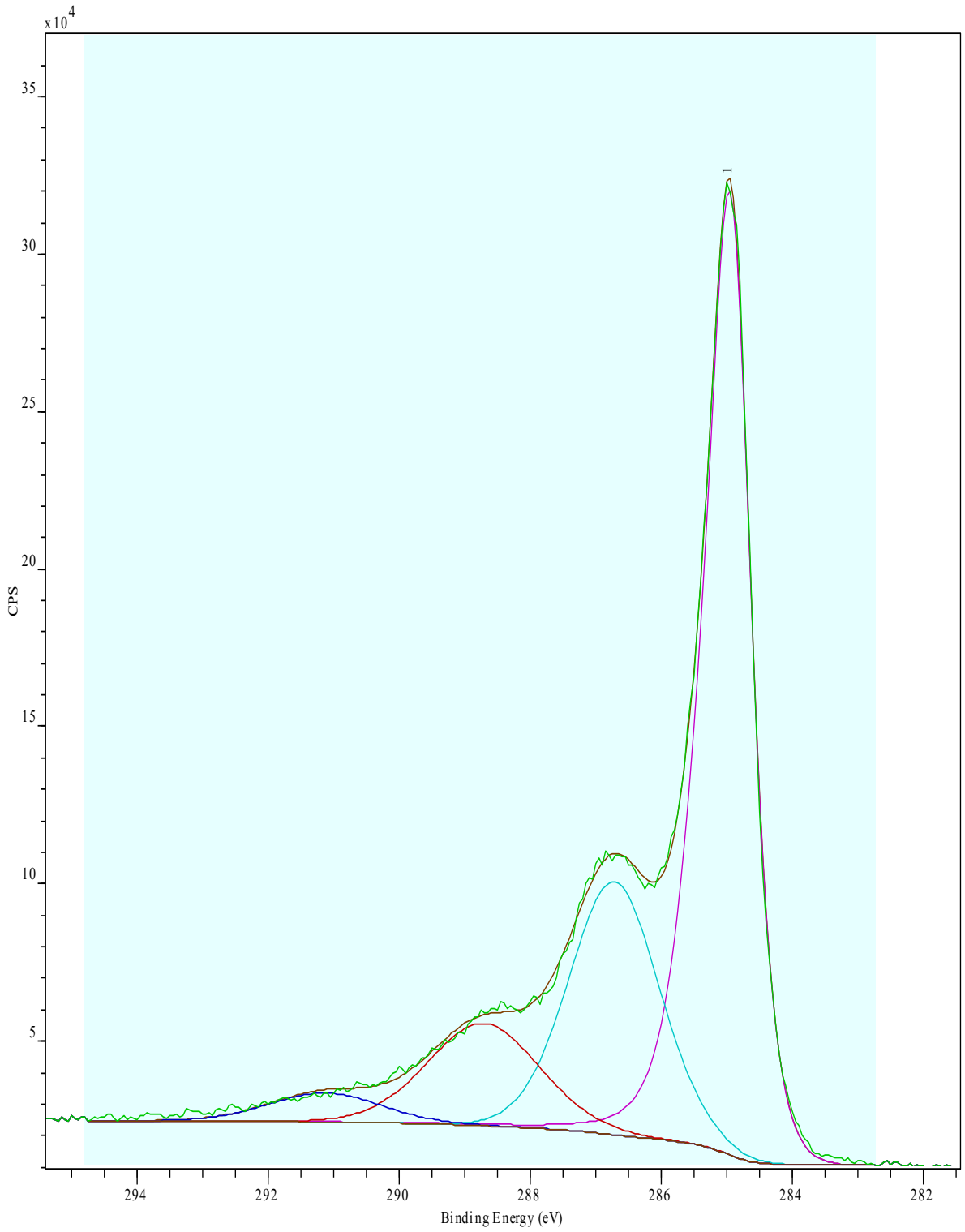

A 13. Fitted C1s XPS spectrum of Spectracarb 2225 carbon cloth treated with 1.0 M H_2SO_4 performed at the Canadian Light Source.

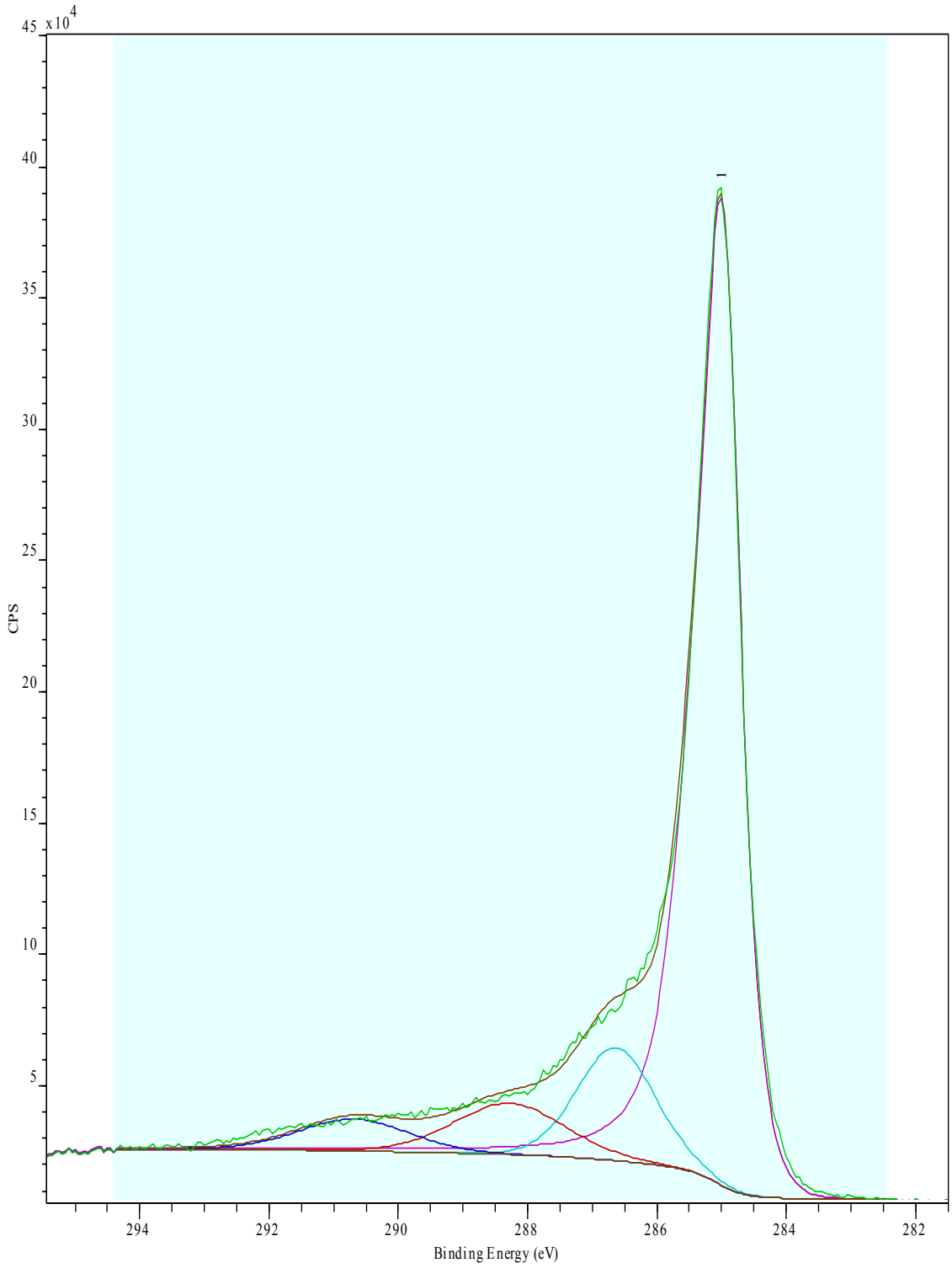

A 14. Fitted C1s XPS spectrum of Spectracarb 2225 carbon cloth electrode cycled for two cycles from 0.0 to 1.0 V vs. SHE at 1.0 mV/s in 1.0 M H_2SO_4 performed at the Canadian Light Source.

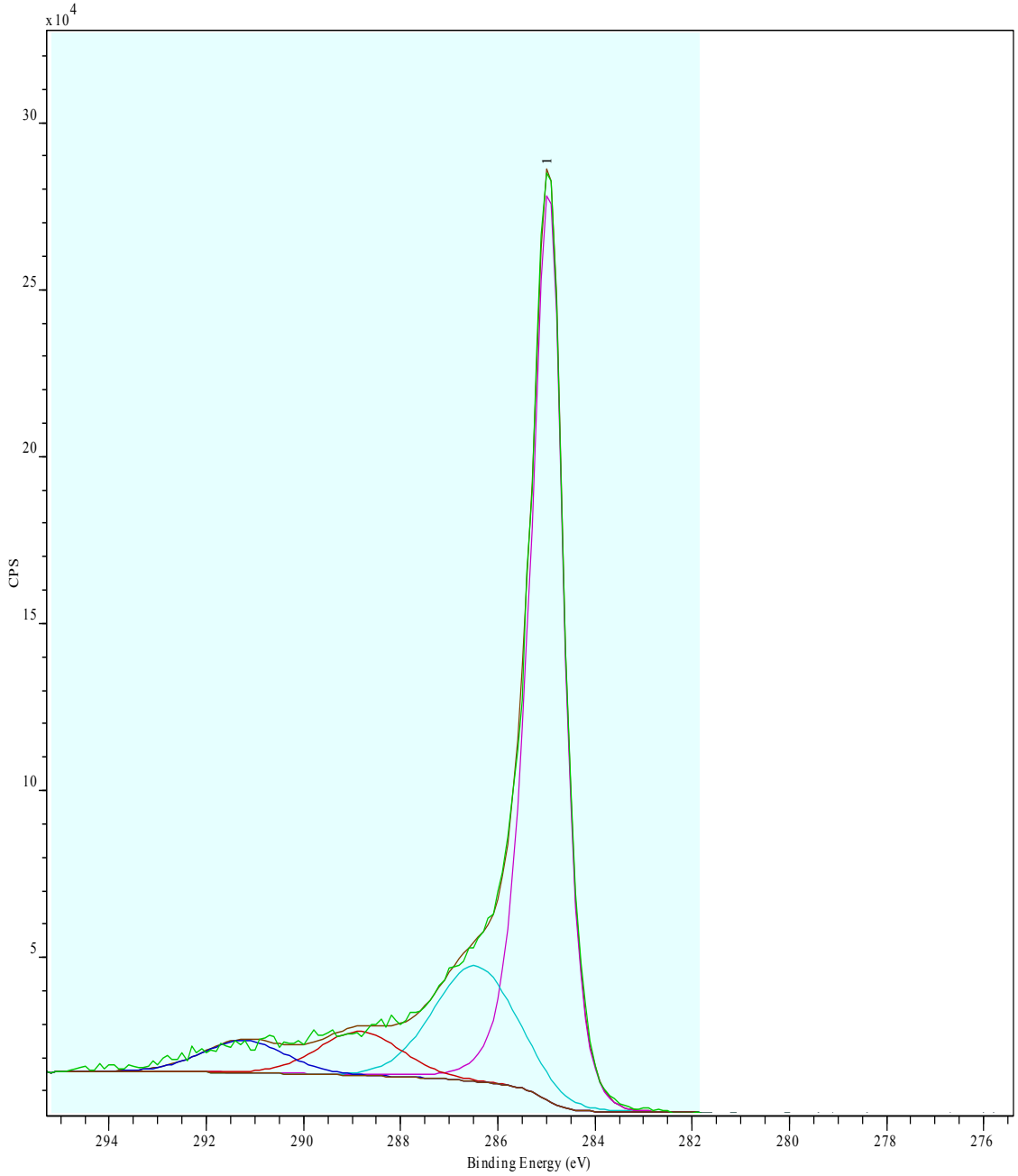

A 15. Fitted C1s XPS spectrum of Spectracarb 2225 carbon cloth electrode cycled for one day from 0.0 to 1.0 V vs. SHE at 1.0 mV/s in 1.0 M H_2SO_4 performed at the Canadian Light Source.

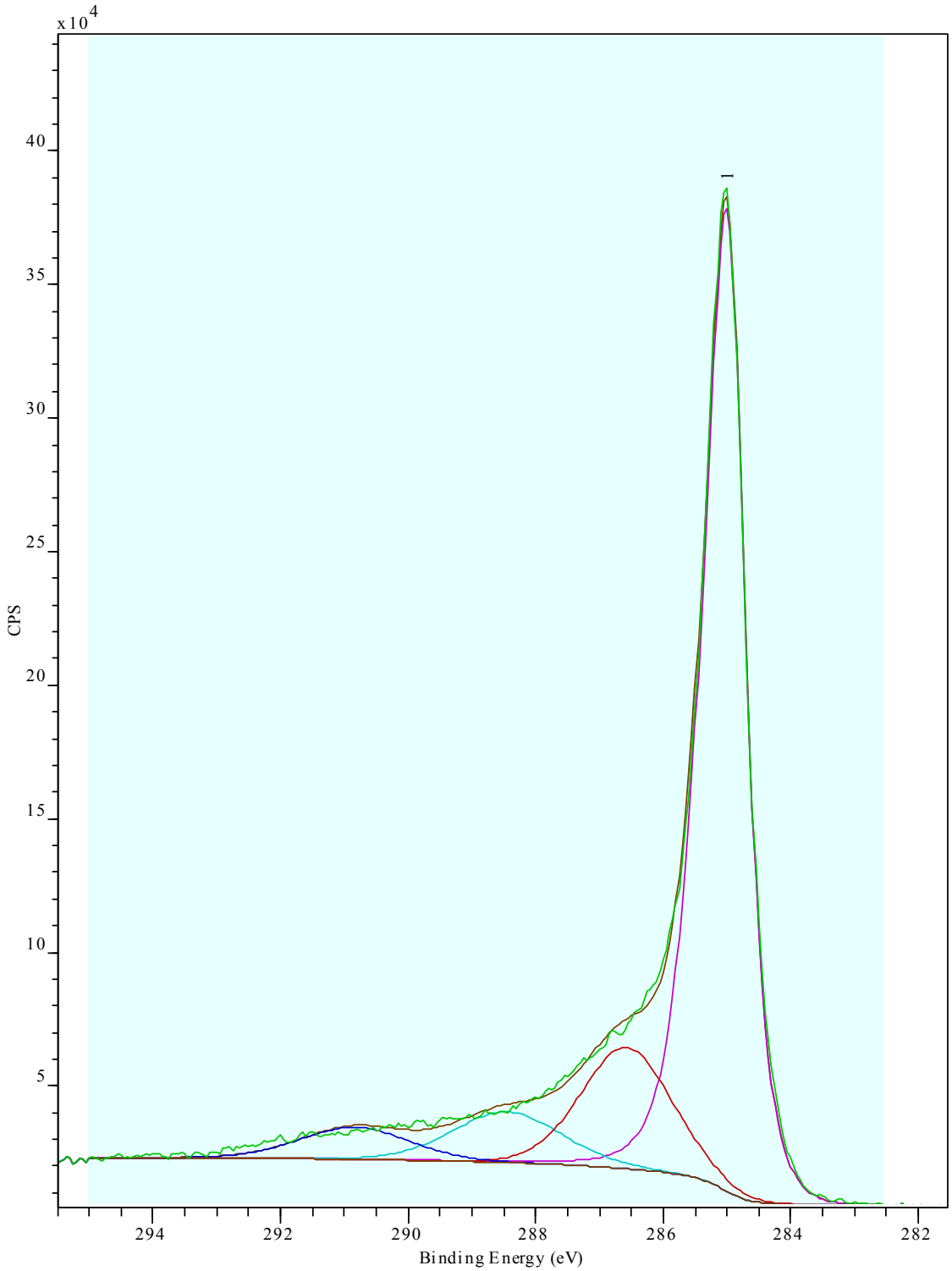

A 16. Fitted C1s XPS spectrum of Spectracarb 2225 carbon cloth electrode cycled for two days from 0.0 to 1.0 V vs. SHE at 1.0 mV/s in 1.0 M H_2SO_4 performed at the Canadian Light Source.

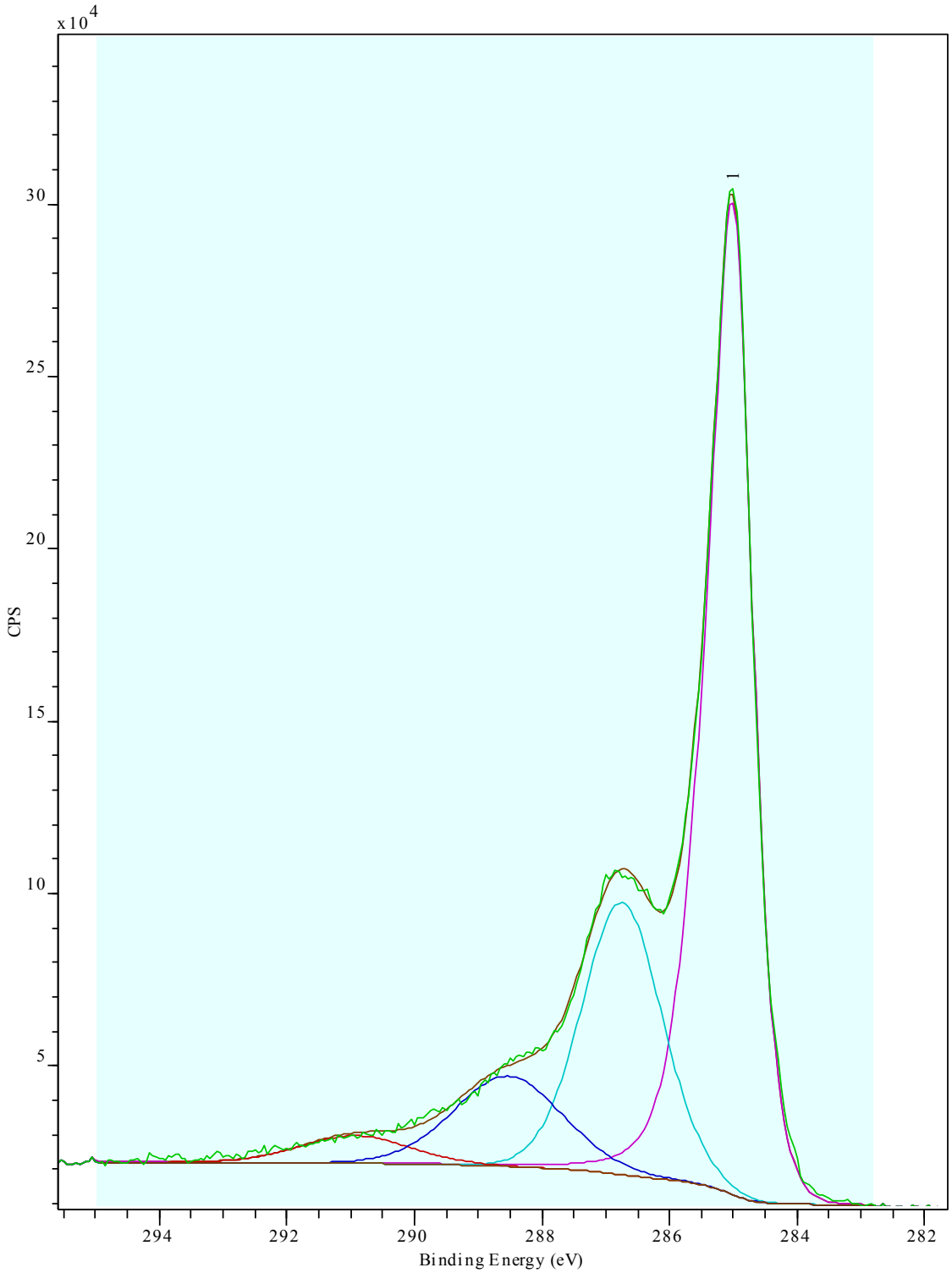

A 17. Fitted C1s XPS spectrum of Spectracarb 2225 carbon cloth electrode cycled for one week from 0.0 to 1.0 V vs. SHE at 1.0 mV/s in 1.0 M H_2SO_4 performed at the Canadian Light Source.

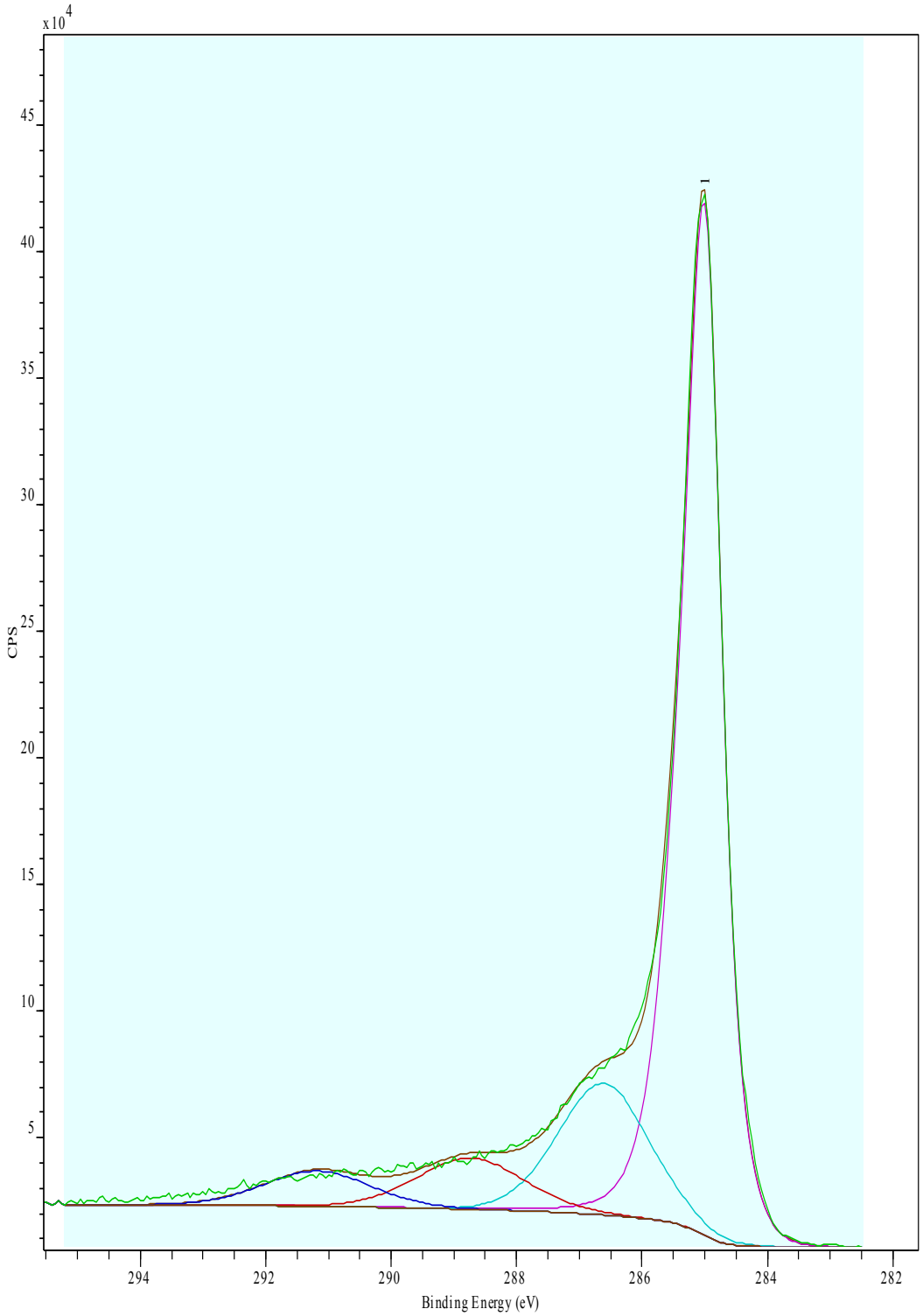

A 18. Fitted C1s XPS spectrum of Spectracarb 2225 carbon cloth electrode cycled for one week from 0.0 to 1.0 V vs. SHE at 1.0 mV/s in 1.0 M H_2SO_4 and extracted at 0.0 V performed at the Canadian Light Source.

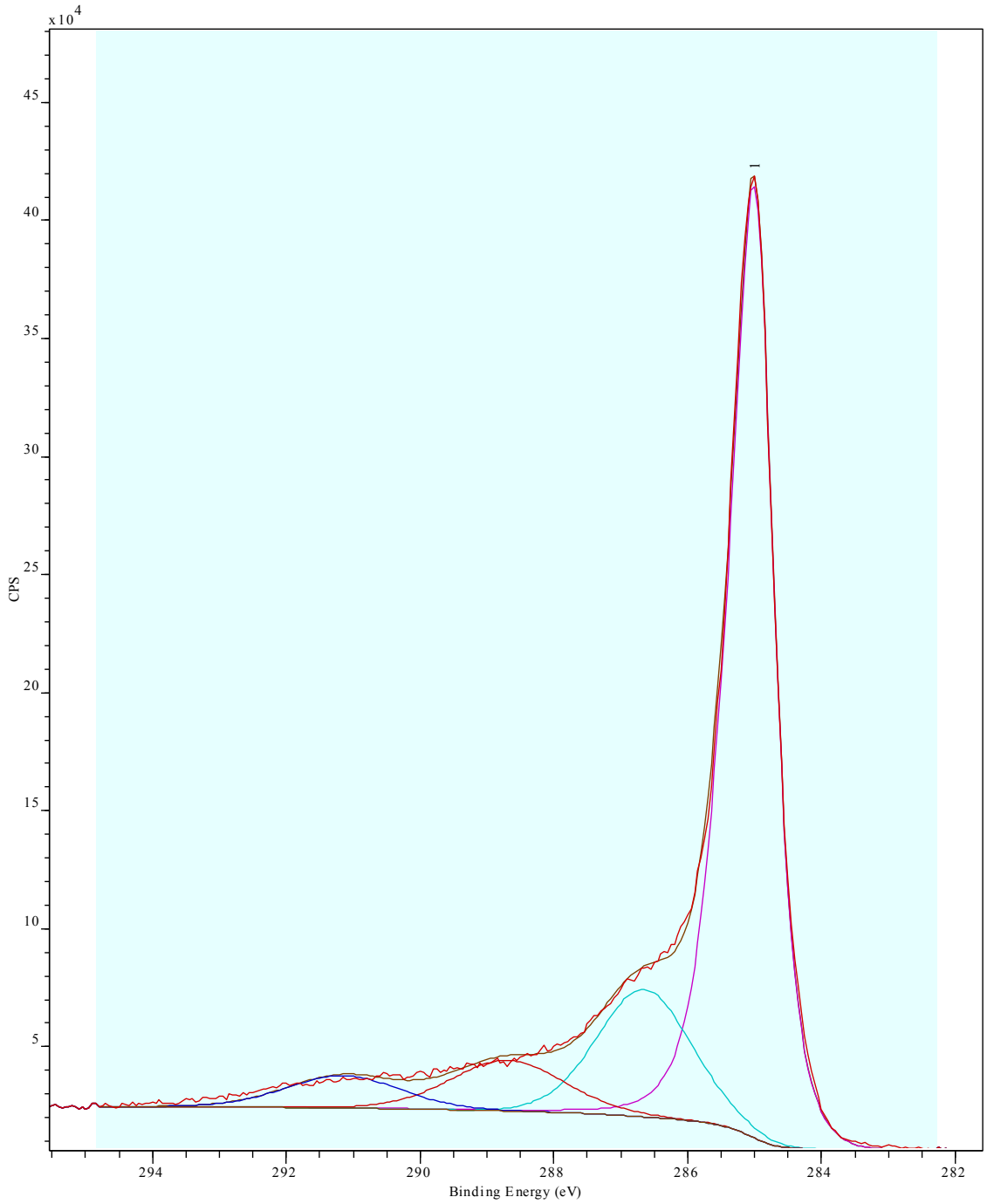

A 19. Fitted C1s XPS spectrum of Spectracarb 2225 carbon cloth electrode cycled for one week from 0.0 to 1.0 V vs. SHE at 1.0 mV/s in 1.0 M H_2SO_4 and extracted at 0.5 V performed at the Canadian Light Source.

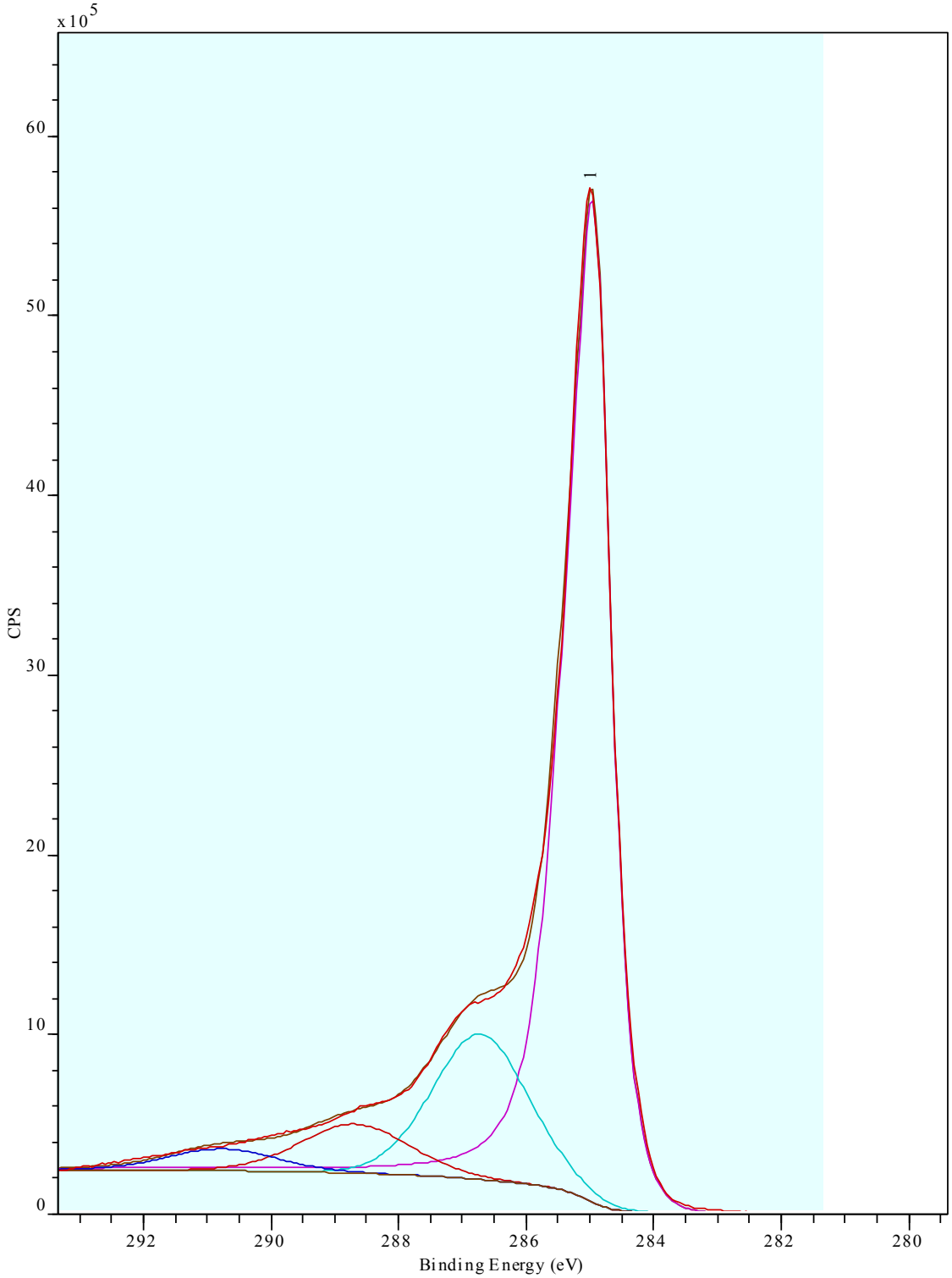

A 20. Fitted C1s XPS spectrum of Spectracarb 2225 carbon cloth electrode cycled for one week from 0.0 to 1.0 V vs. SHE at 1.0 mV/s in 1.0 M H_2SO_4 and extracted at 1.0 V performed at the Canadian Light Source.

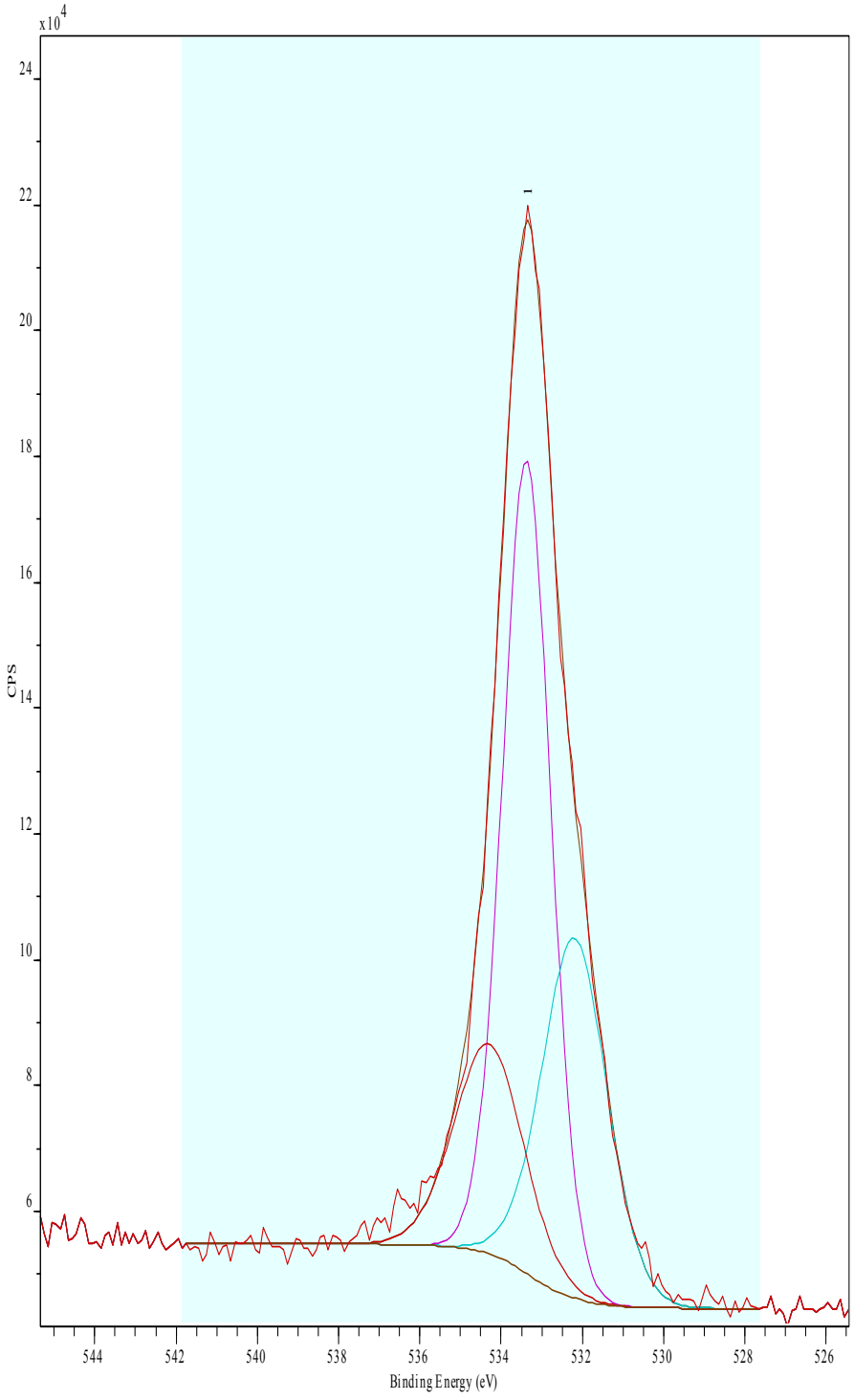

A 21. Fitted O1s XPS spectrum of Spectracarb 2225 carbon cloth treated with 1.0 M H_2SO_4 performed at the Canadian Light Source.

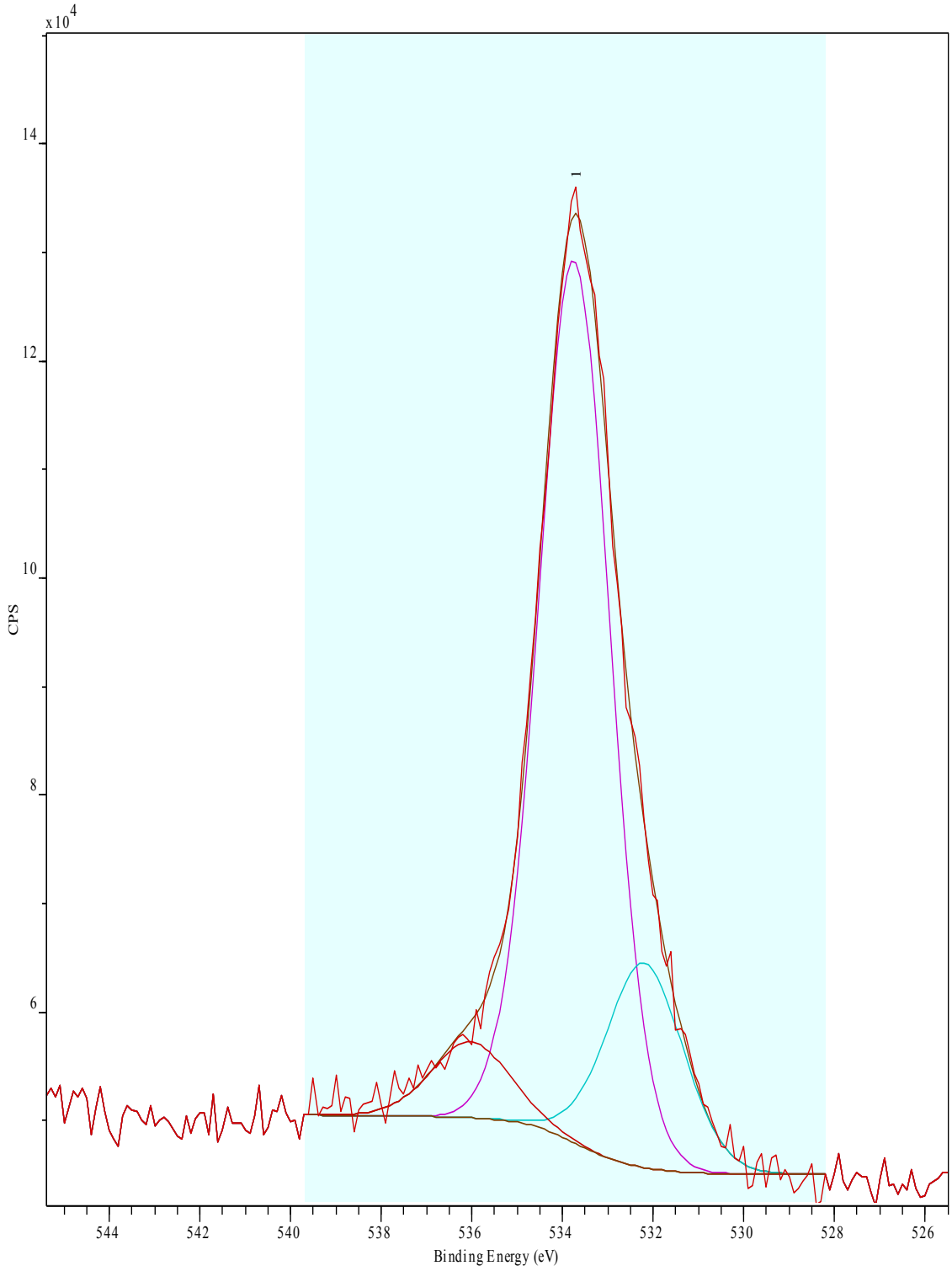

A 22. Fitted O1s XPS spectrum of Spectracarb 2225 carbon cloth electrode cycled for two cycles from 0.0 to 1.0 V vs. SHE at 1.0 mV/s in 1.0 M H_2SO_4 performed at the Canadian Light Source.

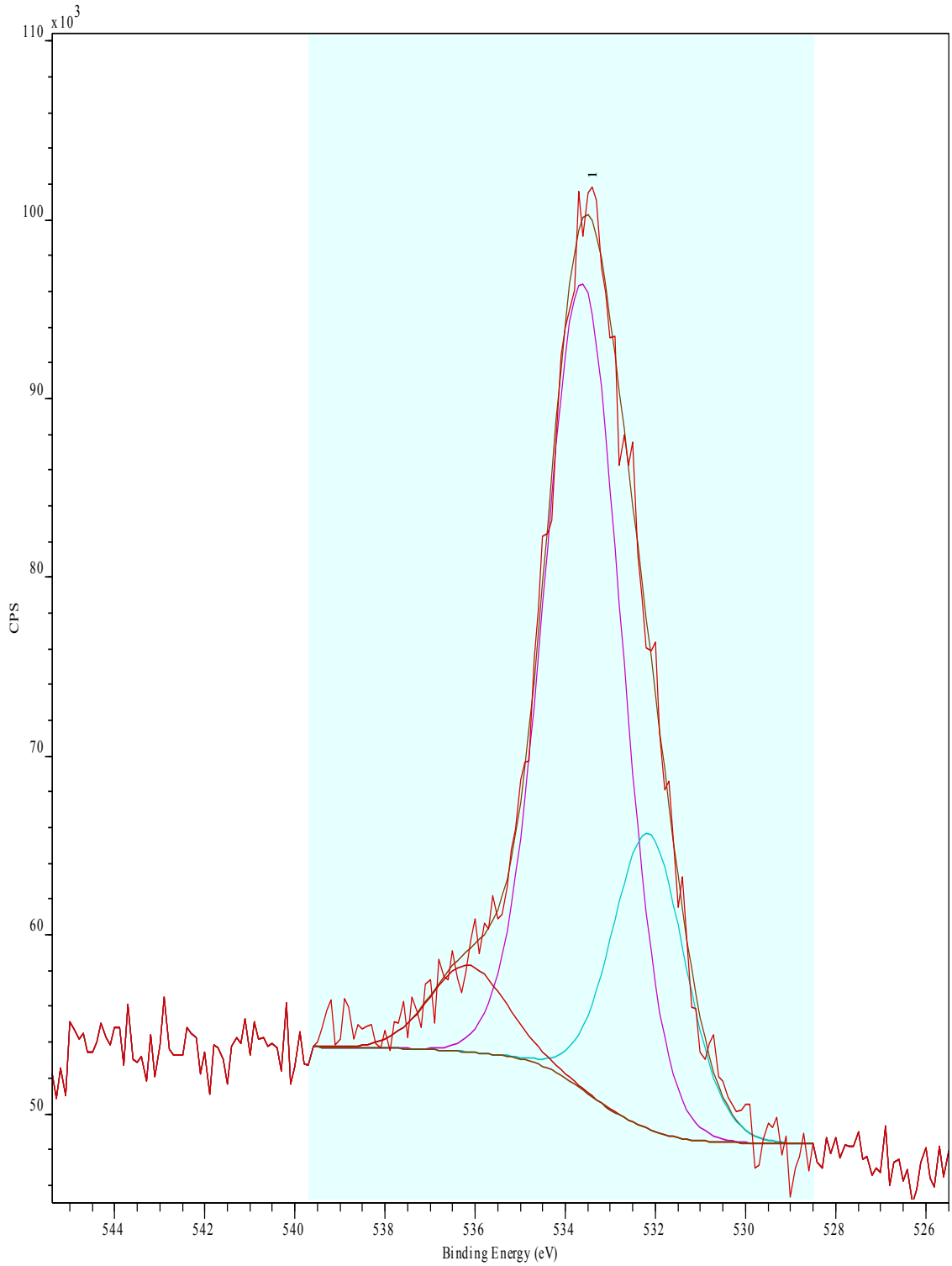

A 23. Fitted O1s XPS spectrum of Spectracarb 2225 carbon cloth electrode cycled for one day from 0.0 to 1.0 V vs. SHE at 1.0 mV/s in 1.0 M H_2SO_4 performed at the Canadian Light Source.

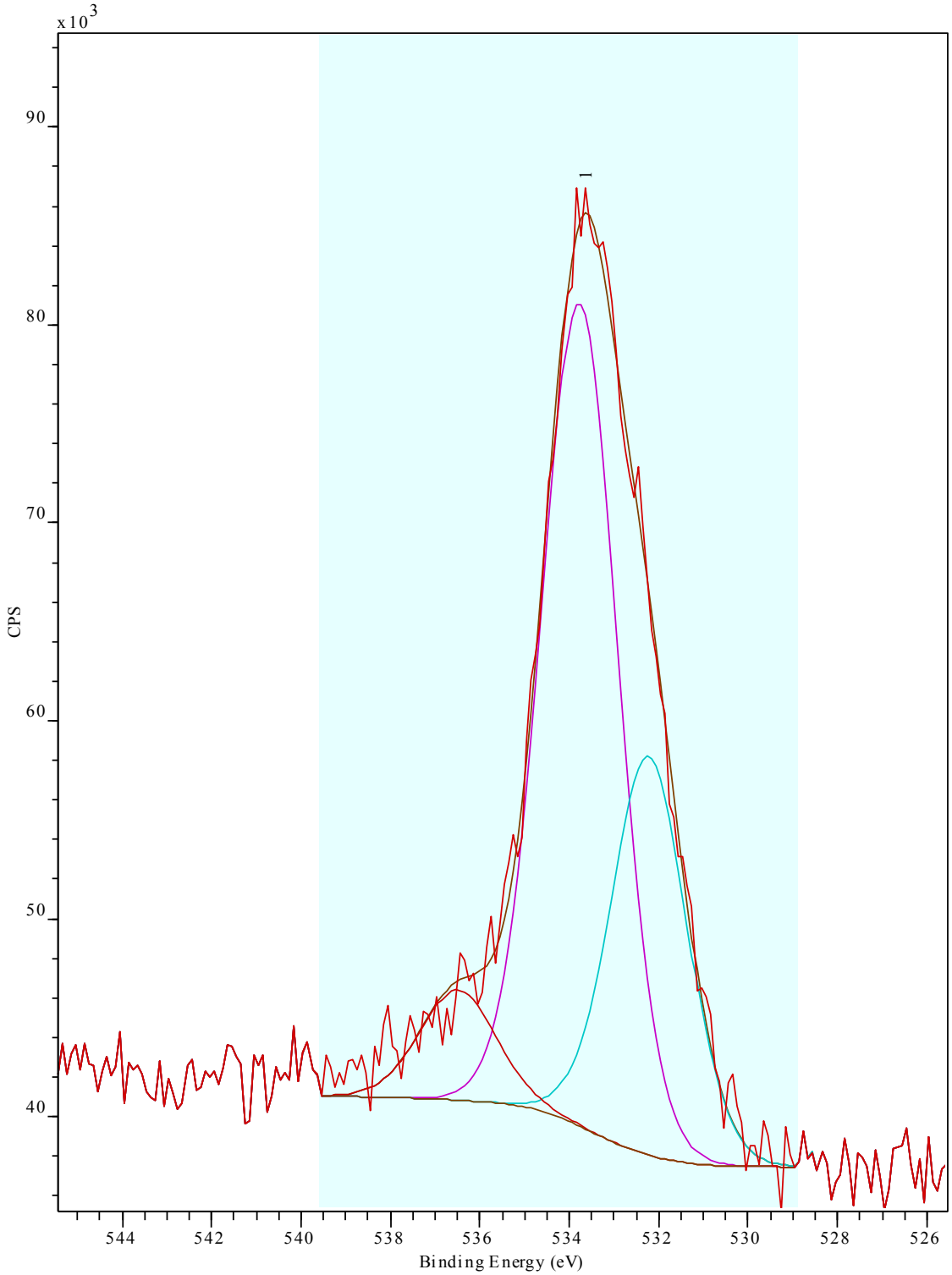

A 24. Fitted O1s XPS spectrum of Spectracarb 2225 carbon cloth electrode cycled for two days from 0.0 to 1.0 V vs. SHE at 1.0 mV/s in 1.0 M H_2SO_4 performed at the Canadian Light Source.

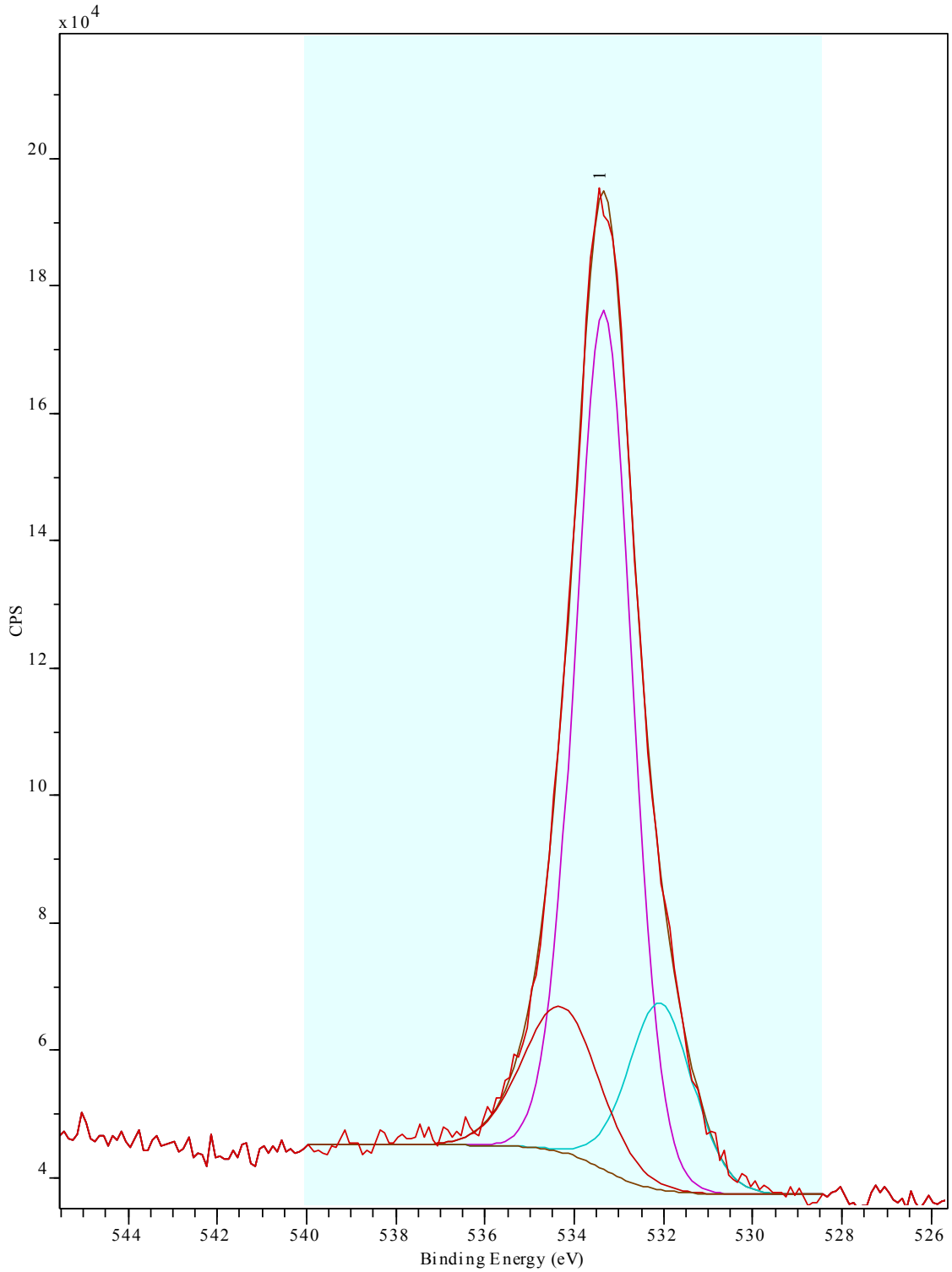

A 25. Fitted O1s XPS spectrum of Spectracarb 2225 carbon cloth electrode cycled for one week from 0.0 to 1.0 V vs. SHE at 1.0 mV/s in 1.0 M H_2SO_4 performed at the Canadian Light Source.

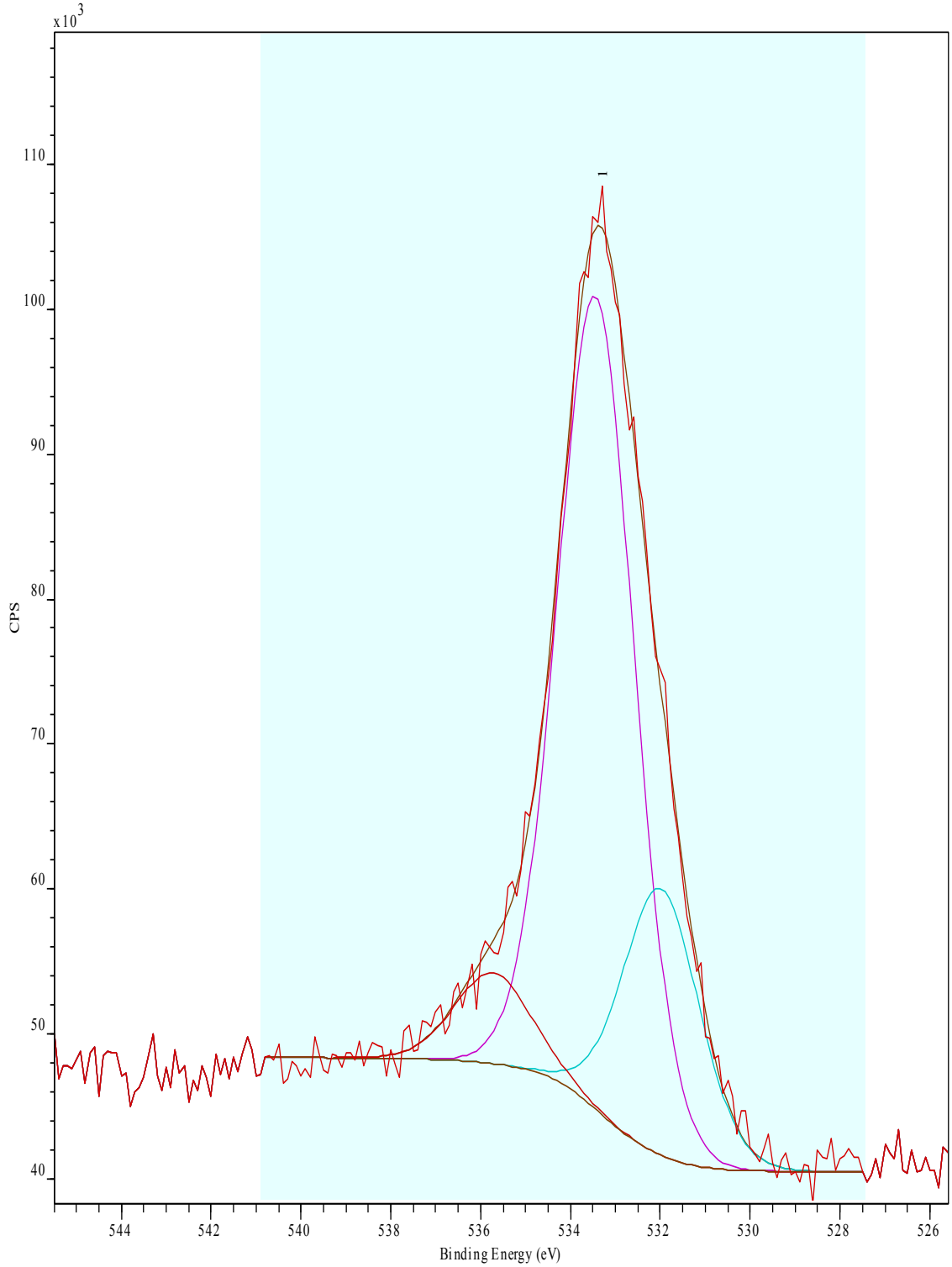

A 26. Fitted O1s XPS spectrum of Spectracarb 2225 carbon cloth electrode cycled for one week from 0.0 to 1.0 V vs. SHE at 1.0 mV/s in 1.0 M H_2SO_4 and extracted at 0.0 V performed at the Canadian Light Source.

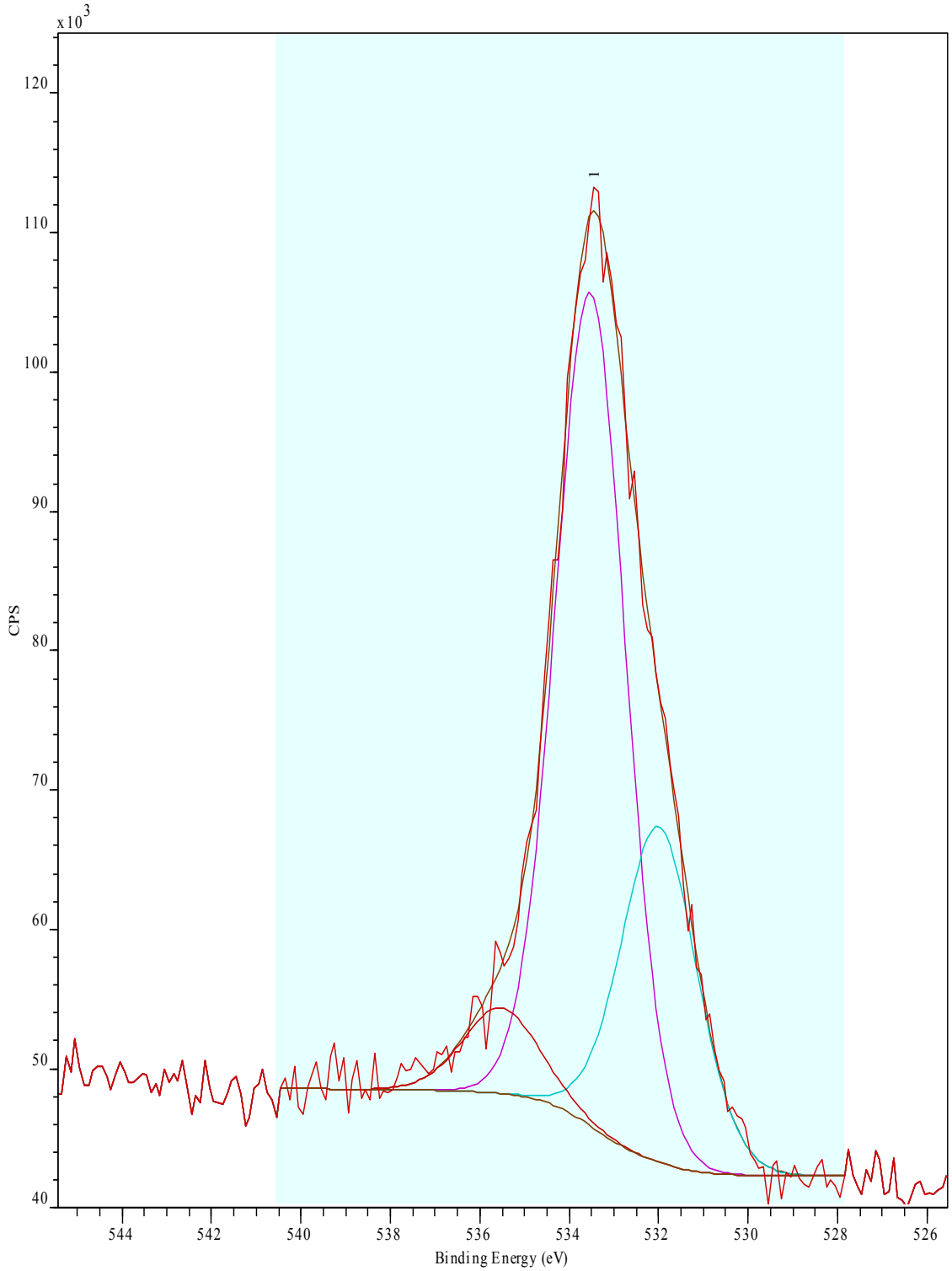

A 27. Fitted O1s XPS spectrum of Spectracarb 2225 carbon cloth electrode cycled for one week from 0.0 to 1.0 V vs. SHE at 1.0 mV/s in 1.0 M H_2SO_4 and extracted at 0.5 V performed at the Canadian Light Source.

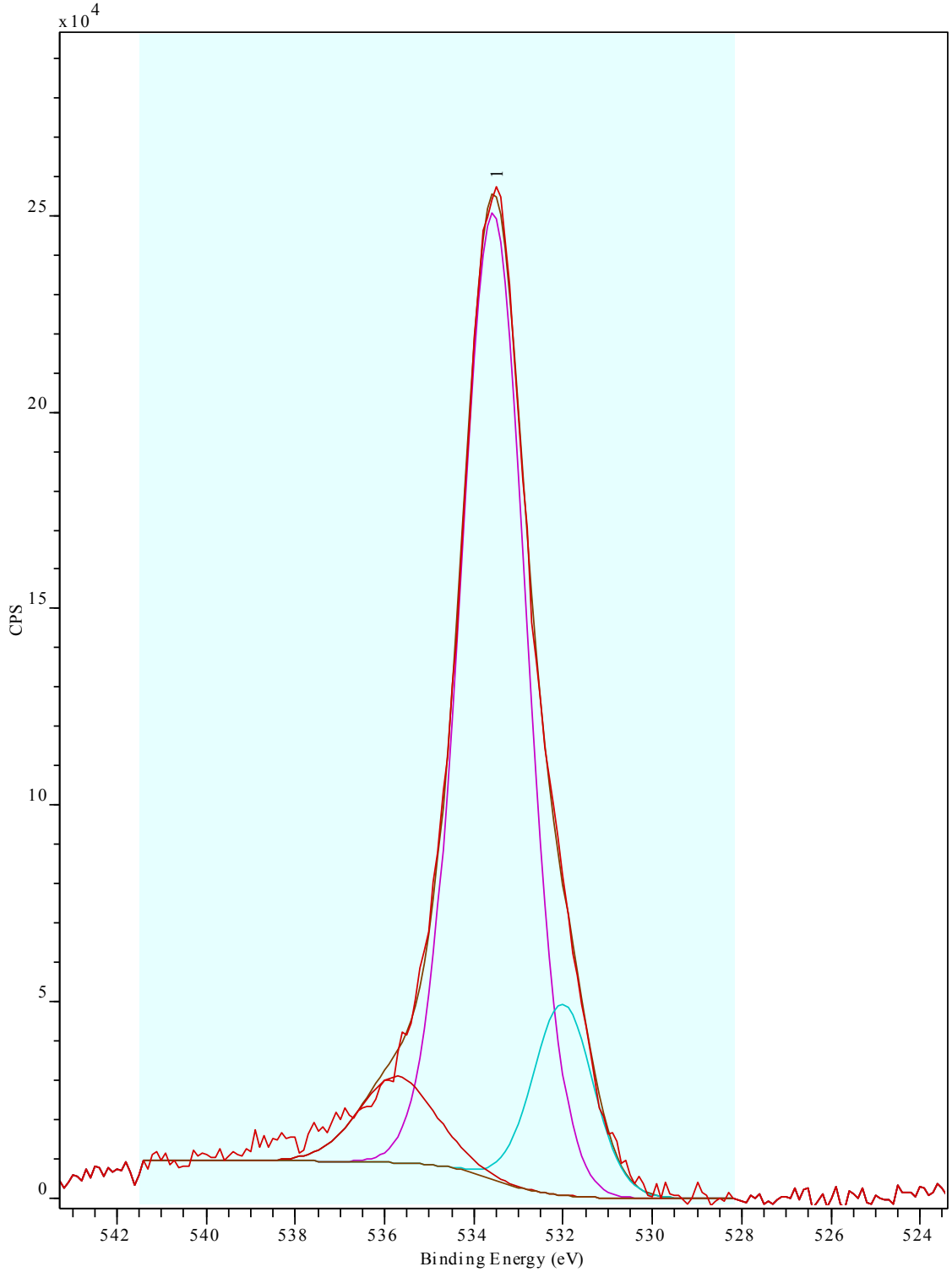

A 28. Fitted O1s XPS spectrum of Spectracarb 2225 carbon cloth electrode cycled for one week from 0.0 to 1.0 V vs. SHE at 1.0 mV/s in 1.0 M H_2SO_4 and extracted at 1.0 V performed at the Canadian Light Source.

A.2 Raw data for Endpoint Determination Data in the Standardization of the Boehm Titration

A 29. Comparison of endpoints determined by phenolphthalein vs. pH meter: phenolphthalein data.

Titration	Volume NaOH (mL)	Volume HCl (mL)	pH at endpoint
1	9.20	10.00	8.55
2	9.23	10.00	8.56
3	9.23	10.00	8.78
average	9.22		8.63
SD	0.02		0.13
%RSD	0.19		1.51

A 30. Comparison of endpoints determined by phenolphthalein vs. pH meter: pH meter data.

Titration	Volume NaOH (mL)	Volume HCl (mL)	pH at endpoint
1	9.18	10.00	6.92
2	9.19	10.00	6.93
3	9.19	10.00	6.99
average	9.19		6.95
SD	0.01		0.04
%RSD	0.06		0.55

A 31. Comparison of endpoints determined by methyl red vs. pH meter: methyl red data.

Titration	Volume NaOH (mL)	Volume HCl (mL)	pH at endpoint
1	10.00	10.86	5.97
2	10.00	10.83	5.92
3	10.00	10.70	5.98
average		10.80	5.96
SD		0.09	0.03
%RSD		0.79	0.54

A 32. Comparison of endpoints determined by methyl red vs. pH meter: pH meter data.

Titration	Volume NaOH (mL)	Volume HCl (mL)	pH at endpoint
1	10.00	10.54	7.05
2	10.00	10.40	6.97
3	10.00	10.28	7.01
average		10.41	7.01
SD		0.13	0.04
%RSD		1.3	0.57

A.3 Raw Data from the Boehm Titration on Spectracarb 2225 Carbon Cloth

A 33. Amounts of functional groups on Spectracarb 2225 carbon cloth based on the Boehm titration, before averaging.

	n_{CSF} ± uncertainty (µmol/g)			
Time of electrochemical cycling	Reacted with $NaHCO_3$	Reacted with Na_2CO_3	Reacted with NaOH	Reacted with HCl
Not cycled	-32 ± 73	214 ± 140	190 ± 23	389 ± 26
Not cycled	-12 ± 73	330 ± 140	185 ± 23	389 ± 26
Not cycled	-27 ± 73	191 ± 140	192 ± 23	373 ± 26
1	57 ± 68	306 ± 116	528 ± 27	339 ± 23
1	52 ± 68	326 ± 116	528 ± 27	334 ± 23
1	57 ± 68	323 ± 116	544 ± 27	326 ± 23
2	80 ± 70	405 ± 137	488 ± 23	323 ± 25
2	85 ± 70	411 ± 137	520 ± 23	323 ± 25
2	88 ± 70	425 ± 137	518 ± 23	320 ± 25
4	121 ± 72	421 ± 127	606 ± 24	320 ± 24
4	124 ± 72	434 ± 127	604 ± 24	306 ± 24
4	138 ± 72	459 ± 127	611 ± 24	297 ± 24
7	79 ± 91	394 ± 130	715 ± 27	375 ± 31
7	97 ± 91	361 ± 130	707 ± 27	367 ± 31
7	94 ± 91	356 ± 130	691 ± 27	364 ± 31
Not cycled, soaked in electrolyte	--	--	--	136 ± 24
Not cycled, soaked in electrolyte	--	--	--	144 ± 24
Not cycled, soaked in electrolyte	--	--	--	136 ± 24

A 34. Average amounts of functional groups on Spectracarb 2225 carbon cloth based on the Boehm titration.

Time of electrochemical cycling (days)	n_{CSF} ± uncertainty (µmol/g)			
	Reacted with $NaHCO_3$	Reacted with Na_2CO_3	Reacted with NaOH	Reacted with HCl
Not cycled	-29 ± 126	203 ± 242	189 ± 40	384 ± 46
1	56 ± 117	318 ± 202	533 ± 47	333 ± 40
2	84 ± 122	413 ± 237	509 ± 40	322 ± 43
4	128 ± 124	438 ± 220	607 ± 41	307 ± 41
7	90 ±157	371 ± 226	704 ± 47	369 ± 53
Not cycled, soaked in electrolyte	--	--	--	139 ± 41

A 35. Summary of acidic and basic groups on Spectracarb 2225 carbon cloth calculated based on the Boehm titration.

Time of electrochemical cycling (days)	n_{CSF} ± uncertainty (µmol/g)			
	Carboxylic groups	Lactonic groups	Phenolic groups	Basic groups
Not cycled	-29 ± 126	232 ± 273	-13 ± 245	384 ± 46
1	56 ± 117	263 ± 233	215 ±207	333 ± 40
2	84 ± 122	329 ± 266	95 ± 240	322 ± 43
4	128 ± 124	310 ± 253	169 ± 224	307 ± 41
7	90 ± 157	280 ± 275	338 ± 231	369 ± 53
Not cycled, soaked in electrolyte	--	--	--	139 ± 41